PARAMETRIC CHARACTERIZATION OF AN EXPERIMENTAL VERTICAL AXIS HYDRO TURBINE

by

George William Rawlings

BASc, University of British Columbia, 2005

A THESIS SUBMITTED IN PARTIAL FULFILLMENT OF THE REQUIREMENTS FOR THE DEGREE OF

MASTER OF APPLIED SCIENCE

in

The Faculty of Graduate Studies

(Mechanical Engineering)

THE UNIVERSITY OF BRITISH COLUMBIA

(Vancouver)

April 2008

ABSTRACT

The current research focuses on the design, fabrication, and testing of an experimental vertical axis tidal current turbine model to obtain first hand experimental data for use in validating numerical codes. In addition to obtaining repeatable experimental results using an entirely new system developed for the UBC towing tank, a parametric study was performed examining the effects of parasitic drag, tip losses, angle of attack, cambered blades, and shaft fairing on a free-stream device. The impacts on overall efficiency of each characteristic are quantified, leading to a prediction for the maximum efficiency of a free-stream device in the absence of losses.

Upon the application of a venturi-style duct, significant gains were demonstrated in the shaft power acquired, as well as in the reduction of torque fluctuations. Application of downstream deflectors provided a further decrease in torque fluctuations with minimal decrease in efficiency, which is significant for structural considerations. A maximum Ck value of 0.473 was obtained for the ducted device compared to 0.272 for the free-stream case; however, the power produced was 12% less than what may be expected from a free-stream rotor of cross-sectional area equivalent to the duct capture area. An investigation into drag characteristics of a free-stream device further quantified the drag coefficient that may be expected, as well as the fluctuations of forces in parallel with the free-stream flow.

Experimental results were then compared with a commercial RANS solver CFD model from a parallel study. This validation will enable further numerical refinement of the optimum tip-speed ratio and solidity values identified in previous research, as well as further advancements into angle of attack, airfoil profile, and ducting configurations. Lastly, a case study was presented using specifying a ducted 3.375m x 3.375m rotor operating in Quatsino Narrows on Vancouver Island capable of powering approximately 17 homes.

TABLE OF CONTENTS

LIST OF TABLES

LIST OF FIGURES

LIST OF SYMBOLS, NOMENCLATURES, AND ABBREVIATIONS

A	Turbine cross-sectional area (0.914m x 0.686m)
AoA	Blade angle of attack (leading edge rotated outwards is positive)
Bk	Betz coefficient = 16/27
c	Blade chord
Cd	Drag coefficient
C_k	Power coefficient
CI	Confidence Interval
Cl	Lift coefficient
C_p	Power coefficient accounting for Betz limit
C_{TF}	Torque fluctuation coefficient
CFD	Computation fluid dynamics
D	Drag force
DAQ	Data acquisition
deg, °	Degrees
FFT	Fast Fourier Transform
HMCS	Her Majesty's Canadian Ship
kWh	Kilowatt-hour
l	Length
m	Metres
MW	Mega-watt
n	Number of blades
N	Number of observations in a sample (for standard deviation calculation)
NI	National Instruments
NRC	National Research Council of Canada
r	Turbine radius (centre of shaft to ¼ chord)
ρ	Density
P_A	Extracted power = torque*angular frequency for current experiments

RPM	Revolutions per minute
s	Seconds
T_{avg}	Average torque
T_{max}	Maximum torque
T_{min}	Minimum torque
TSR	Tip-speed ratio
μ	Viscosity
UBC	University of British Columbia
V, v	Free-stream velocity
VAHT	Vertical Axis Hydro Turbine
ω	Turbine angular velocity
″, in	Inches

ACKNOWLEDGEMENTS

Firstly, I would like to extend a sincere thank you to Dr. Sander Calisal for providing me with the opportunity to venture into the field of ocean energy. His openness to new ideas, guidance in all aspects related to fluid dynamics, and constant push to discover more is a first-class example of how research should be conducted. Secondly, thank you to Jon Mikkelsen for his almost daily consultation, as well as his demonstrated commitment to enhancing student experiences and providing new opportunities for every student showing an interest in marine engineering.

To those in the lab, we've accomplished a large amount of work and have been fortunate to do it so well as a group. Specifically, Voytek Klaptocz has been a great example by simply getting stuff done when it matters and making sure everyone's having a good time doing it, all the while being a valuable resource for ideas and general guidance. Yasser Nabavi and Mahmoud Alidadi have demonstrated immense dedication to the project and I am grateful for the time we have spent chasing ideas, as well as their repeated patience when explaining concepts. Similarly, thank you to Ye Li for his keenness to help out whenever possible. A large number of co-op and visiting students have also made valuable contributions to the project through work on design drawings, instrumentation, data acquisition, and data analysis. Those include Florent Cultot, Cameron Fraser, John Axerio, Robby Chen, Pierre Leplatois, Bo Zulonas, and Thomas Chabut.

I would also like to extend my appreciation to Blue Energy, and in particular Jon Ellison, for both their financial contributions to the research as well as the good times we shared during the experiments. Additionally, thank you to Western Economic Diversification for the funding of experimental equipment and personnel to make the project possible.

Lastly, thank you to my friends for their patience and to my family for their unwavering support in whatever I choose to do, and encouragement to do it right.

1 INTRODUCTION

The mounting evidence substantiating human-caused climate change [1], as well as the pending shortage of fossil fuels [2], is creating an increasing demand for clean, renewable sources of energy. Harnessing wind and photovoltaic energy is among the more traditional means of renewable energy capture; however, increasing attention is being turned to the world's oceans as a resource for wave, tidal, and thermal energy extraction. Canada is fortunate to possess vast wave and tidal energy resources. The Canadian wave resource is estimated to be 146,500 MW, or more than double the current electricity demand, though it should be noted that only a fraction of this total may be extracted and converted to useful power due to power conversion, socio-economic factors, or technology limitations [3]. Similarly, Canada is endowed with abundant tidal current resources. Recent estimates put Canada's tidal current resource at 42,240 MW based on examination of sites with over 1MW of in-stream power, again with only a fraction of that being extractable. Figure 1-1 below provides the distribution of this resource, equivalent to approximately 63% of Canada's current electricity demand [3]. In addition to the significant resource available, tidal currents are advantageous in that they are highly reliable and predictable, and the extraction of this energy using low-head turbines is expected to be environmentally benign [4]. Tidal current energy extraction differs from tidal barrage type power plants (existing in France and Nova Scotia), which function primarily as dams and release water in a controlled manner after the water level on one side of the dam has dropped.

Dr. Barry Davis, former Chief Hydrodynamic Designer for the HMCS Bras D'Or Hydrofoil Ship and Aerodynamic Loads Analyst for the Avro Arrow, was one of the first people to recognize the potential of tidal current energy extraction and began focusing his research here in 1978. Building upon the National Research Council of Canada's (NRC) development of the Darrieus vertical axis wind turbine, he applied the technology to low head hydro applications [4]. Dr. Davis' research led to an extensive research program during the 1980's developing the vertical axis hydro turbine (VAHT) funded by over $1.3 million Canadian dollars. This work, completed as Nova Energy in collaboration with the NRC, led to a number of demonstration projects, the publication of multiple reports, and several independent assessments validating the technology; however, due to the low cost of fossil fuels and the lack of political support for further development of tidal energy at the time, neither Nova Energy nor its successor Blue Energy could establish any major projects through the 1990s.

In 2005, Blue Energy approached the University of British Columbia (UBC) to inquire about developing a computational fluid dynamics (CFD) model of the turbine to update their technology. Numerical models are a particularly useful tool in the field of tidal energy extraction as they:

- Can be linked with an optimizer tool to efficiently conduct parametric studies and determine optimum turbine parameters
- May evaluate designs at various scales, thus minimizing unknown scaling effects when changing turbine size
- Can calculate blade loads used for mechanical calculations or incorporated directly into Finite Element Analysis software
- Permit two-phase simulations that can predict cavitation inception
- May incorporate site-specific current data, accurately predicting power output including cut-in and cut-out operating regimes
- Enable examination of turbine interaction and provide insight into productive / destructive interference
- Allow for flow visualization enabling prediction of environmental effects

This need for numerical model development led to a collaborative research agreement and the ongoing research into the VAHT at UBC. In the meantime, since Dr. Davis' research in the 1980's, the market price of a barrel of oil had risen from $18 USD [5] per barrel in 1985 to over $100 USD in 2008, rendering tidal energy a feasible method of energy extraction. A number of tidal energy technology developers have also entered the market, attracted by current tidal energy cost estimates of 11 – 25 ¢/kWh, and future estimates in the 5 – 7 ¢/kWh range [6].

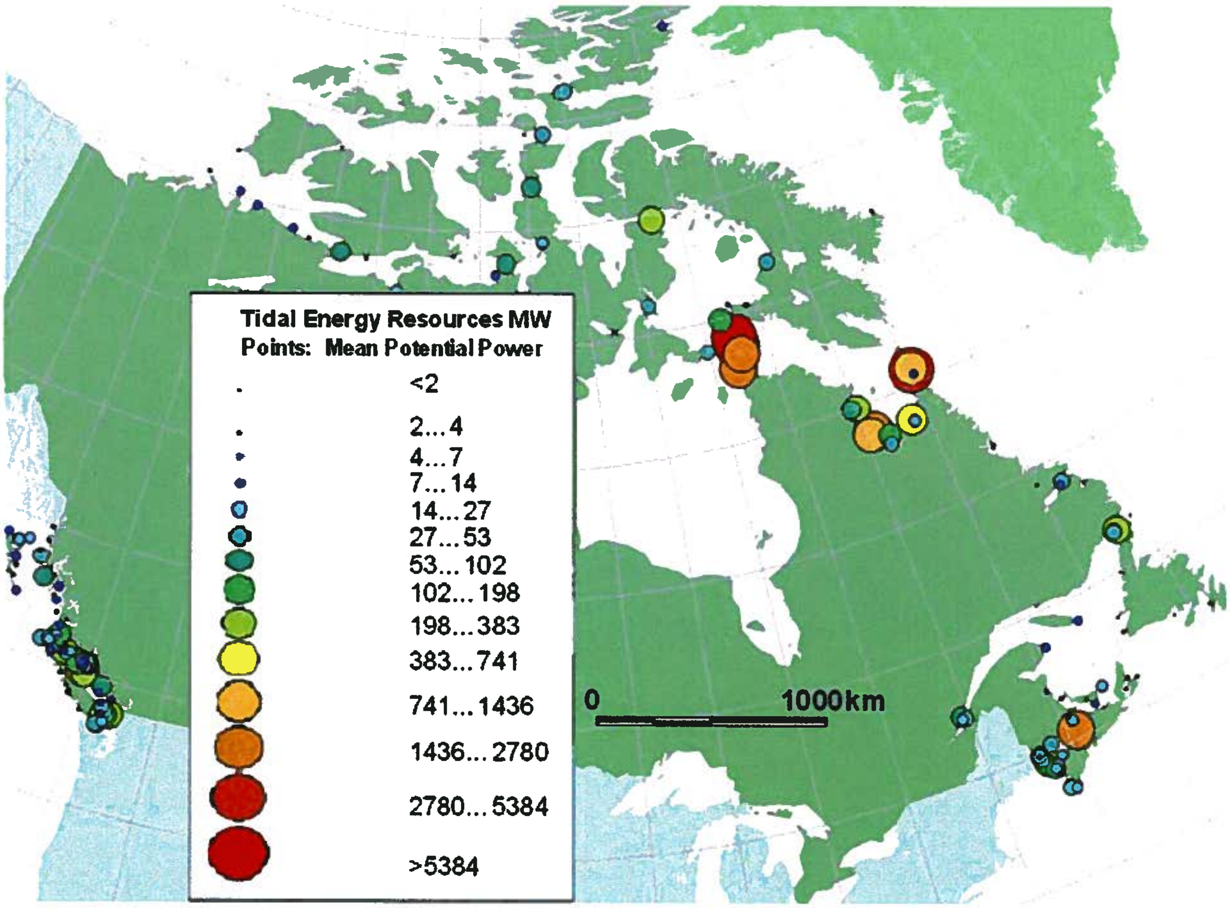

Figure 1-1: Distribution of Canada's in-stream tidal current resource [3].

1.1 Turbine Operating Principles

The vertical axis turbine is a lift-driven device consisting of vertical foils (typically 3 or 4) mounted perpendicular to the flow, usually to a spinning central shaft as shown in Figure 1-2. This differs from a horizontal axis device, which is often similar to a wind turbine or ducted impeller or propeller mounted to the seabed. As the foils rotate, typically at 2-3 times the free-stream flow velocity, the free-stream flow inducess an angle of attack on the foil. The resultant of the lift and drag forces generated by the foil may be reduced to radial and tangential components, of which the tangential component drives the turbine rotation. Figure 1-3 illustrates this concept when a blade passes across the upstream side of the turbine. As the turbine continues to rotate, the relations between the vectors shift, and as a result tangential force is generated primarily in the regions upstream and downstream of the shaft. This causes torque fluctuations, or torque ripple, of the turbine due to blades passing in and out of torque-generating regions. Similarly, the radial component of the force on the blades and the drag forces on the turbine fluctuate with blade position. These cyclic loads are of concern when designing for turbine reliability and longevity.

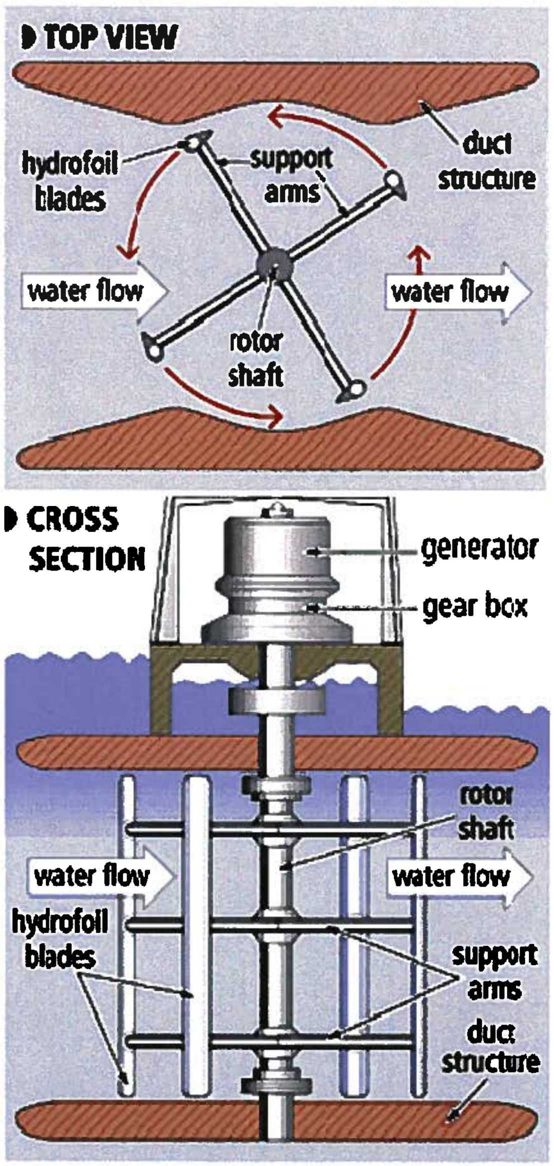

Figure 1-2: Vertical axis turbine schematic [7].

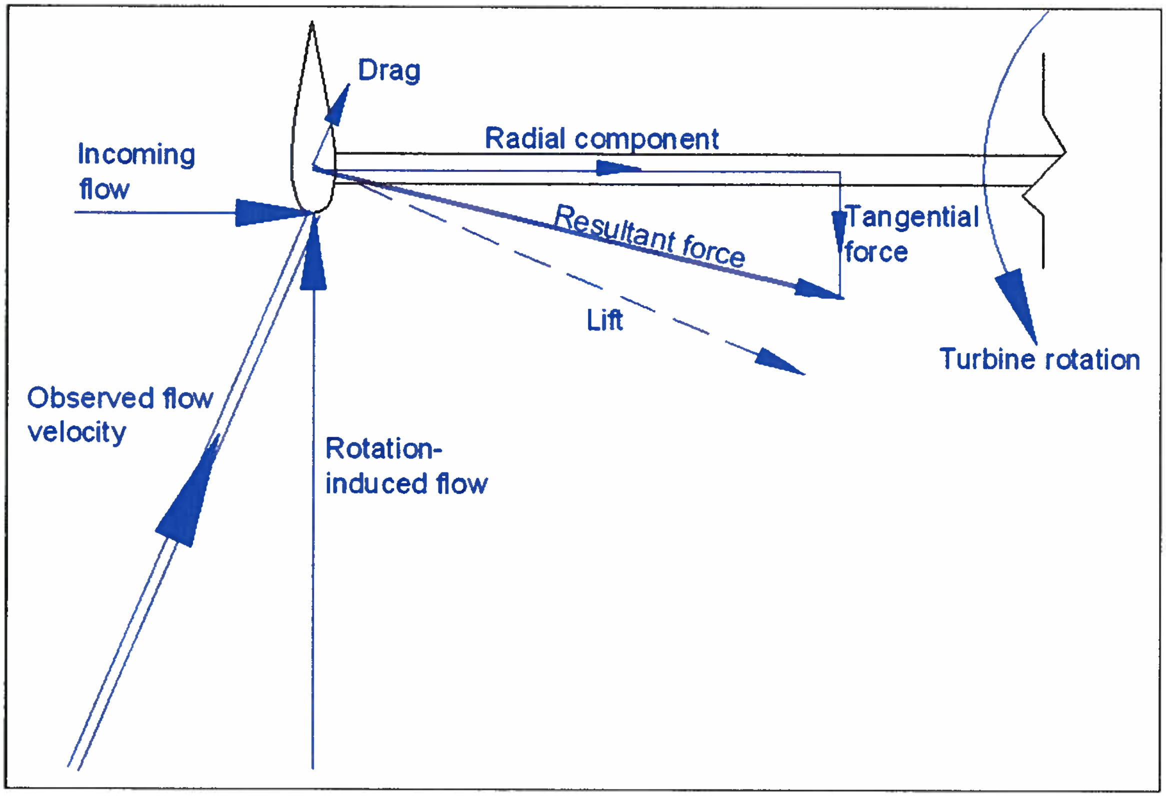

Figure 1-3: Turbine driving force generation.

These torque fluctuations are much less evident in horizontal-axis designs, and the primary arguments against the vertical-axis turbine are that the torque ripple is difficult to manage both for structural integrity and generator function, and that efficiency is lost given the turbine blades are only generating torque through select regions of each revolution. Conversely, there are a number of advantages unique to the vertical axis turbine, encouraging further examination:

- Generators may be easily stored above the water surface and directly driven by the shaft
- Only a single bearing is required underwater
- Turbine rotates in same direction regardless of flow direction
- The vertical design is conducive to stacking multiple turbines under bridges or other existing infrastructure

Until functional commercial units of both horizontal and vertical axis turbines are established and the cost per kWh is compared on a site-by-site basis, the design most suitable to tidal current applications remains unknown.

1.2 Previous Work / Motivation

Prior to Davis' work, Templin examined key parameters affecting Darrieus wind turbine operation by plotting power coefficient (Cp) as a function of tip-speed ratio (TSR) and solidity [8].

$$Cp = \frac{P_A}{\frac{1}{2}.\rho.V^3.A}.\frac{1}{Bk} \qquad \textbf{Equation 1}$$

$$TSR = \frac{r.\omega}{V} \qquad \textbf{Equation 2}$$

$$solidity = \frac{n.c}{r} \qquad \textbf{Equation 3}$$

In the Cp calculation above, it is interesting to note the extracted power (P_A) is divided by the power available in the free-stream passing through the turbine cross-sectional area, which would be the equivalent of efficiency for a free-stream device. This Cp value is then divided by the Betz coefficient (Bk = 16/27), which is the maximum theoretical efficiency for a free-stream turbine according to idealized wind theory [9], thus yielding the efficiency of the device compared to the theoretical maximum extraction possible.

Davis then adapted Templin's work to tidal turbines and generated a number of reports in collaboration with the NRC, upon which many of the initial turbine parameters and dimensionless coefficients were based for the UBC series of tests. Davis initiated the use of the power coefficient (Ck) to quantify turbine performance. This is similar to Cp above, though it is not divided by the Betz coefficient:

$$Ck = \frac{P_A}{\frac{1}{2}.\rho.V^3.A}$$ **Equation 4**

It should be noted that the Ck value is often used interchangeably with efficiency, though this is only appropriate when used in free-stream applications. This is because the addition of ducting, or operation in a confined flume or tank, will enhance the turbine power output; however, the power output (P_A) is still only being divided by an extractable power term that is a function of the free-stream velocity and cross-sectional area of the turbine, instead of a function the effective velocity through the turbine which is altered by the duct or confined domain, or a function of the increased area affected by the duct cross-sectional area or the domain boundaries. As per Davis, power output data discussed below is presented in terms of Ck. The available Davis reports were as follows:

Table 1-1: Available Davis et al. reports

Report Title	Synopsis
NEL-002: Water Turbine Model Trials [10]	Flume tank tests of vertical and horizontal axis water turbines.
NEL-021: Ultra Low Head Hydroelectric Power Generation Using Ducted Vertical Axis Water Turbines [11]	Vertical axis water turbine flume tank tests with caissons, walls, and vane duct configurations.
NEL-022: Ultra Low Head Hydroelectric Power Generation Using Ducted Vertical Axis Water Turbines [12]	Continuation of NEL-021 with a more robust model.
NEL-038: Research and Development of a 50kW to 100kW Vertical Axis Hydro Turbine for a Restricted Flow Installation [13]	Installation of 70 kW turbine within a dam in Nova Scotia.
NEL-070: The Ducted Vertical Axis Hydro Turbine for Large Scale Tidal Energy Applications [14]	Investigates application of vertical axis turbine in a 474 turbine tidal fence.
NEL-081: Commissioning and Testing of a 100kW Vertical Axis Hydraulic Turbine [15]	Examines repaired and enhanced version of model in NEL-038.

Numerical model validation requires both power extraction data and torque data as a function of blade angle. Torque data as a function of blade angle, also known as a torque curve, is critical to provide insight into the regions where torque generation may be enhanced to improve turbine performance, or may be altered to reduce torque ripple. Unfortunately, though discussed briefly by Davis et al. [12], the reports above did not contain sufficient torque curve data for model validation.

Aside from Davis et al., Gorlov patented a vertical axis turbine using helical blades to distribute the torque loading in 1994 (U.S. Patent 5451127) and continues development work in Korea [16]. Given the commercial nature of this venture, efficiency data and torque curve data is closely guarded. Similarly, research has been undertaken in Italy by the Ponte di Archimede S.p.A. Company and the University of Napoli on a turbine with a patented passive angle of attack adjustment mechanism [17,18]; though no publicly available torque curve data has been found. The United Kingdom is a leader in tidal energy technology given the active resource in Northern Scotland and generous government incentives promoting technology development. The former Department of Trade and Industry sponsored three reports on vertical-axis tidal turbines, though only one attempted experimental trials for numerical model validation and provided no useful quantitative data due to a number of factors, including excess friction in the gearbox and a less than ideal experimental flume facility [19]. Other recent efforts include a group from the University of Buenos Aires [20] that has looked into ducting effects, and a group from the University of Edinburgh [21] that has developed a number of numerical models and a conceptual design, though both are lacking experimental data for validation.

Considering torque curve data that was able to be located, Shiono et al. [22] only provided torque curve data upon turbine start-up, and Highquest [23] obtained torque curve data limited to 2 or 3 turbine revolutions on a chart recorder in 1987, providing little accuracy for validation. Secondly, the literature search outlined above revealed no investigation into the drag forces on the turbine during operation, making mechanical design (particularly bearing specification) very difficult.

Apart from the apparent lack of available turbine performance, torque ripple, and drag data, a number of factors affect one's ability to properly use another researcher's experimental data for model validation:

- Flume/towing tank blockage affects turbine performance and must be well documented
- Drive-train losses may affect power output or dampen torque readings
- Shaft and mounting arms affect turbine performance through interference effects and parasitic drag, and geometry and effects of each must be examined
- Knowledge of revolution speed fluctuations is required as performance is highly dependent on TSR

This lack of data and need for comprehensive first-hand knowledge of the experimental setup and parameters provided the motivation for the experimental investigation presented in this thesis.

1.3 Objectives / Scope of Work

The primary purpose of this thesis is to acquire baseline power output and torque ripple data for both a free-stream and ducted vertical axis current turbine for the purpose of validating numerical models, which are currently being developed by two other graduate students. These tests will also serve to enhance understanding of work completed by previous researchers, as well as investigate a number of turbine parameters and quantify their corresponding effects on performance. More specifically:

- Acquire power coefficient data for both a free-stream and ducted vertical axis turbine in the UBC campus towing tank
- Acquire torque fluctuation data for both a free-stream and ducted vertical axis turbine over the course of a turbine revolution
- Investigate effects of TSR, blade angle of incidence, cambered blades, and various ducting configurations on turbine performance and torque fluctuations. Effects of shaft fairings, arms, and foil end plates are also examined
- Experimentally investigate magnitude of forces parallel to the free-stream flow on the turbine for future design applications (referred to as drag forces)

Chapter 2 below outlines the entirely new system developed for conducting tests in the UBC towing tank. This includes the requirement for a secondary carriage to accommodate the turbine testing. An overview of the data acquisition (DAQ) software, instrumentation, experimental procedure, and data analysis program is also provided as well as the baseline model parameters.

Chapter 3 presents the experimental power coefficient and torque curve results from the three experimental test programs and discusses their significance. An overview of the recorded drag data is also provided. Chapter 4 examines experimental errors and compares select power output, torque curve, and drag curve results with theory. These results are then used to develop a case study specifying a sample unit capable of powering 17 homes in Quatsino Narrows on Vancouver Island. Chapter 5 contains conclusions and recommendations for future work.

2 EXPERIMENTAL SETUP AND PROCEDURE

All instrumentation, data acquisition equipment and software, experimental equipment, and data analysis software was purchased, built, or written specifically for this research program and is described below.

2.1 Towing Tank and Carriage Overview

Experimental testing was conducted in the UBC campus towing tank, which is a 200' long by 12' wide by 8' (7' of water) deep fresh water tank. The main cantilevered carriage, typically used for ship model testing, runs on rails alongside the tank. The tank is oriented in the east-west direction and runs were performed traveling both towards the wave-maker (due east) and towards the dock (due west). A secondary carriage spanning the width of the tank was constructed and attached to the main carriage and used as the testing platform for the turbine, as shown in Figure 2-1 and Figure 2-2. The use of the secondary carriage was necessary to accommodate the large turbine device:

- Support increased weight and drag force compared to typical ship hull model tests
- Facilitate turbine installation and removal
- Provide easy access for adjustments
- Serve as a platform for the large amount of instrumentation including motor and drive-train

The secondary carriage was fabricated of welded aluminum c-channel in two halves that were then bolted together. Two rubber wheels rested on both the outer rail and the side of the tank opposite the main carriage, while two v-grooved wheels ran along the rail closest to the water. The entire secondary carriage was bolted to the front of the main carriage, with a diagonal brace providing added support.

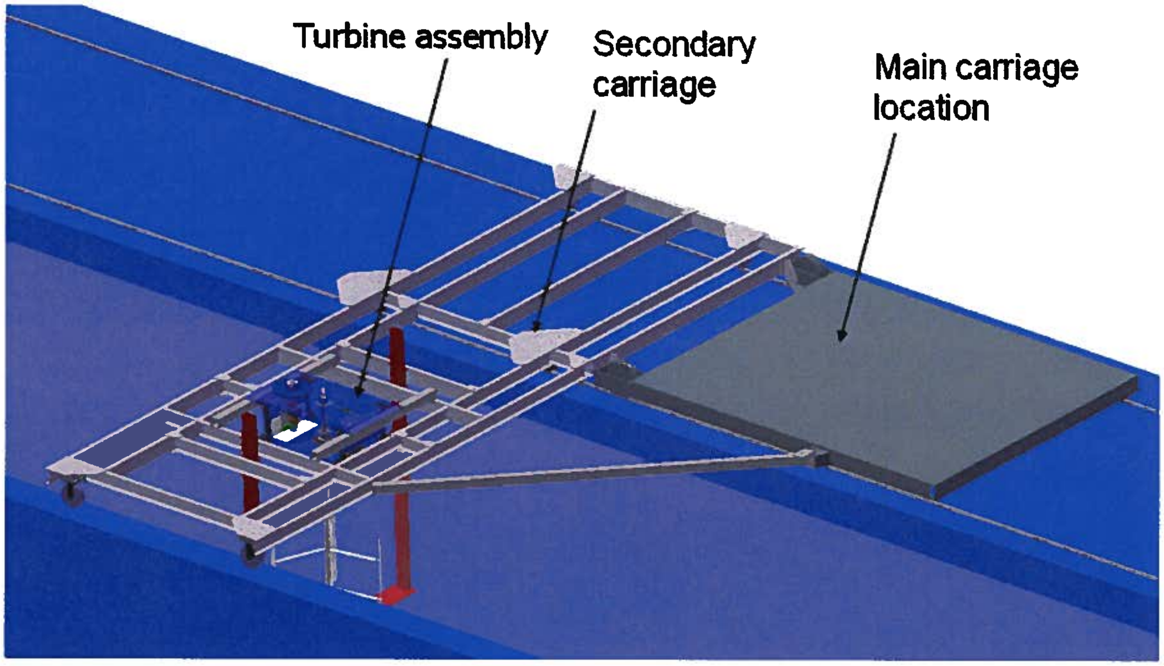

Figure 2-1: Secondary carriage and turbine assembly drawing.

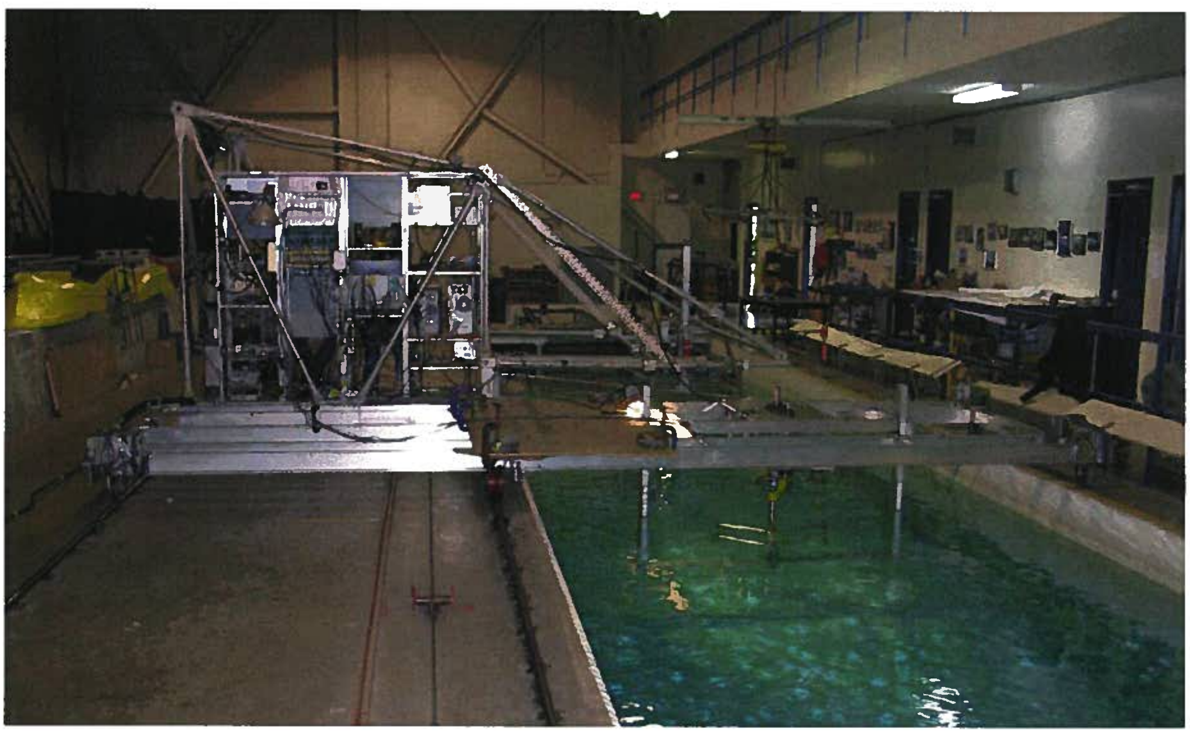
Figure 2-2: Towing tank facility with main and secondary carriage.

2.2 Baseline Model Parameters

The three turbine blades are attached to a central shaft that is supported at both ends by ball bearings. The top bearing is mounted on the force balance, while the bottom bearing is constrained to a horizontally-mounted bottom plate supported by two vertical rectangular beams forming a u-shaped frame. These beams are bolted to the secondary carriage and stiffened using 3 guy wires each; two extending in the plane of the flow direction (one forwards and one backwards) up to the secondary carriage, and the third extending in the plane perpendicular to flow direction and out towards the side up to the secondary carriage. The turbine assembly with arms supporting the blades at the ¼ span locations is shown in Figure 2-3 below, along with the supporting frame and force balance for mounting the instrumentation.

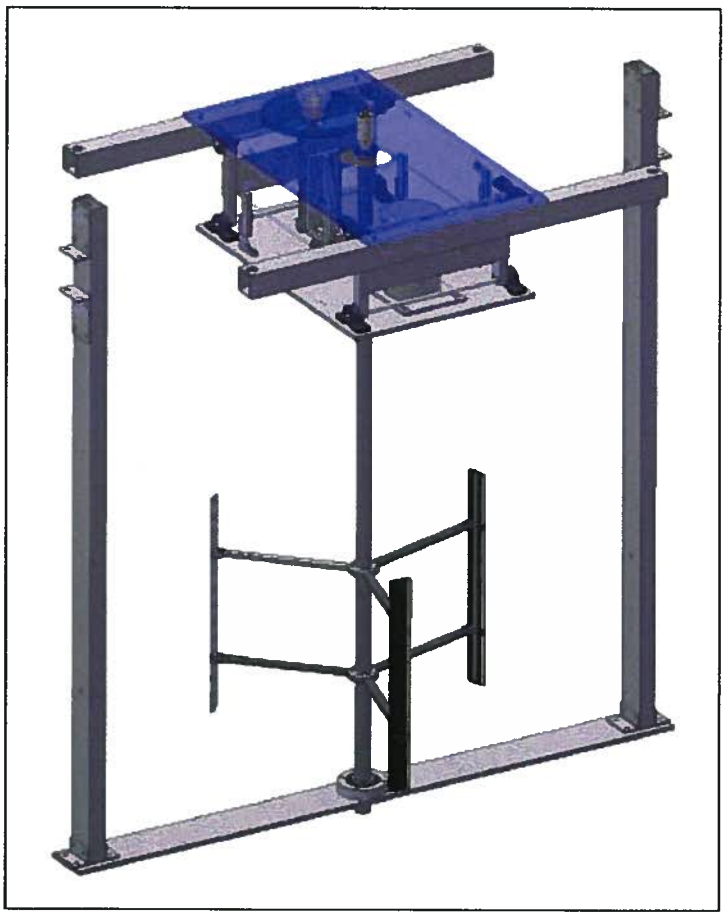

Figure 2-3: Turbine assembly with force balance and frame.

Principal model parameters are provided in Table 2-1 and Figure 2-4:

Table 2-1: Principal model turbine parameters.

PARAMETER	DIMENSION / CHARACTERISTIC
Diameter (across foil chord)	36 in
Number of blades	3
Blade span	27 in
Blade profile	NACA 63_4-021 and 63_4-421
Chord length	2.70 in ideal; 2.57 in manufactured
Shaft outer diameter	1.9 in

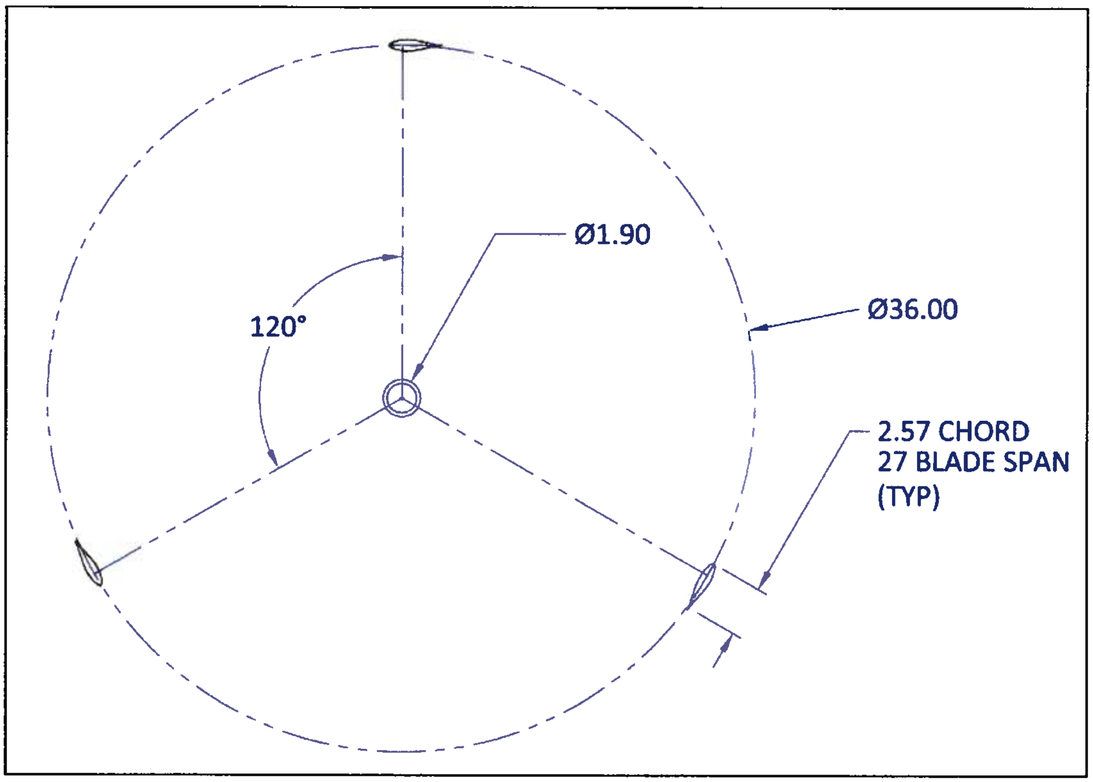

Figure 2-4: Turbine rotor nomenclature (top view, inches).

Arm profiles supporting the blades varied between test programs and therefore are not listed above. Appendix A and Appendix B contain component sizing calculations and part drawings respectively. Specific turbine and ducting position within the towing tank is discussed in Section 3 for each case presented.

2.3 Instrumentation

2.3.1 Instrumentation Components

The components used for measuring drag force, torque, turbine angle, and for driving the turbine were as follows:

- 3HP Micro Max motor 182TCZ TEFC from Marathon Electric with Parker SSD AC vector drive controller and braking resistor kit (may be used for both driving and braking turbine) (7/8" shaft; 230V, 4.6A, 5400 max. safe rpm)
- 2 of PT-Global SG-PT4000-500 lb s-type load cells
- Futek Torque Sensor, 0 - 369 ft lb, 0.2% accuracy, aluminum, 2mV/Voutput , 7" length (TRS300)
- Accu-Coder 776-B-S-2048-R-PP-E-P-A-N 1-7/8" through-bore encoder (2048 increments per revolution)
- U.S. Digital encoder digital-analog converter (used with encoder)
- CONEX gearbox B091020.LAARJ, TEXTRON fluid and power. Ratio 20:1, SHC 634 lubrication, helicoidal gear geometry

Additional specifications on the components above may be found in Appendix C. Carriage speed was monitored using a pre-existing system on the towing carriage.

2.3.2 Drive-train / Force Balance Configuration

Model revolution speed was controlled using an AC motor, and for the first two test programs chains and sprockets drove the turbine shaft, as well as provided the ratios necessary to scale the revolution speeds between the turbine and motor shafts. The motor, chains and sprockets, and lay-shaft (consisting of the torque sensor) all mounted to the bottom plate of the force balance as shown in Figure 2-5. This lower plate was hung from the top plate using two pairs of hinged arms and was thus free to translate relative to the top plate; additionally, large holes were cut in the top plate to allow the main turbine shaft and lay-shaft to pass through without contact. Two load cells (one on each side of the force balance) were then used to ground the bottom plate relative to the top, and thus measure the forces on the bottom plate. To accelerate the turbine to the desired rotation speed, the motor drove the lay-shaft, which consisted of the torque sensor and adaptive couplings mounted vertically on two bearings, at a 14:72 ratio. The lay-shaft then drove the main turbine shaft at a 20:36 ratio. Alternately, when the motor was acting as a brake to slow the turbine rotation, the system drove in the reverse direction. This chain and sprocket system was used to facilitate drag force measurement using this force balance design, as well as to allow for flexibility to change the sprocket ratios should the motor or torque sensor not performed as anticipated. Lastly, the encoder was mounted directly around the main turbine shaft above the top bearing.

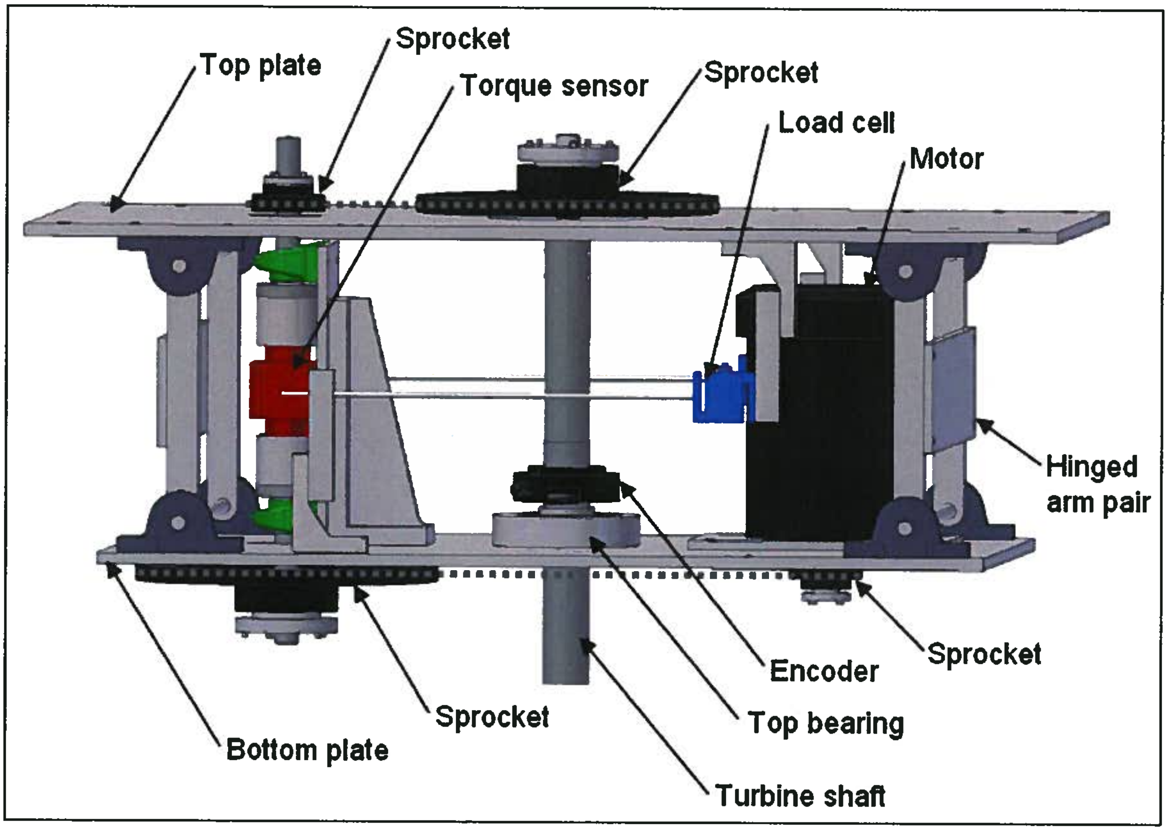

Figure 2-5: Force balance and instrumentation configuration.

For the third test program, the chain and sprocket drive-train was replaced with a 20:1 gearbox, and the force balance plates were rigidly joined using a plate and aluminum channel (Figure 2-6). This was an attempt to reduce revolution speed fluctuations (discussed in Section 4.1.3 below) by using a more rigid system with the 90° worm gear drive, and thus drag measurements were no longer recorded. A second bearing was added to the top plate to minimize shaft deflections, and a flexible coupling was used to couple the torque sensor and gearbox.

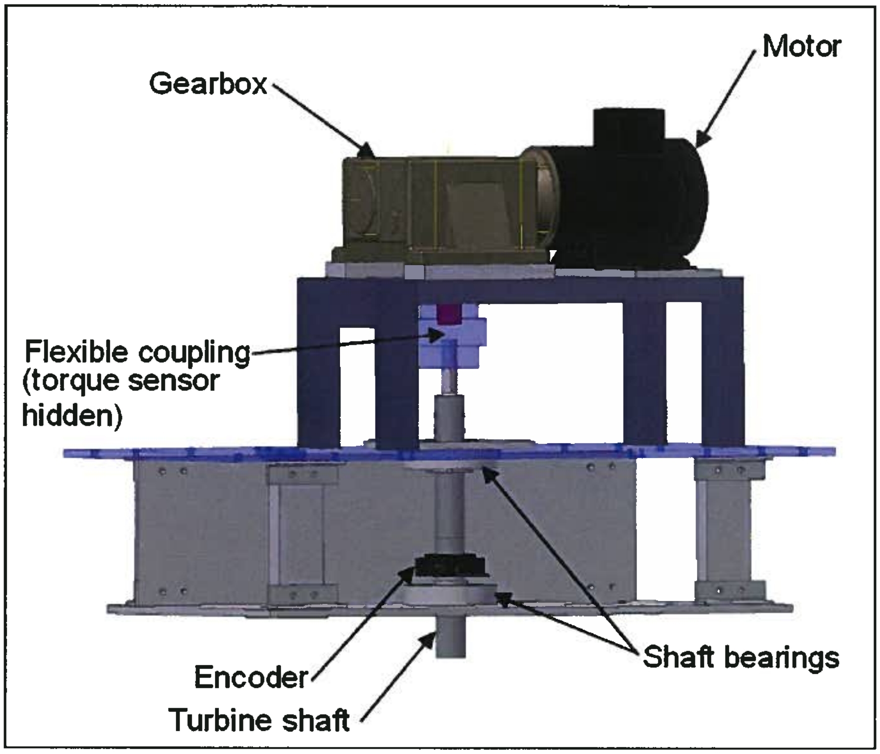

Figure 2-6: Gearbox drive-train configuration.

2.4 Data Acquisition System

The following National Instruments (NI) data acquisition hardware components were used for these trials:

- 1 cDAQ-9172 8-slot USB Chassis with rail mounting kit
- 1 NI 9205 32-Channel +/- 10V 250 ks/s 16-bit analog input module used with encoder and carriage speed
- 1 NI 9237 4-Ch 50 ks/s per channel 24-bit analog input module used with torque sensor

Supplementary DAQ hardware information may be found in Appendix C.

Labview software was developed to take 100 samples on each channel (angle, torque, carriage speed, and load cell 1 and 2 where necessary). Each set of 100 samples was then averaged and written to an output file, and this sequence was performed at a frequency of approximately 240 Hz, or every 0.00406 seconds. Table 2-2 below provides number of degrees of revolution per data point for representative velocity and TSR values.

Table 2-2: Degrees of revolution per sample for representative carriage speeds and TSR values.

	Number of Degrees per Sample			
Velocity (m/s)	TSR = 1.5	TSR = 2	TSR = 2.5	TSR = 3
1.5	1.14	1.53	1.91	2.29
2	1.53	2.04	2.54	3.05

2.5 Calibration

Calibration of the instrumentation components was performed as required. The torque sensor utilized a manufacturer supplied constant that was verified in the lab. Routine checks using the shunt resistor were then performed validating the 0-500Nm range. Similarly, routine checks were used to verify that the angular encoder was accurate over 0-360°. Lastly, each load cell was connected one at a time and calibrated by applying a force (typically up to 16 lb) to the lower force balance plate using a rope and pulley system.

2.6 Experimental Procedure

For each test run, a standard procedure was followed:

1. The carriage and turbine were stopped while the waves dissipated on the water surface and the vortices dissipated in the tank
2. The turbine was manually rotated such that a blade was in the 180° position and the encoder was reset to 180° (0° corresponds to when a blade is heading directly into the oncoming flow as discussed Section 2.7 below)
3. The DAQ system and motor driving the turbine were started
    a. If drag data was being recorded, then the DAQ system was started and allowed to run for a few seconds to record values at zero velocity before starting the turbine and allowing it to reach the desired revolution speed
    b. If no drag data was being recorded, the turbine was started and allowed to reach the desired revolution speed; the DAQ system then started to record
4. The carriage accelerated up to speed while the motor maintained the turbine at the desired revolution speed

5. The carriage ran down the tank at the desired speed for the maximum allowable distance
6. The carriage was decelerated to a stop
7. The DAQ system was stopped and the motor driving the turbine was turned off, allowing the turbine to come to rest

Figure 2-7 below illustrates this procedure (case 2.b) using a plot of torque measurement vs. cumulative angle of turbine rotation for a typical run; the duration of the recorded data period was 31.5 seconds.

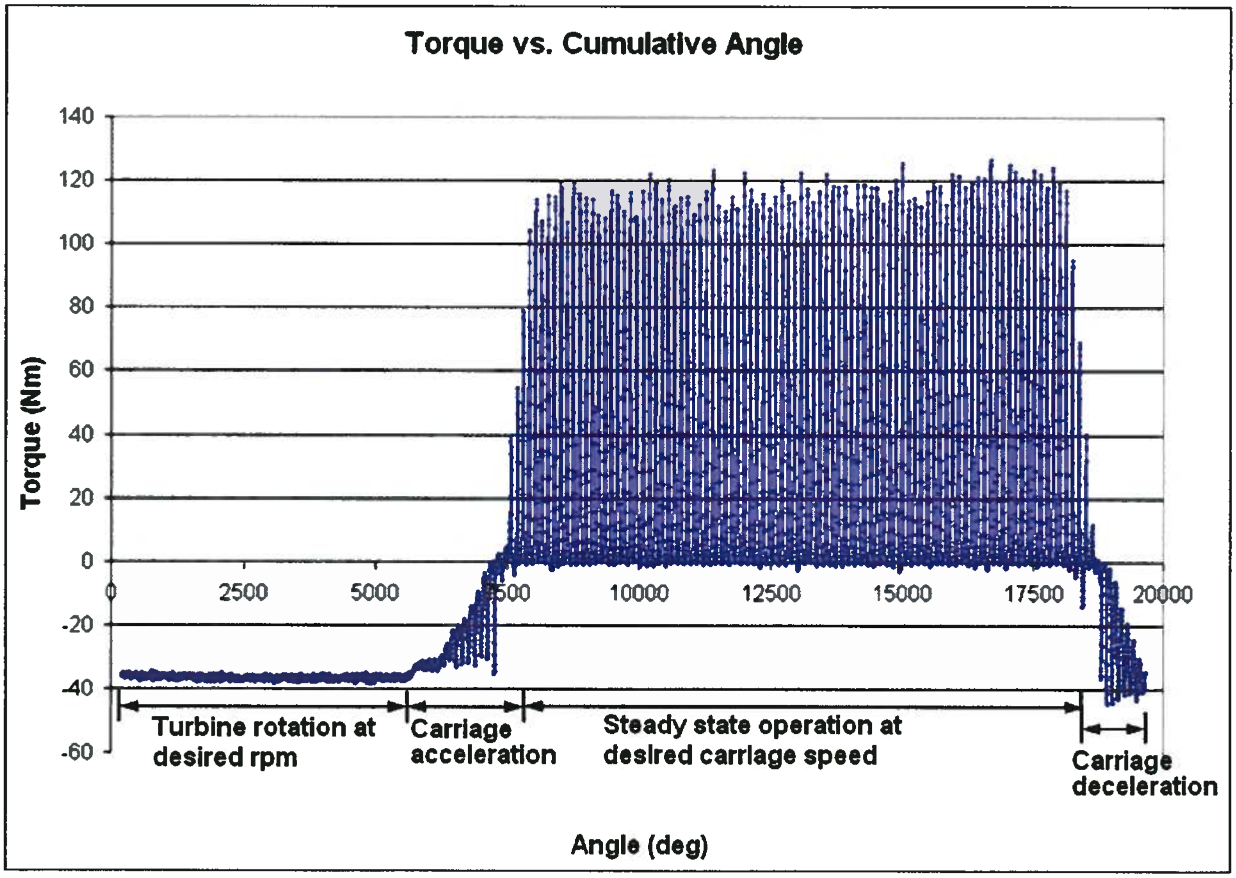

Figure 2-7: Typical run description (run duration 31.5 sec).

2.7 Data Processing Methodology

A Matlab program was developed to first read the raw data files output from the DAQ program, then format the data, and subsequently facilitate "on-the-spot" data analysis. This analysis primarily consisted of plotting loads recorded by each individual load cell, the total load, the torque values, or the turbine revolution speed versus either time or revolution angle (either cumulative or reduced to over 1 revolution). The raw data files were processed such that the recorded parameters from the different test programs could be plotted on the same plots, enabling comparison. Figure 2-8 displays the primary Matlab program user interface.

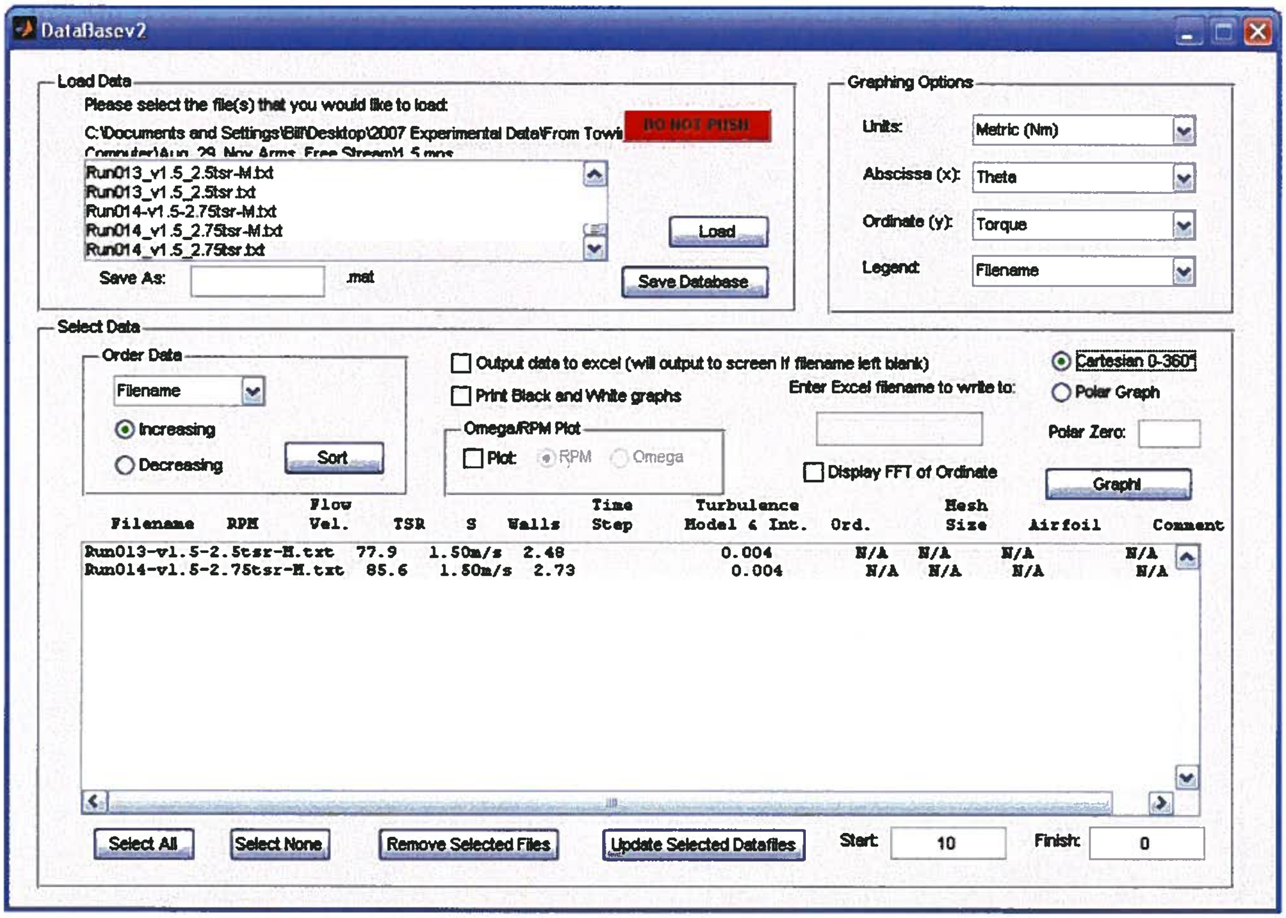

Figure 2-8: Matlab program interface.

2.7.1 Data Selection and Averaging

The Matlab program was written to select the range of data at outside of the carriage acceleration and deceleration periods and thus suitable for analysis. Examining the carriage velocity data column, the beginning and end of the range of data at the desired carriage velocity was specified. 10% of the length of this specified range was further eliminated from either end, leaving the middle 80% of the data at the constant velocity to be written to a new Matlab file (with a "-M" extension to the file name) for further analysis as shown in Figure 2-9. This method of selecting the steady-state range was tested during experiments and provided consistent torque profiles at either end of the range. Columns written in the "-M" file included Time, Theta, Torque, RPM, Carriage Velocity, Time-step, as well as Load Cell1, Load Cell 2, and Total Load where applicable. Calculations were performed as necessary to complete the columns above:

- Shaft revolution speed ratios were applied to the torque values when the lay-shaft experimental setup was used.
- Moment arm ratios were applied as needed to the drag force calculation (further discussed in Section3.5).
- Instantaneous angular velocity, and subsequently RPM, for a given point was the average of the 12 closest points to minimize data spikes from the small interval (change in theta over time-step) used for calculation.

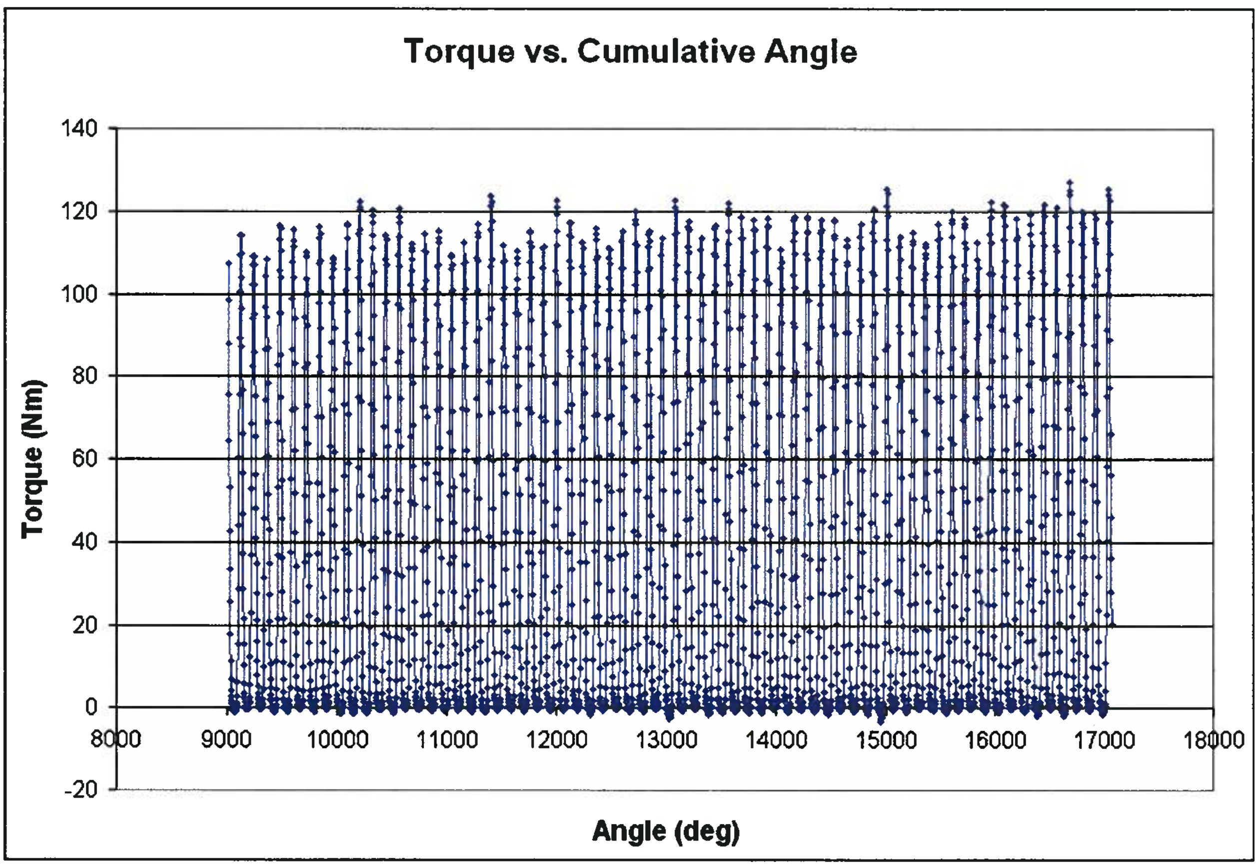

Figure 2-9: Range of data at steady-state for analysis.

An ensemble averaging technique was then used to collapse the data onto one turbine revolution. The torque values over each revolution for a single run were plotted over 360 degrees, or overlaid on each other, as shown by the small points in Figure 2-10. The data was then isolated into 4 degree increments, as demonstrated in Figure 2-11, in which an average (cross) is obtained from the overlaid data points for each increment. Figure 2-10 also displays the resulting average torque curve over one revolution.

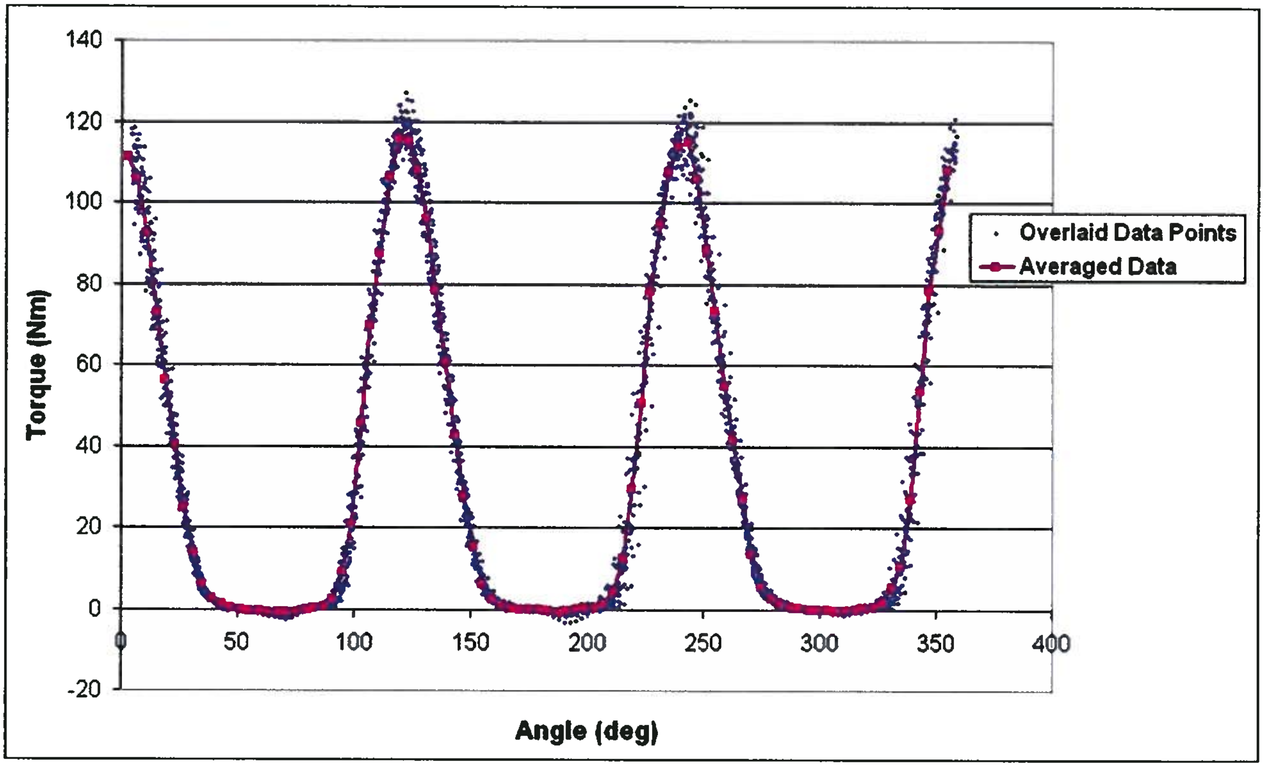

Figure 2-10: Torque vs. Angle of Revolution overlaid over one turbine revolution.

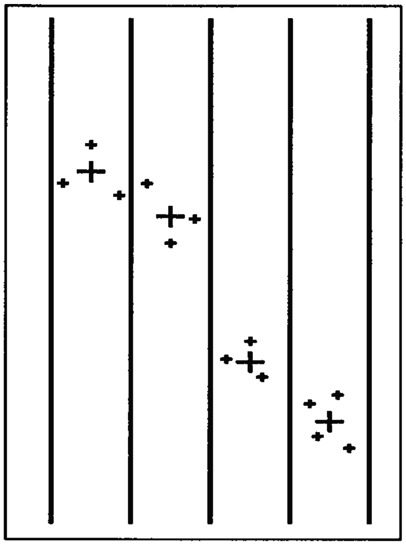

Figure 2-11: Ensemble averaging.

2.7.2 Data Presentation

Data is typically presented in three forms. Firstly, plots are often given as power coefficient vs. tip-speed ratio, demonstrating the capability of the device to extract power from the free-stream current. The two other plots are used to enhance understanding of the turbine operation, and provide the parameter of interest (typically torque) vs. angle of rotation in both Cartesian (ie. Figure 2-10) and Polar (ie. Figure 2-12) coordinates. Because Polar plots typically distort the plots and don't easily display negative values, they are primarily used as a visualization tool for highlighting the regions of turbine revolution that could benefit from flow adjustment to enhance turbine performance as well as reduce torque fluctuations. Figure 2-12 illustrates the torque generated by a three-bladed turbine oriented such that at 0 degrees a blade is headed directly into the flow. Flow enters the turbine from the top of the image (90^{o}) and rotation is counter-clockwise. The 3 peaks are created as torque is generally produced by each blade as it passes through approximately 90^{o}-120^{o} in the region upstream of the shaft.

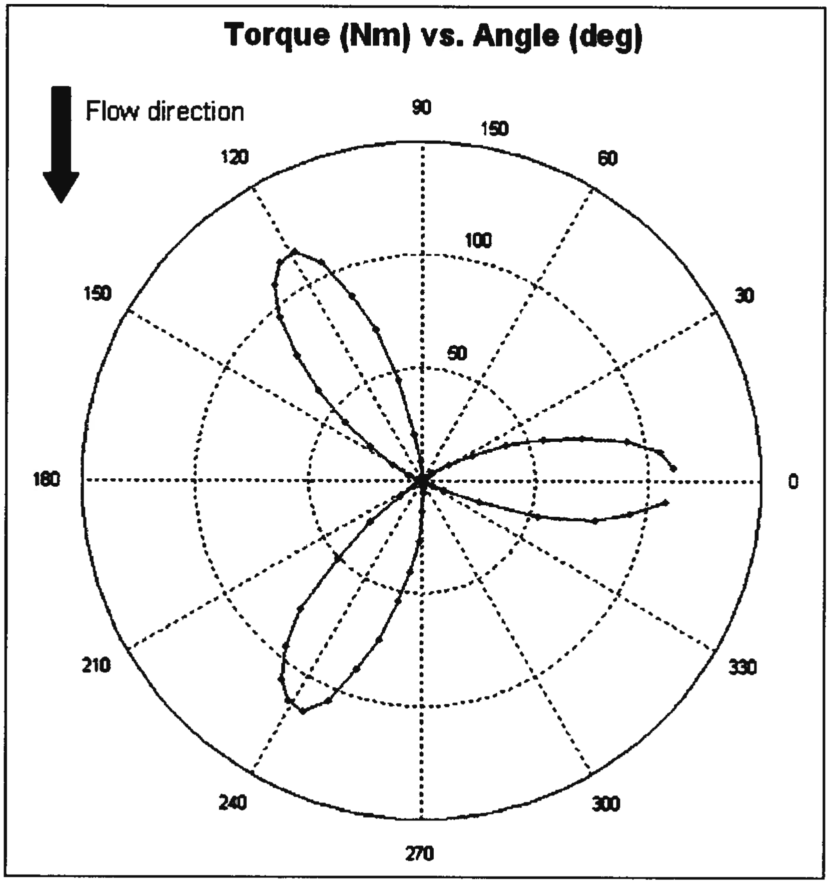

Figure 2-12: Example of Polar plot (counter-clockwise rotation).

3 EXPERIMENTAL RESULTS

The specific setup and results for each test program conducted are discussed in the Sections 3.2 through 3.4. Experimental errors and measurement accuracy are later discussed in Section 4.1.

3.1 Angle of Attack and Revolution Angle Notation

Blade incidence angle (commonly referred to as angle of attack – AoA) was investigated in a number of the experiments, and is considered positive when the leading edge of the blade was rotated outwards from the main shaft as shown in Figure 3-1 below.

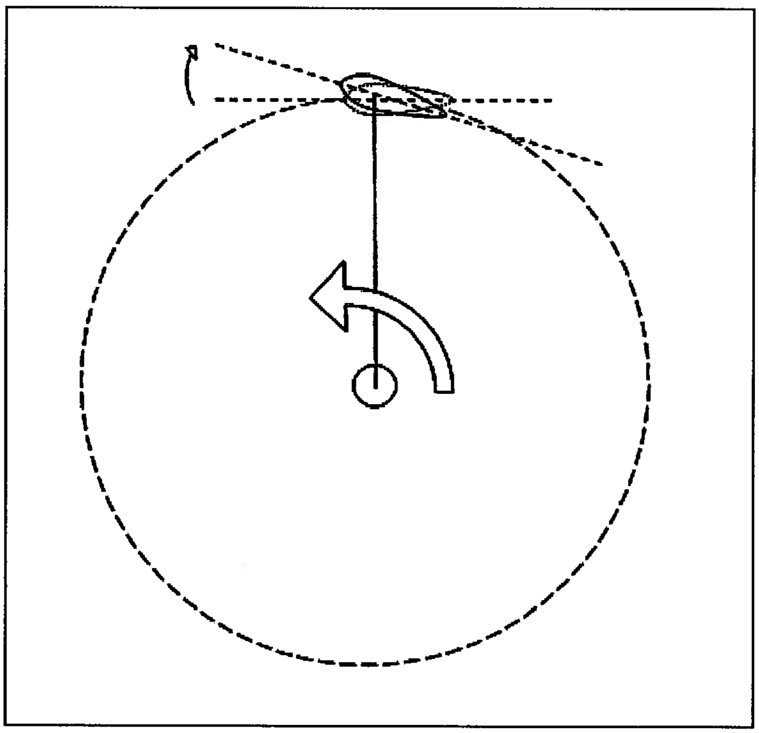

Figure 3-1: Angle of attack notation.

Blade position over the course of a revolution is also of importance when reading plots and understanding turbine operation. For the results presented below, a blade is considered to be at 0 degrees when it is headed directly into the flow, and is at 180 degrees when it is moving in the same direction as the flow. This is illustrated in Figure

3-2 below, with a blade generally producing torque at approximately the 90 degree position and 270 degree position, as it passes perpendicular to the free-stream flow.

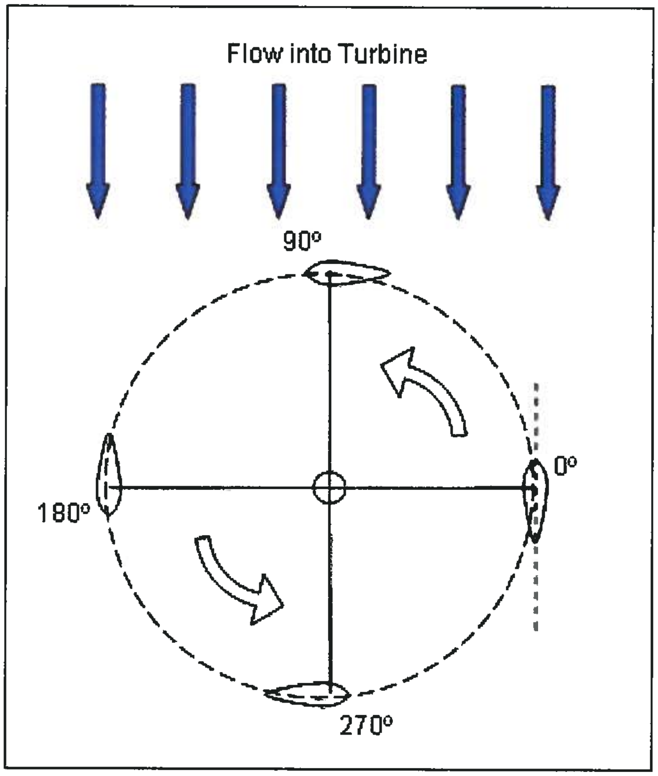

Figure 3-2: Flow direction relative to blade angular position.

3.2 Test Program Overview

Three programs were performed in August 2006, November 2006, and Aug/Sep 2007. Table 3-1 provides details on model configuration and parameters examined during each test program. It should be noted that for each test program the arm profiles were subsequently reduced, while specific arm profiles, end plate specifications, and other turbine parameters may be found in Appendix B. A detailed run log may be found in Appendix D.

Table 3-1: Test program and corresponding parameters.

TEST PROGRAM	PROGRAM DETAILS
August 2006 (approx. 575 runs)	• Chain and sprocket drive-train

TEST PROGRAM	PROGRAM DETAILS

	• High-profile arms (configuration A) supporting blades at ¼ chord
	• Symmetric blade profile 63_4-021
	• Parameters tested:
	    o Blade angles of attack -5, 0, 3, 5, 10
	    o Carriage velocities 1, 1.25, 1.5, 1.75, 2 m/s
	    o TSR values 1.25 – 3.5 at 0.25 increments
	    o Single blade
	    o Arms without blades attached

November 2006
(approx. 460 runs)
	• Chain and sprocket drive-train
	• Medium-profile arms (configuration B) supporting blades at ¼ chord
	• Symmetric blade profile 63_4-021
	• Parameters tested:
	    o Carriage velocities 1 – 2 m/s at 0.25 increments
	    o TSR values 1.25 – 3.5
	    o Free-stream turbine at AoA = -3,0,3,5 deg
	    o Single blade at AoA = 3 deg
	    o Ducted turbine with open ends at AoA = 0,3,5 deg
	    o Medium profile arms without blades

Aug/Sep 2007
(approx. 340 runs)
	• Gearbox drive-train
	• Parameters tested:
	    o TSR values 1.5 – 3.5 at 1.5 m/s carriage speed, and 1.5 – 2.75 at 2 m/s carriage speed
	    o Medium-profile arms at ¼ locations vs. low-profile (NACA 0012) arms at ends and middle of blades
	    o Medium-profile arms with circular and foil end plates
	    o 2 vs. 3 arms (foils end supported with removable

TEST PROGRAM	PROGRAM DETAILS
	arm at centre) o Symmetric blade 63_4-021 at AoA = 0, and cambered blade 63_4-421at AoA = 0, 5 deg o Single blade o Duct with end covers and deflectors at varying positions o Shaft fairing with single blade, 3 blades, and ducted turbine o Low-profile arms without blades

3.3 Free-stream Turbine

Figure 3-3 below illustrates turbine positioning within the tank for both the high and medium profile arms (profiles A and B discussed in Section 3.3.3) supporting the blades at the ¼ chord locations. Figure 3-4 highlights the change in turbine position to accommodate ducting with end caps when the low-profile (NACA 0012) supporting arms were used at the ends, and usually middle, of each blade. The following tests and parameters are discussed in Sections 3.3.1 through 3.3.8:

- 3.3.1 Velocity / Reynolds Number Effects
- 3.3.2 Drive-train Comparison
- 3.3.3 Arm Profile Reduction
- 3.3.4 Single-blade
- 3.3.5 Angle of Attack
- 3.3.6 Cambered Blades
- 3.3.7 Blade End Plates
- 3.3.8 Shaft Fairing

Lastly, Section 3.3.9 summarizes these results.

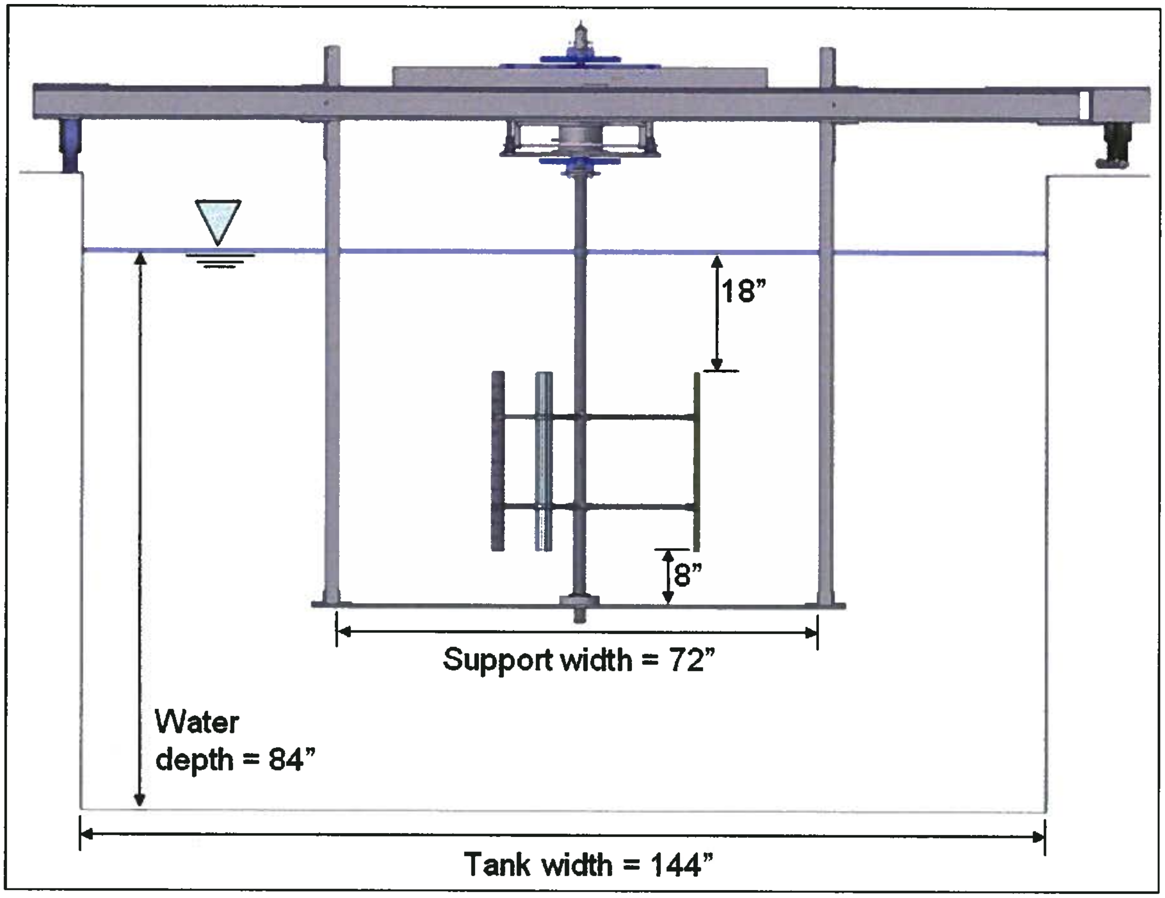

Figure 3-3: Free-stream turbine positioning (arm profiles A and B).

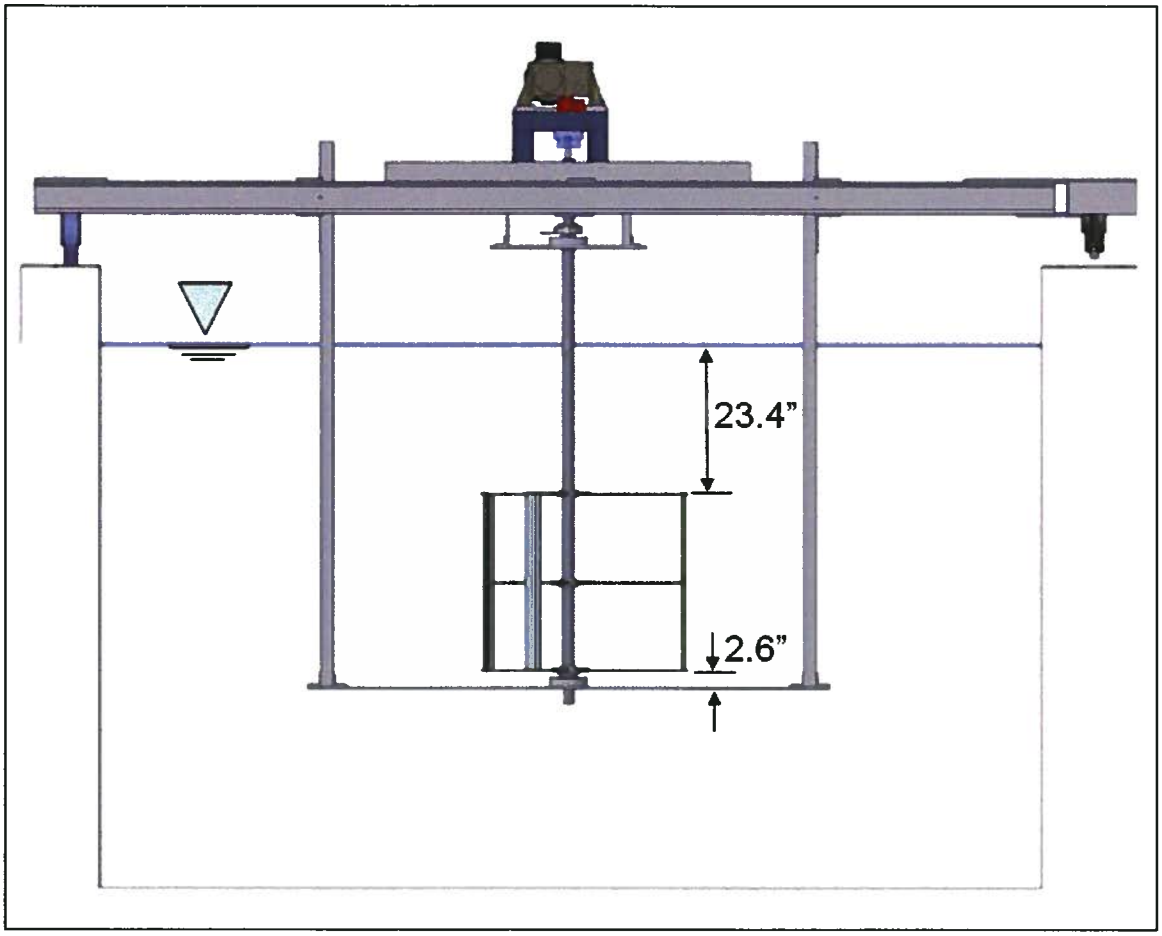

Figure 3-4: Arm profile C free-stream turbine positioning.

3.3.1 Velocity and Reynolds Number Effects

Reynolds number, and as a result free-stream velocity and tip-speed ratio, affect turbine performance. Table 3-2 below illustrates the range of Reynolds numbers observed at the primary velocities and TSR values examined. As these values range between 32 600 and 522 000, the foil is in a transition region and the lift coefficient will be significantly affected as the turbine velocity is increased. Figure 3-5 and Figure 3-6 provide lift coefficient and lift/drag coefficient respectively vs. angle of attack for a NACA 63_4-021 foil at Re = 200 000 and Re = 500 000 [24]. These results were obtained using CFD software, as it is very difficult to find experimental data for such coefficients at the range of angles of attack needed for turbine analysis at the Reynolds numbers of interest. At Re = 500 000, Cl / Cd may be 35% larger than for Re = 200 000, greatly affecting turbine performance. These effects are evident in Figure 3-7, demonstrating improved turbine efficiency with increasing free-stream velocity. This is a positive result, as at larger commercial scales turbine performance considering Reynolds effects should improve.

$$\mathrm{Re} = \frac{\rho . v . l}{\mu} \qquad \textbf{Equation 5}$$

Table 3-2: Reynolds numbers at varying velocities and TSR values for a free-stream device.

		TSR			
Velocity (m/s)	Angle (deg)	1.5	2	2.5	3
1	0	1.63E+05	1.96E+05	2.28E+05	2.61E+05
	90, 270	1.18E+05	1.46E+05	1.76E+05	2.06E+05
	180	3.26E+04	6.53E+04	9.79E+04	1.31E+05
1.5	0	2.45E+05	2.94E+05	3.43E+05	3.92E+05
	90, 270	1.77E+05	2.19E+05	2.64E+05	3.10E+05
	180	4.90E+04	9.79E+04	1.47E+05	1.96E+05
2	0	3.26E+05	3.92E+05	4.57E+05	5.22E+05
	90, 270	2.35E+05	2.92E+05	3.52E+05	4.13E+05
	180	6.53E+04	1.31E+05	1.96E+05	2.61E+05

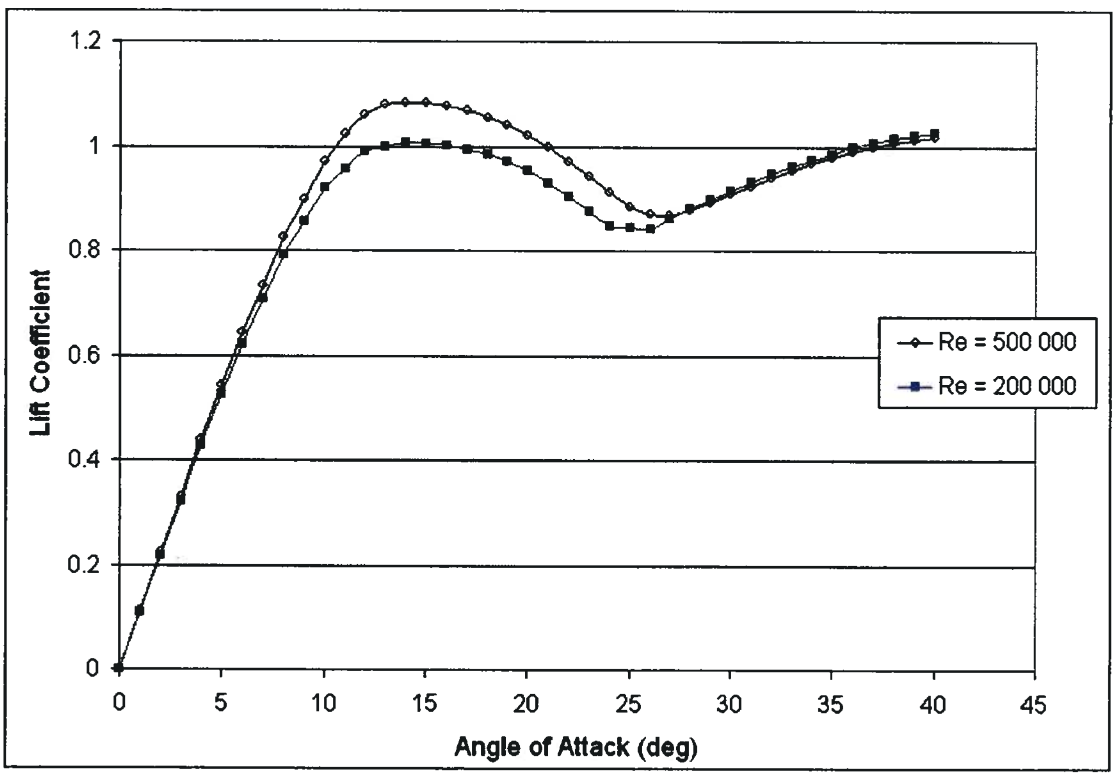

Figure 3-5: Lift Coefficient vs. Angle of Attack using CFD for 63_4-021 at Re = 200 000, 500 000.

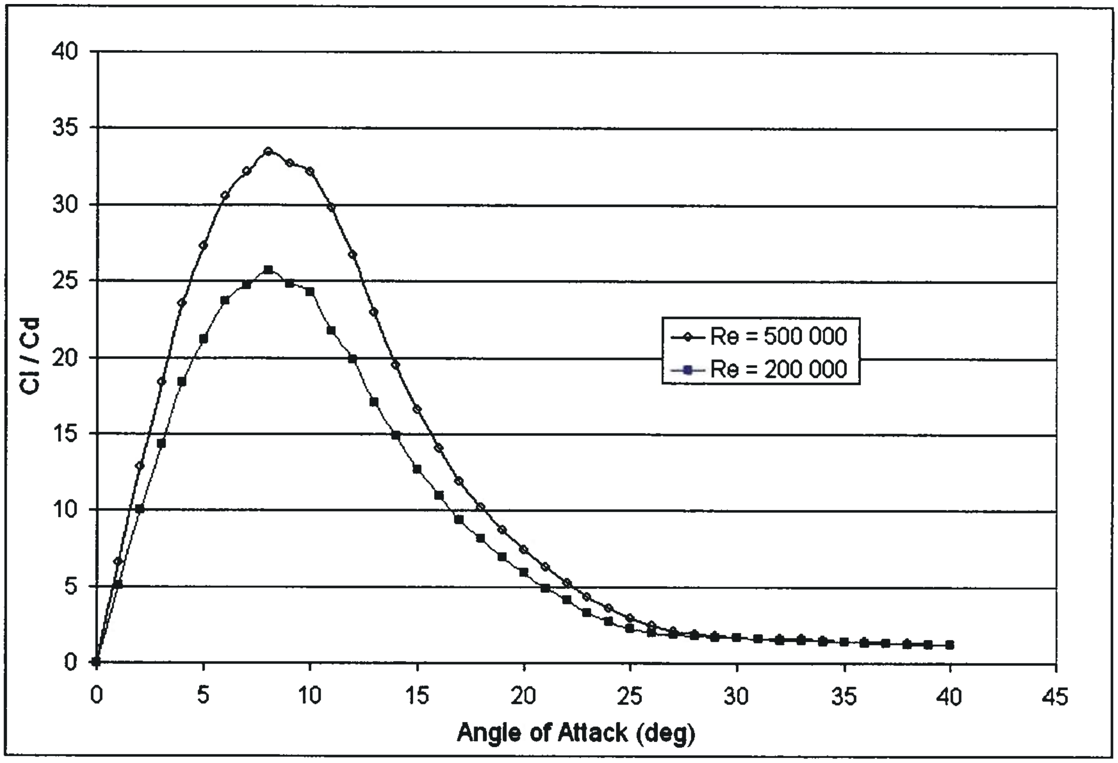

Figure 3-6: Cl / Cd vs. Angle of Attack for 63_4-021 at Re = 200 000, 500 000.

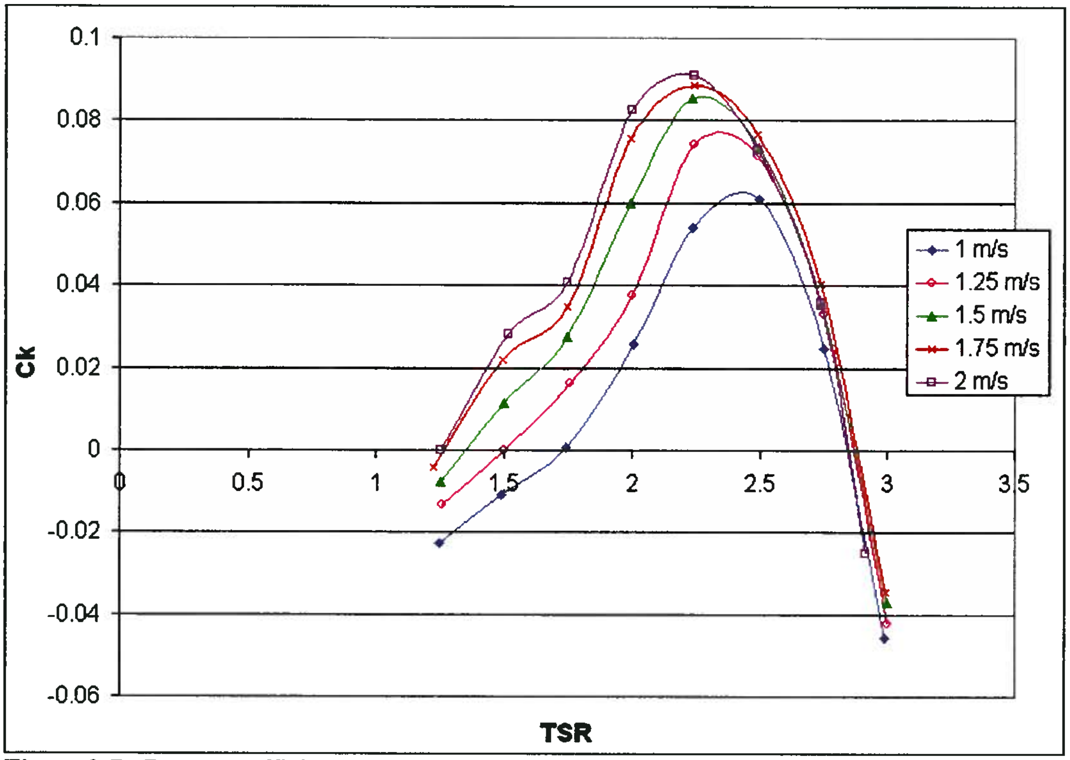

Figure 3-7: Power coefficient (Ck) vs. tip-speed ratio (TSR) at varying velocities.

Upon removing the airfoils and testing the supporting arms to investigate parasitic drag, at all velocities the power coefficient as a function of TSR is quite consistent (Figure 3-8). This indicates the Reynolds number effects are having a more significant impact on the lift characteristics of the foil than on the drag characteristics of the supporting arms (supporting arm effects are discussed in more detail in Section 3.3.3, along with connections between arm and foil). The supporting arms operate at lower Reynolds numbers, primarily due to the majority of the arm length is at a shorter radius leading to lower velocities, and thus are further from the sensitive transition region.

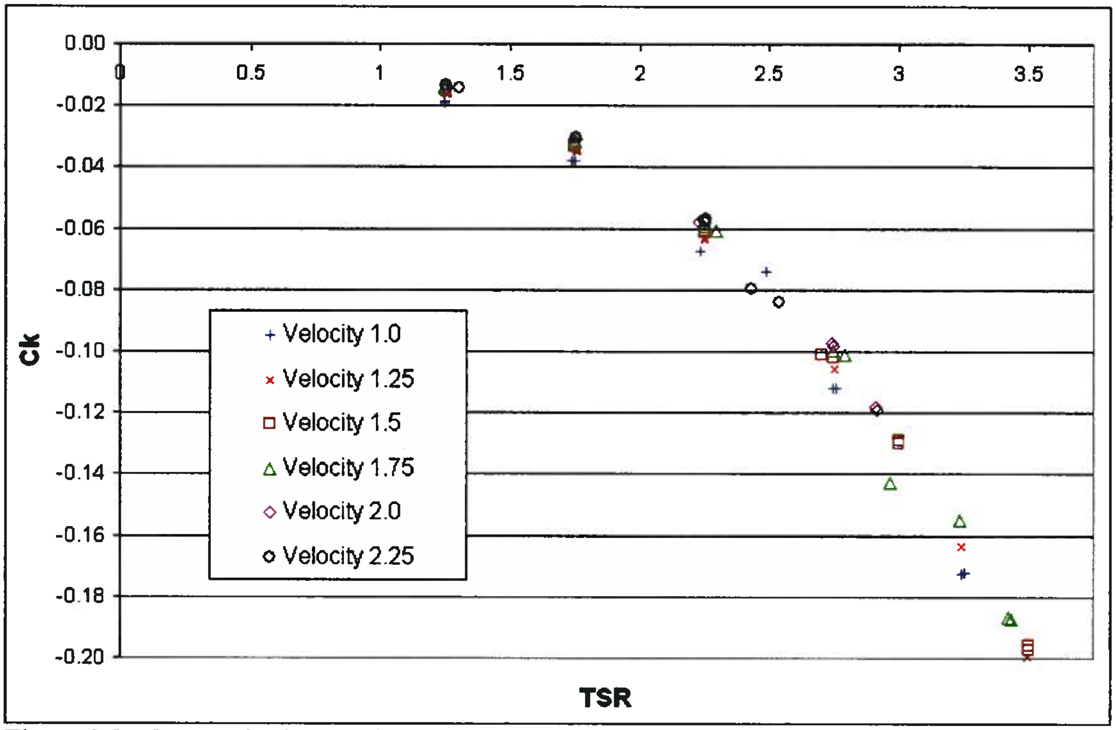

Figure 3-8: Ck vs. TSR illustrating power loss due to parasitic drag from arm configuration A.

3.3.2 Drive-train Comparison

It is important to compare similar turbine configurations using the two different drive-trains to ensure that the data from each program was reasonably similar, given turbine operating efficiency should be the same regardless of the drive-train used to drive or break the turbine; however, one may expect minor differences in the efficiency and torque curve plots, primarily due to the fact that in the chain/sprockets drive-train the torque sensor also served as a lay shaft and was not linked directly in-line with the turbine shaft as it was with the gearbox.

Figure 3-9 provides the power coefficient vs. TSR for runs using the different drive-trains at both 1.5 m/s and 2 m/s at the optimum operating TSR values of a free-stream turbine. The higher efficiency at 2 m/s, is attributed to Reynold's number effects, as discussed in Section 3.3.1.

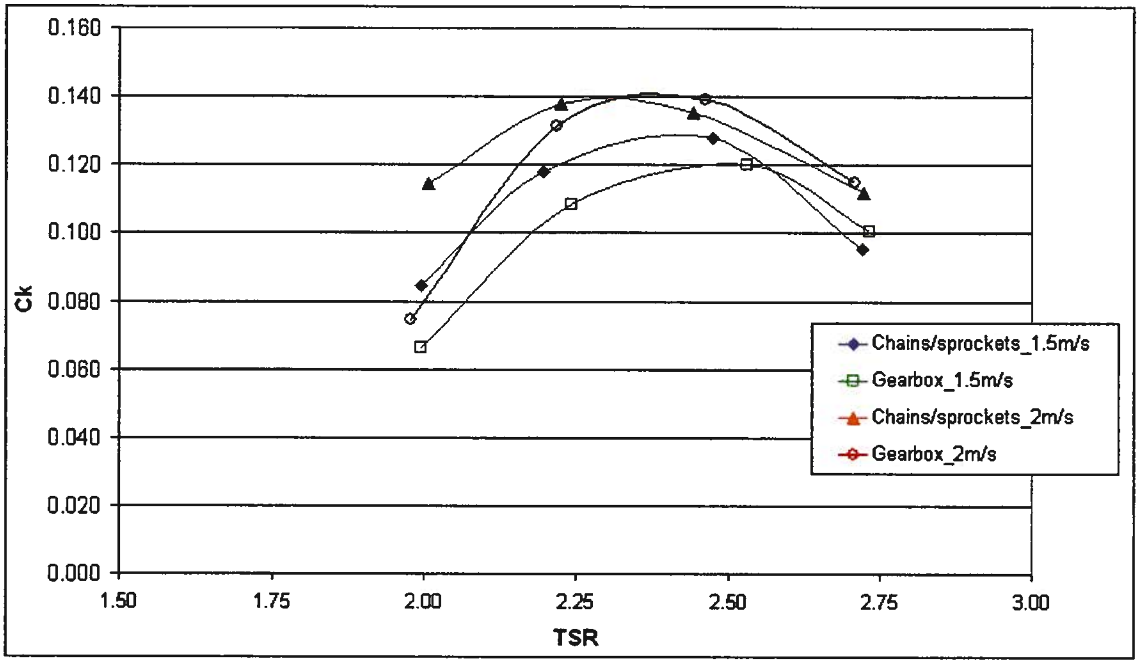

Figure 3-9: Ck vs. TSR drive-train comparison (medium profile arms).

The efficiencies above show percent differences typically on the order of 10%, though less agreement is observed at 2 m/s and with a TSR of 2. Apart from measurement accuracies, differences in the curves may result from:

- With the layshaft, power is transmitted through a chain and additional bearings before being registered by the torque sensor, so one may expect this drive system to have lower power, as is the case at higher TSR values, while flexing in the chain/sprocket system could also have an effect.
- Fly-wheel effects of the sprockets about the torque sensor and flexing in the system may also serve to minimize the tendency of the chain/sprocket configuration to require/receive driving torque from the motor, thus artificially increasing the apparent efficiency.

Figure 3-10 and Figure 3-11 illustrate the torque curves at the optimal TSR values (2.25, 2.5, 2.75) at 1.5 m/s and 2 m/s respectively. It is evident that the chains/sprockets drive-train configuration has lower, wider torque peaks observed by the torque sensor at both velocities due to flexing in the chains absorbing shock in the system, and inertial effects of the sprockets. Alternately, the flexible coupling used with the gearbox drive-train allowed for a small amount of backlash, leading to the flattening of the curve observed as torque magnitude passes through zero. This backlash likely also produced a slamming effect once the coupling re-engaged, leading to sharper, higher peaks than what may actually be observed in an ideal system.

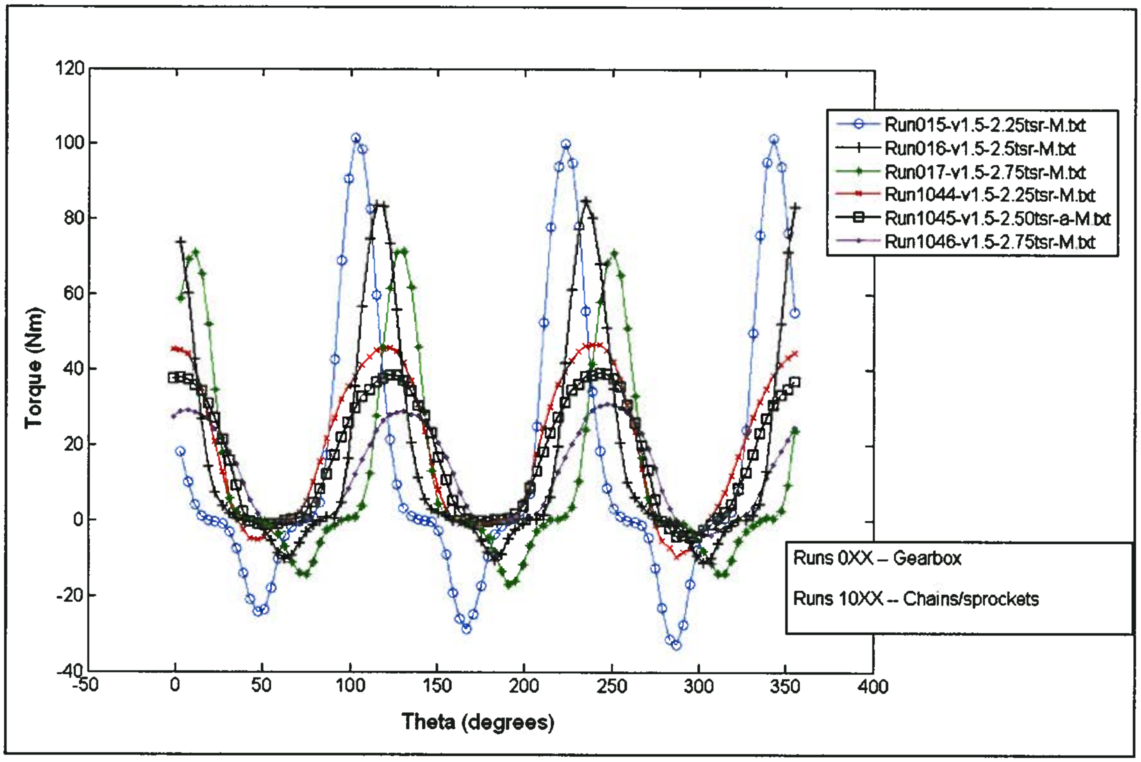

Figure 3-10: Torque vs. Angle of Revolution comparing chains/sprockets with gearbox drive at TSR = 2.25, 2.5, 2.75, v=1.5 m/s.

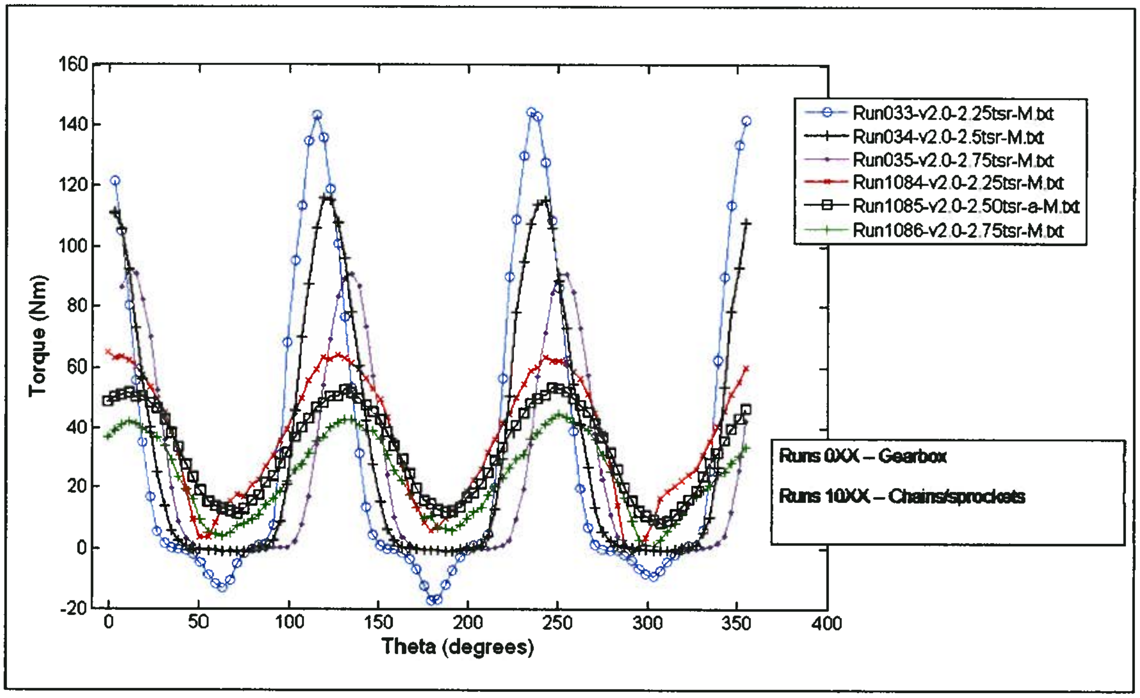

Figure 3-11: Torque vs. Angle of Revolution comparing chains/sprockets with gearbox drive at TSR = 2.25, 2.5, 2.75, v=2.0 m/s.

Frequencies of torque input are also masked by the chains/sprockets drive-train. Table 3-3 provides the expected frequencies of torque ripple based on blade position, as well as the observed frequencies which were obtained by running a Fast Fourier Transform on the torque data for runs at 1.5 m/s and TSR=2.5. Figure 3-12 provides the frequency content of these runs, and it is evident that the higher frequencies have a greater influence with the gearbox drive train.

Table 3-3: Expected and observed torque frequencies for gearbox and chains/sprockets drive-train.

		Expected Experimental Frequencies (rad/sec)					Primary Observed Frequencies from FFT			
Run #	Drive-train	rad/sec	1 pulse/blade	2 pulses/blade	3 pulses/blade	4 pulses/blade				
Run1045a	Chains/sprockets	8.12	24.36	48.72	73.08	97.44	24.32	48.6	72.95	–
Run016	Gearbox	8.30	24.90	49.80	74.70	99.60	24.69	49.4	74.14	98.77

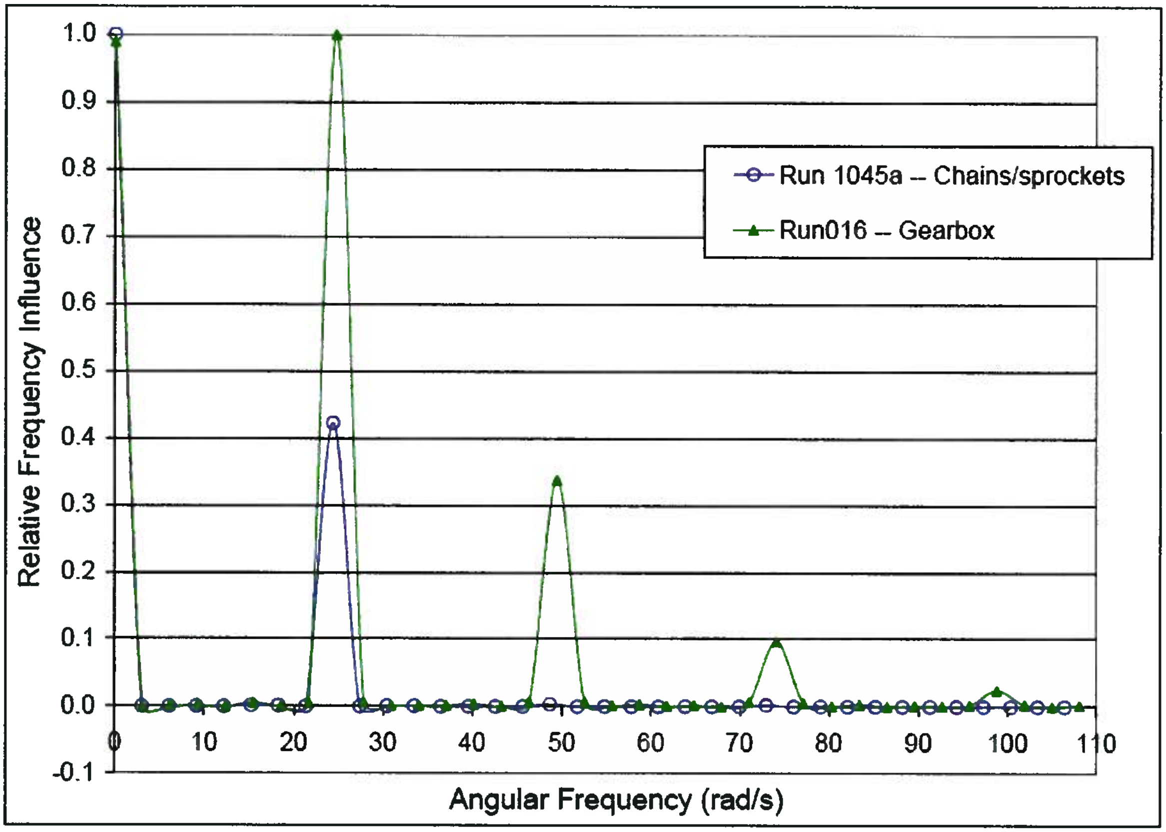

Figure 3-12: Torque data normalized frequency content for chains/sprockets and gearbox drive-train (free-stream, 1.5 m/s, 2.5 TSR).

Recognizing these differences in the drive-trains, it is reasonable to have confidence in the efficiencies obtained in using either drive-train; however, one must recognize that the chains/sprockets configuration masks the peak torque values. Alternately, the play in the flexible coupling of the second configuration leads to a bucketing of the torque curve, and potentially sharper, higher peaks due to impact in the coupling when it re-engages. It is reasonable to expect that the true torque curve in an ideal system would lie between the two, likely closer to the gearbox drive-train case.

3.3.3 Arm Profile Reduction

Figure 3-13 illustrates the various arm profiles examined during the test programs. It is important to notice the clamping mechanism allowing for adjustable angle of attack used for profiles A and B. Upon removing the blades to examine the power absorbed by the arms, a large portion of the clamping mechanism was also removed, greatly reducing the parasitic drag compared to when the blade was mounted. The ends and middle connections used for profile C are also shown.

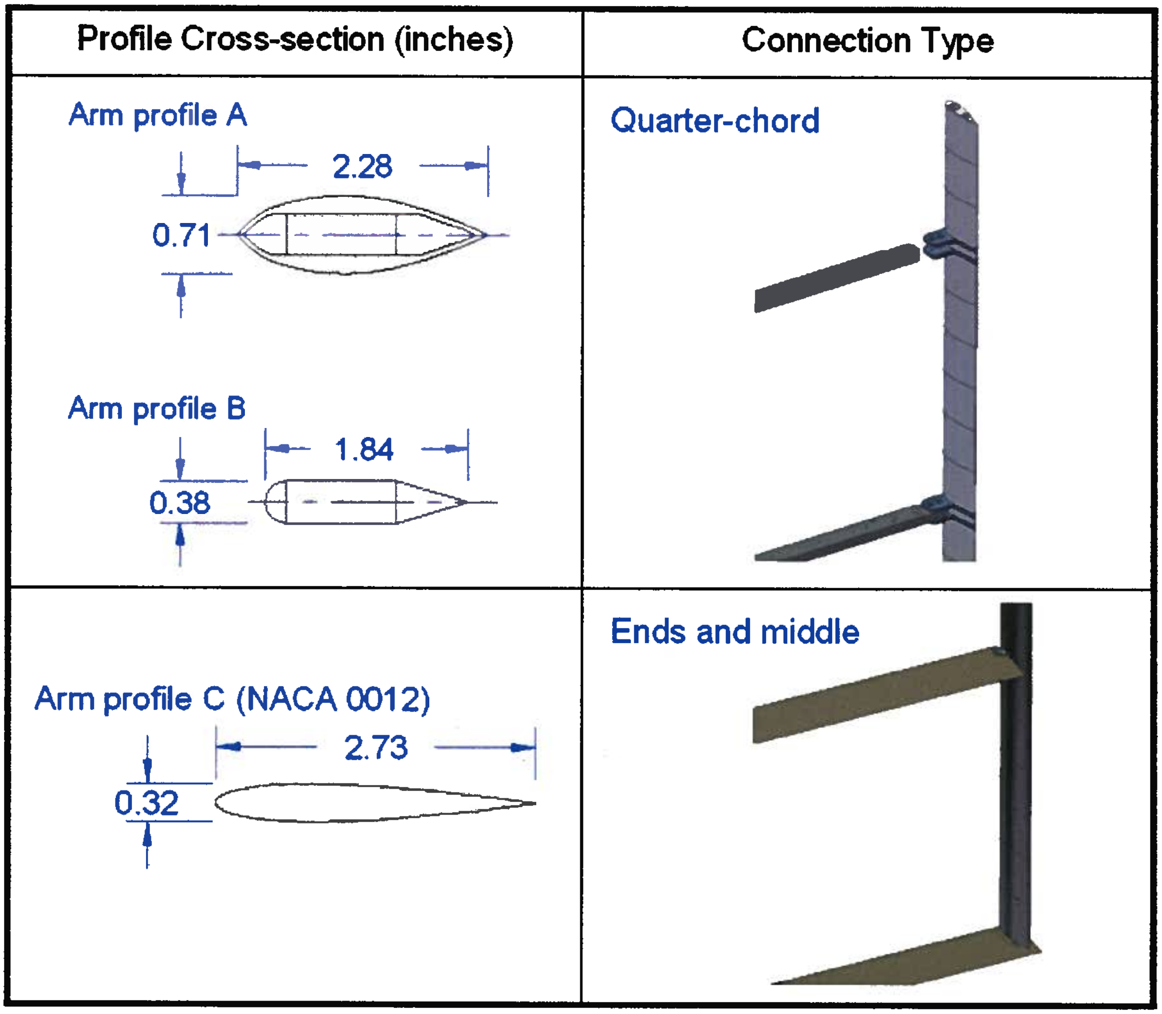

Figure 3-13: Arm profile cross-sections and connections.

Figure 3-14 below provides Ck vs. TSR of the turbine model using the various arms illustrated in Figure 3-13 above. Efficiency significantly increases with each subsequent decrease in arm profile. The most significant jump comes when changing from arm profile B to C, even though configuration C has a third central arm. This is primarily due to reduced drag, but also due to the end-plate effect gained from mounting the arms at the ends of the blades, as well as the increased working span of the foil compared to the ¼ chord mounted configurations. The more stream-lined design of configuration C also performs better at a higher TSR, indicating the foil provides better performance at TSR closer to 2.75 or 3, but the trade-off with parasitic drag from the bulkier arms lowers the optimal TSR ratio with configuration B. A further significant increase in performance is gained when removing the middle arm and running with the blade mounted using arms only at the ends. The Ck value of the two arm configuration decreases much more slowly at TSR values of 3 – 3.5, indicating better performance at a larger range of TSR values, which is beneficial for performance over a range of current speeds. The large difference in performance between 2 and 3 arms at TSR > 2.25 may be explained by the v^2 dependency of arm drag having a larger relative impact at higher rotation speeds, and thus removal of the middle arm creates a significant drop in resistance. Additionally, the middle arm does not improve lift characteristics about the end of the foil as the end arms do, so its removal is purely reducing parasitic drag and not reducing lift generated by the foil.

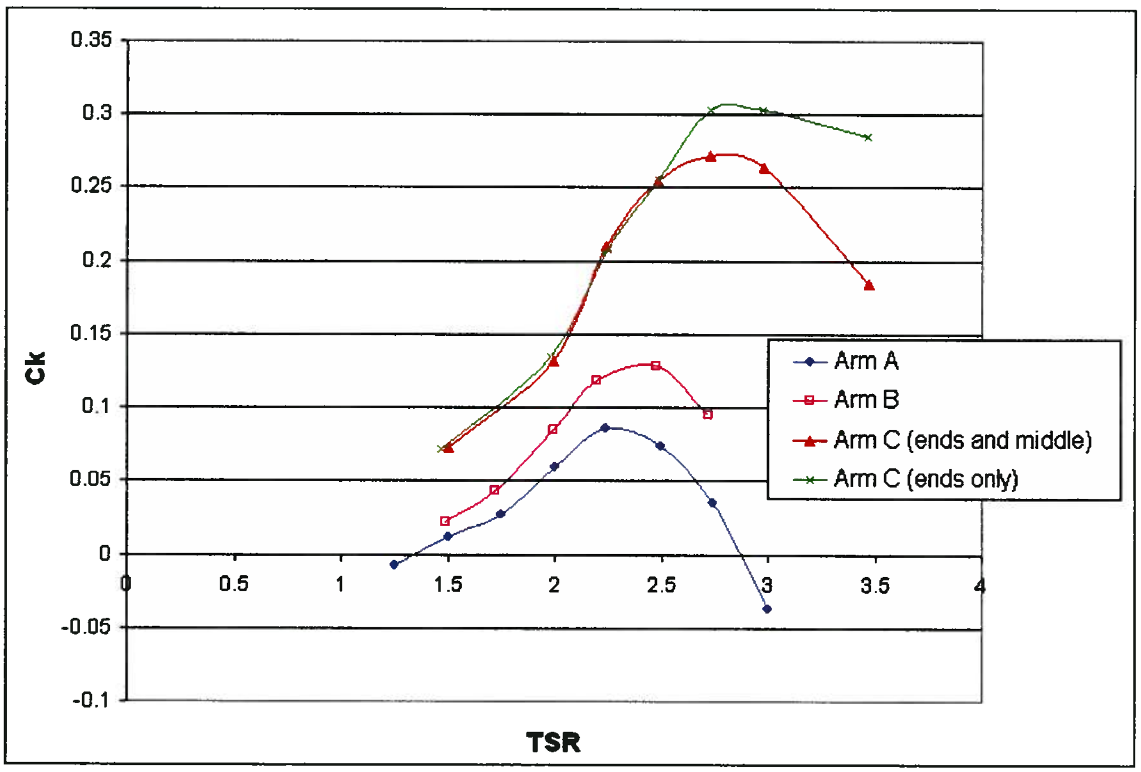

Figure 3-14: Ck vs. TSR for supporting arm comparison at 1.5 m/s.

To facilitate comparison with theory, which typically ignores arm effects or requires an empirical formulation, the parasitic drag induced by the arms must be known. Figure 3-15 presents Ck vs. TSR of the various arm configurations when running the turbine model with the blades removed. Though this plot provides insight into what Ck losses are occurring due to the drag on the arms, simple subtraction of these Ck values from those in the plot above does not simulate an ideal case without parasitic drag for the following reasons:

- ¼ span mounting of the foils reduces span of the blade working as an airfoil
- Positioning the arms at the ends of the foil will affect tip losses
- Upon removing the blades for these tests, bolt heads, etc. are also removed and thus in the assembled case parasitic drag will be larger. This was particularly the case for arm configurations A and B, where their mounting configuration incorporated a clamping mechanism about the arm, which added much drag but was removed with the blade (Figure 3-13 above).

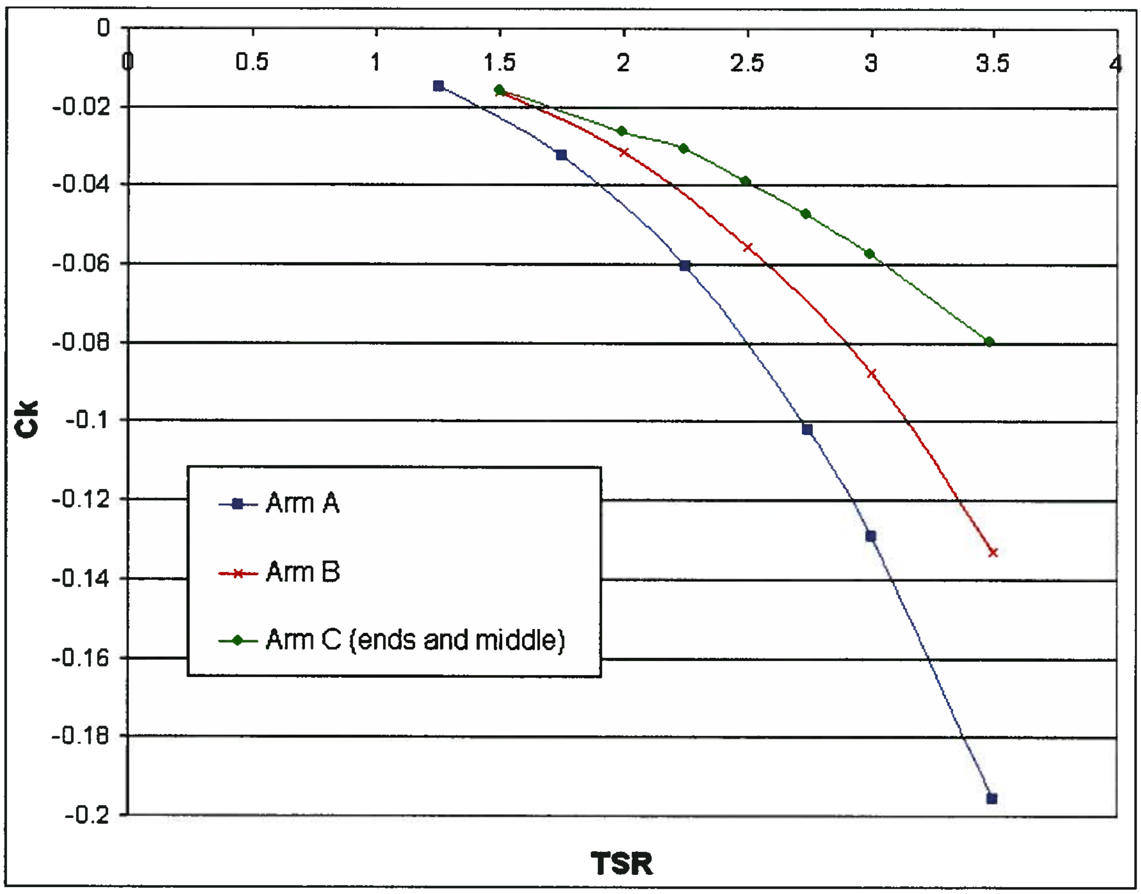

Figure 3-15: Ck vs. TSR of varying arm configurations (blades removed) at 1.5 m/s.

Torque curves comparing arm profiles B and C (ends and middle) are provided in Figure 3-16 below. Arm profile C has significantly higher torque peaks transmitted to the shaft due to the reduced drag from the arms, though it is interesting to note that profile C demonstrates more negative torque readings at TSR = 2.25 and 2.5.

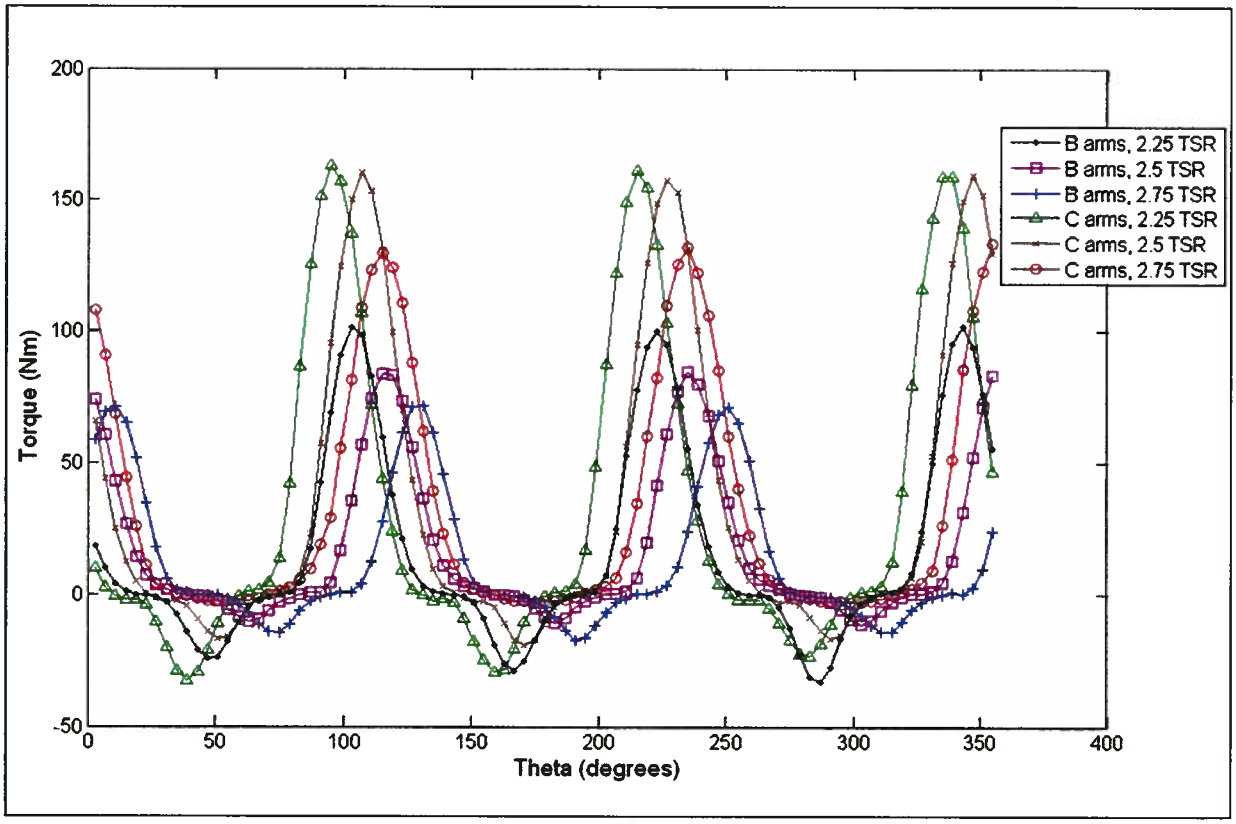

Figure 3-16: Torque vs. Angle of Revolution for arm profiles B and C (ends and middle) at 1.5 m/s and varying TSR.

Figure 3-17 provides the torque curves at 1.5 m/s comparing the three arms (profile C) for each blade vs. the case when just the end arms were supporting the blades at TSR = 2.75 and 3. As one might expect, the removal of the middle arm leads to significantly higher torque peaks (hollow data points), which is reflected in the increased Ck value in Figure 3-14.

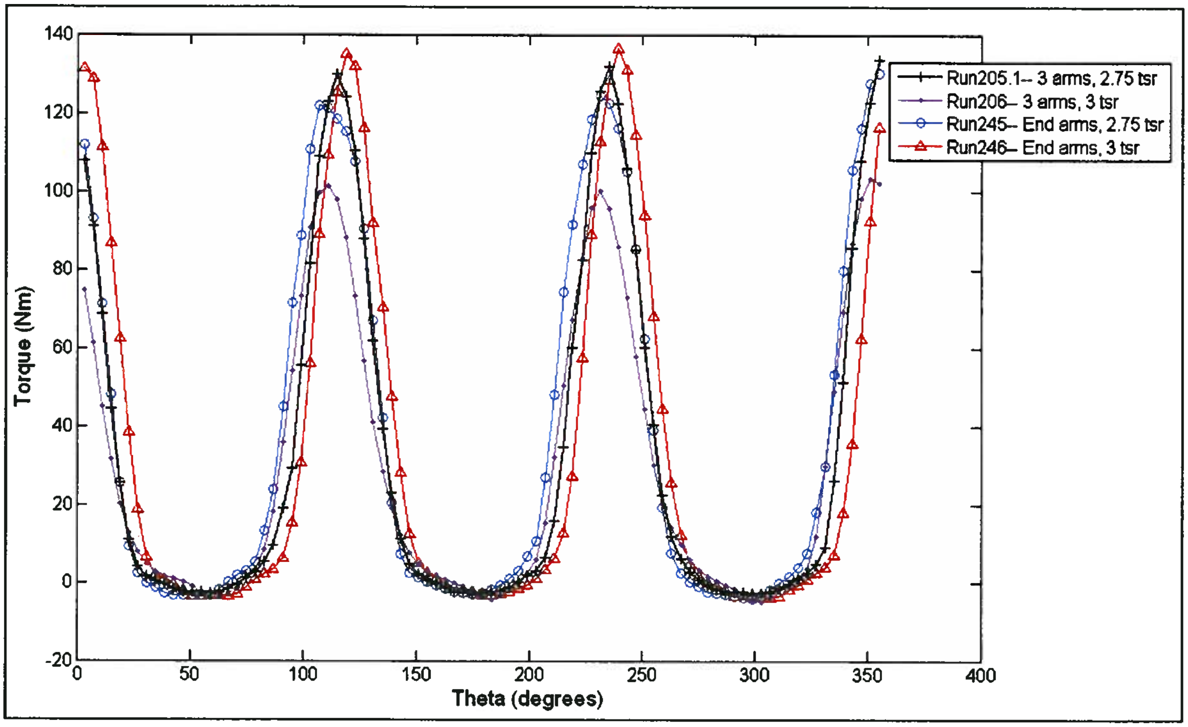

Figure 3-17: Torque vs. Angle of Revolution for 3 arms and end arms only at TSR=2.75, 3 and v=1.5 m/s.

The plots above (primarily Figure 3-14) demonstrate an improvement in turbine performance by a factor of four simply when going from arm profile A to C; Section 3.3.7 further examines the effect of tip losses on turbine performance.

3.3.4 Single-blade

Figure 3-18 below provides Ck vs. TSR for a 3-bladed test (arm configuration C), and two single-bladed tests (arm configurations B and C) at 1.5 m/s using the gearbox drive-train. It is apparent that interference and flow disruption play a significant role in reducing the power output of the 3-bladed configuration. At the highest Ck value for the 3-bladed test (TSR = 2.5), the single blade efficiency is 55.5% that of the 3-bladed design. Beyond this TSR value, the 3-bladed efficiency drops, while the single bladed efficiency continues to climb.

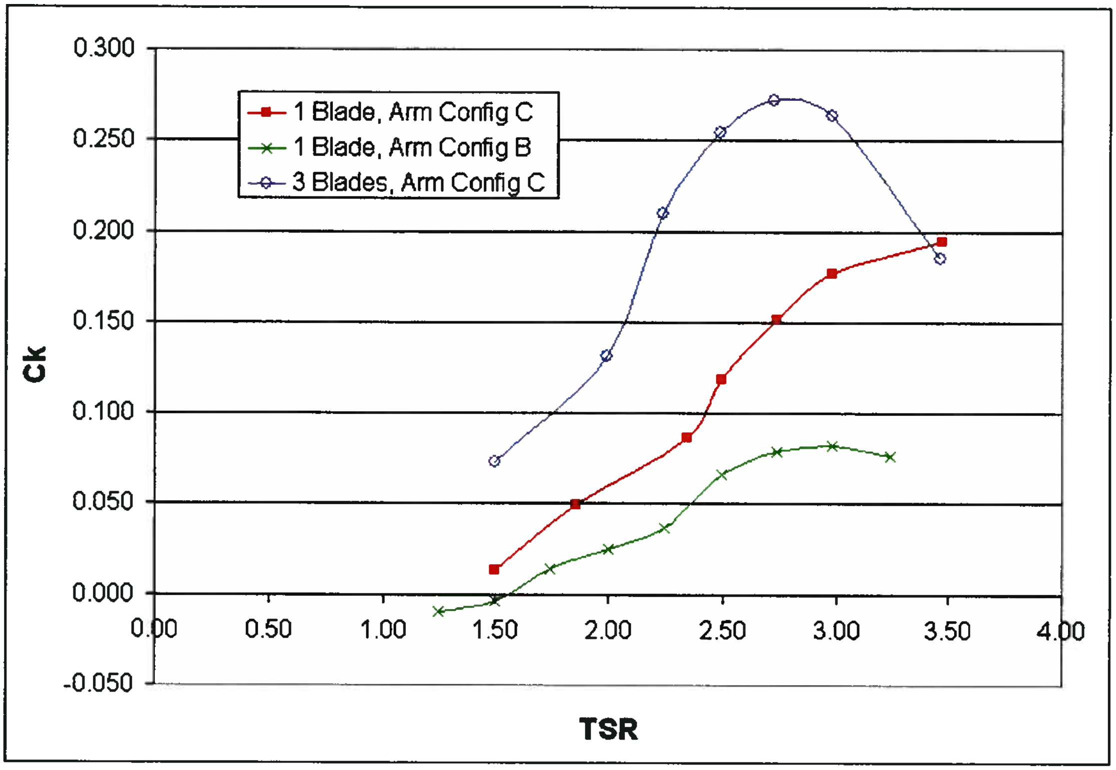

Figure 3-18: Ck vs. TSR for single and 3-bladed tests at 1.5 m/s.

Figure 3-19 illustrates the torque output of the single-blade test over a revolution at 1.5 m/s for TSR = 2.5, 3, 3.5. The double peak at the primary torque-producing region (near 90^{o}) is believed to be caused by flow separation on the blade. When the flow separates due to the large angle of attack induced by the free-stream flow, the drag increases and the turbine produces less torque until the flow re-attaches. Meanwhile, near 270^{o}, a double peak in torque creation due to a loss in lift caused by vortices shed by the shaft may be observed.

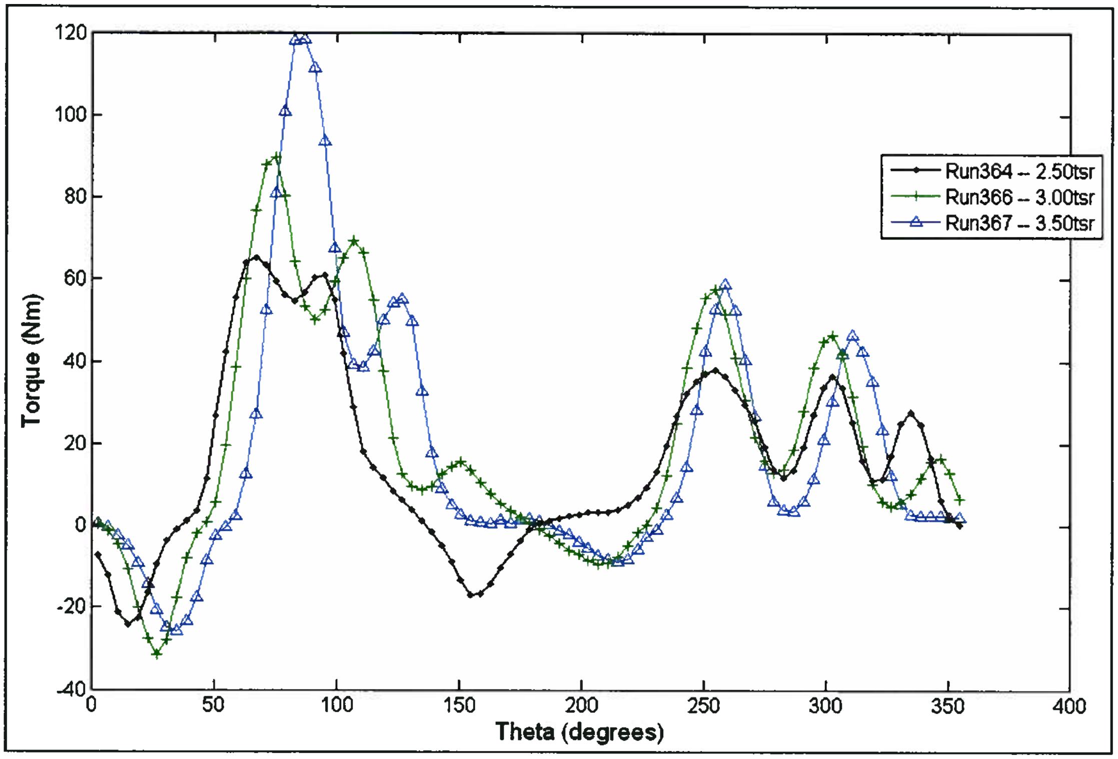

Figure 3-19: Torque vs. Angle of Revolution at 1.5 m/s for a single blade test.

Figure 3-20 superimposes three sets of torque data (TSR = 2.5 at 1.5 m/s) from the single-blade tests phased at 120° and compares them to the 3-bladed experimental test. The 3-bladed experimental result varies greatly from the superimposed single-blade result, and this is likely due to a combination of a number of factors:

- Interference and vortex shedding disrupts the flow at the downstream blades, reducing ability to cleanly create lift
- The additional power being extracted by the multiple blades changes pressure distribution at the front of the turbine, affecting the amount of torque available for extraction at the 90° position
- The phase shift observed between the peaks is believed to be caused by the fluctuating turbine revolution speed due to the larger forces involved (discussed further in Section 4.1.3)

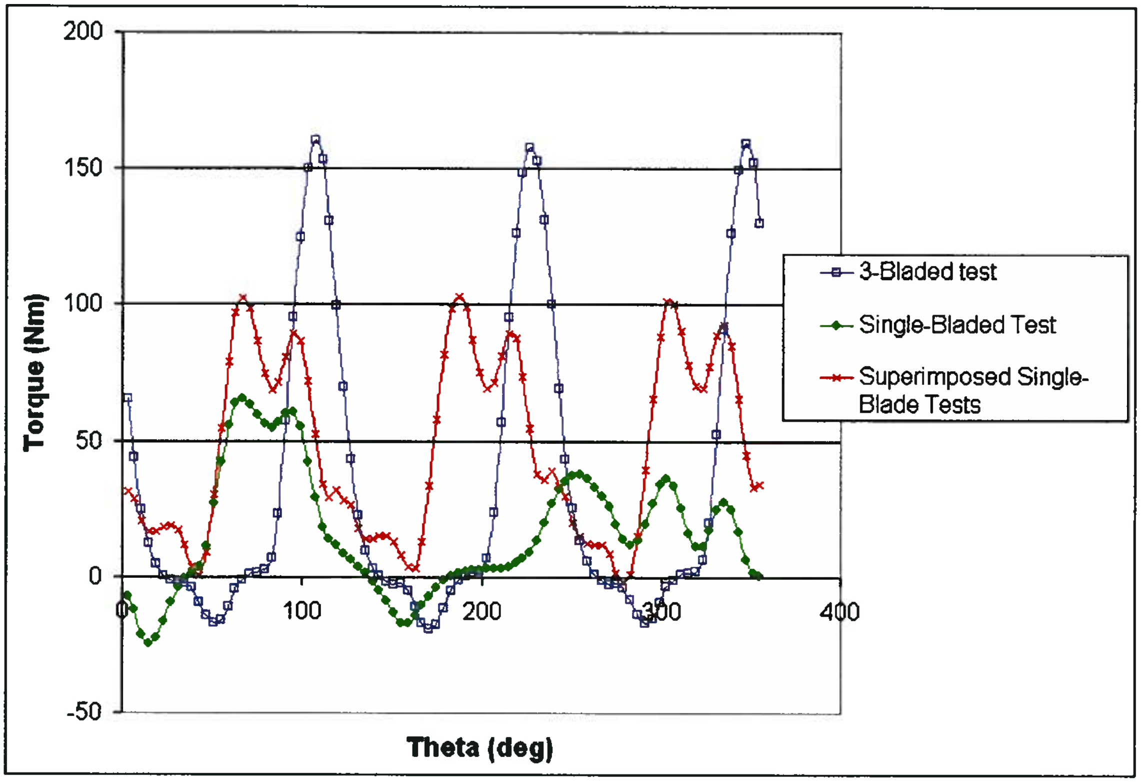

Figure 3-20: Torque vs. Angle of Revolution at 1.5 m/s for a 3-blade test, single-blade test, and 3 superimposed single-blade tests.

Lastly, an interesting result was obtained when comparing tests done using arm profiles B and C, as shown in Figure 3-21 at 1.5 m/s with a TSR = 3 (both using the gearbox drive-train). Similar shaft interference is obtained in the vicinity of 270°, though surprisingly the larger arm profile (B) shows higher torque values. Meanwhile, across the 90° position, a near opposite torque profile is created. An explanation for this is that across 90° the added drag from the arms and clamping mechanism, as well as tip losses, reduce the torque generated, while just before 270° vortex interactions with the arms or clamping mechanism may be acting on the arms to enhance performance. Lastly, the dual peak observed in the 90° position with the lower profile arm is likely due to flow separation on the blade. With profile B, it is hypothesized that the large clamping mechanism at the ¼ chord locations, as well as tip losses, result in a much less pure observation of flow separation characteristics and instead yield a single pulse. Similar results were obtained at different TSR values.

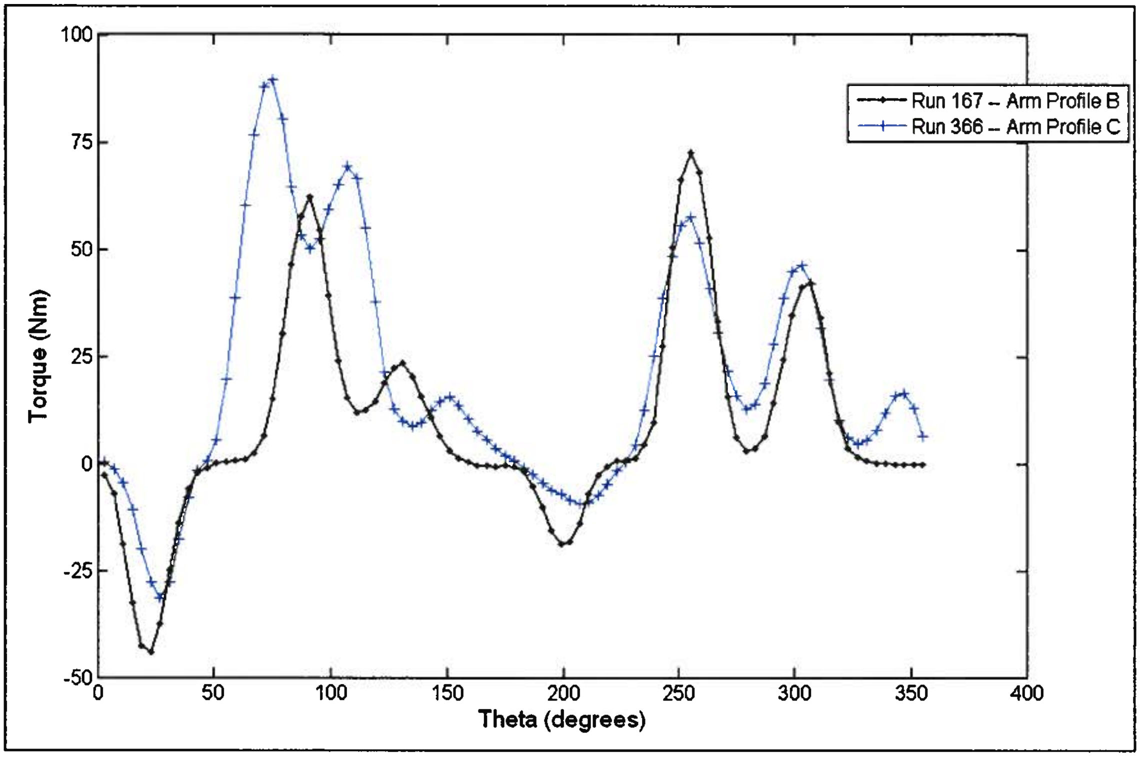

Figure 3-21: Torque vs. Angle of Revolution for a single-blade test with arm profiles B and C at TSR=3, v=1.5 m/s.

3.3.5 Angle of Attack

Blade set angles of attack of -5, -3, 0, 3, 5, and 10 degrees were tested throughout the test programs. 0, 3, 5 and -3 degrees provided the most insightful results and are discussed below. -3 degrees reduced turbine performance by almost 50%, while -5 and 10 degrees were highly ineffective. Figure 3-22 presents Ck vs. TSR at 2.0 m/s for AoA = 0, 3, and 5 degrees.

It is interesting to note that at TSR < approximately 2.35, an AoA = 3 yielded the best performance, while at TSR > approximately 2.35 an AoA = 5 provided better performance. In the vicinity of 90° of the turbine revolution (ie. directly upstream of the shaft), having a positive preset angle of attack decreases the angle of attack observed by the blade; meanwhile, in the vicinity of 270° (directly downstream of the shaft), a preset angle of attack on the blade increases the observed angle of attack on top of that caused by the free-stream flow. These are the most significant angles of attack experienced by the blades (not accounting for vortex interactions) and are provided in Table 3-4 and Table 3-5.

Table 3-4: Blade angle of attack at varying TSR and preset angle values at the 90° angle of revolution.

	Angle of Attack (degrees) at 90° Position		
TSR	**Flow-induced Angle**	**Net Angle (3° preset)**	**Net Angle (5° preset)**
2	26.6	23.6	21.6
2.25	24.0	21.0	19.0
2.5	21.8	18.8	16.8
2.75	20.0	17.0	15.0

Table 3-5: Blade angle of attack at varying TSR and preset angle values at the 270° angle of revolution.

	Angle of Attack (degrees) at 270° Position		
TSR	**Flow-induced Angle**	**Net Angle (3° preset)**	**Net Angle (5° preset)**
2	26.6	29.6	31.6
2.25	24.0	27.0	29.0
2.5	21.8	24.8	26.8
2.75	20.0	23.0	25.0

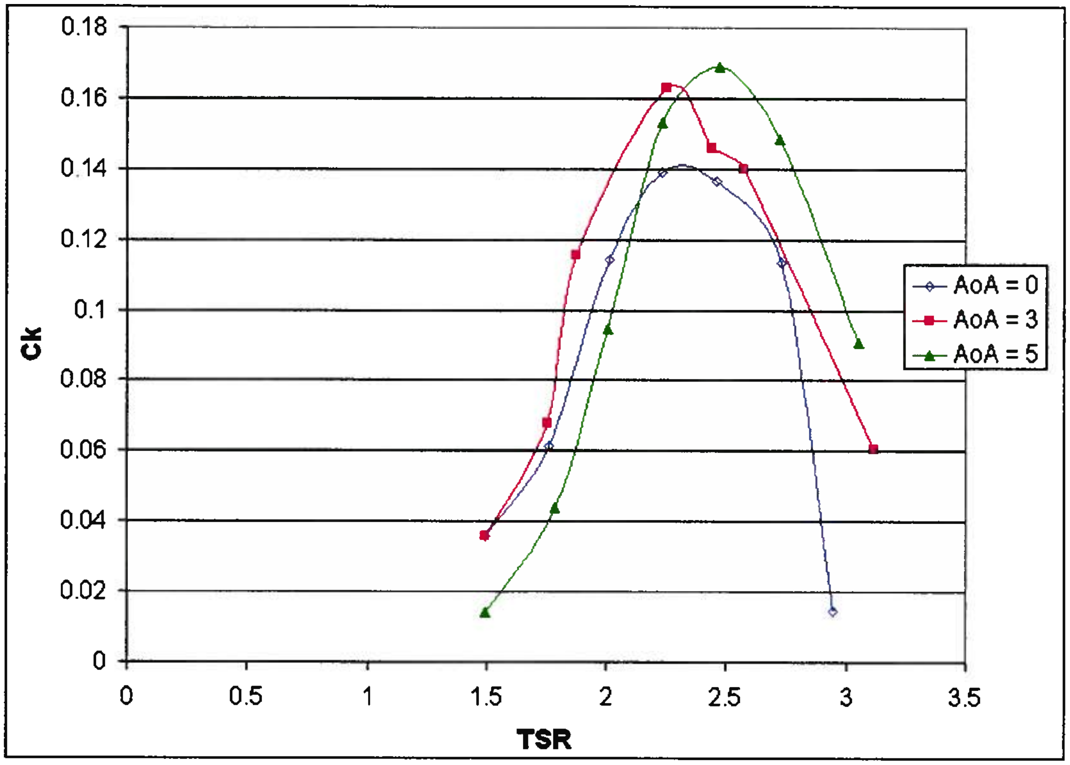

Figure 3-22: Ck vs. TSR for AoA = 0, 3, 5 degrees at 2 m/s.

Figure 3-23 illustrates the torque generated at a TSR = 2.25, which is generating higher peaks than at TSR = 2.5 (Figure 3-25). This is because larger angles are being experienced at 90° at the lower TSR value, generating more lift. A contributing factor to this is the dynamic stall effect, which tends to delay stall [25] that typically occurs near AoA = 8° for the 63_4-021 airfoil at these Reynolds numbers (2.92E05 to 3.82E05 for 2 m/s). Also at TSR = 2.25, the 5° angle of attack generates larger peaks due to reduced stall upstream of the turbine, while it also creates similar, or slightly worse, low torque values downstream of the shaft due to an increased tendency to stall.

At TSR = 2.5, the peak values in general are lower, though the turbine performance is better. This is due to the fact that the low-points in the torque curve are higher than at TSR = 2.25. This is caused by less stalling around the back of the turbine since the angle induced by the free-stream flow is smaller at the higher TSR value. Comparing the 3° and 5° preset angles of attack, 5° is creating substantially higher peaks due to reduced stall upstream of the turbine. Downstream of the shaft, both angles create similar negative torque peaks. One should note that this is a simplified assessment of the situation, as dynamic stall and vortex shedding onto the downstream blades play a significant role; however, flow visualization capturing these phenomena is extremely difficult. A key conclusion from this examination is that optimal angles of attack likely lie in the vicinity of 2 to 5 degrees, and are dependent on operating tip-speed ratio. Polar plots (Figure 3-24 and Figure 3-26) are also provided to aid with visualization.

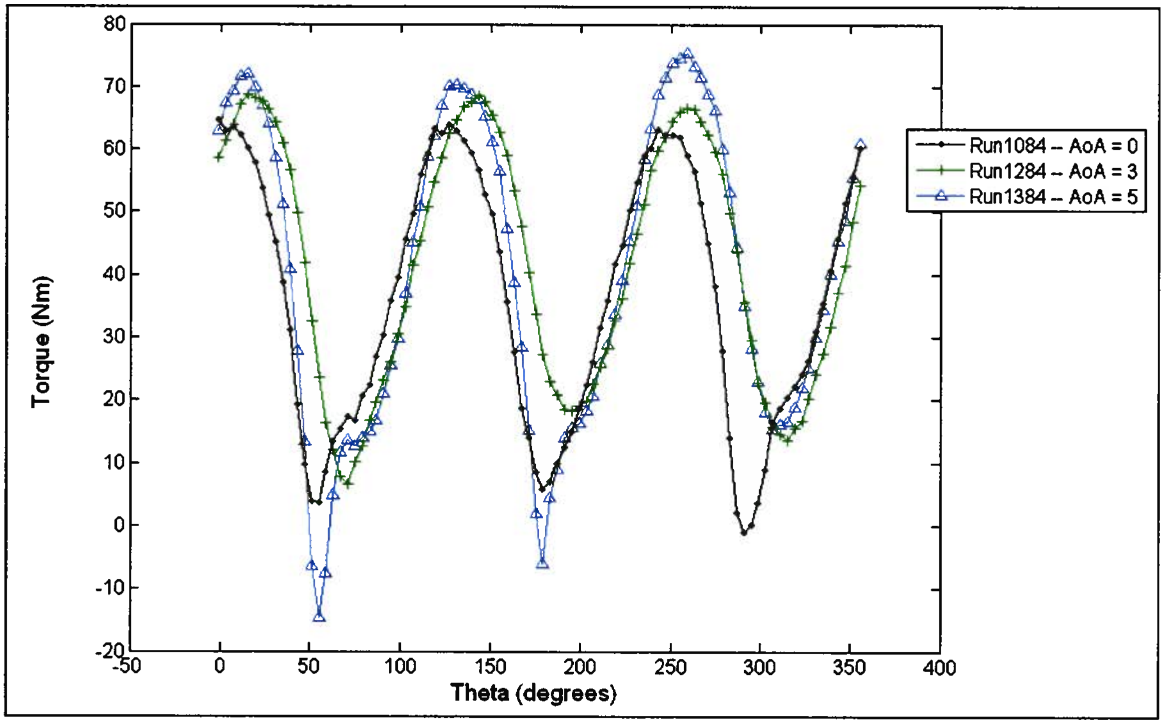

Figure 3-23: Torque vs. Revolution Angle for AoA = 0, 3, 5 deg at 2 m/s, TSR = 2.25.

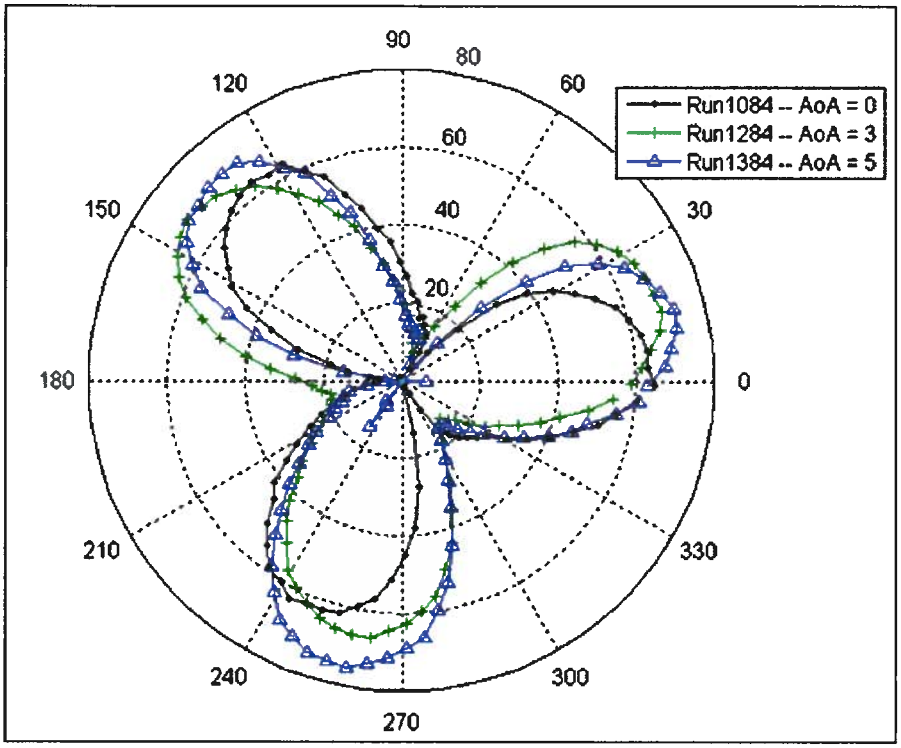

Figure 3-24: Polar Plot of Torque vs. Revolution Angle for AoA = 0, 3, 5 deg at 2 m/s, TSR = 2.25.

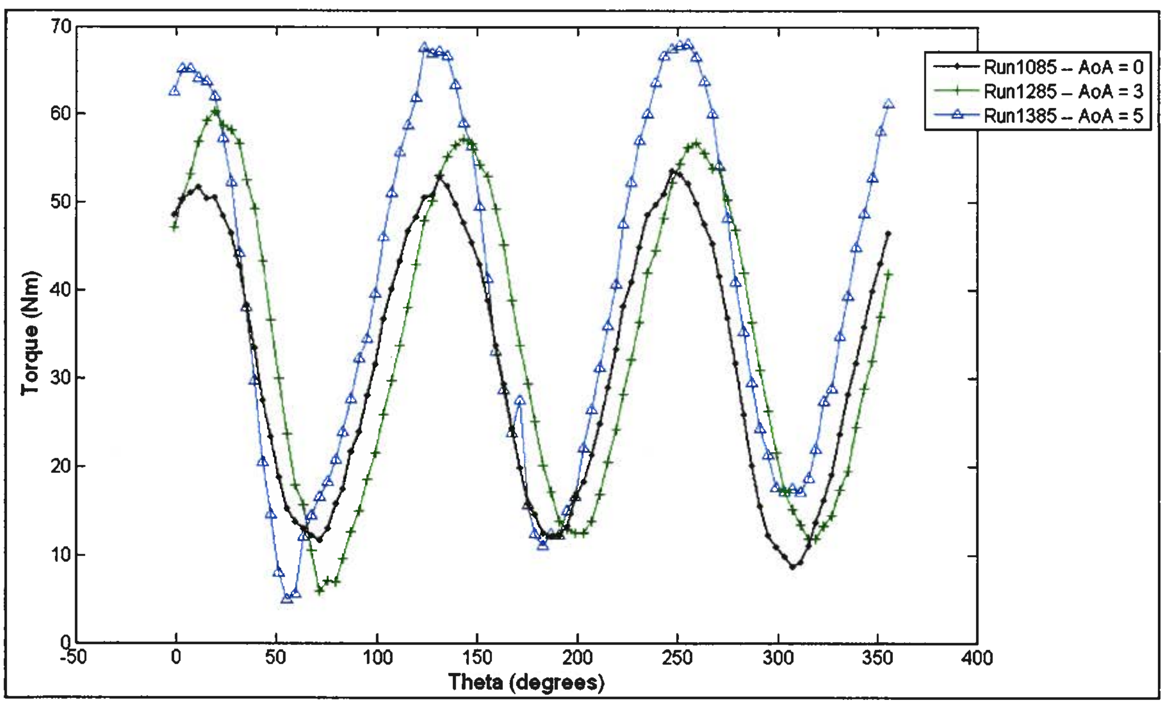

Figure 3-25: Torque vs. Revolution Angle for AoA = 0, 3, 5 deg at 2 m/s, TSR = 2.5.

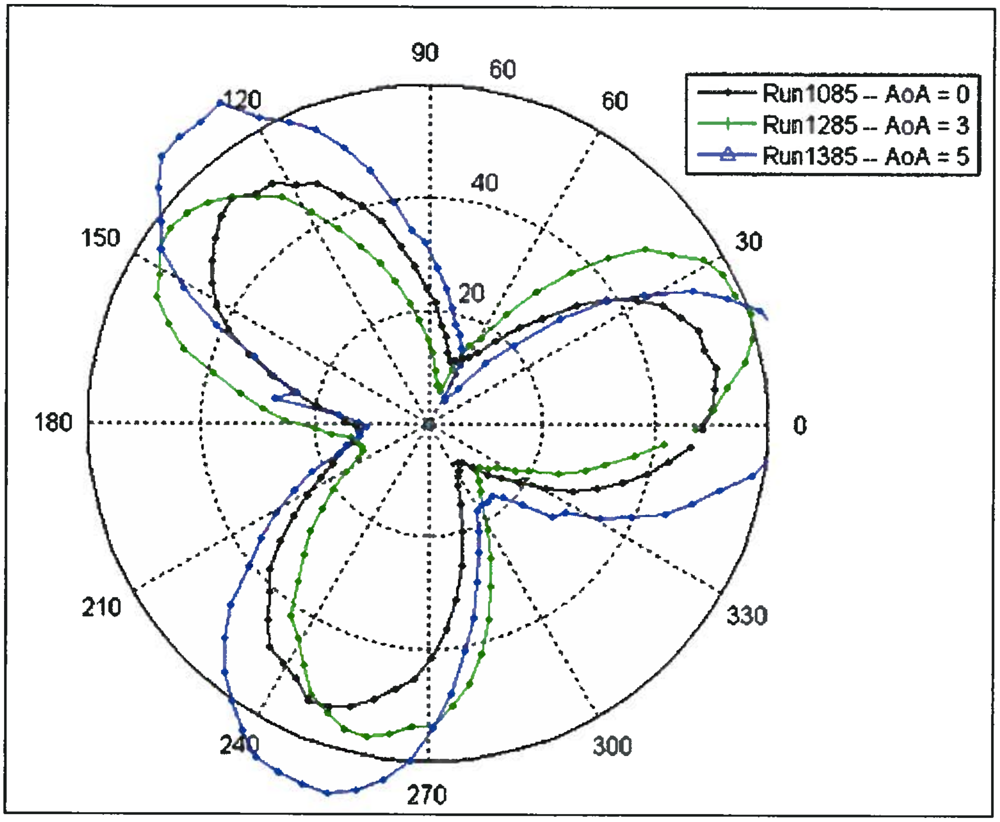

Figure 3-26: Polar Plot of Torque vs. Revolution Angle for AoA = 0, 3, 5 deg at 2 m/s, TSR = 2.5.

Lastly, Figure 3-27 illustrates the torque curves generated with a preset AoA = -3 and 0 deg at 1.75 m/s. The reduced torque peak at AoA = -3 indicates that this angle is significant enough to increase the angle of attack observed by the blade past its stall point, reducing its ability to produce torque in the vicinity of 90°. The more negative lows in the torque curve indicate that this was also effective at reducing torque generated in the vicinity of 270° by reducing the observed angle of attack.

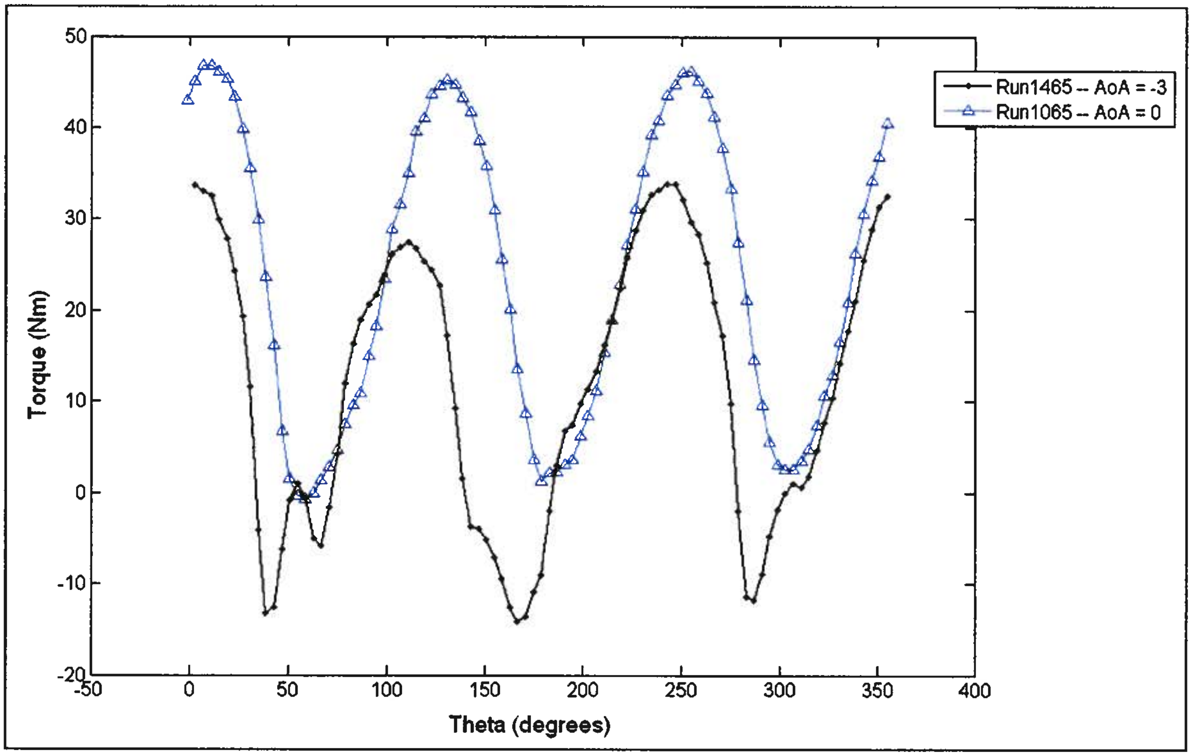

Figure 3-27: Torque vs. Revolution Angle for AoA = -3 deg at 1.75 m/s, TSR = 2.5.

3.3.6 Cambered Blades

Investigation using cambered blades was performed using a cambered version (63_4-421) of the symmetric blade tested above. Power coefficient vs. TSR at 1.5 m/s is plotted in Figure 3-28 for the cambered blade at AoA = 0° and 5°, as well as for the symmetric blade case. It is apparent that the cambered blade offers a substantial increase in efficiency, especially at 5°.

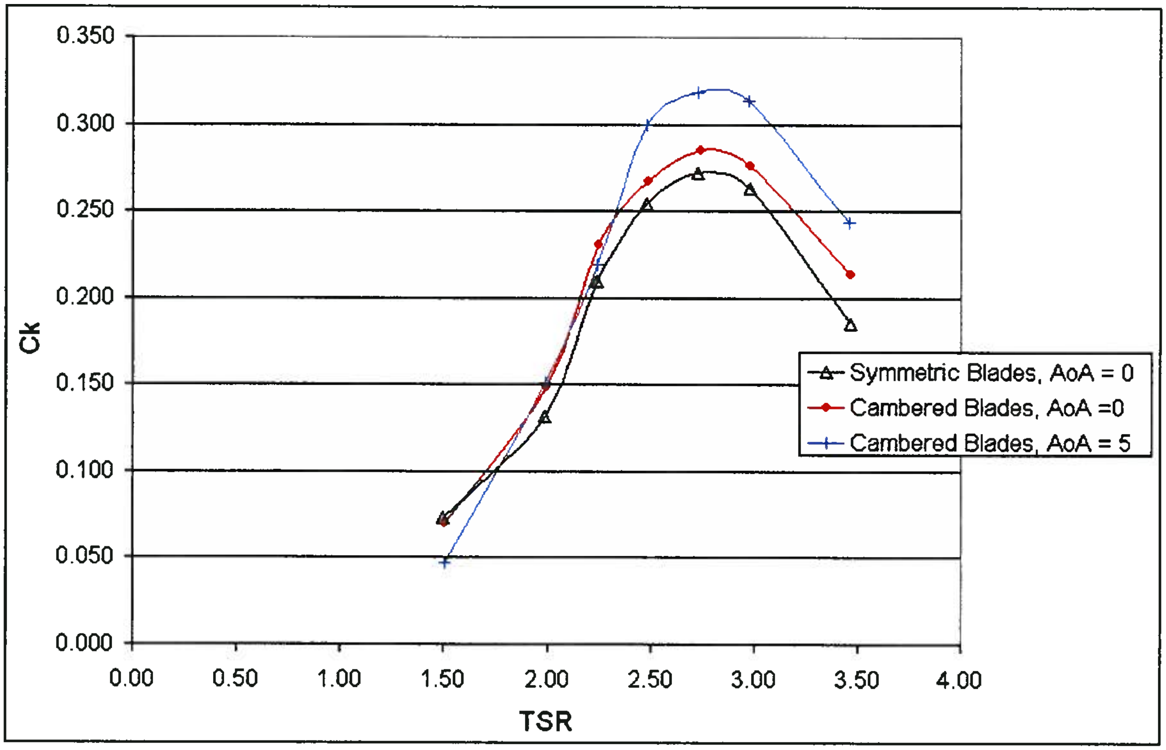

Figure 3-28: Ck vs. TSR for cambered (0 and 5 deg) and symmetric (0 deg) blades at 1.5 m/s.

Examining the torque curves, Figure 3-29 provides torque vs. angle of revolution for the symmetric blade (AoA = 0) and the cambered blade (AoA = 0 and 5) for the optimum TSR = 2.75 at 1.5 m/s. As expected, the symmetric blade produces higher peaks as a blade passes near the 90°, because the cambered blade is effectively flying upside down. However, the cambered blade at 5° is effective in reducing this upside down angle of attack, and produces greater torque than the 0° cambered blade case. Additionally, as the cambered blade passes downstream of the turbine near 270°, the cambered blade is better suited to producing lift in this location, increasing the minimum torque values observed. This also appears to produce torque over a greater range, as indicated by the wider peaks, leading to improved turbine performance.

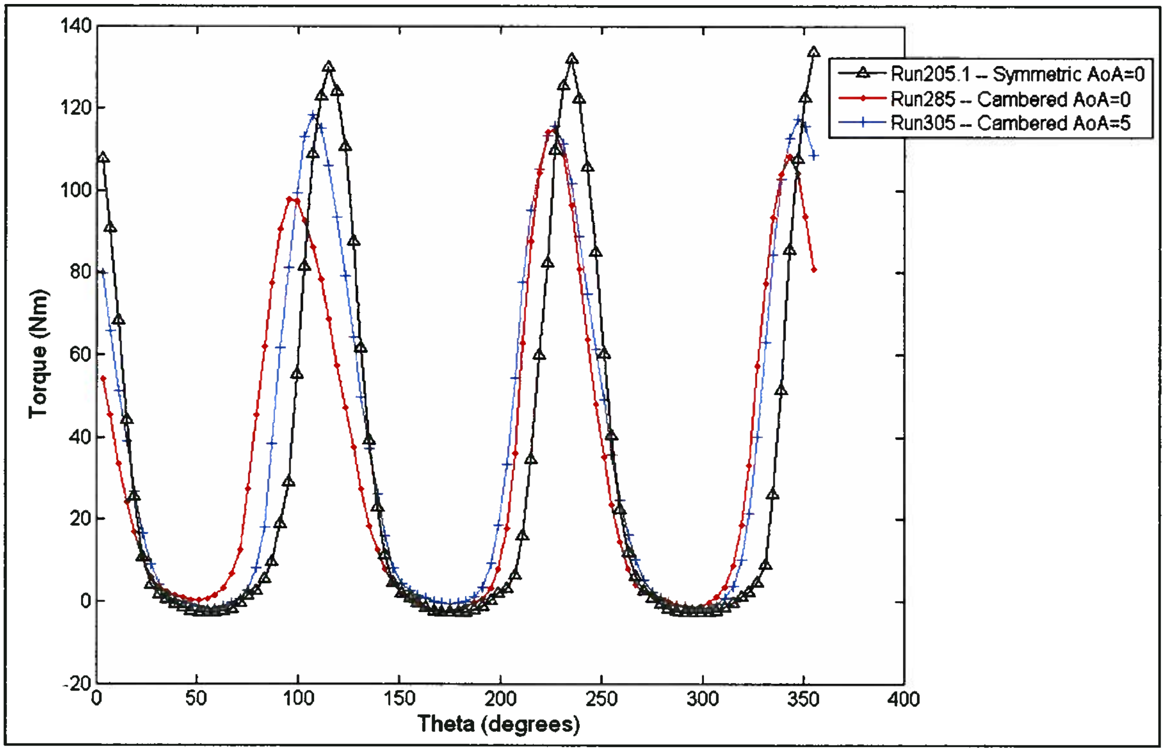

Figure 3-29: Torque vs. Angle of Revolution for symmetric (0 deg) and cambered (0 and 5 deg) at 1.5 m/s and TSR = 2.75.

3.3.7 Blade End Plates

Proof of concept tests were performed using end plates on the blades to examine the possibility of reducing tip losses when supporting arms were mounted at the ¼ chord positions. Riley examined the use of end plates [26] and demonstrated that end plates with a foil-shaped cross-section were advantageous. Therefore, rectangular end plates with length equal to the chord and width of 1.5" with a NACA 0012 cross-section profile were applied, as suggested by Klaptocz [27]. Additionally, disc shaped end plates [0.25" thick] with a rounded edge and diameter equal to the foil chord were also tested given the circular path the turbine blade travels. Figure 3-30 displays the NACA 0012 (with flattened edge to sit flush on the foil) end plate and the circular end plate mounted to the blade.

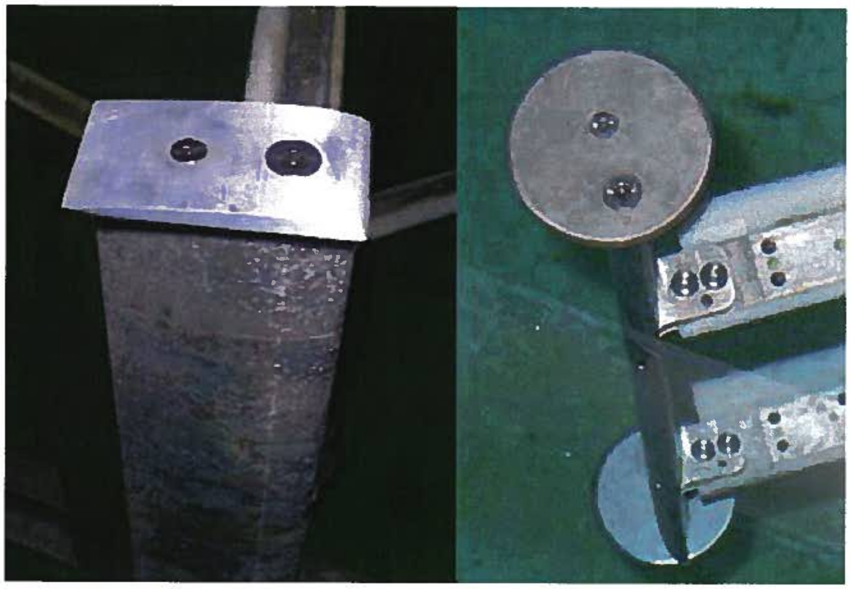

Figure 3-30: NACA 0012 profile and circular end plates.

Figure 3-31 and Figure 3-32 below provide Ck vs. TSR for the end plate configurations compared to the case without end plates at 1.5 m/s and 2 m/s respectively. At both speeds the NACA 0012 end plates provided the best results, increasing the Ck value by 16% (at 1.5 m/s) and 12% (at 2 m/s). The circular end plates also demonstrated an improvement over the case without.

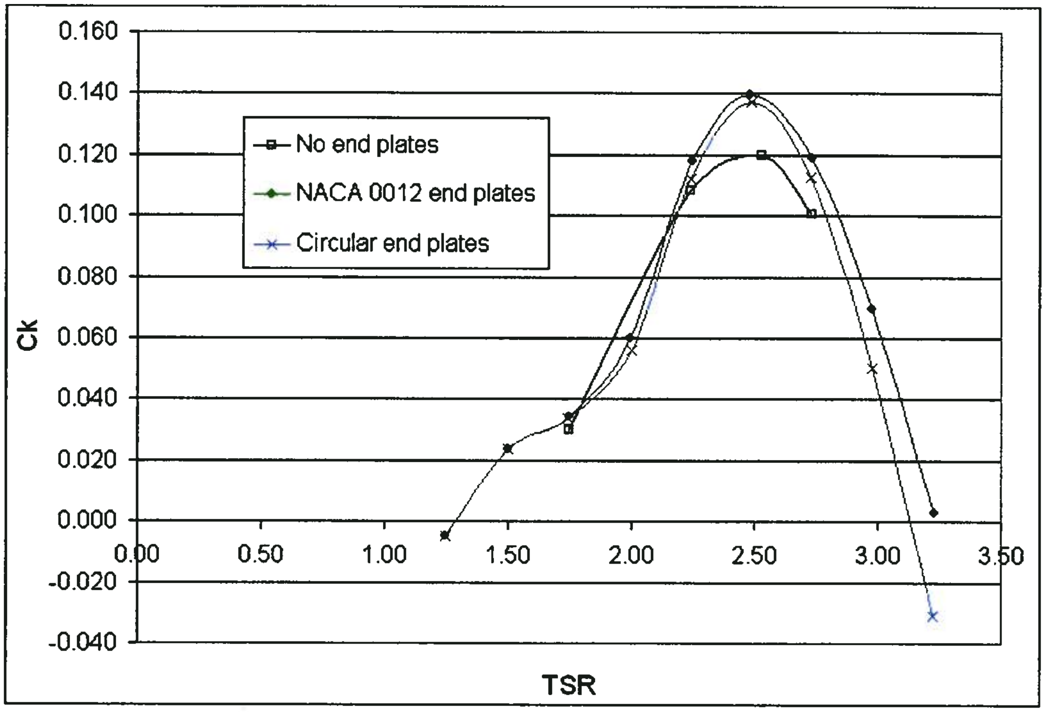

Figure 3-31: Ck vs. TSR for end plate comparison at 1.5 m/s.

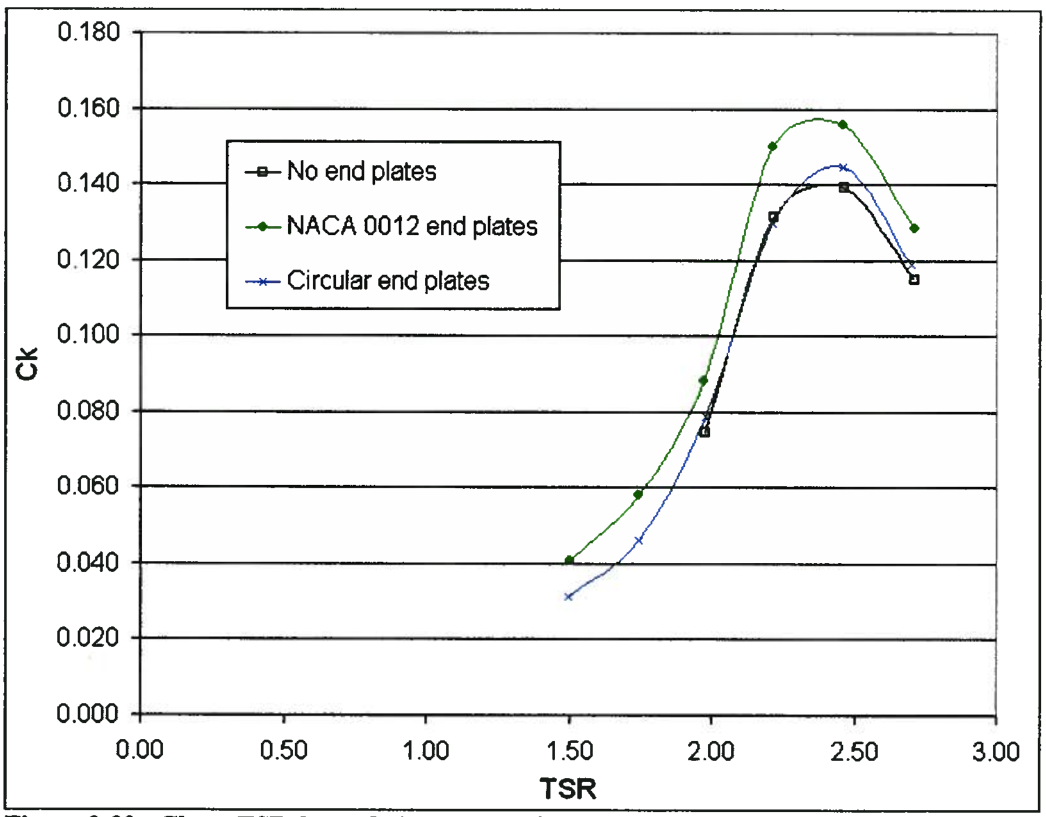

Figure 3-32: Ck vs. TSR for end plate comparison at 2 m/s.

Considering the torque curves, at 1.5 m/s (Figure 3-33) the NACA 0012 appears to produce increased torque peaks, while the circular end plates produces smaller and slightly wider torque peaks which rarely enters a negative torque region. Conversely, at 2 m/s (Figure 3-34) the NACA 0012 end plates produce lower, wider torque curves while the circular end plates produce higher torque peaks. Lastly, it is possible to create thinner disc end plates, which would reduce associated drag and improve performance.

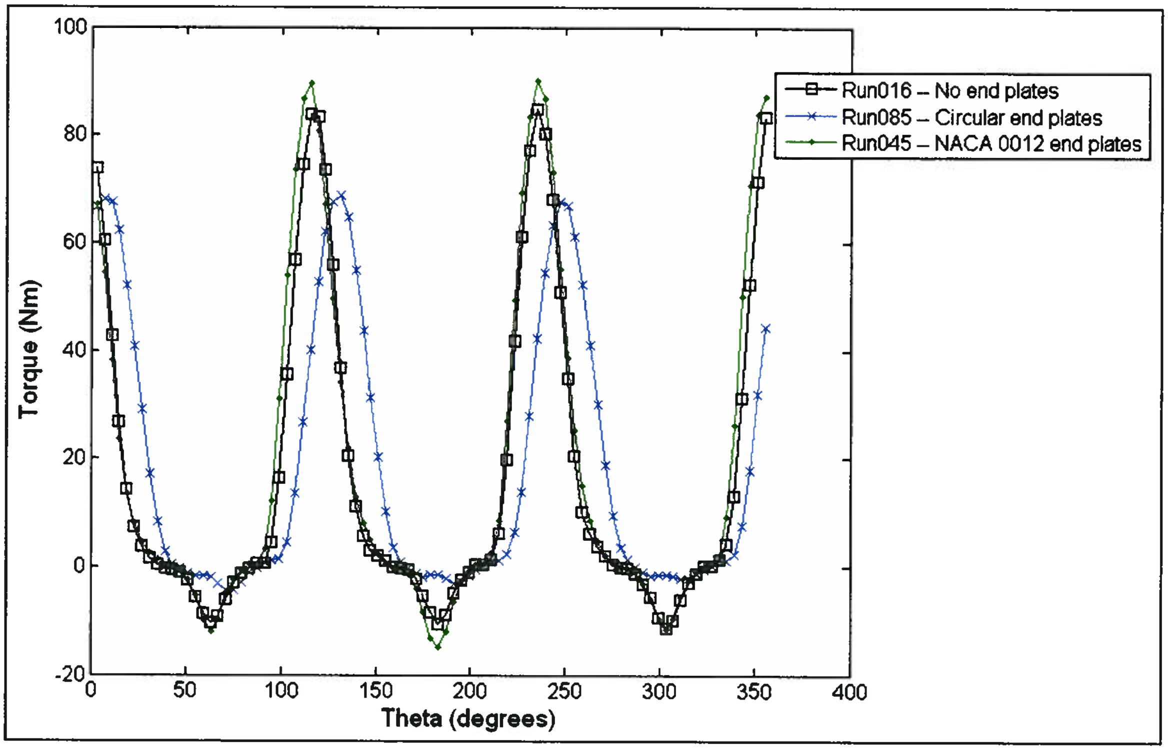

Figure 3-33: Torque vs. Revolution Angle comparing end plates at 1.5 m/s.

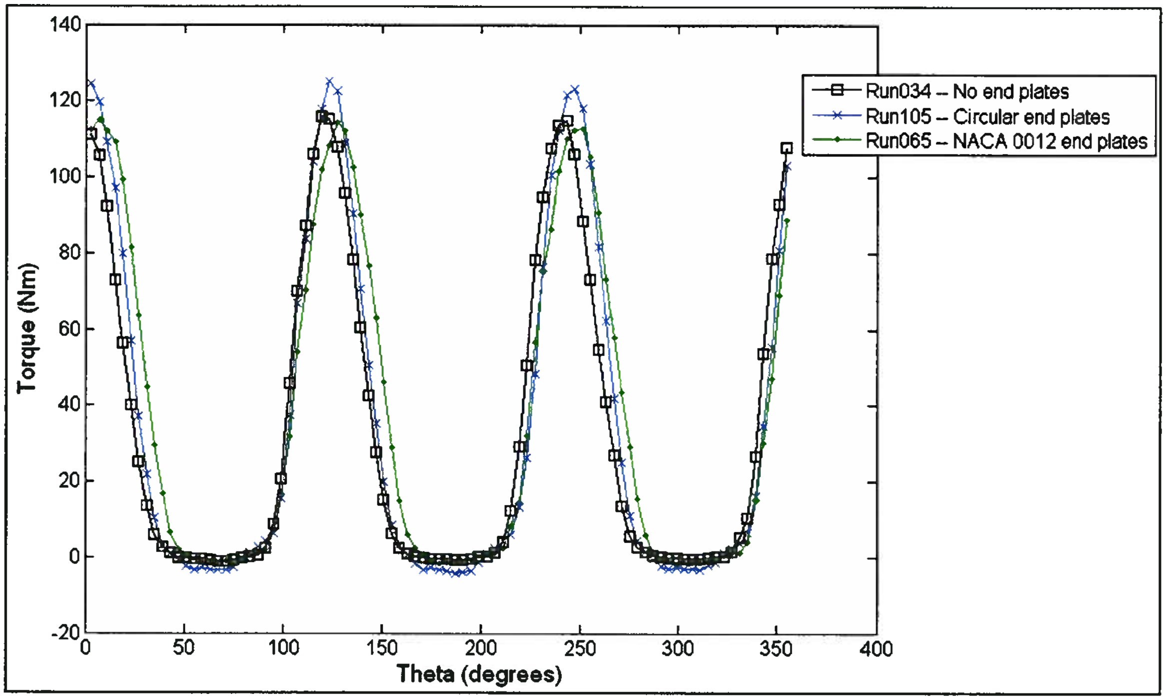

Figure 3-34: Torque vs. Revolution Angle comparing end plates at 2 m/s.

3.3.8 Shaft Fairing

Given the interference observed in the single blade tests, fairings were fabricated and placed around the shaft as an attempt to minimize the shaft vortices (Figure 3-35). Figure 3-36 below provides Ck vs. TSR for runs with and without the shaft fairing at 1.5 and 2 m/s. Tests were conducted using arm configuration C, and a fairing was placed each between the upper/middle arms and the middle/lower arms. For both speeds, the fairings either reduced performance or had negligible effect.

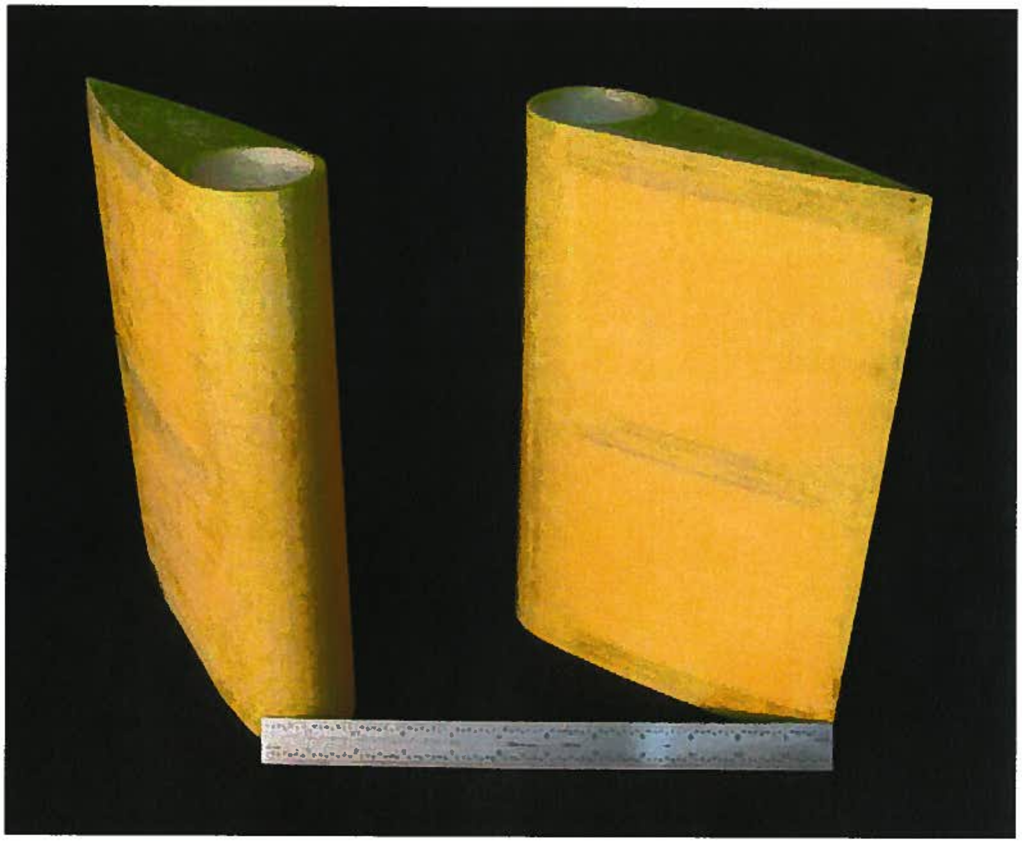

Figure 3-35: Shaft fairings.

Figure 3-37 displays torque curves for the cases with and without shaft fairing for a TSR = 2.75 at 1.5 m/s. The fairing reduces the torque peaks, as well as shifts the peaks approximately 12 degrees to the left, or earlier in the rotation. A similar effect was observed at 2 m/s. Friction is the likely cause of the reduced torque peak, while different vortex interactions, as well as the reduced torque peaks resulting in less revolution speed fluctuation, are the most reasonable explanation for the phase shift in torque curve (revolution speed fluctuations discussed below in Section 4.1.3).

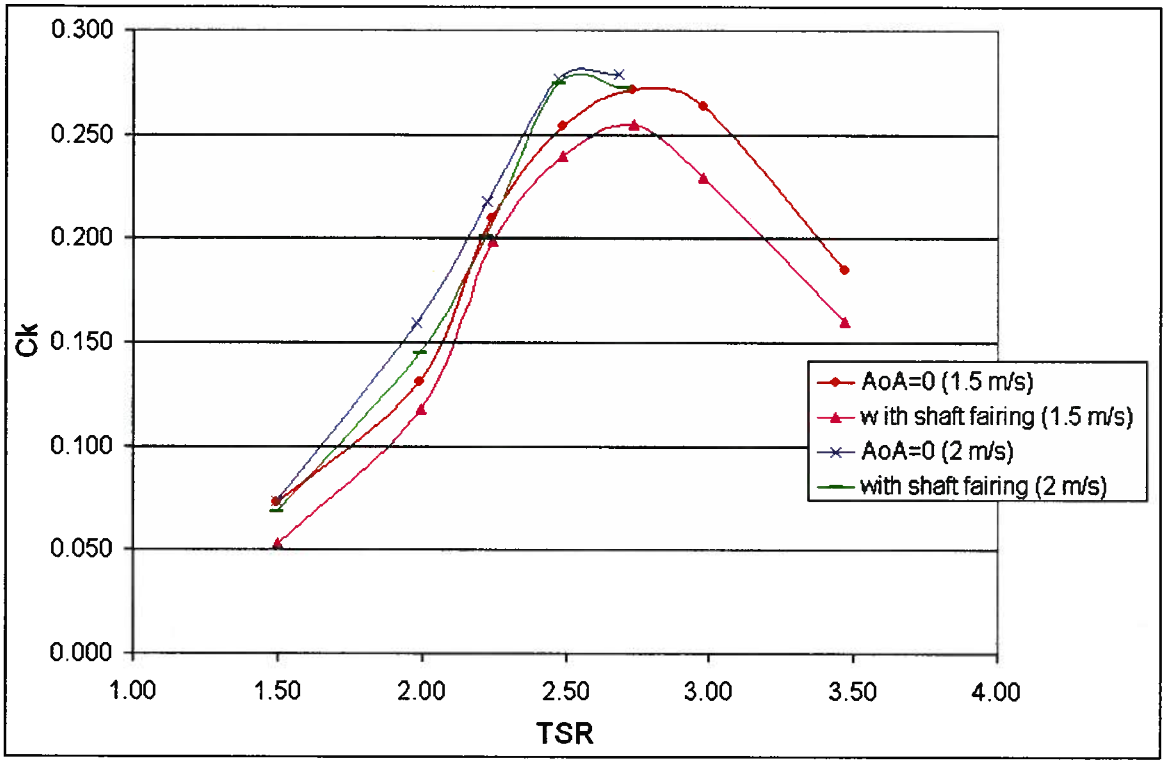

Figure 3-36: Ck vs. TSR with and without shaft fairing (1.5 and 2 m/s).

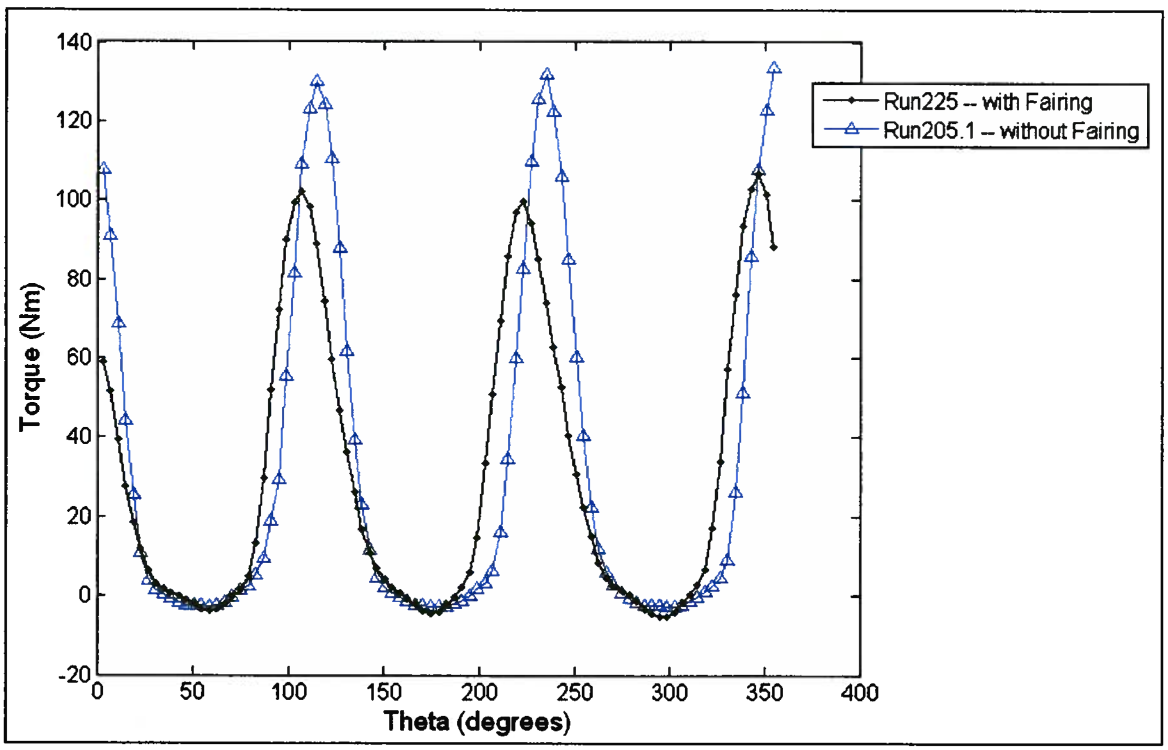

Figure 3-37: Torque vs. Revolution Angle with and without shaft fairing at 1.5 m/s, TSR=2.75.

Tests were also conducted for a single blade with the shaft fairing, as shown in Figure 3-38. Figure 3-39 provides torque vs. revolution angle with and without the shaft fairing. The fairing appears to smooth out the torque curve downstream of the turbine near 270° as one might expect, though the general effect of the fairing was to reduce the average torque by 4 % (Ck = 0.151 without the shaft fairing for a single blade vs. 0.145 for the case with the shaft fairing). This reduction in power is likely caused by additional friction between the fairing and shaft, as well as an increase in frontal area of the shaft increasing the effective blockage of the turbine and causing more flow to pass around.

Figure 3-38: Single blade with installed shaft fairing.

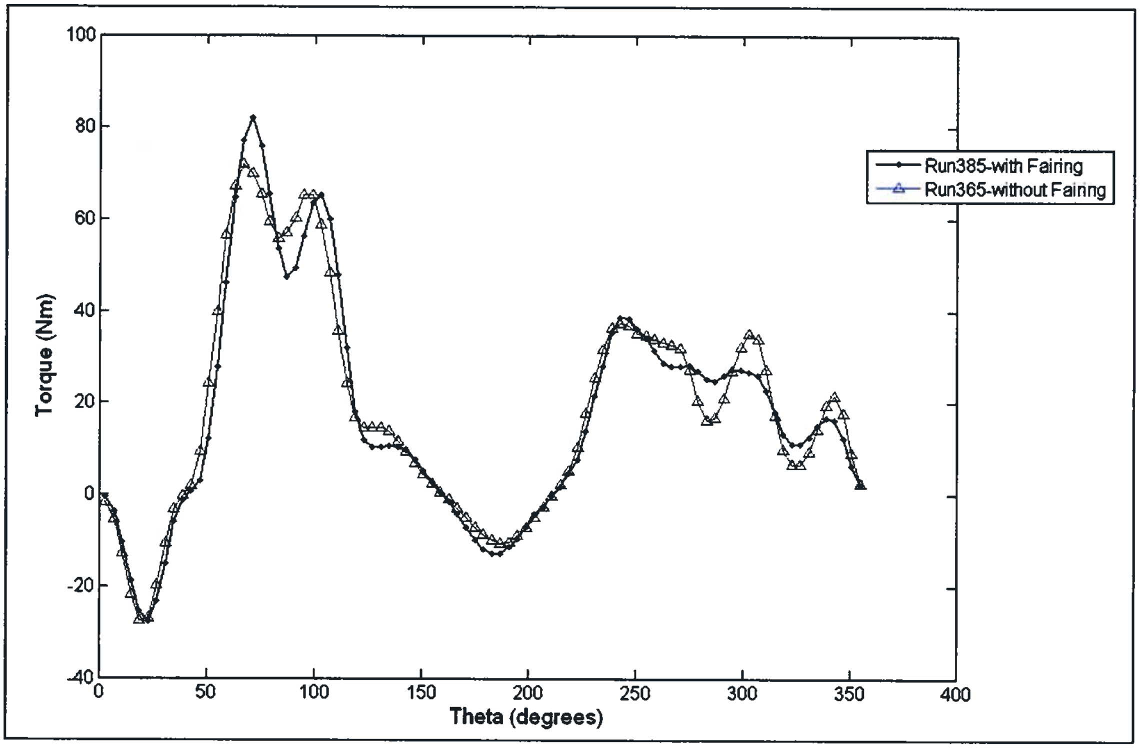

Figure 3-39: Single Blade Torque vs. Revolution Angle with and without shaft fairing at 1.5 m/s, TSR=2.75.

3.3.9 Summary

Considering the data above, it becomes possible to summarize the improvements to be gained from each parameter by comparing to its baseline configuration. NACA 0012 end plates were shown to increase the baseline Ck value by 12.2% and 16.6% at 1.5 m/s and 2 m/s respectively, though in general the contribution of tip losses to overall device performance will reduce with increasing aspect ratio. Angle of attack provided a notable improvement over the baseline case of 0° (tested with arm profile B), as at 1.5 m/s 3° and 5° increased the Ck value by 21.1% and 14.8% respectively, while at 2 m/s 3° and 5° increased the Ck value by 17.3% and 21.6% respectively.

Table 3-6 below summarizes the incremental improvements achieved over the 3-armed baseline (profile C) for the following cases: 2 arms at the ends only, cambered blades at 0° and 5°, and shaft fairing application.

Table 3-6: Maximum Ck and percent increase over free-stream baseline.

Case	Maximum Ck	% change
3 arms (baseline)	0.272	--
2 arms	0.303	11.4%
Cambered blade (0° AoA)	0.285	4.8%
Cambered blade (5° AoA)	0.319	17.3%
Shaft fairing	0.255	-6.3%

Using this data, it is possible to hypothesize the maximum efficiency of a free-stream, 3-bladed rotor. As moving from 3 to 2 arms yielded an increase in Ck of approximately 0.031, it seems reasonable that in the absence of all arms, the Ck may increase by an additional 0.062; however, one must recognize that removing end arms will also allow for tip losses (Ck = approximately 0.02 at this aspect ratio). Assuming tip losses may be eliminated by some other hypothetical means, the maximum efficiency of this device would be approximately 0.365. The shift to cambered blades at 5° further increased Ck by a value of 0.047, bringing our theoretical maximum Ck value, without arms or tip losses using the cambered blade at 5°, to 0.412. Two other major components affecting rotor design and not examined as part of this thesis are solidity and foil shape. Recognizing these, a rotor with Ck of 0.45 in the absence of all losses seems to be a reasonable theoretical maximum after using numerical codes or an extensive experimental program to pin-point optimum solidity and foil shape/angle of attack.

3.4 Ducted Turbine

Figure 3-40 provides a dimensioned plan view of the venturi-type ducting installed around the turbine, while Figure 3-41 illustrates the ducting position within the tank. A top and bottom was installed as shown in Figure 3-41, and a large Plexiglas window was installed to allow for removal of the turbine while leaving the ducting in place, as well as to facilitate visualization. The duct shape was determined based on previous NRC trials [11] as well as what was suitable for the current experimental setup. Results for the venturi-type ducting (Section 3.4.1) and ducting with flow deflectors (Section 3.4.2) are discussed below.

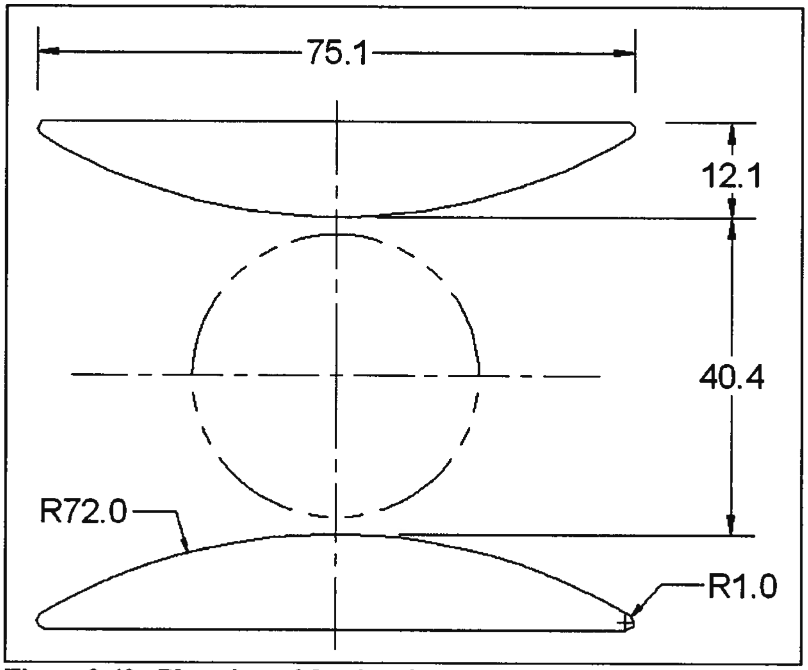

Figure 3-40: Plan view of ducting (inches).

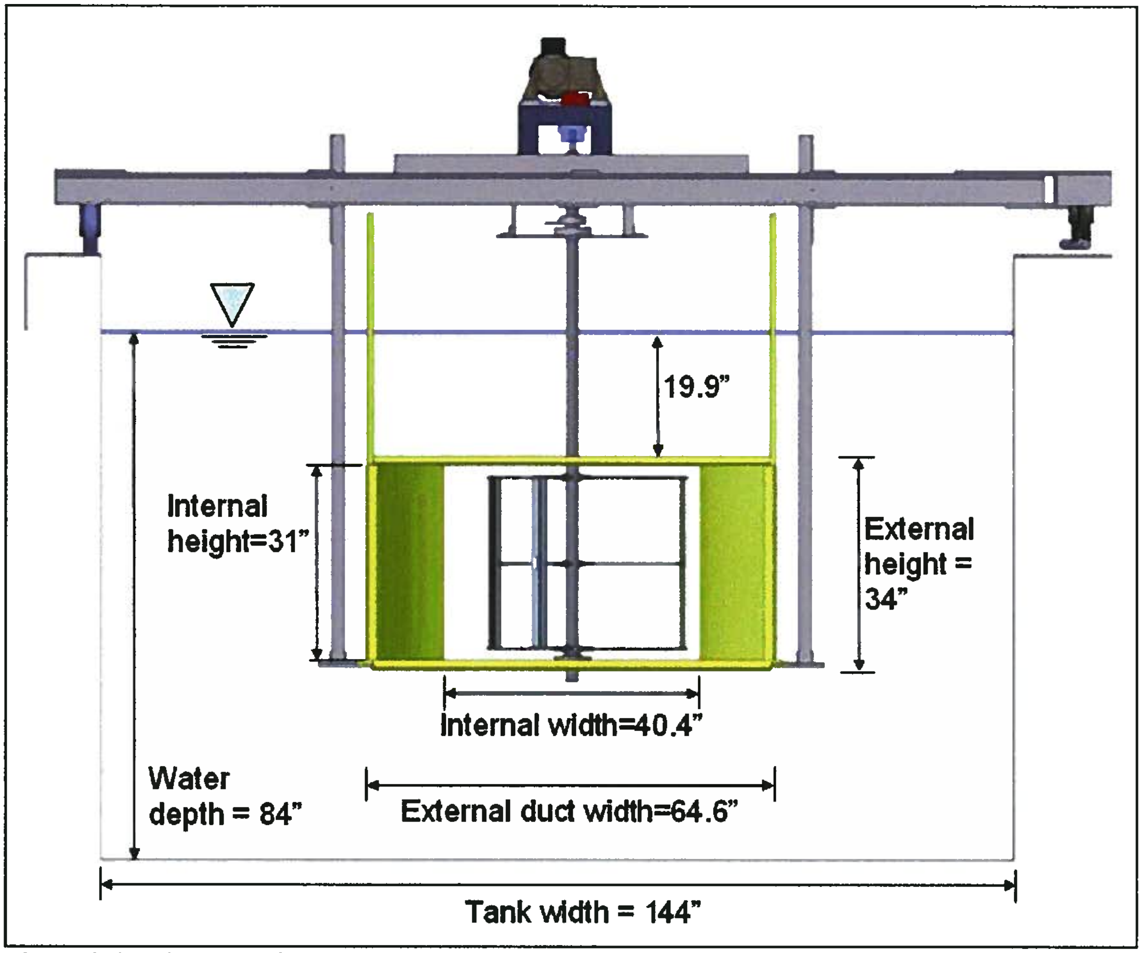

Figure 3-41: Cross-section of towing tank with ducting and turbine.

3.4.1 Venturi-type Ducting

Figure 3-42 provides Ck vs. TSR for the free-stream and ducted turbine at 1.5 m/s. The ducted turbine greatly enhances power output from the turbine, though Ck is still calculated based on the turbine area, and not the duct frontal area affecting the flow. Secondly, TSR is calculated relative to the free-stream velocity, and not relative to the accelerated velocity through the duct, explaining why the highest Ck value is occurring at a higher TSR value for the ducted case.

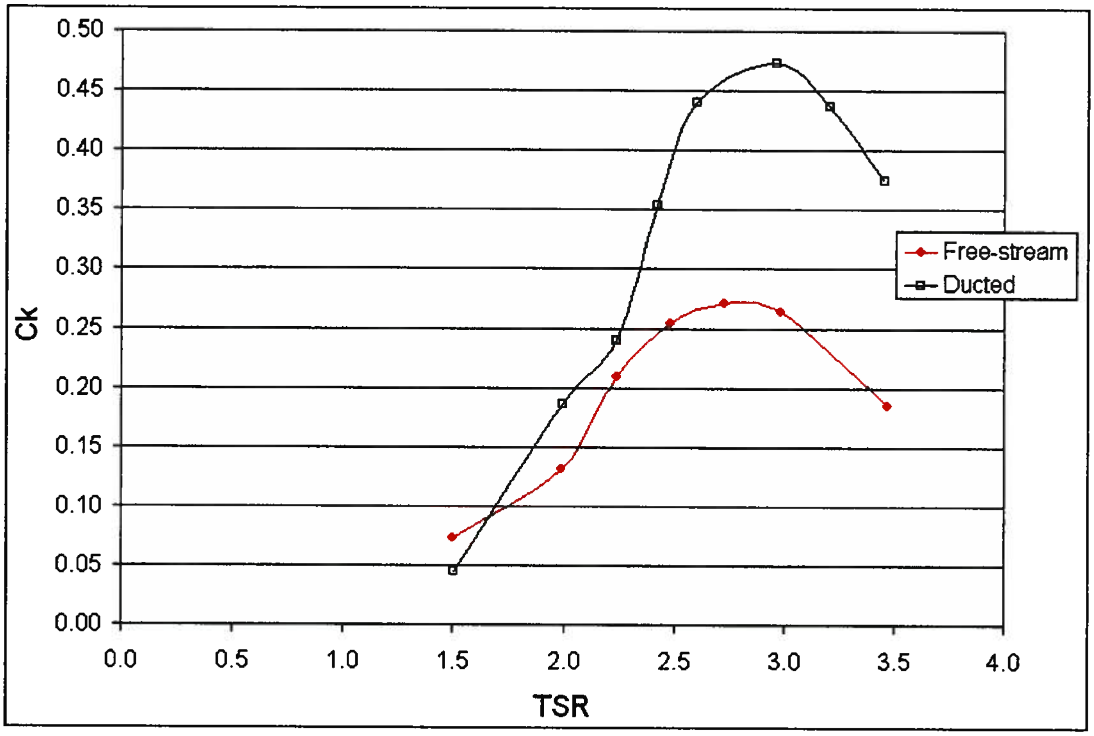

Figure 3-42: Ck vs. TSR for the free-stream and ducted turbine at 1. 5 m/s.

It is interesting to compare the power harnessed by the ducted turbine vs. the power that would be extracted by a free-stream turbine of capture area equivalent to the duct (approximately 32.5" x 63.1") operating at the Ck values obtained in previous tests. This is provided in Figure 3-43 which indicates the ducted turbine captured a peak of 501 W, while a free-stream turbine of equivalent capture area may be expected to harness 560 W, not accounting for Reynolds' effects. Therefore, the ducted configuration tested was approximately 12% less efficient than an equivalent-sized free-stream turbine, having a peak Ck value based on the capture area of 0.239, vs. 0.272 for the free-stream device. A free-stream device of equivalent size to the ducted device tested may be capable of generating more power due to more flow passing through the device given there is less blockage in the absence of a duct, as well as the increased diameter and blade size of the free-stream device is capable of producing larger torque forces on the shaft.

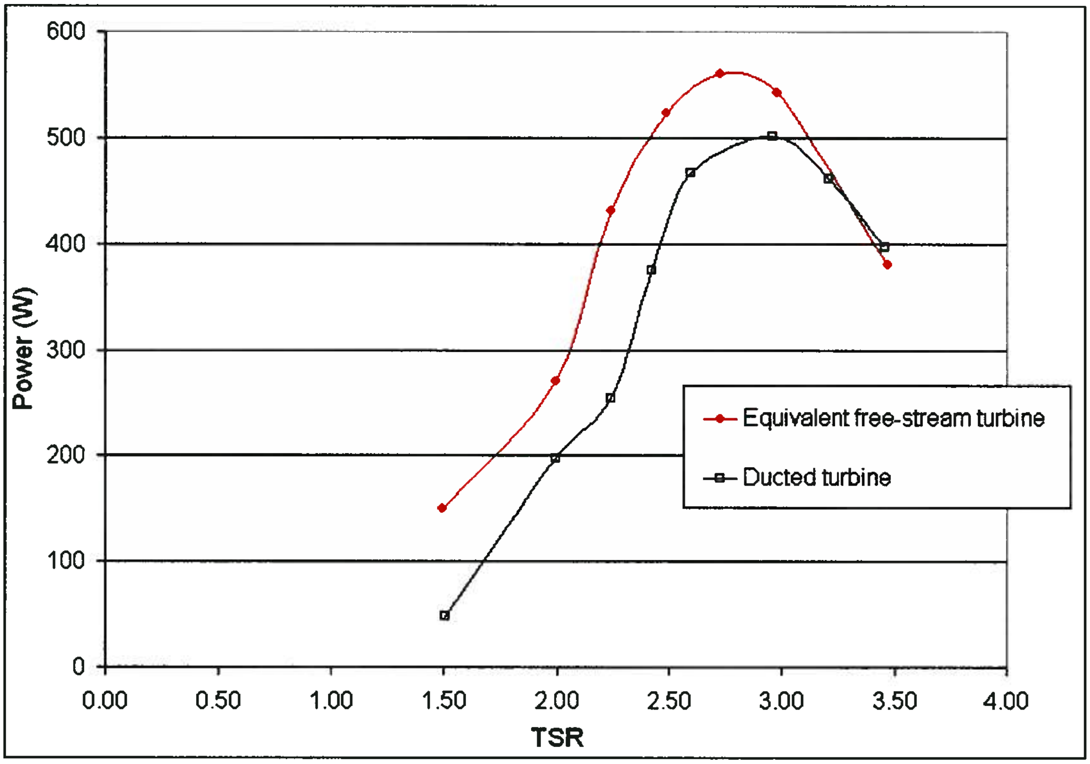

Figure 3-43: Extracted Power (W) vs. TSR for the tested ducted turbine and a free-stream turbine of equivalent capture area at 1.5 m/s.

Considering torque curves for the free-stream vs. the ducted turbine, Figure 3-44 illustrates the torque curves for the free-stream turbine at 1.5 m/s, while Figure 3-45 provides torque curves for the ducted device at 1.5 m/s. The most significant (and surprising) result is the decrease in amplitude of the torque curve for the ducted configuration once a TSR of 2.75 or greater is reached. A similar decrease in torque ripple was observed in the 2 m/s ducted tests beginning at TSR = 2.5. It is convenient to define a torque fluctuation coefficient calculated as follows from values of the torque curve:

$$C_{TF} = \frac{T_{\max} - T_{\min}}{T_{avg}} \qquad \textbf{Equation 6}$$

where: T_{max} = maximum torque

T_{min} = minimum torque

T_{avg} = average torque

C_{TF} facilitates comparison of torque curve fluctuations, which are a key parameter in the mechanical design of the device as reduced fluctuations may greatly enhance both reliability and operation life of the device.

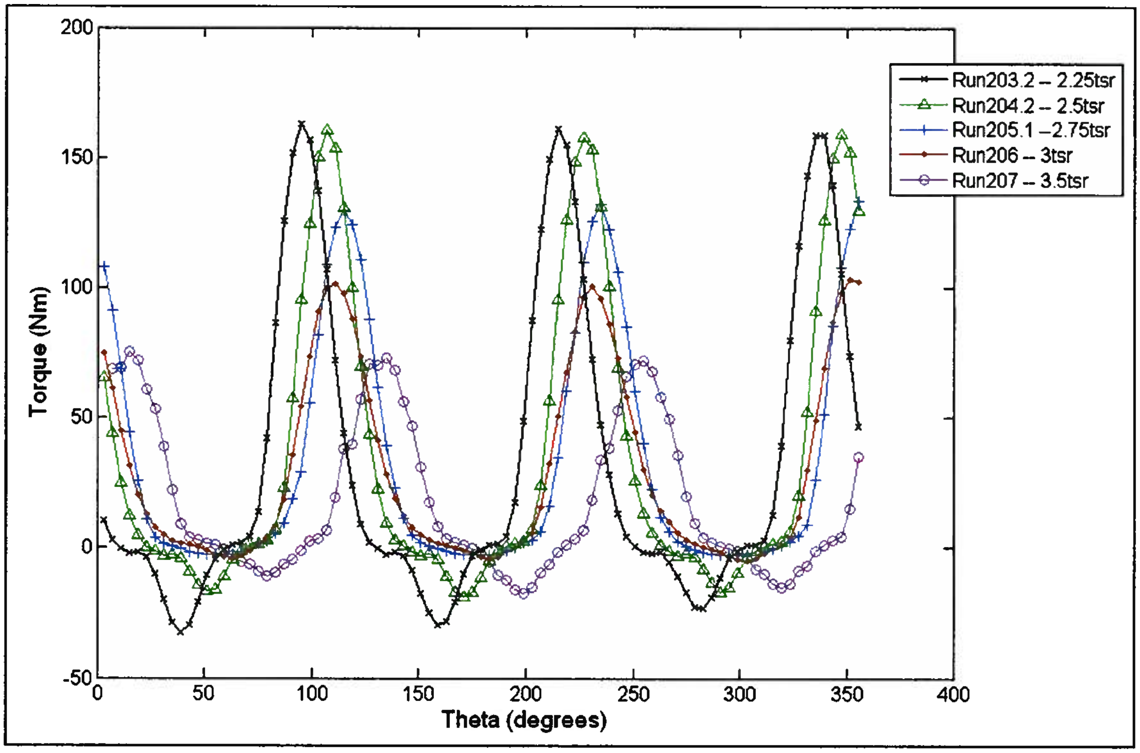

Figure 3-44: Torque vs. Revolution Angle for free-stream turbine at 1.5 m/s.

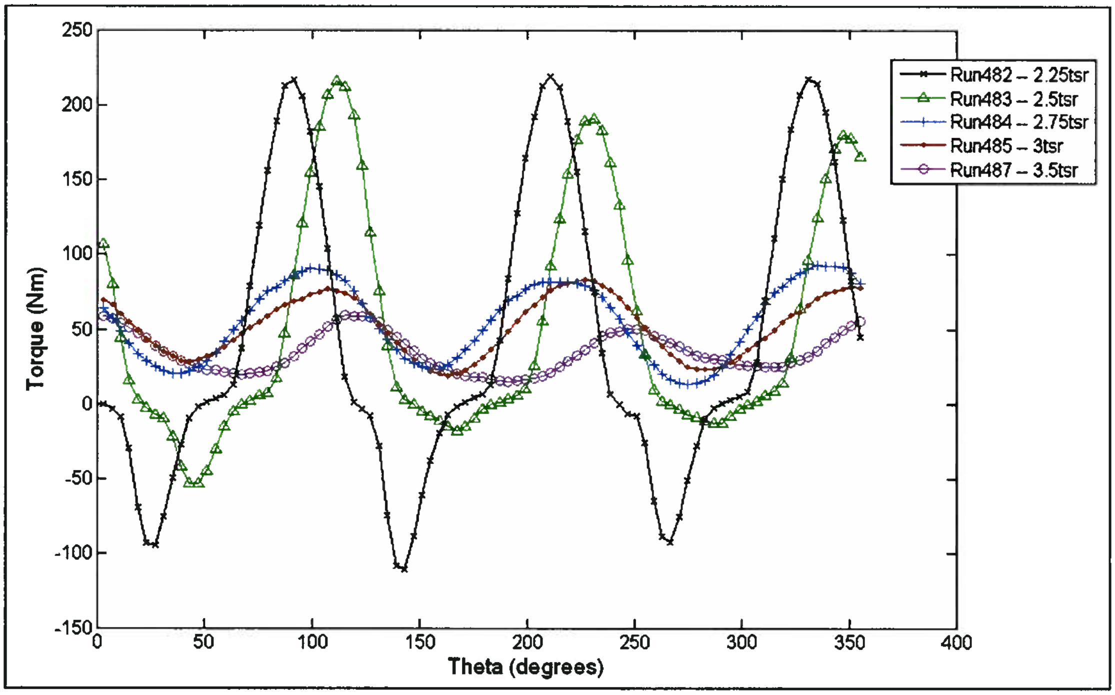

Figure 3-45: Torque vs. Revolution Angle for ducted turbine at 1.5 m/s.

Table 3-7 below tabulates torque fluctuation coefficient for both a free-stream and ducted turbine in the runs shown above.

Table 3-7: Torque fluctuation coefficient for a free-stream and ducted turbine.

	C_{TF}		
TSR Value	**Free-stream**	**Ducted**	**Percent Change**
2.25	6.48	9.54	47.2%
2.5	5.44	5.71	5.0%
2.75	4.24	1.45	-65.8%
3	3.8	1.25	-67.1%
3.5	5.4	1.26	-76.7%

This decrease in C_{TF} is primarily due to the duct constraining the flow and not allowing it to expand and slow in way of the downstream blade, thus increasing the available power; altered vortex interactions compared to the free-stream case may also be increasing performance of the downstream blade though flow visualization would be required to be certain. Lastly, tests were also conducted with the ducted configuration and the shaft fairing. As for the free-stream result, a slight decrease in performance was observed for all runs, except for TSR=2.75 at 2 m/s which showed a 6% increase in performance. This point is believed to be an outlier, but may warrant future investigation should the device be re-examined.

3.4.2 Ducting with Deflectors

In place of testing a large variety of duct shapes which are both expensive and laborious to construct, 4 deflectors were fabricated to be placed at various locations within the duct to adjust the flow. Figure 3-46 below illustrates deflector positioning and size, with additional details in Appendix B. The configurations tested were as follows:

- All four deflectors
- Blades spinning towards (deflectors 1 & 3)
- Blades spinning away (deflectors 2 & 4)
- Downstream (deflectors 1 & 2)
- Upstream (deflectors 1 & 2 while running in opposite direction; equivalent to 3 & 4 with flow direction as shown on diagram)

The rationale behind the use of the deflectors was to reduce the cross-sectional area, and thus increase the speed and available power, in the blade positions where the turbine is generating the most torque (90° and 270°). Additionally, deflectors were offset from the ducting to allow for flow to pass in-between, limiting separation that may occur behind the deflector. This design was developed by Yasser Nabavi and Voytek Klaptocz [28].

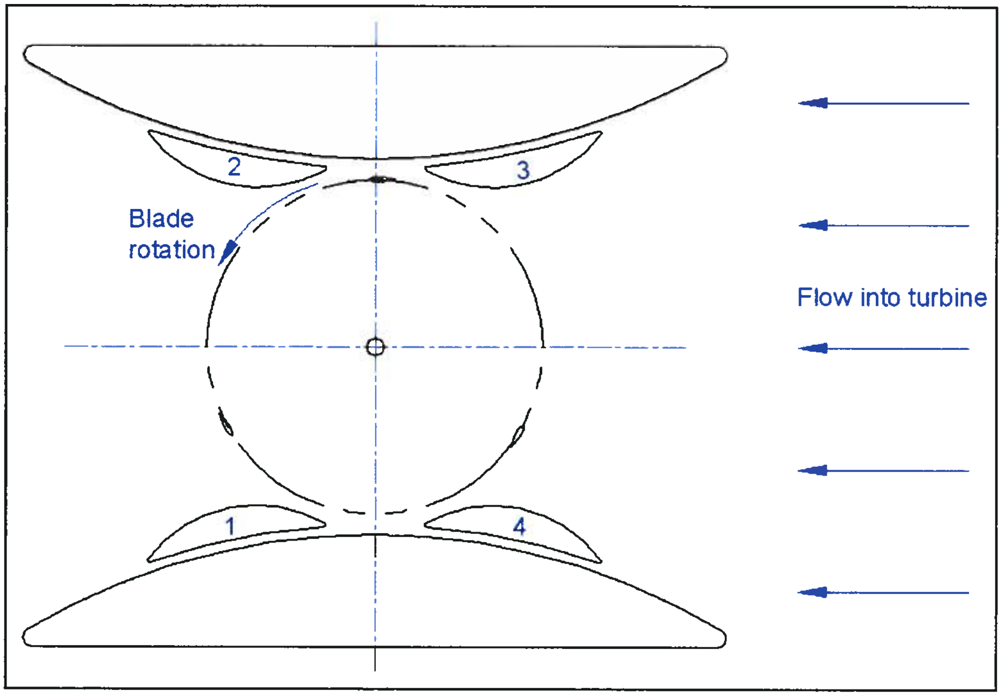

Figure 3-46: Ducting with deflectors.

Figure 3-47 below provides Ck vs. TSR for the various deflector configurations, as well as for the plain venturi-type duct. The configuration without deflectors produced the highest Ck values, and this is likely due to the deflectors reducing the flux through the ducting assembly and thus reducing the available power to be extracted by the rotor. The 4-deflector and upstream deflector designs appear to be the least efficient, likely due to increasing resistance to the flow before the rotor, while the downstream deflectors as well as 1+3 and 2+4 yield similar peak Ck values.

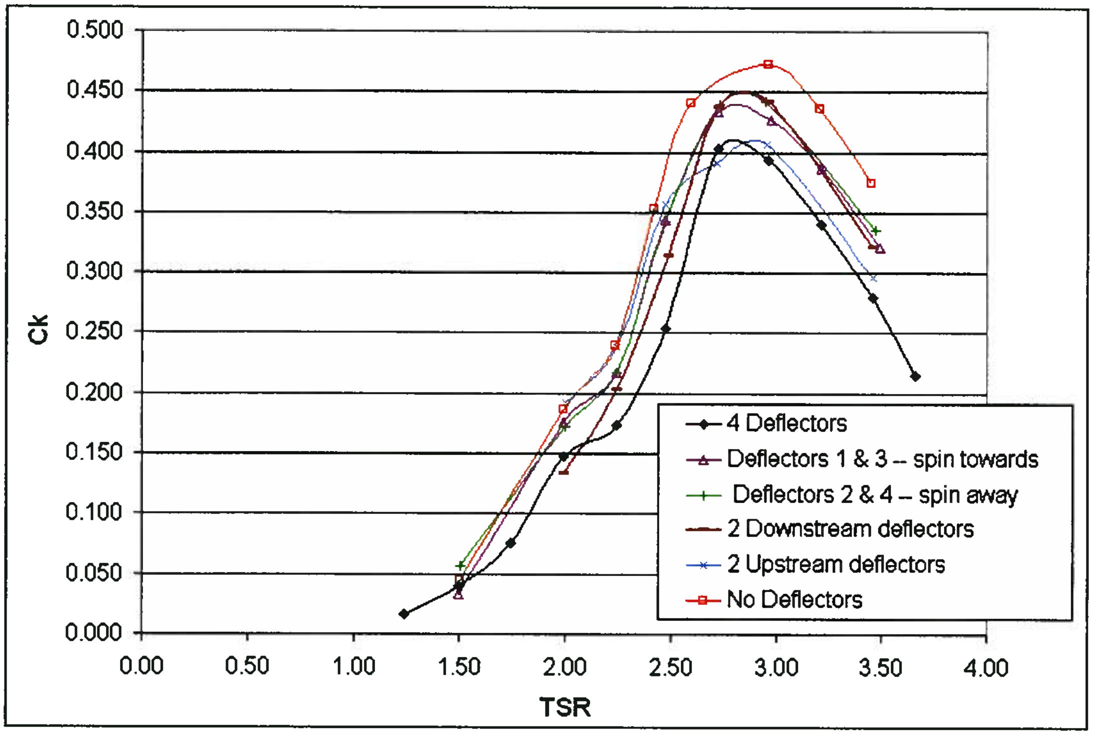

Figure 3-47: Ck vs. TSR for duct and deflector configurations.

The primary significance of the deflector designs is observed when examining the torque curves of the various configurations. Maximum Ck values were observed at TSR values of 2.75 and 3, and Figure 3-48 and Figure 3-49 provides torque curves for the various configurations at TSR = 3. The downstream deflectors (solid dashes) greatly reduce the torque fluctuations observed, believed to be due to higher torques at the downstream blade caused the smaller cross-sectional area and resulting higher flow velocities. Conversely, the deflectors upstream of the turbine appear to cause much greater torque fluctuations due to the increased velocity passing past the blade upstream of the turbine, which is already producing the majority of the torque.

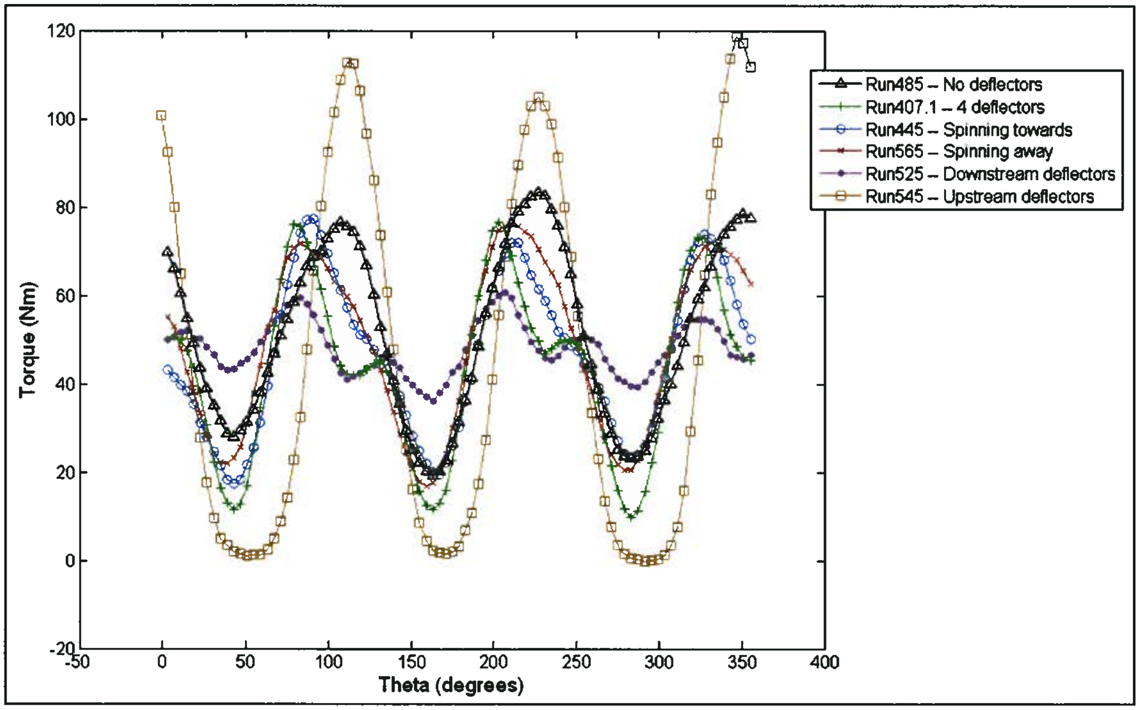

Figure 3-48: Torque vs. Angle of Revolution for ducted and deflector configurations.

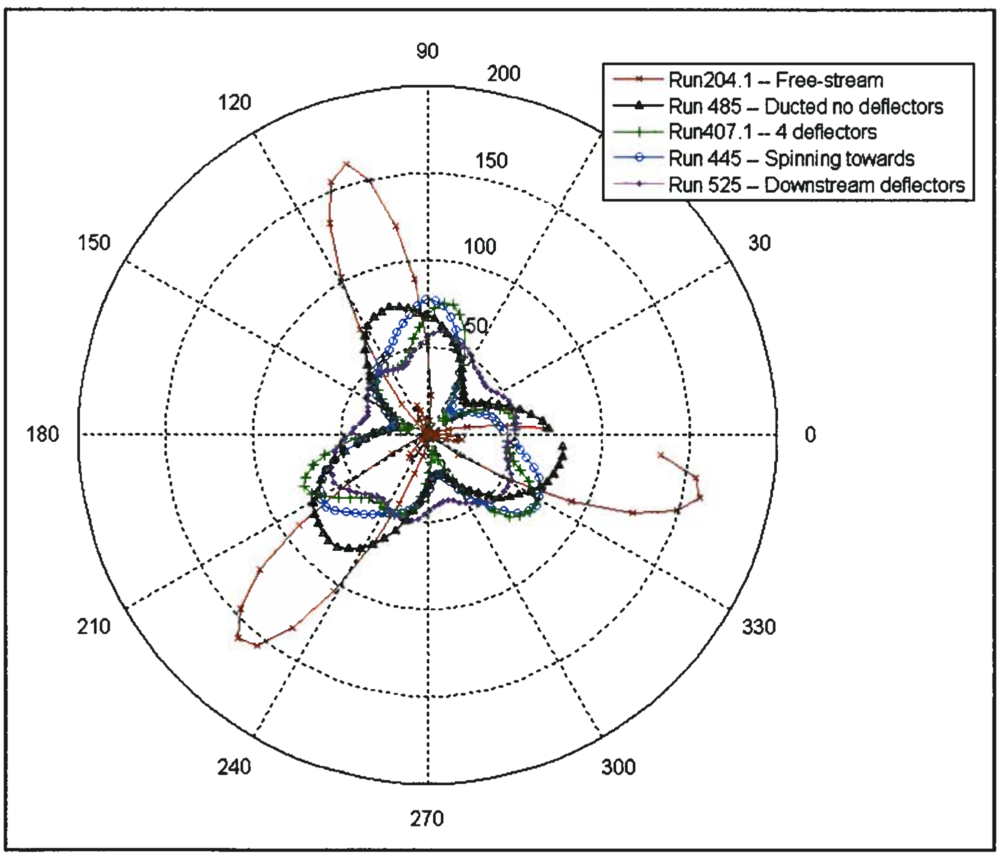

Figure 3-49: Polar plot of Torque vs. Angle of Revolution for ducted configurations.

Table 3-8 below provides the maximum Ck values and corresponding C_{TF} for the various ducted configurations examined, as well as for the free-stream case. The downstream deflectors offer a 62% reduction in the torque ripple experienced by the shaft over the case without deflectors. This is considered due to the reduced cross-sectional area in way of the deflectors at the downstream positions of the blades, which increases flow velocity and thus lift extracted in this position, resulting in a torque generation more comparable to the 90° position upstream of the shaft. Lastly, in the figure above it should be noted that reduced torque fluctuations resulted in reduced revolution speed fluctuations (Section 4.1.3)shifting the peaks back closer to their theoretical position near 90°.

Table 3-8: Maximum Ck and corresponding C_{TF} for ducted turbine configurations (1.5 m/s).

Case	Ck Value	% Ck Change	C_{TF}	% C_{TF} Change
No deflectors	0.473	--	1.25	--
Downstream deflectors	0.442	-6.6%	0.47	-62.4%
All four deflectors	0.393	-16.9%	1.4	12.0%
Spinning towards deflectors	0.426	-9.9%	1.17	-6.4%
Spinning away from deflectors	0.442	-6.6%	1.23	-1.6%
Upstream deflectors	0.407	-14.0%	2.67	113.6%

3.4.3 Summary

As for the free-stream case, it is possible to quantify the effect of the various ducting configurations compared to the baseline free-stream case. Table 3-9 below provides maximum Ck value, Ck percentage increase over the free-stream baseline, and coefficient of torque fluctuation.

Table 3-9: Maximum Ck, percent change, and torque fluctuation coefficient.

Case	Ck Value	% Ck Change	C_{TF}	% C_{TF} Change
Free stream (baseline)	0.272	--	4.24	--
No deflectors	0.473	73.9%	1.25	-70.5%
Downstream deflectors	0.442	62.5%	0.47	-88.9%
All four deflectors	0.393	44.5%	1.4	-67.0%
Spinning towards deflectors	0.426	56.6%	1.17	-72.4%
Spinning away from deflectors	0.442	62.5%	1.23	-71.0%
Upstream deflectors	0.407	49.6%	2.67	-37.0%

As expected, ducting around the rotor increases power output; however, the power obtained from the ducting design tested is less than what may be expected from a free-stream turbine of equivalent cross-sectional area. Recognizing this, ducting (especially with modifications such as the downstream deflectors) is demonstrated to greatly reduce torque ripple. Additional potential benefits such as structural support for the bottom bearing and to facilitate mooring render ducting a prospective enhancement to a turbine design requiring a comprehensive cost-benefit analysis.

3.5 Drag Force

No previous documentation has been found on the forces parallel to the free stream flow acting on the turbine rotor, and subsequently the shaft bearings. These forces are a combination of drag forces on the shaft and supporting arms, as well as the component of the lift and drag forces on the turbine blades acting parallel to the free-stream flow. For this thesis, the combination of forces parallel to the free-stream flow will be referred to collectively as drag forces.

A means of approximating the drag force on the turbine was devised by measuring the force at the top bearing using the force balance, estimating the centre of action of the drag forces, and balancing moments about the bottom (self-aligning) bearing to solve for the magnitude of the drag force. Figure 3-50 below illustrates the location of the assumed and measured forces. Analytical calculations demonstrated that the blades and arms may be expected to account for approximately 83-93% of the forces parallel to the free-stream flow, while the shaft and arms account for the remaining forces. Given the centre of the blades and arms is 21.5" above the bottom bearing and the centre of the shaft is 26" above the bottom bearing, this results in an assumed centre of force about 22" above the bottom bearing to within approximately +/- 15%. The broad range is due to the simplified analytical calculations as well as the dynamic nature of the system, but is sufficient for this preliminary investigation. With the top bearing 68" above the lower bearing and the force balance measuring the load parallel to the free stream on this top bearing, it is possible to use moment calculations and determine that the drag load at the turbine is 68/22 times the in-line load measured at the force balance.

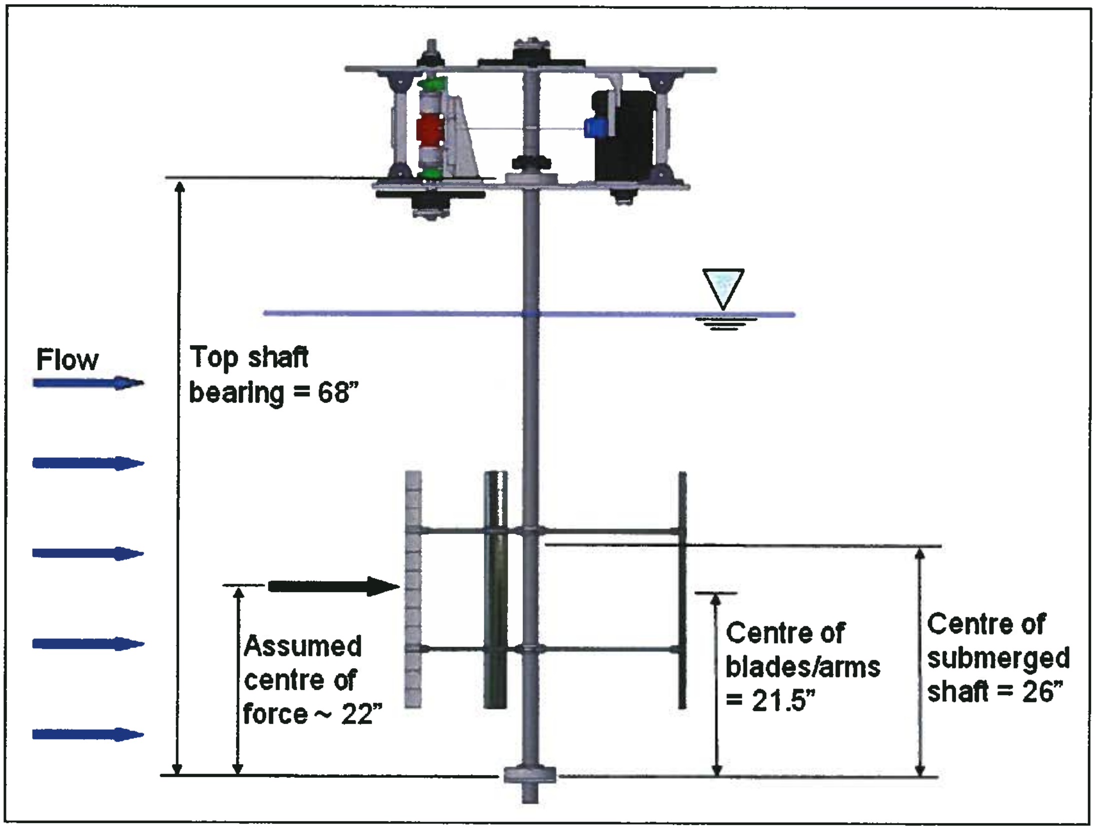

Figure 3-50: Side view providing location of assumed centre of drag force.

Figure 3-51 provides drag force of a free-stream turbine vs. TSR for angles of attack at 0° and 3° for TSR values between 1.5 and 3 at velocities between 1m/s and 2m/s. Using this measured drag force (D), it is possible to calculate a drag coefficient (Cd) for the turbine as follows:

$$Cd = \frac{D}{\frac{1}{2}.\rho.v^2.A}$$ **Equation 7**

Drag coefficient vs. TSR for these same trials is provided in Figure 3-52. The data for velocities of 1.5, 1.75, and 2 m/s collapses reasonably close together, while the data for 1m/s yields slightly higher drag coefficients. As these drag forces are a combination of resistance on the shaft and arms, as well as components of lift and drag on the foil parallel to the flow, Reynolds effects will be present and it is apparent that at the lower Reynolds numbers in the 1m/s tests the result is increased relative drag forces on the device. A linear trend line fit through the combined 1.5, 1.75, and 2m/s data points yields an equation with slope of 0.41 and y-intercept = -0.16 (R^2 = 0.91). This enables a rough approximation for the drag coefficient of the tested device at varying TSR values over this range of Reynolds numbers. One must exercise caution if attempting to extrapolate these results directly to other vertical axis turbines of different solidities, or proportionally larger shaft and arm sizes, as all of these will affect the magnitude of the drag forces generated.

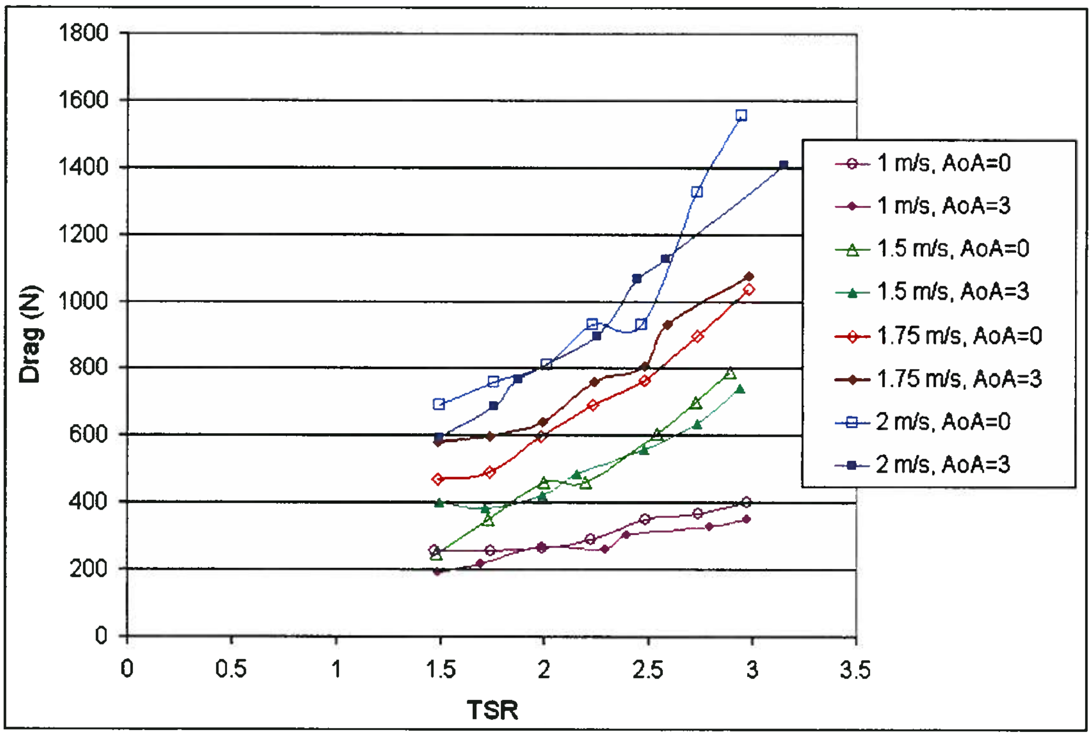

Figure 3-51: Drag Force vs. TSR for a free-stream turbine at varying velocity.

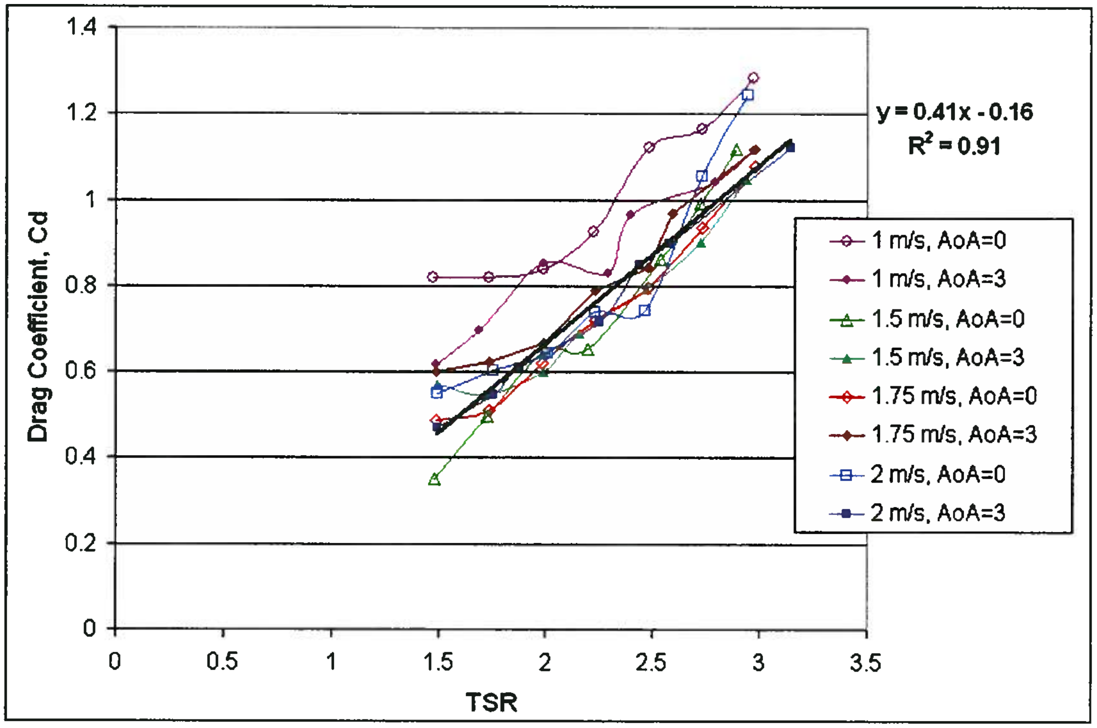

Figure 3-52: Drag Coefficient vs. TSR with trend line for data at v=1.5, 1.75, 2m/s.

As for the torque curves, it is possible to plot drag data as a function of revolution angle. Figure 3-53 provides drag force vs. revolution angle at the TSR values for which optimal power is typically being generated. The most drag is being produced in the vicinity of 90° as one might expect, since this is where peak torque is typically being generated, and a large component of the lift generating this torque is in the free-stream direction, resulting in drag on the device. Of note are the smaller peaks for the TSR=2 and TSR=2.25 cases, which occur at frequencies of approximately 57.8 rad/s and 64.1 rad/s respectively as determined by performing a Fast Fourier Transform (FFT) on the data set within the analysis software. This occurrence is discussed further after examining the single-blade case below. Figure 3-54 provides drag force vs. revolution angle at 2 m/s for TSR=2, 2.25, 2.5, 2.75. It is apparent that these high frequency oscillations have disappeared, and clean drag curves are obtained with peaks near the 90° position.

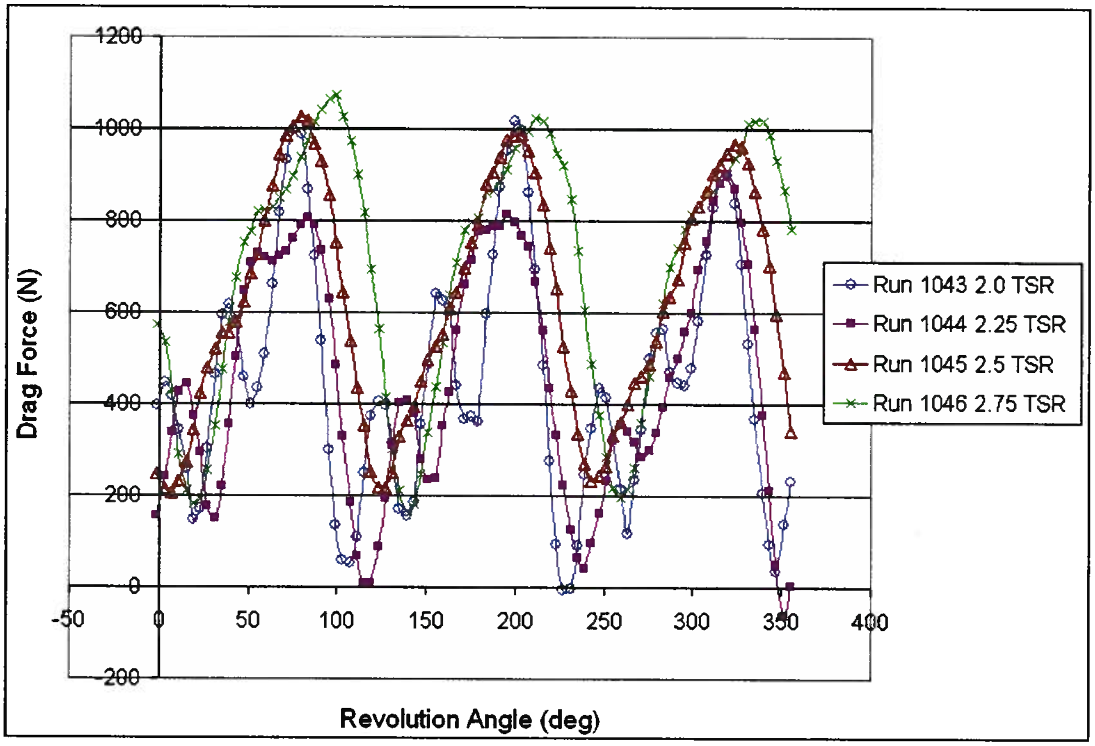

Figure 3-53: Drag Force vs. Revolution Angle at 1.5 m/s, AoA=0.

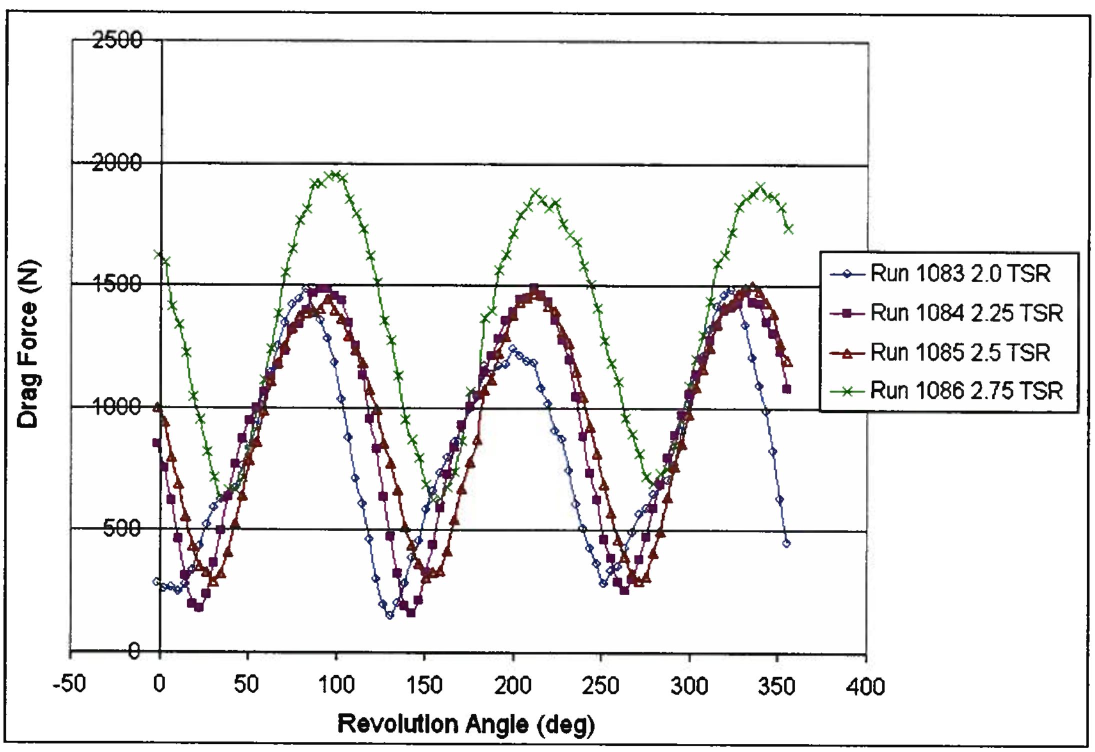

Figure 3-54: Drag Force vs. Revolution Angle at 2 m/s, AoA=0.

Considering the experimental tests with only a single blade attached to the shaft, Figure 3-55 provides drag coefficient vs. TSR for both the single and 3-bladed case at 1.5 m/s with AoA=3. A single-blade device has approximately 2/3 of the drag coefficient of a 3-bladed turbine.

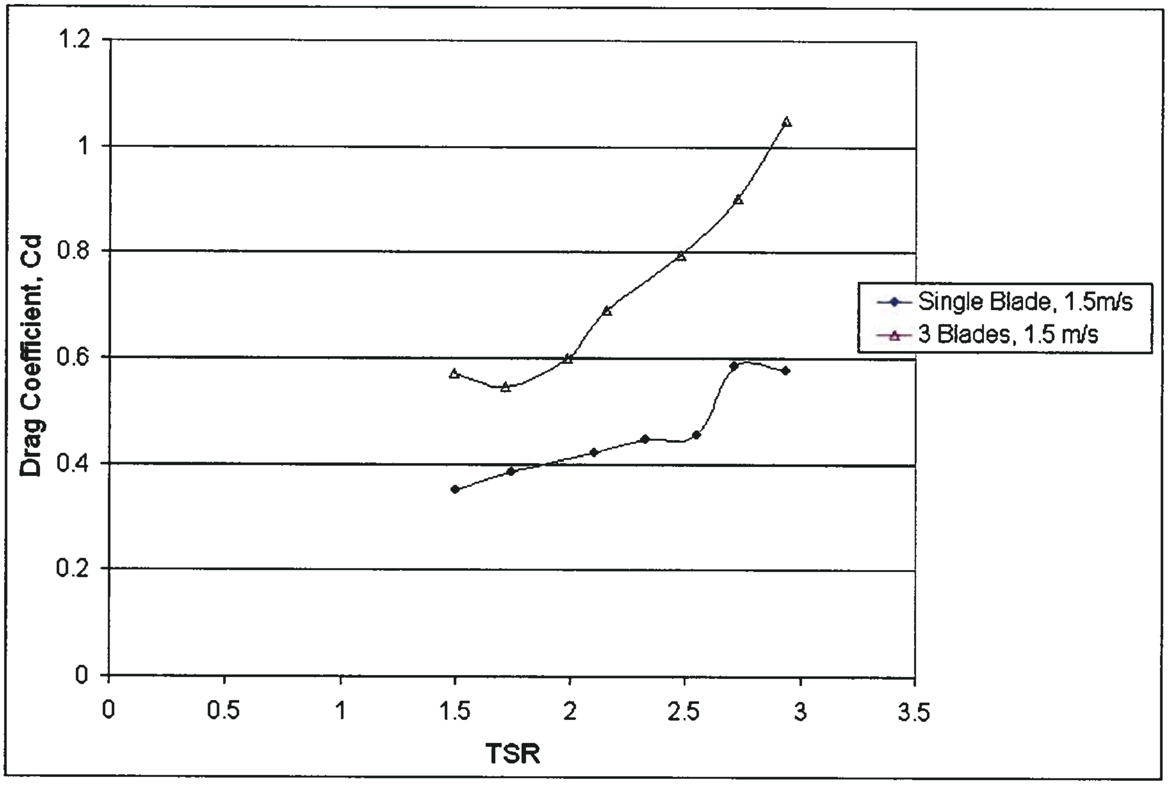

Figure 3-55: Drag Coefficient vs. TSR for a single and 3-bladed device at 1.5m/s, AoA=3.

Examining single-blade drag vs. revolution angle (Figure 3-56), drag is again being generated in the 90° and 270° regions, as is torque. The high-frequency oscillations, however, are apparent at TSR values of 2, 2.25, and 2.5, and are less apparent at TSR=2.75.

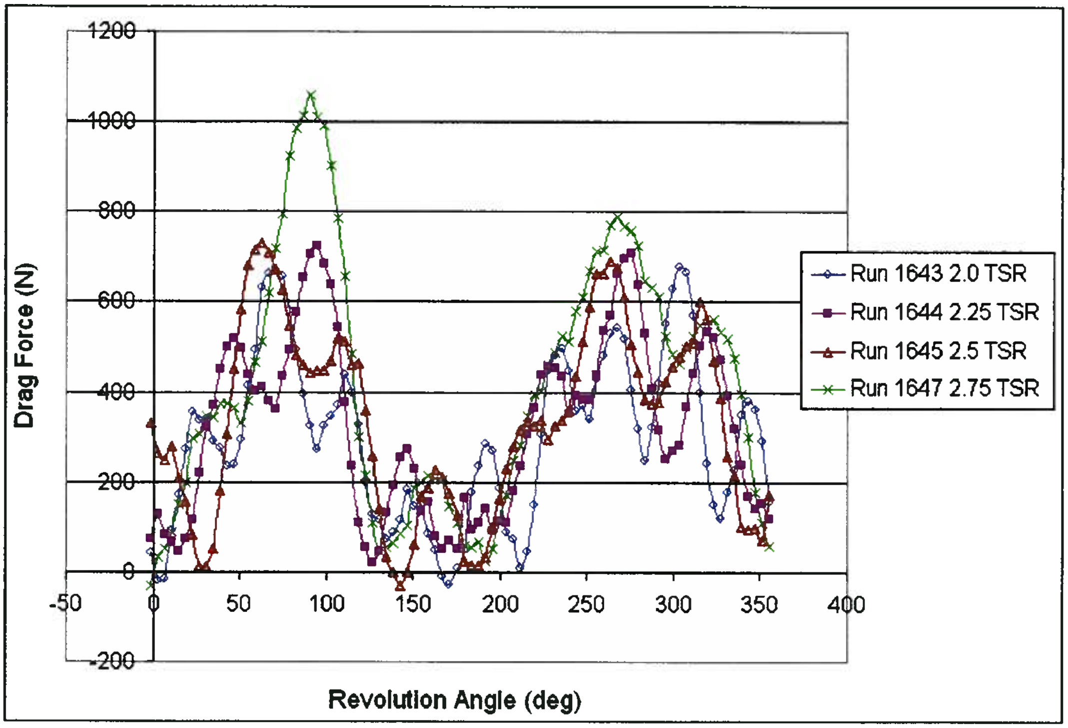

Figure 3-56: Drag Force vs. Revolution Angle for a single blade at 2 m/s, AoA=3.

Table 3-10 provides expected frequencies based on the turbine revolution speed for both one primary pulse (ie. at 90°) and two primary pulses (ie. at 90° and 270°) per blade per revolution. Approximate observed frequencies obtained from a FFT on the recorded data are also provided. The observed frequencies are where one may expect based on the turbine blade frequency and the two pulses per blade; however, there is the unique frequency at about 57-63 rad/s that isn't easily explicable by blade pulsing, and that disappears at higher drag forces. Additionally, these oscillations appear with both the single-bladed and 3-bladed device at about the same frequency, making it unlikely that this is due to arm forces or flow around the foils separating and then re-attaching. If that was the case, this frequency near 57-63 Hz would appear at much different values when comparing the 3-bladed and single-blade device. Considering this, it is reasonable to conclude that the oscillation was at a natural frequency of the force balance / load cell configuration. At higher velocities and drag forces, this oscillation has disappeared, hinting to the fact that these higher loads were perhaps capable of dampening the motion at the force balance. Lastly, the vortex shedding frequency on the shaft was predicted to be approximately 345 rad/s, while the natural frequency for the shaft was predicted to be 622 rad/s, both of which are too high to be responsible for the oscillations discussed here.

Table 3-10: Expected and observed experimental drag force frequencies.

		Expected Experimental Frequencies (rad/s)				Primary Observed Frequencies (rad/s)		
		Radians / sec	Blade Frequency	Expected Frequency (2 pulses per blade)	Expected Frequency (3 pulses per blade)			
3 Blades	2.0 TSR	6.54	19.61	39.23	58.84	18.28	39.65	57.93
	2.25 TSR	7.21	21.62	43.25	64.87	21.30	42.60	63.90
	2.5 TSR	8.11	24.32	48.63	72.95	24.32	48.63	63.84
Single Blade	2.0 TSR	6.91	6.91	13.82	20.73	6.47	12.88	57.99
	2.25 TSR	7.64	7.64	15.28	22.92	–	15.77	63.02
	2.5 TSR	8.37	8.37	16.75	25.12	–	15.58	59.31

3.5.1 Summary

The drag force measurements above provide an insightful first look into the magnitude of drag forces that may be expected on a vertical axis hydro turbine. The high frequency oscillations (57-63 Hz) appear to dampen out at higher velocities and drag loads, indicating that they are likely caused by a natural frequency in the flexibility of the load cell / force balance system. Lastly, the equation approximating Cd [Cd = 0.41*tsr – 0.16] only accounts for forces parallel to the free-stream flow, and much further work is required to understand the interaction between parasitic drag forces, lift/drag forces acting on the turbine blades, and the net forces observed by the bearings, which are likely to have a variable direction during turbine revolution.

4 DISCUSSION

Below, measurement errors and repeatability are discussed, followed by a comparison with the numerical predictions and a general discussion on sources of error.

4.1 Measurement Accuracy

Typically, when considering measurement accuracy and error, one must consider both systematic error and random error. Random error is the experimental error that occurs given no two runs will yield exactly the same result due to random variation in the experimental setup and surrounding conditions. Systematic error results from an erroneous method that is repeated with each test and consistently provides a similar inaccurate result. Random errors are addressed below in the form of measurement uncertainty, ensemble averaging for obtaining torque curve data points, and run repeatability. Revolution speed variation is a source of systematic error and is examined in Section 4.1.3.

4.1.1 Instrumentation Uncertainty and Data Point Averaging

Precision of the recorded values affects measurement accuracy, and this uncertainty is typically specified with the instrumentation component being used. Error is also attributed to the DAQ component reading and amplifying the signal, as well as any other signal conversion devices. Table 4-1 below provides the uncertainty associated with the torque sensor and angular encoder.

Table 4-1: Torque sensor and encoder uncertainty (percent of rated output) and absolute error.

Item	Torque Sensor	Encoder
Sensor	0.20%	0.10%
Digital-Analog Converter	--	0.50%
DAQ Card	0.10%	0.04%
Sum	0.30%	0.64%
Absolute Error (extreme case)	1.5 Nm	2.27 deg

These maximum errors due to instrumentation are very small, and given the number of data points recorded and the averaging techniques applied, these uncertainties do not provide a good understanding of the accuracy of each data point. Considering the torque curves, it is more useful to know the standard deviation of the ensemble averaged data used to obtain the plots. Figure 4-1 and Figure 4-2 provide standard deviation of the data points used for obtaining torque curves of the free-stream device at 1.5 and 2 m/s with the gearbox drive-train at TSR=2.5. Representative 95% CI obtained from the standard deviations are also provided for three locations on the first peak and are circled. The magnitude of the standard deviations are similar for each plot, though one difference is that at 2 m/s the torque values do not drop significantly below zero. The play in the coupling in way of torque values about zero and the resulting steep slopes contribute to the fluctuating standard deviations observed.

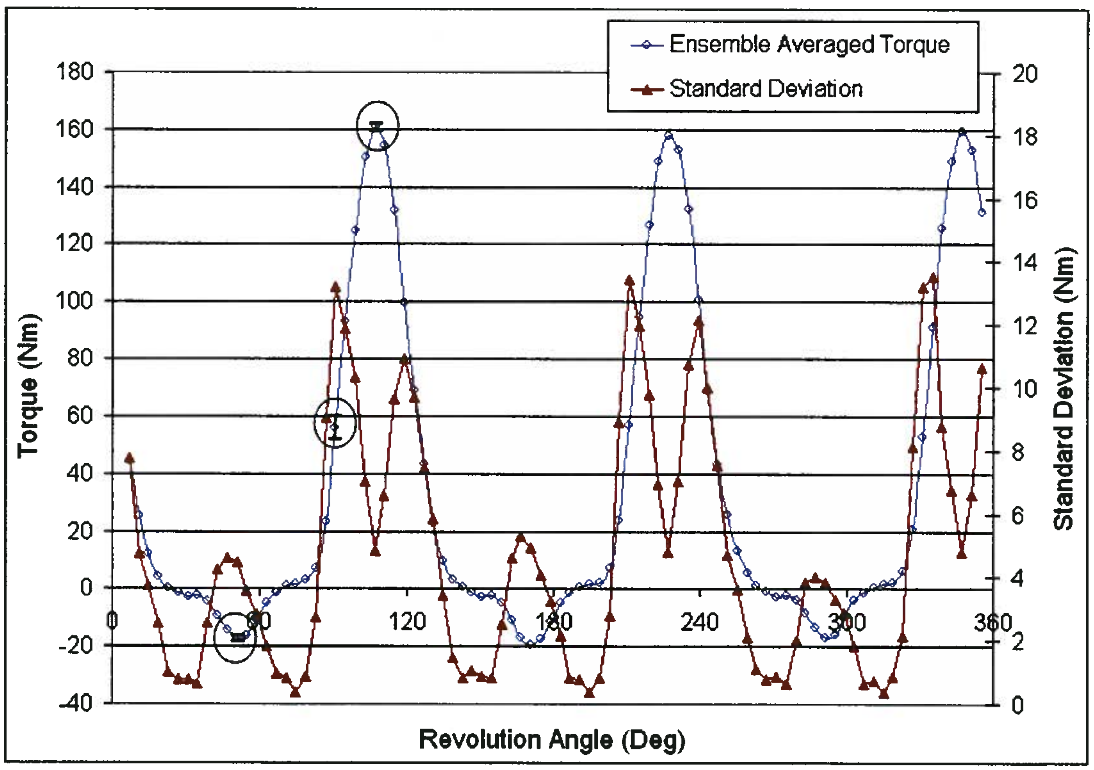

Figure 4-1: Standard Deviation and Torque vs. Revolution Angle for a free-stream device with gearbox drive-train at 1.5 m/s and TSR=2.5 (N ~ 34).

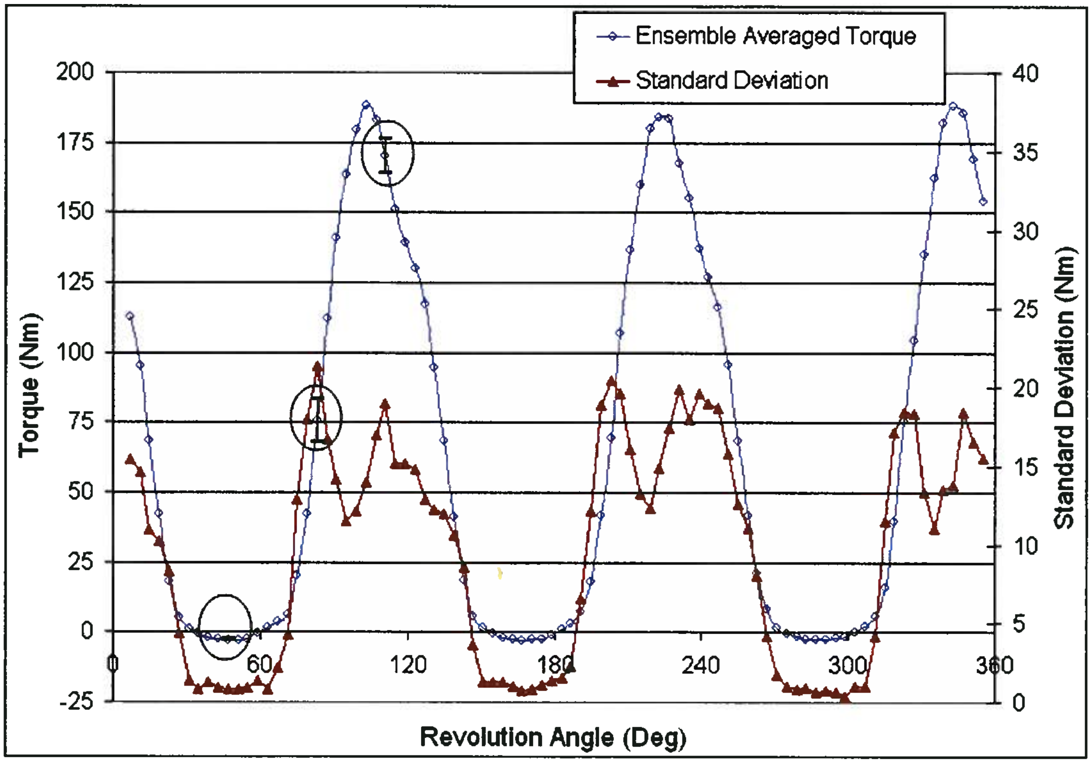

Figure 4-2: Standard Deviation and Torque vs. Revolution Angle for a free-stream device with gearbox drive-train at 2 m/s and TSR=2.5 (N ~ 52).

Figure 4-3 provides a similar plot for the free-stream device using the chains and sprockets drive-train at 2 m/s with TSR=2.25. The combination of dampening from the chains and sprockets system, as well as lack of play in the coupling, significantly reduces the standard deviation values to be consistently less than 4, though the peak torque values have also been decreased by a factor of approximately 3 from the gear-box drive-train case.

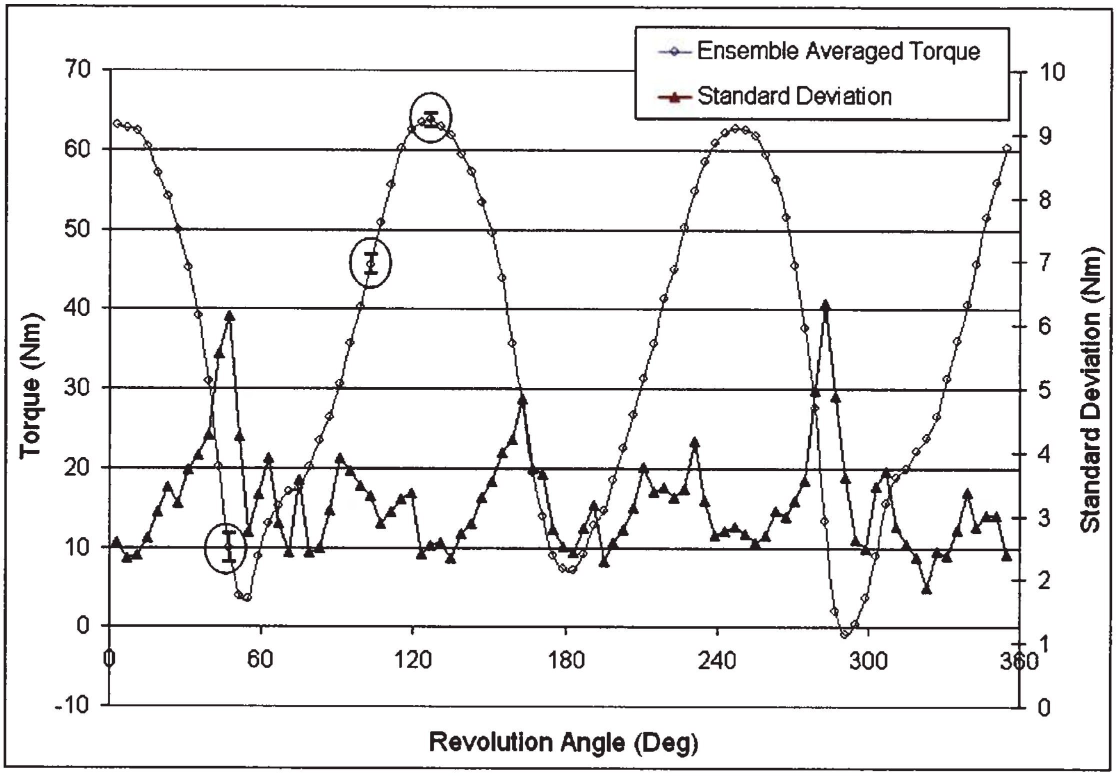

Figure 4-3: Standard Deviation and Torque vs. Revolution Angle for a free-stream device with chains/sprockets drive-train at 2 m/s and TSR=2.25 (N ~ 33).

Lastly, for the case with ducting and gearbox drive-train (Figure 4-4), the reduced torque fluctuations also lead to reduced standard deviations. In this case, the standard deviation is consistently less than 3, with peak torque values ranging up to approximately 80 Nm. The standard deviation above is used to create error bars in efficiency plots when comparing with theory (Section 4.2.2).

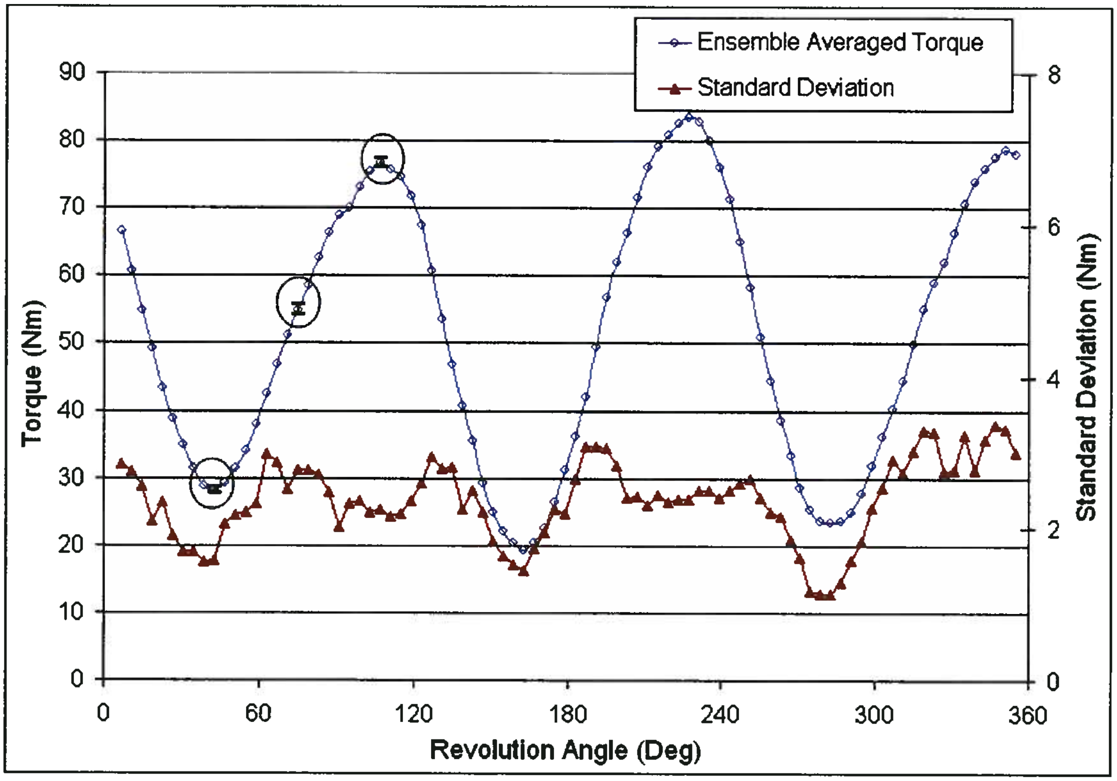

Figure 4-4: Standard Deviation and Torque vs. Revolution Angle for a ducted device with gearbox drive-train at 1.5 m/s and TSR=3 (N ~ 45).

4.1.2 Run Repeatability

Given the time constraints due to working in the towing tank facility and the number of parameters requiring investigation, it was not possible to conduct a large number of repeated runs for completion of a comprehensive statistical analysis. Table 4-2 below compares Ck values for repeated runs using the gearbox drive-train for both free-stream (arm profiles B and C) and ducted tests. The percent difference between a series of runs completed at a given set of conditions and their respected mean is provided.

For free-stream runs, 18 of the 29 repeated runs have a percent difference of less than 1% in magnitude from their respective mean value. 6 of the 29 are between 1-2%, while the remaining 5 values are between 2-4%. This repeatability is acceptable considering carriage speed, torque, and revolution speed are all being recorded and used for the calculation of the Ck value. Examining the ducted device, 75% of the points have a percent differences less than 2%, with the remaining points having differences of 2.74% -

4.2%. A larger error for the ducted device is reasonable given the size of the duct being towed through the water resulting in large disturbances in the flow and increased forces, and thus flexing, on the mounting structure. Runs noted as being in the opposite direction were performed towards the wavemaker instead of the dock so as to investigate consistency between directions. This enabled runs with duct deflectors upstream of the turbine to be performed without having to move deflectors from the downstream position.

Table 4-2: Gearbox drive-train repeated run percent variation in Ck.

	Run #	Speed (m/s)	Nominal TSR	Ck	% Difference*	
Free-Stream Arm Profile B	15	1.5	2.25	0.109	0.66%	
	112	1.5	2.25	0.107	-0.66%	
	16	1.5	2.50	0.120	-3.13%	
	113	1.5	2.5	0.128	3.13%	
	17	1.5	2.75	0.100	-2.03%	
	114	1.5	2.75	0.105	2.03%	
	33	2	2.25	0.131	-0.06%	
	116	2	2.25	0.132	0.06%	
	34	2	2.50	0.139	0.59%	
	117	2	2.5	0.138	-0.59%	
	35	2	2.75	0.115	0.02%	
	118	2	2.75	0.115	-0.02%	
Free-Stream Arm Profile C	203.1	1.5	2.25	0.208	0.26%	
	203.2	1.5	2.25	0.209	0.76%	
	203.3	1.5	2.25	0.206	-1.02%	
	204.1	1.5	2.5	0.254	-1.25%	
	204.2	1.5	2.5	0.254	-1.01%	
	204.3	1.5	2.5	0.267	3.96%	
	204.4	1.5	2.5	0.253	-1.70%	
	213	2	2.25	0.219	0.88%	
	213.1	2	2.25	0.214	-1.46%	
	213.2	2	2.25	0.217	0.33%	
	213.3	2	2.25	0.217	0.24%	
	214	2	2.5	0.277	0.39%	
	214.1	2	2.5	0.276	-0.13%	
	214.2	2	2.5	0.277	0.26%	
	214.3	2	2.5	0.272	-1.28%	
	214.4	2	2.5	0.276	0.06%	
	214.5	2	2.5	0.278	0.69%	
Ducted Arm Profile C	482	1.5	2.25	0.239	0.68%	
	622	1.5	2.25	0.236	-0.68%	
	483	1.5	2.5	0.354	-1.88%	
	623	1.5	2.5	0.368	1.88%	
	484	1.5	2.75	0.441	-2.74%	
	624	1.5	2.75	0.455	0.45%	
	501	1.5	2.75	0.461	1.72%	
	502	1.5	2.75	0.456	0.56%	opposite direction
	485	1.5	3	0.473	3.01%	
	625	1.5	3	0.467	1.60%	
	503	1.5	3	0.458	-0.42%	
	504	1.5	3	0.440	-4.19%	opposite direction

* calculated as (Run-Mean)/Mean for each condition

Table 4-3 below compares Ck values for sample free-stream runs repeated with the chains and sprockets drive-train. Percent differences are on the order of 1% from the mean values, though a slightly higher variation may be expected than above due to the flexing in the chain and sprockets system.

Table 4-3: Sample chain/sprockets drive-train repeated run percent variation in Ck

Run #	Speed (m/s)	Nominal TSR	Ck	% Difference*
1045	1.5	2.5	0.1284	0.73%
1045b	1.5	2.5	0.1266	-0.73%
1085	2	2.5	0.1367	-1.03%
1085b	2	2.5	0.1395	1.03%

* calculated as (Run-Mean)/Mean for each condition

Just as Ck values should be equal for each run at the same conditions, torque curves should also match over a revolution cycle. Figure 4-5 provides torque vs. revolution angle for repeated runs at 1.5 m/s and TSR=2.5, while Figure 4-6 and Figure 4-7 provide Cartesian and polar plots respectively of repeated runs at 2 m/s, TSR=2.5. It is evident that the peak locations are very repeatable, providing consistent knowledge on which regions of a revolution are in need of performance enhancement. The polar plot is a nice visualization tool, accentuating that torque is generally created as a blade passes across the flow upstream of the turbine.

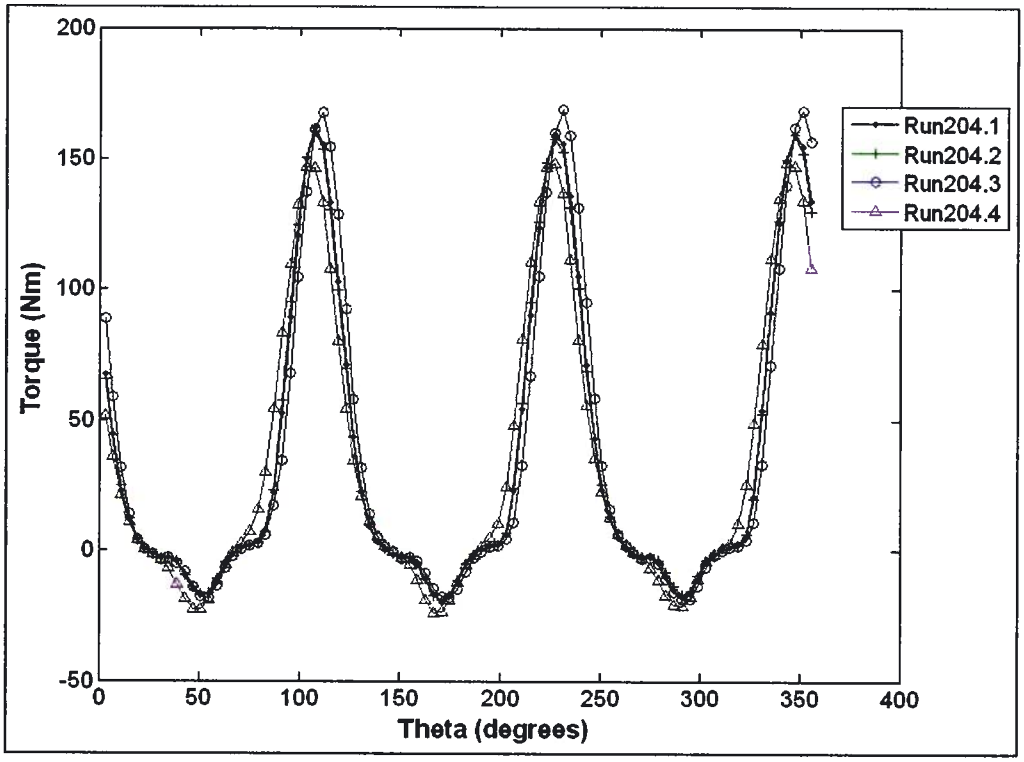

Figure 4-5: Torque vs. Revolution Angle for repeated runs with gearbox drive-train at 1.5 m/s, TSR=2.5 (arm profile C).

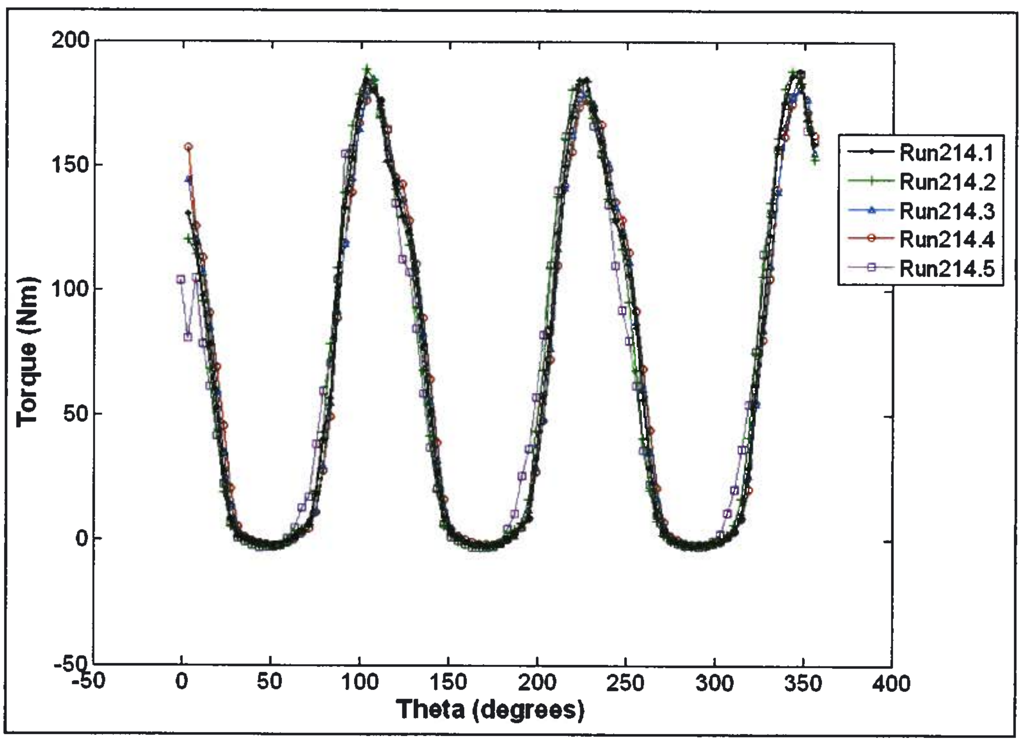

Figure 4-6: Torque vs. Revolution Angle for repeated runs with gearbox drive-train at 2 m/s, TSR=2.5 (arm profile C).

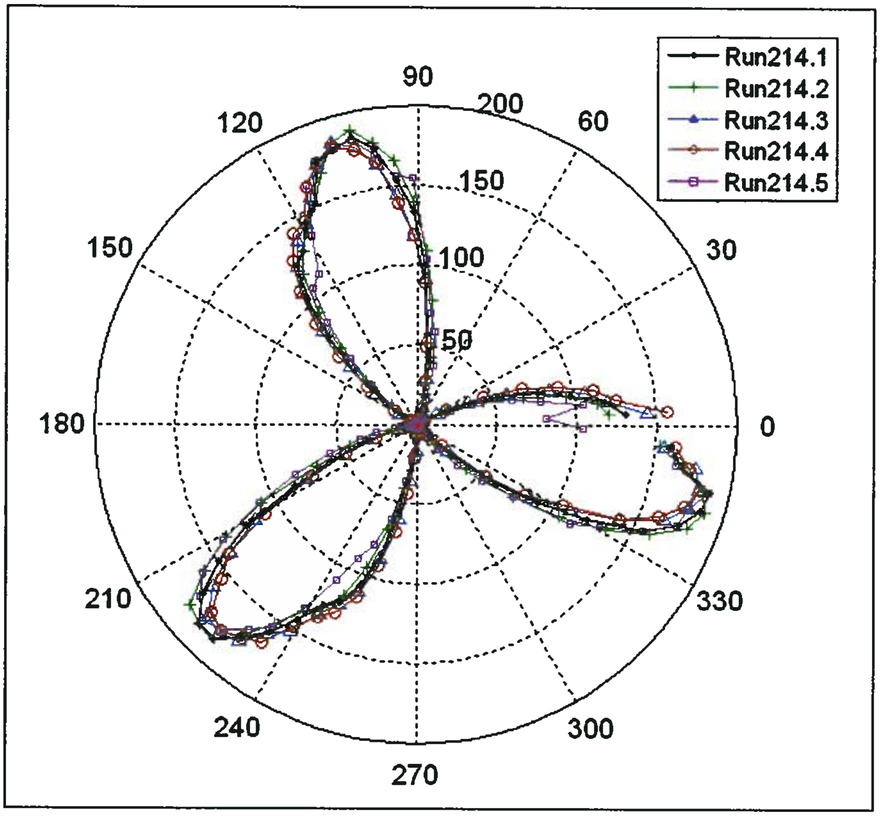

Figure 4-7: Polar plot of Torque vs. Revolution Angle for repeated runs with gearbox drive-train at 2 m/s, TSR=2.5 (arm profile C).

Figure 4-8 provides torque curves for the ducted configuration, again highlighting repeatability of the system. It is particularly impressive considering tests were conducted on different days amongst configuration changes. Lastly, Figure 4-9 provides repeated runs with the chains and sprockets drive-train for TSR=2.5 at speeds of 1.5 and 2 m/s. Again, repeatability is reasonable given the flexibility in the chain and sprockets drive-train, and flexing of the force balance.

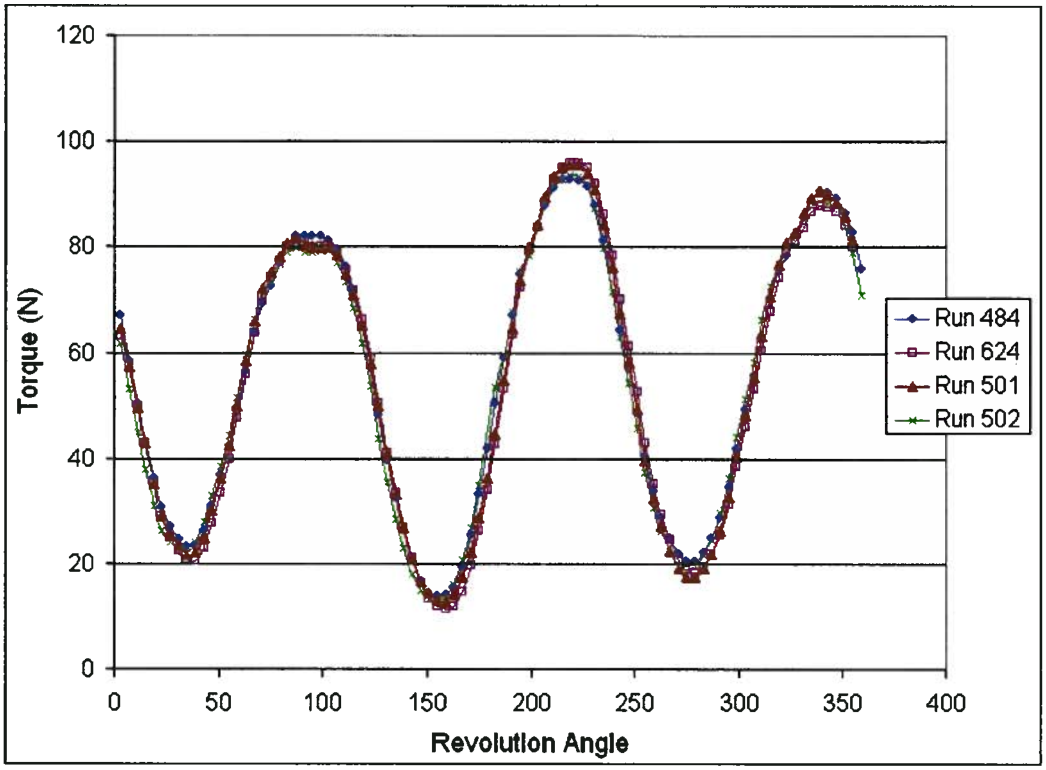

Figure 4-8: Torque vs. Revolution Angle for ducted repeated runs with gearbox drive-train at 1.5 m/s, TSR=2.75.

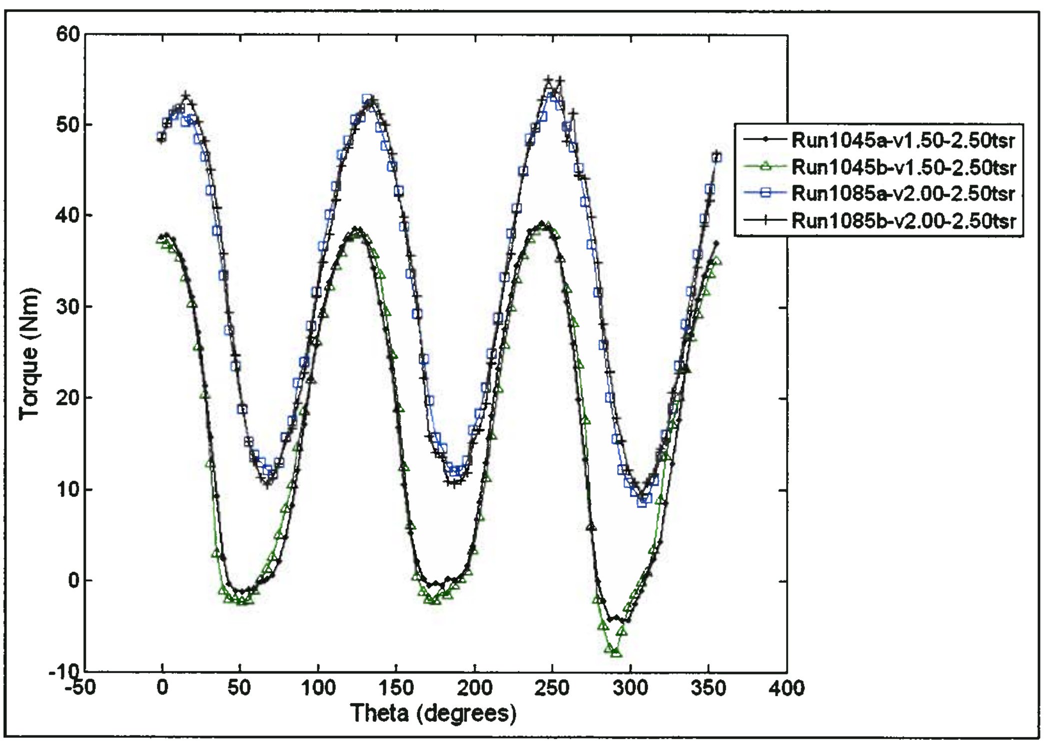

Figure 4-9: Torque vs. Revolution Angle for repeated runs with chains/sprockets drive-train at 1.5 and 2 m/s, TSR=2.5 (arm profile B).

4.1.3 Revolution Speed Variation

When comparing to numerical predictions, it was observed that the peak torque locations were phased to a higher revolution angle than expected (discussed further in Section 4.2.2). Data examination revealed a fluctuating revolution speed due to the torque being generated. This is illustrated in Figure 4-10 for runs at 1.5 m/s at varying TSR values with the chains and sprockets drive-train. The revolution speed (rpm) provided is representative as it is a spline fit through the multiple data points based on very small sampling periods; however, it provides insight into what is occurring. Additionally, as RPM and torque are being plotted vs. revolution angle, any average taken from this plot will be artificially increased compared to the true average over time of the run. When plotted against time, less time is spent at the angles with higher torque generation and revolution speed; however, when plotting against revolution angle equal weighting is given to all points in the revolution, skewing the average. Averages displayed in the legend provide the true average revolution speed when taken over the time duration of the run. It is interesting to note that the peak revolution speed typically occurs earlier in the rotation, or closer to 90° as one may expect. As the motor controller responds to the increasing rpm, it acts as a brake and the torque continues to increase for another 25° or so as the turbine is slowed. This process is repeated for all TSR values.

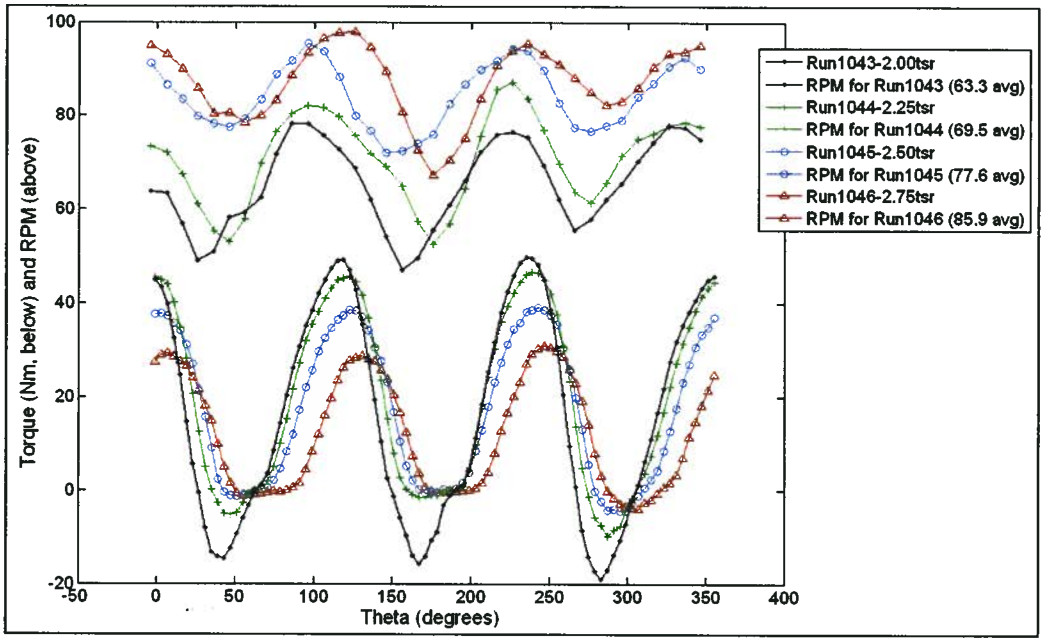

Figure 4-10: Torque (below) and RPM (above) vs. Revolution Angle for runs with chains/sprockets drive-train at 1.5 m/s.

Hypothesizing that the chains and sprockets drive-train, as well as the flexing in the load cells, was adding to the cause of the revolution speed fluctuation, the chain and sprockets drive-train was replaced with a gearbox and the bottom force-balance plate was fixed firmly to the carriage. Figure 4-11 provides the resulting revolution speed and torque values recorded at the same condition as in Figure 4-10 (profile B arms, 1.5 m/s). Much higher peaks were recorded with torque sensor and coupling attached directly in-line with the shaft, and though the revolution signal was much cleaner, fluctuations still occurred on the order of +/- 15-20% of the target value. Given the magnitude of these fluctuations (ie. from -60 Nm to 90 Nm at a frequency of 3 Hz for TSR=2.0), it is not surprising that these fluctuations occurred. Again, the maximum revolution speed peaks appeared closer to 90° where maximum torque was expected, and the subsequent torque peak appeared approximately 25° later.

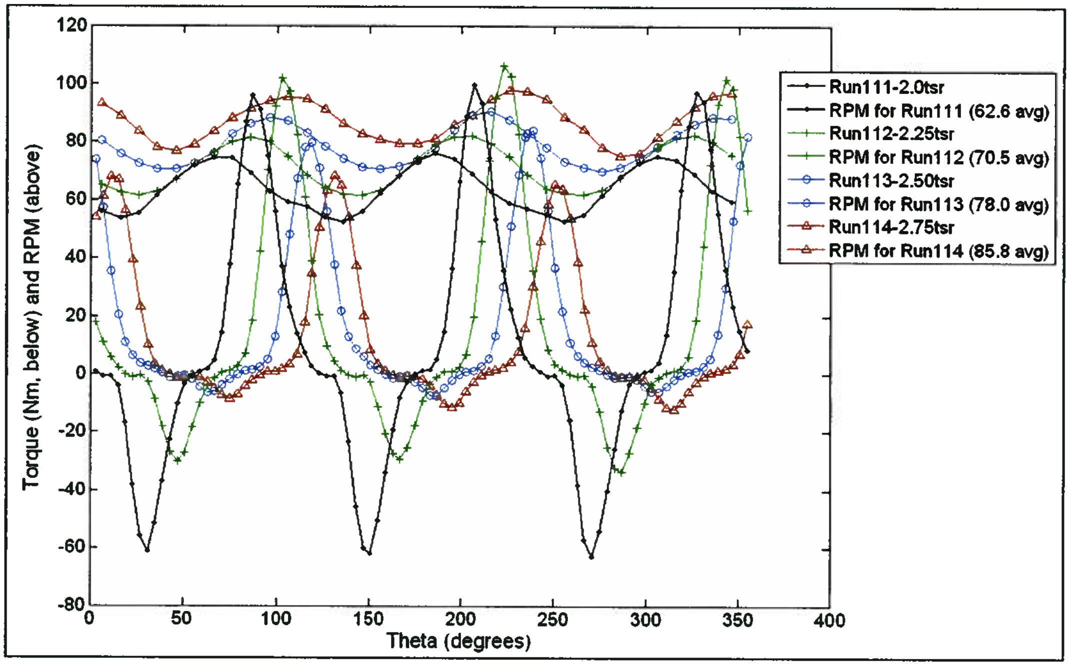

Figure 4-11: Torque (below) and RPM (above) vs. Revolution Angle for runs with gearbox drive-train at 1.5 m/s.

Not surprisingly, the observed reduction in torque ripple when using ducting also corresponded to a reduction in revolution speed fluctuations. Figure 4-12 provides torque curves for the ducted turbine at 1.5 m/s, while Figure 4-13 provides revolution speed vs. revolution angle for the same runs. Worth noting are the way the revolution speed mimics the torque ripple at TSR=1.5, indicating that revolution and torque ripple are closely tied. Secondly, it is interesting to note that the drop in torque ripple at TSR=2.75 greatly reduces the revolution speed fluctuations (ie. from approximately +/- 29% at TSR=2.5 to +/- 8% at TSR=2.75). Importantly, with the reduction in revolution speed fluctuations, the position of the peak also shifts back in revolution angle from 103° to 95°. It has been demonstrated that in the absence of external factors, an increase in TSR value shifts the torque peak to increasing angle of revolution; however, due to the reduction in torque speed fluctuations and revolution speed fluctuations, in this case the torque peak has shifted to the left with the increase in TSR. This is strong evidence that the revolution speed fluctuations are responsible for a phasing of the torque curve when comparing with numerical predictions, with the largest torque fluctuations leading to a peak phase shift of 20-25°.

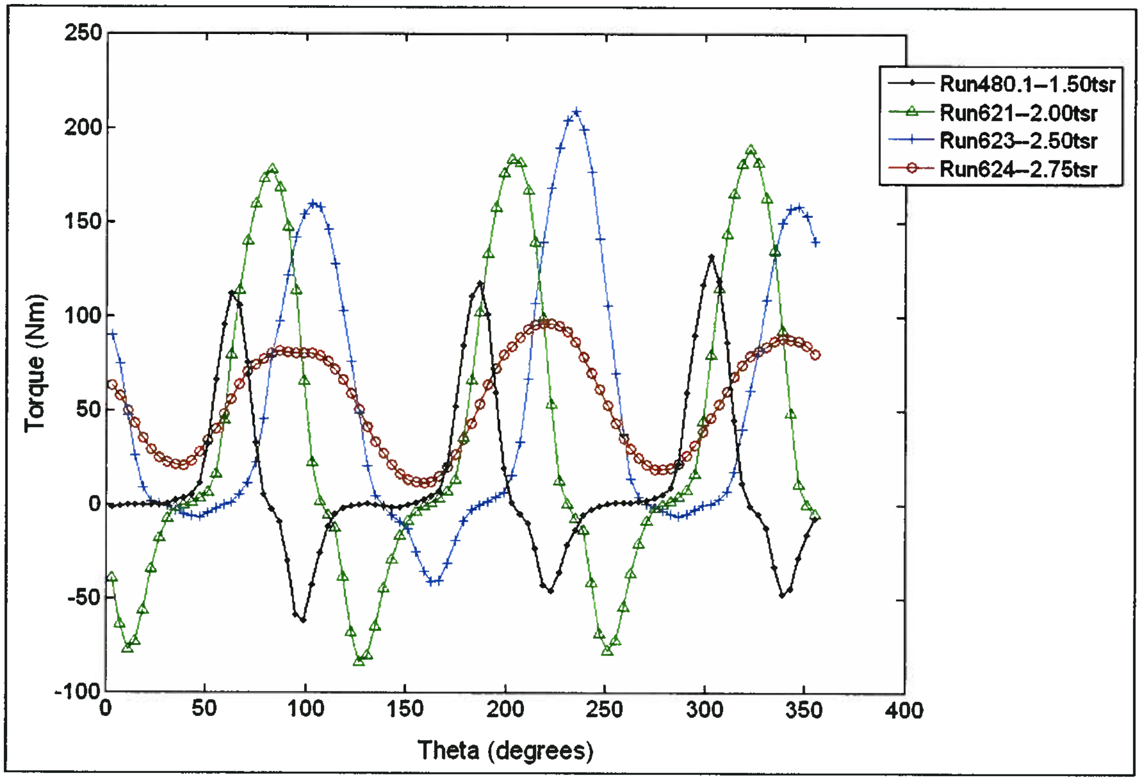

Figure 4-12: Torque vs. Revolution Angle for ducted device at 1.5 m/s.

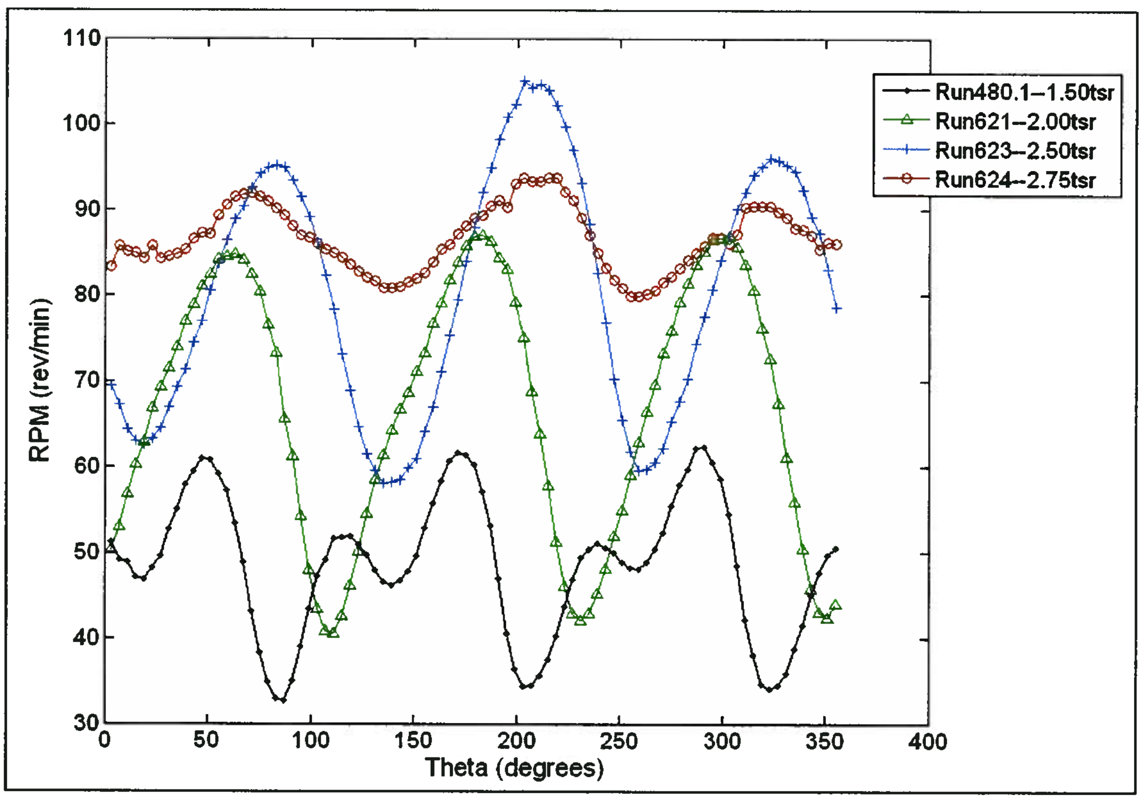

Figure 4-13: RPM vs. Revolution Angle for ducted device at 1.5 m/s.

Additionally, with the revolution speed fluctuations, torque values observed will be less than the peak torques that would exist in a constant revolution speed system, as some of the torque will have gone into accelerating the turbine revolution speed.

4.2 Comparison with Numerical Predictions

Below, an overview of the numerical model used for comparison to theory is provided. This is followed by a comparison of experimental and numerical Ck values and torque curves.

4.2.1 Numerical Model Overview

The numerical model used for comparison to experimental results was developed by Nabavi [28] using the commercial RANS code FLUENT. A two-dimensional, incompressible, unsteady solver was used in conjunction with a Spalart-Allmaras turbulence model. An extensive examination into grid density was also conducted, and a fine structured grid around the blades contained within a sliding unstructured ring in way of the turbine blades was used (Figure 4-14). This combination of parameters provided the best compromise between accuracy, computational cost and reliability, though it still took upwards of two weeks to run a ducted turbine simulation. Lastly, domain size was also examined to ensure that the blockage ratio in the 2D simulations (same percent as 3D blockage in the experiments) was consistent with free-stream results. For the free-stream device, this corresponded to 8% blockage, and for the ducted device this corresponded to 18%. Extensive discussion on the numerical model is beyond the scope of this thesis, and details may be found in the referenced document [28]. Figure 4-15 provides a sample output from a simulation highlighting velocity contours at a TSR=2 and free-stream velocity of 1 m/s.

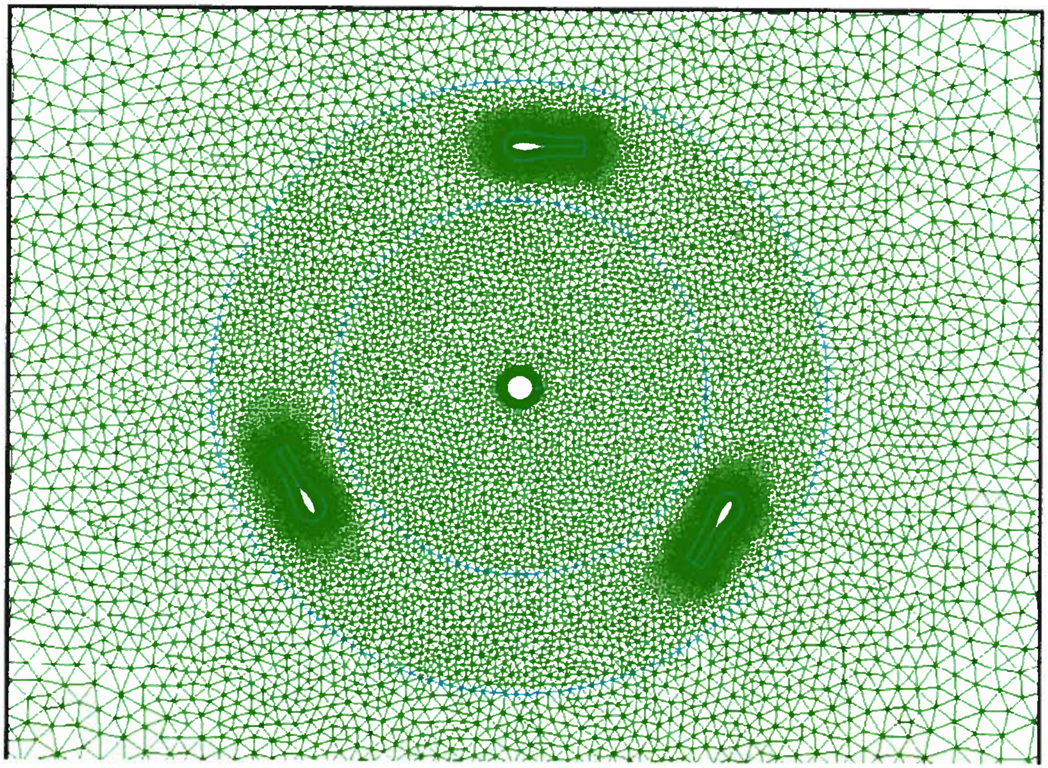

Figure 4-14: Sample grid around the blades and shaft.

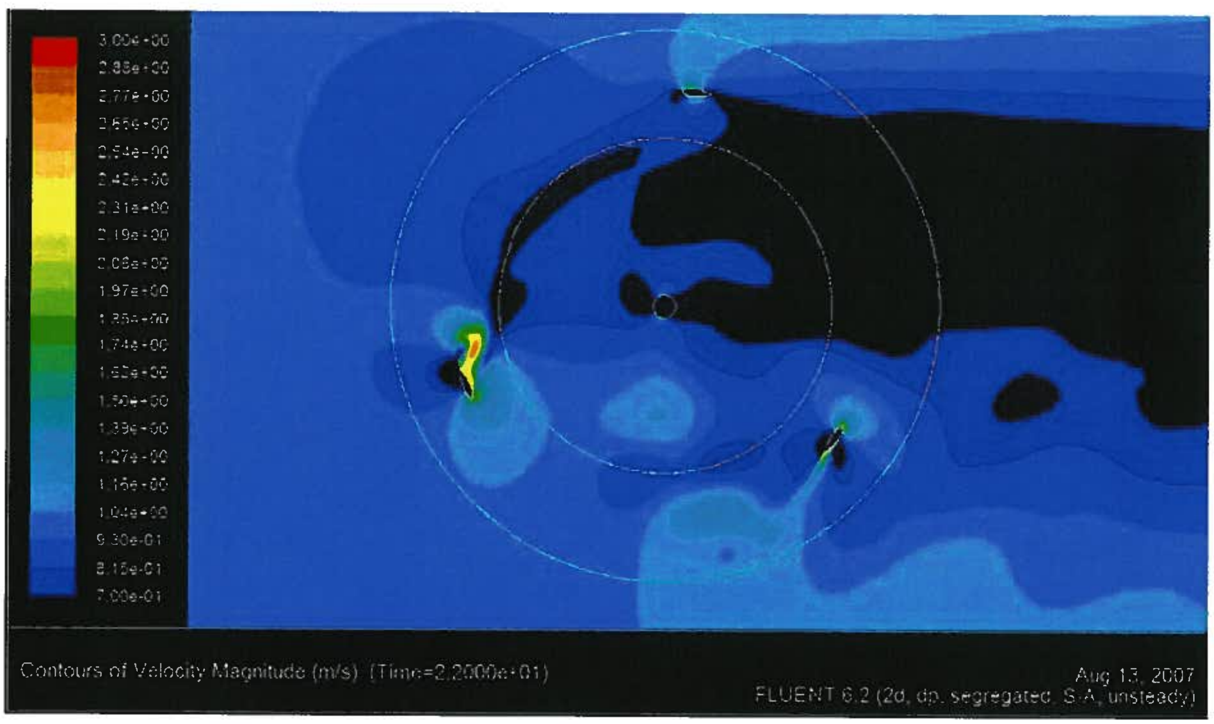

Figure 4-15: Sample velocity contours for a simulation at 1 m/s with TSR=2.

4.2.2 Comparison of Results

Firstly, given the 2-dimensional nature of the numerical models, arm effects were not simulated and must be extracted from the numerical results. Figure 4-16 provides the experimental Ck values obtained for tests with arm profile C without blades to examine power absorbed in the bearings and parasitic arm drag, which were subsequently added to the CFD simulation efficiencies for comparison with experimental data.

Figure 4-17 and Figure 4-18 provide Ck vs. TSR comparing the numerical and experimental results for the free-stream and ducted device. Ck values from the experiments with only arms have been added to the numerically predicted Ck to facilitate comparison. Error bars shown for the experimental tests are a combination of the maximum 95% CI calculated from the standard deviations from the appropriate representative torque curve Section 4.1.1 plus the potential error due to the 1.5 Nm uncertainty from the torque sensor. It should be noted that this is likely an over-estimate of the error, as the maximum standard deviation for one location on the torque curve was assumed to be applied to the average torque for that condition. Errors on the Fluent prediction are from the 1.5 Nm uncertainty in the torque sensor when adding the experimental negative Ck due to the arms.

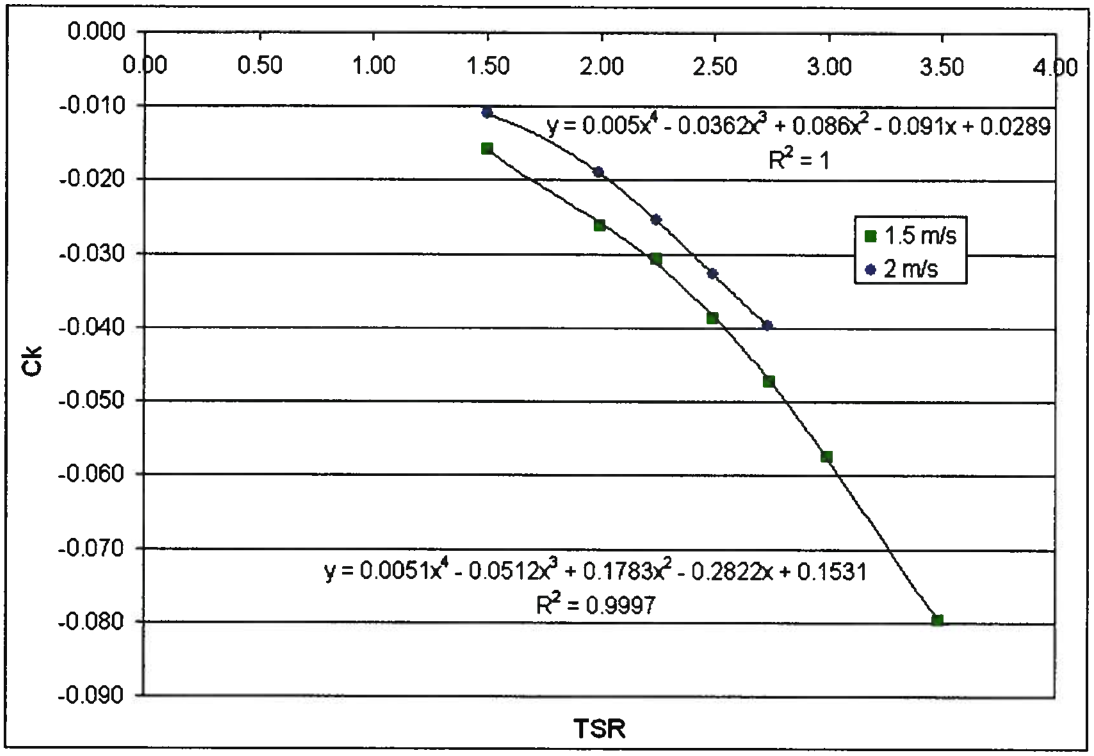

Figure 4-16: Experimental Ck vs. TSR for arm profile C at 1.5 and 2 m/s.

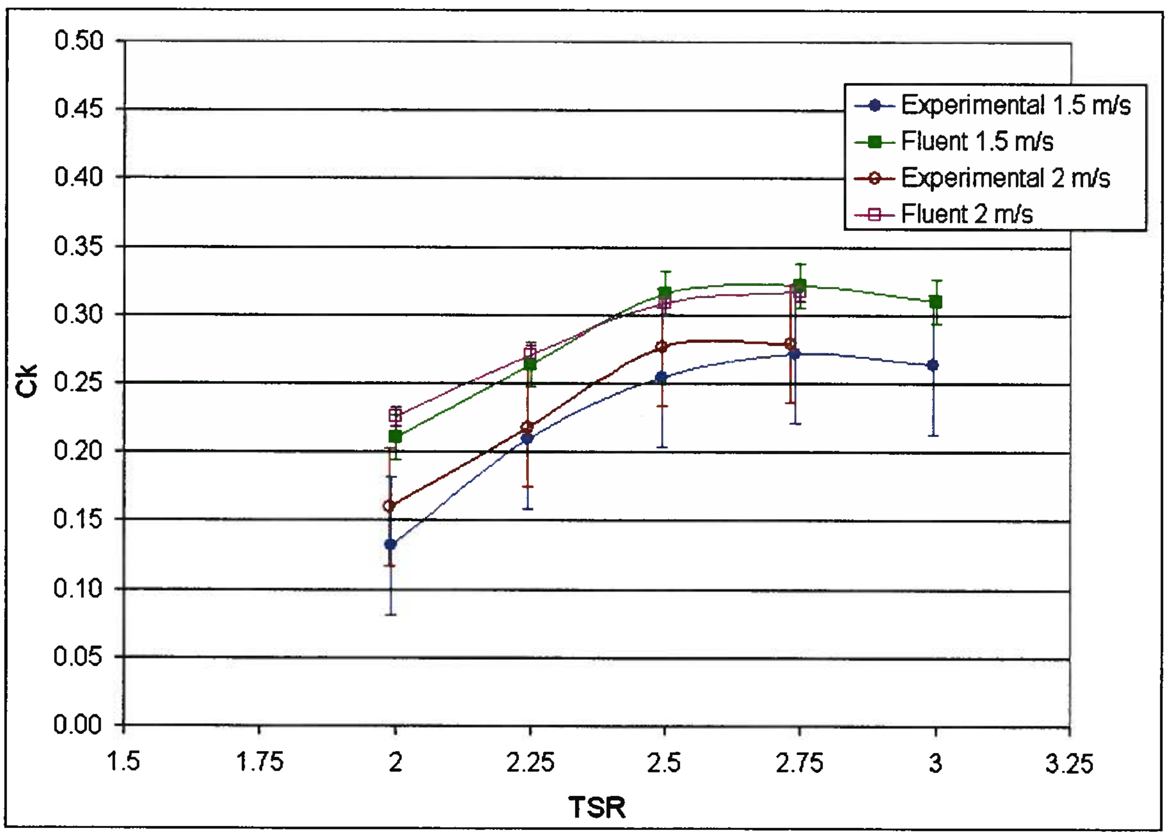

Figure 4-17: Ck vs. TSR for free-stream comparison of experimental and numerical results.

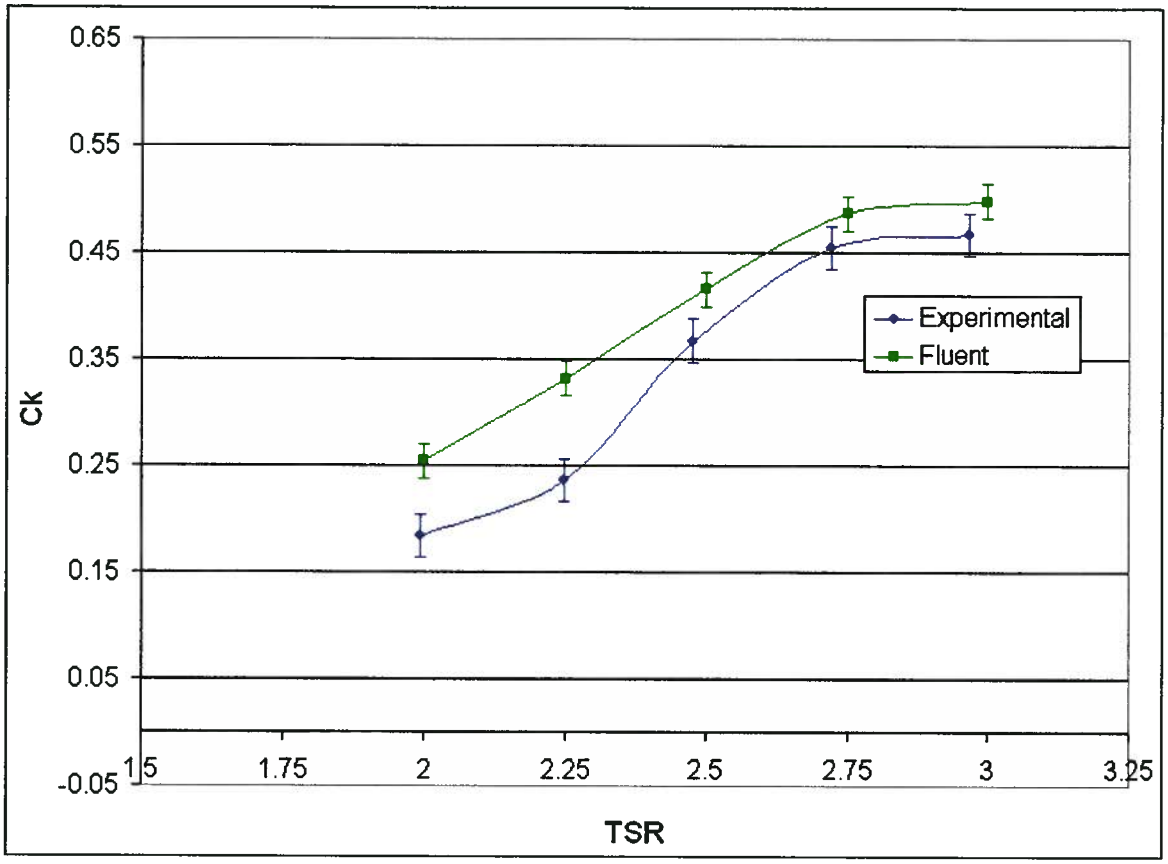

Figure 4-18: Ck vs. TSR for ducted comparison of experimental and numerical results at 1.5 m/s.

The figures above illustrate reasonable agreement between experimental performance and the numerical simulations. The discrepancies observed are likely due to a combination of both experimental and simulation errors. Experimental errors affecting the accuracy of the results are outlined in Section 4.3 below. Though a detailed discussion on potential sources of error in the simulations is beyond the scope of this report and is discussed in detail by Nabavi [28], factors to consider include:

- Turbulence modeling difficulties (including capturing dynamic stall)
- 2-dimensional simulations vs. 3-dimensional experiments
- Inability to fully correct for lost power due to arms and bearings by subtracting results of tests without blades for Ck comparisons
    - Flow disturbance created by the arms reducing lift generated by the foils

- Upon removing the blades, bolt heads and other attachment components creating drag also get removed
- Lost lift on the blades in way of the arm attachments

- Trailing edge of blades in experiments was cropped for manufacturing purposes
- Truncation and round-off errors during simulation calculations

These same factors will also affect torque curve plots. Figure 4-19 and Figure 4-20 compare experimental torque curves (gearbox drive-train with arm profile C at ends only) with Fluent torque curves for the free-stream device. As discussed above, the experimental torque peaks are phased from the theoretical positions due to revolution speed variation. Fluent also predicts shorter, wider peaks, and the lashing in the coupling as the torque transitions through zero is visible in the experimental data.

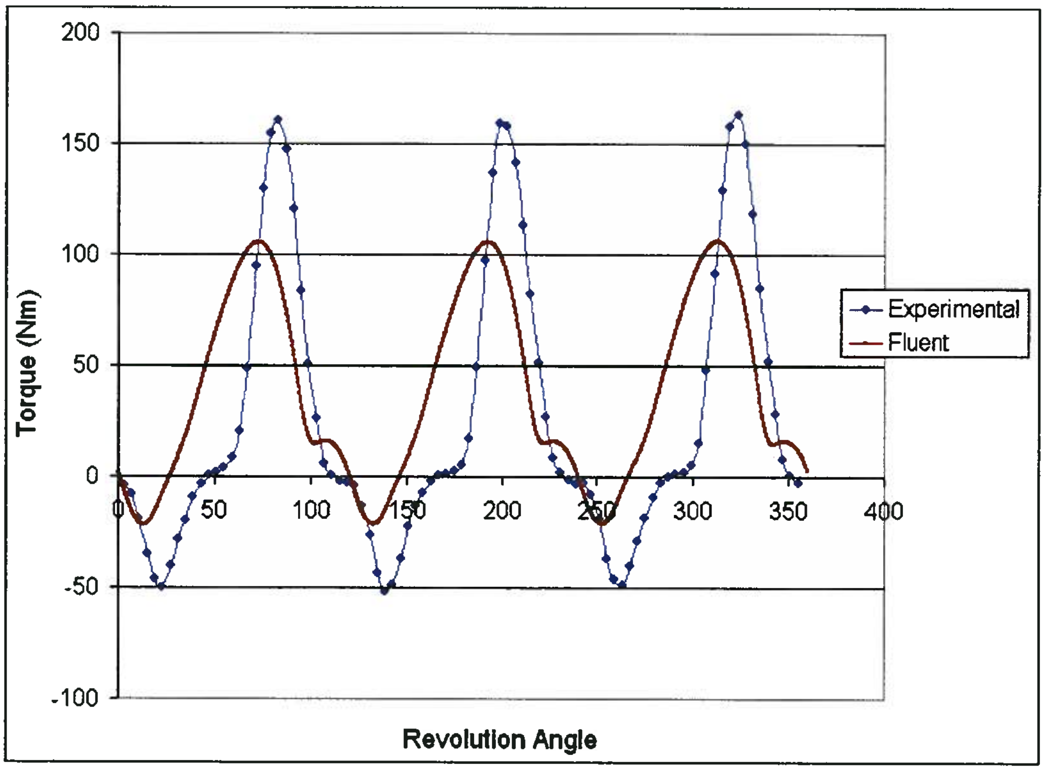

Figure 4-19: Torque vs. Revolution Angle comparing free-stream experiments and Fluent at 1.5 m/s and TSR=2.

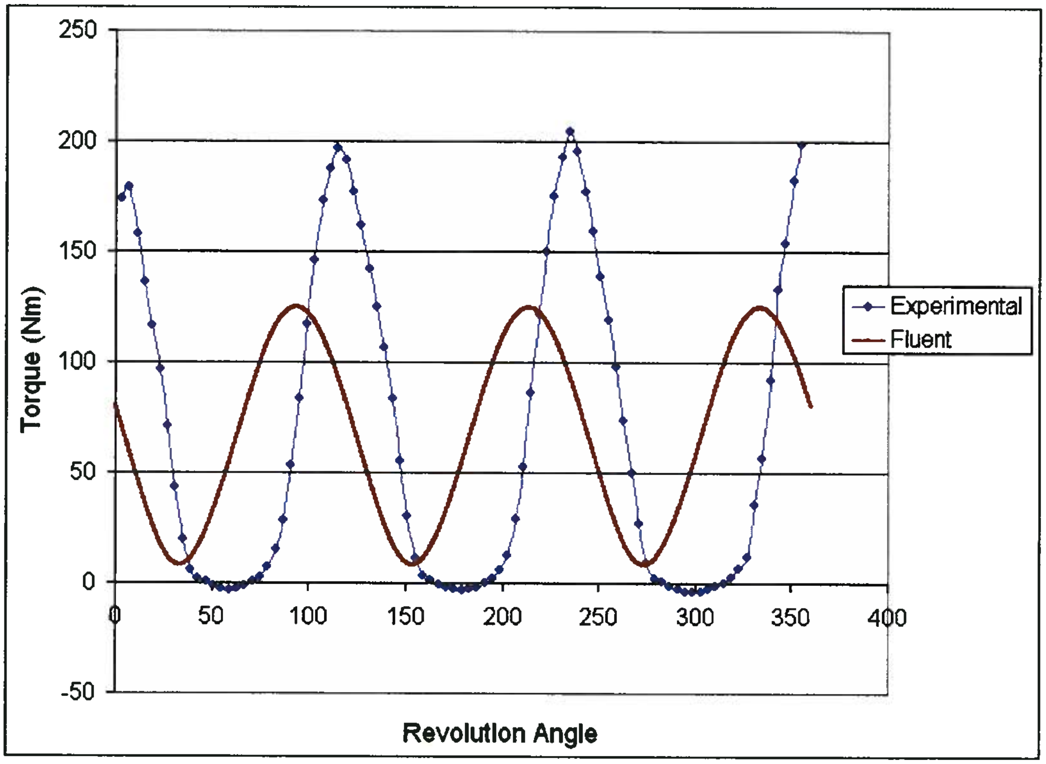

Figure 4-20: Torque vs. Revolution Angle comparing free-stream experiments and Fluent at 2 m/s and TSR=2.75

Comparing ducted experimental results to the simulations, Figure 4-21 (v=2 m/s, TSR=2) again displays phasing between the expected torque peaks and experimental torque peaks, along with more extreme and narrower peaks. Figure 4-22 compares results for a TSR value of 2.75, which as demonstrated above provides a significant decrease in torque ripple and revolution speed fluctuations for the ducted case. Significantly, this decrease in torque ripple (which is also predicted numerically), and consequently revolution speed fluctuations, aligns the peaks of the two data sets very nicely. In this case, phasing is only approximately of 6° instead of the typical 20°-25° degrees. This confirms that the torque ripple and corresponding revolution speed fluctuations are the cause of the peak phasing. Also interesting to note is that the predicted and experimental peaks have similar shapes now that the torque curve does not pass through zero. This is indicative that the play in the coupling may be contributing to a backlash effect, leading to recording of higher and narrower peaks than what would be nominally occurring.

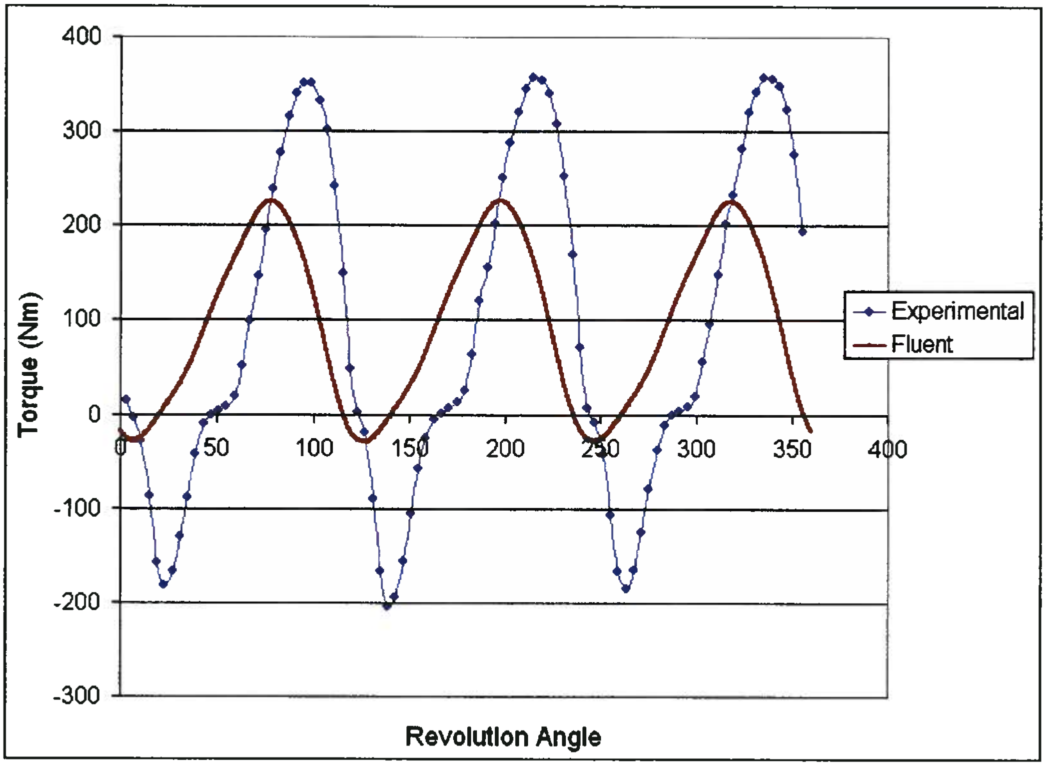

Figure 4-21: Torque vs. Revolution Angle for a ducted turbine at 2 m/s and TSR=2.

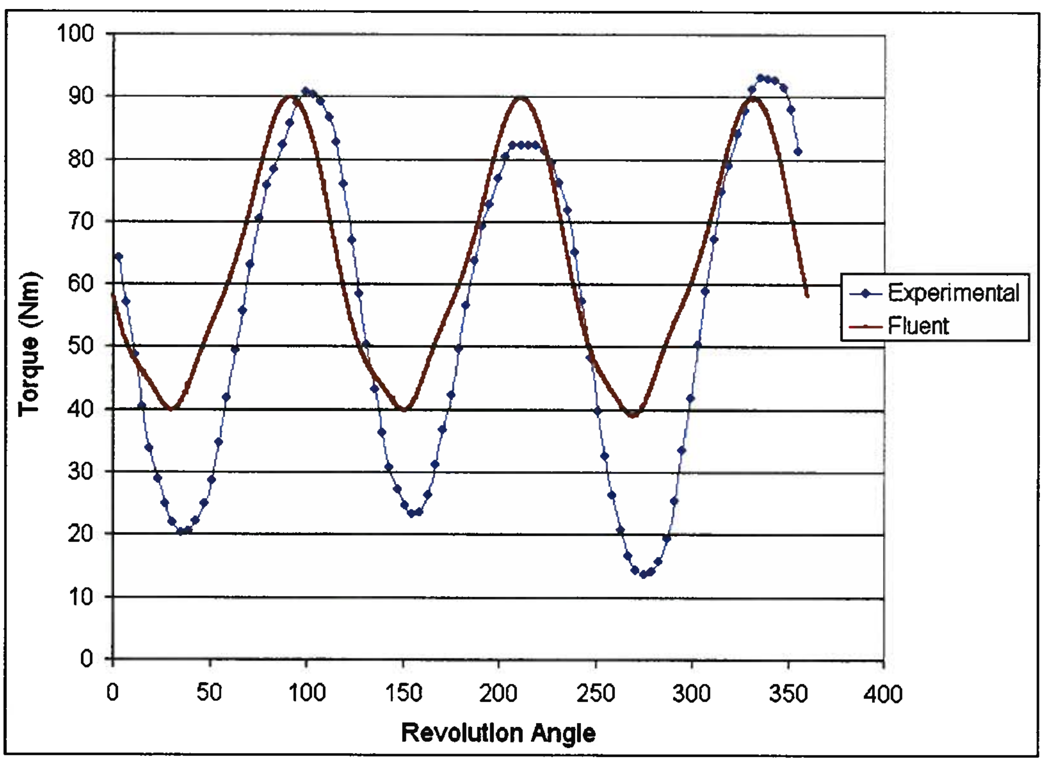

Figure 4-22: Torque vs. Revolution Angle for a ducted turbine at 1.5 m/s and TSR=2.75.

Lastly, Figure 4-23 compares drag force for the experiments and Fluent at 2m/s and TSR=2.75, with torque being displayed below. Given the number of assumptions in the procedure above for balancing moments to record drag and the assumed accuracy on the order of 20%, the results are in good agreement. The average predicted by Fluent is 1290 N, while the average from the experiments is 1325 N. Two significant factors that will raise both averages in the true application are as follows:

- The Fluent simulation does not include shaft drag (predicted to be approximately 155 N)
- When drag was being recorded, the turbine used arm configuration B at the quarter-chord positions, and hence more lift will be generated in an optimized design increasing the drag component on the turbine.

It is also significant that the drag peak position aligns well with both the theoretical torque peak, as well as the theoretical drag peak. This is correct given that at an angular position, drag reading will be independent of the torque reading, which is directly affected by the motor control and phased due to the fluctuating revolution speed.

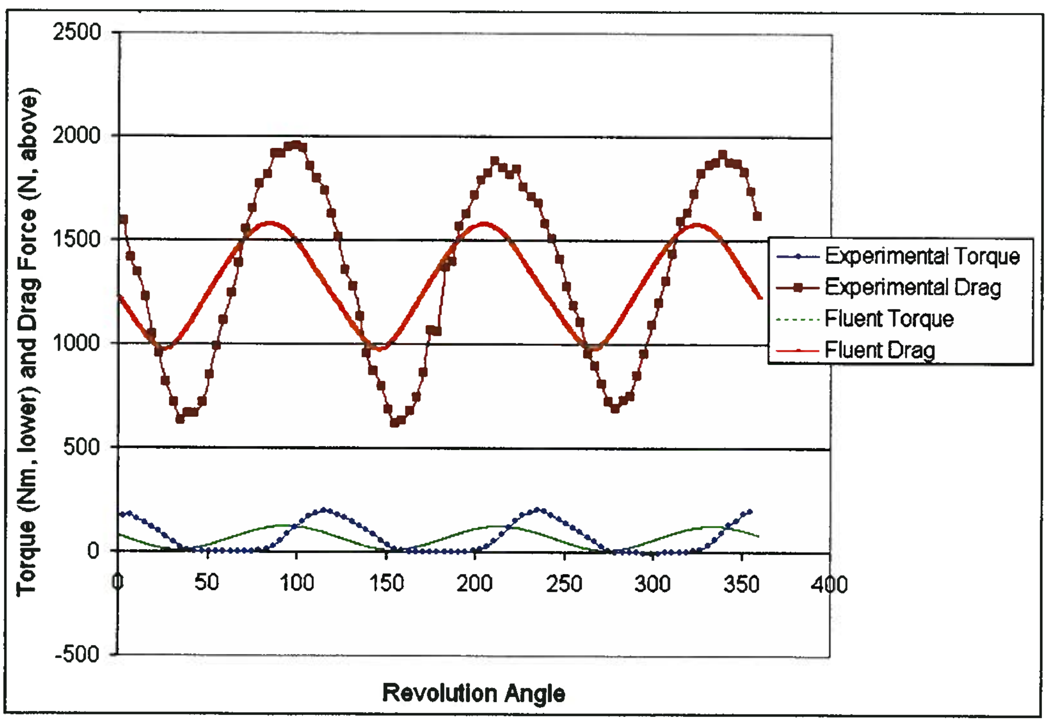

Figure 4-23: Drag Force and Torque vs. Revolution Angle for free-stream Fluent and experiments at 2 m/s and TSR=2.75.

4.3 Sources of Error

In addition to the revolution speed variation that appears to artificially phase the peak in the torque curves up to approximately 25°, additional sources of error include:

- Backlash in the flexible spider coupling used with the gearbox drive-train is potentially affecting the results in two ways:
  - When torque is transitioning through zero a "bucketing" is observed in the torque curve, which should have a much rounder profile.
  - When the play in the coupling re-engages, there is likely a "slamming" effect that creates a narrower torque curve than what would actually occur, with a larger maximum height.
- Considering runs with the chains and sprockets drive train, inertial effects of the sprockets on the lay-shaft torque sensor appear to be dampening out the maximum and minimum torque values.
- Free-surface interactions are an additional potential source of error. With the given time constraints and associated difficulty in producing a structure rigid enough to tow through the tank, the turbine was placed at a depth believed to be deep enough yet still facilitating the structural setup required. After a few seconds of spinning the turbine in a stationary position, disturbance was observed at the free surface; however, with the moving device the accumulation of vortices, and thus large interactions, would be minimized. Waves created by the shaft and surrounding frame as the device was being dragged may also potentially affect the results, though these small variations in pressure are expected to cause error of magnitude well below (if any at all) others identified in the system. Lastly, the comparative nature of these tests examines each parameter under equivalent conditions to observe its effect.
- Blockage of the tank must be considered when extrapolating the results to true free-stream conditions. This would most likely occur with the ducted device, given the 18% blockage of the cross-sectional area of the tank. 2-dimensional simulations revealed blockage should not have a large effect on the result [28]; however, predicted decreases in Ck of 18% and 11% for blockages of 17% and 7.5% respectively when moving to a free-stream condition were predicted by

Bahaj et al. [29] using actuator disk theory for a horizontal device without ducting.

- The angular encoder seemed to wander about 1° or 2° after each run. This is believed to be due to skipping of increments, or truncation error upon digital-analog signal conversion, but was easily managed by resetting the angular position and encoder before each run.
- The method of assuming a centre of force and balancing moments for drag force estimation could likely lead to errors on the order of +/- 20%. Additionally, initial readings on the load cells were tared out before each run; however, settling after the previous run led to variation in the initial readings, and if the force balance system settled in an odd manner this may also introduce error to the measurement. Given the large number of unknowns, one must consider a possible error as large as 25%, though 10% is likely more reasonable.

4.4 Sample Application

From the findings above, it is possible to develop a sample device for the purpose of replacing diesel generators used to power remote communities. Using dwelling and power usage statistics from the B.C. Hydro Remote Community Electrification Program [30], a device capable of producing 257 000 kWh per year was targeted. At 15 000 kWh per year estimated usage per dwelling, this is sufficient for approximately 17 homes. Multiples of these units (ie. for 34, 51, and 68 homes) are consistent with the larger communities targeted for power generation by B.C. Hydro.

A power coefficient of 0.45 was assumed using a ducted device with deflectors and is suitable for the purpose of this exercise. It is likely that a higher value may be achieved through further optimization of the duct and foil, though transmission losses must also be considered. Tidal data for Quatsino Narrows in Northern Vancouver Island was used to assess extractable power from the current. This is considered to be a moderate-high resource, and tidal data is provided in Figure 4-24. Power generation was assumed to begin at a current velocity of 1.5 m/s (minimal extraction is available below this speed), and to cut off at current speeds greater than 3.84 m/s due to structural and cavitation limitations. Generator selection has not been performed as part of this application exercise.

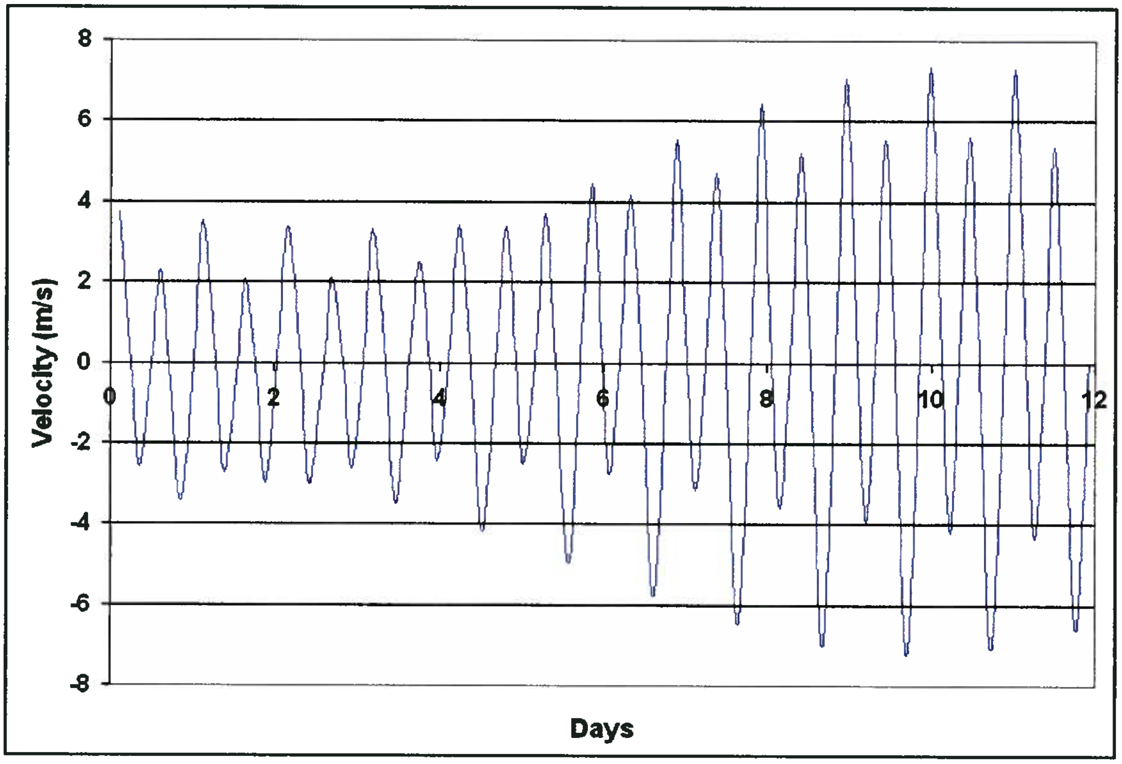

Figure 4-24: Tidal current data.

The resulting rotor required was a 3.375m x 3.375m device assuming an aspect ratio of one, which is suitable for the forces anticipated. Figure 4-25 illustrates the resulting power output from the device as a function of current speed. Torque is also provided, and the dashed lines show maximum and minimum values due to torque fluctuations. Interestingly, maximum and minimum values are also provided for a free-stream device producing the same amount of power should ducting with deflectors not have been used. It is apparent that the resulting stress on the structure due to the large fluctuations would present a significant reliability obstacle. Lastly, Figure 4-26 provides a sketch of a representative configuration for the device to be moored offshore or in a river near the community. The nominal rating of the device at 2.5 m/s (a typical current speed for rating hydro current turbines) is 41 kW.

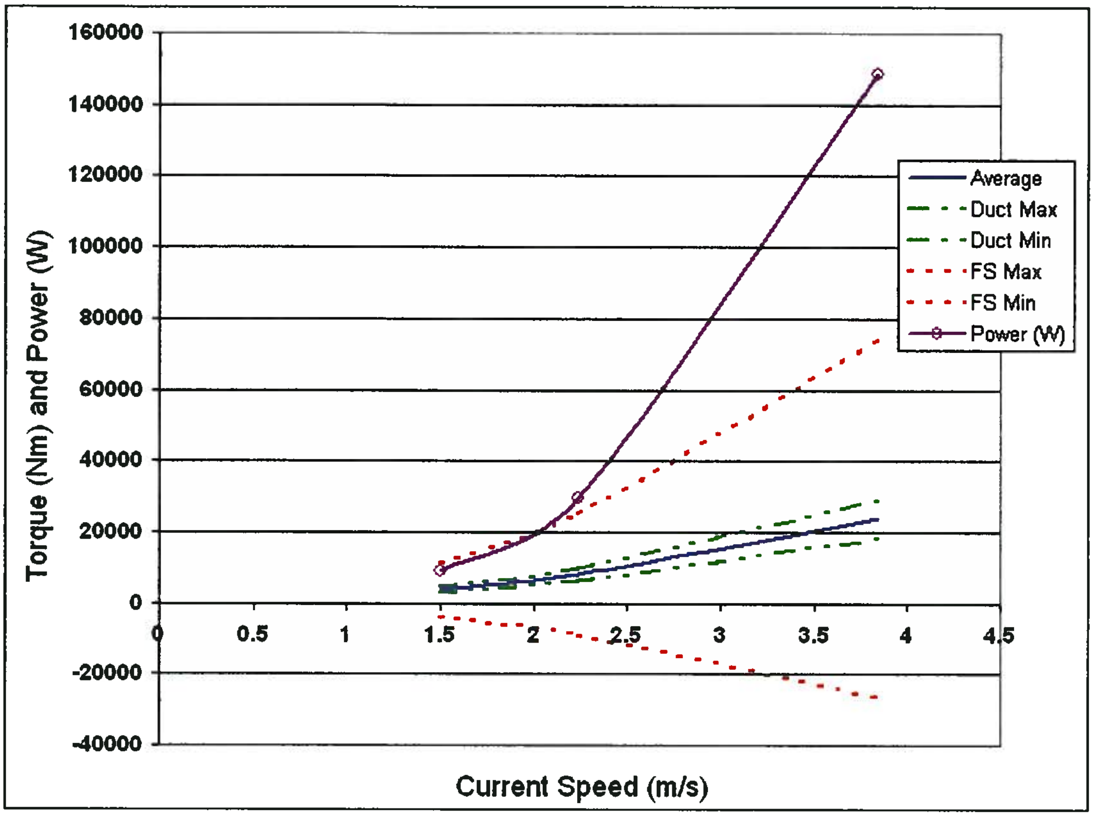

Figure 4-25: Power and torque output.

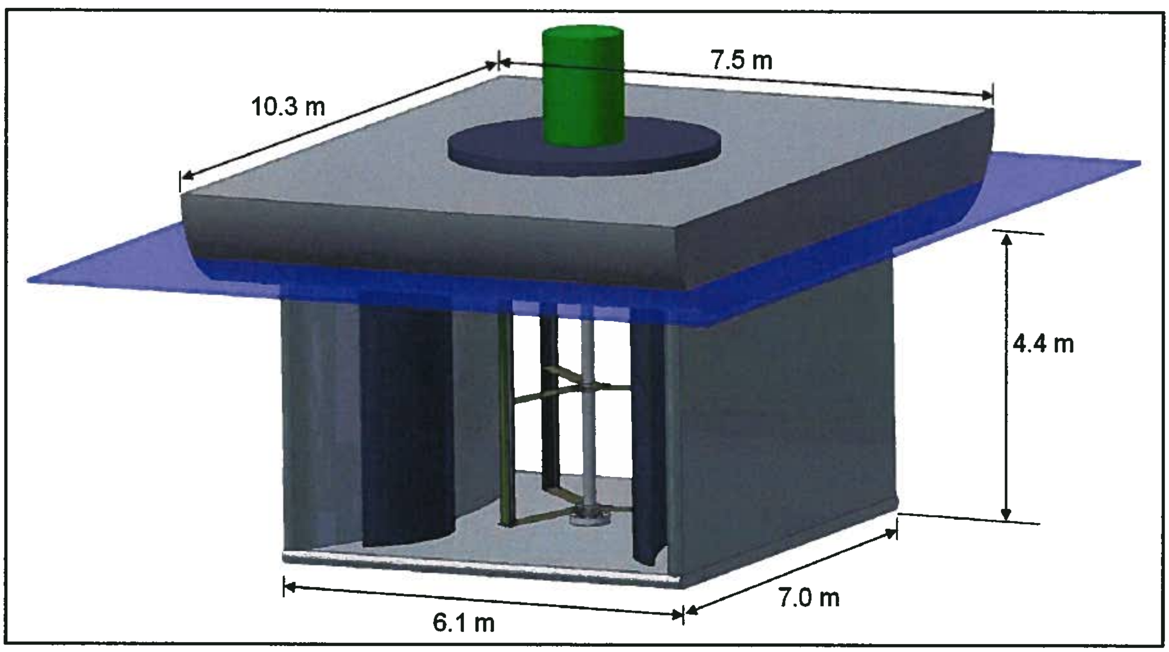

Figure 4-26: Representative device configuration.

5 CONCLUSIONS AND RECOMMENDATIONS

5.1 Conclusions

The research presented above details one of the few available experimental data sets and all associated setup information suitable for the validation of both a free-stream and ducted vertical axis hydro current turbine model. Building upon past NRC research identifying near optimum TSR and solidity ratios, an experimental turbine model (and all associated testing equipment and instrumentation) was built, commissioned, and tested in the UBC campus towing tank. In addition to obtaining repeatable experimental data for use in validating numerical codes, a parametric study was performed yielding baseline data on the effect of a number of parameters. For a free-stream device with span/diameter = 0.75, end plates were shown to increase the baseline Ck value by 16.6% through the reduction of tip losses for the tested aspect ratio. Additionally, changes in angles of attack between 3° and 5° were shown to increase the Ck value by over 21%. Further testing of a 3-armed and 2-armed model allowed for the quantification of arm effects, as well as demonstrated an increase in Ck of 0.047 by applying cambered blades at 5°. This yielded a theoretical maximum performance without tip losses of Ck=0.412. Accounting for further possible optimization of solidity, airfoil shape, and angle of attack, a theoretical maximum of Ck=0.45 in the absence of parasitic and tip losses is reasonable.

Application of a venturi-style duct increased power output by the rotor to a Ck value of 0.473 compared to 0.272 for the free-stream case; however, the power produced was 12% less than what may be expected from a free-stream rotor of cross-sectional area equivalent to the duct capture area. Significantly, the duct provided a decrease in peak torque values, as well as in torque fluctuation coefficient from 4.24 to 1.25, over the free-stream case which is very important for cyclic loading considerations. Subsequent duct configuration changes, as provided in Table 5-1 below, led to an additional reduction in torque fluctuation coefficient. The optimal reduction was provided with two downstream deflectors, providing a Ck = 0.442 and a C_{TF} = 0.47.

Table 5-1: Maximum Ck, percent change, and torque fluctuation coefficient..

Case	Ck Value	% Ck Change	C_{TF}
Free stream (baseline)	0.272	--	4.24
No deflectors	0.473	73.9%	1.25
Downstream deflectors	0.442	62.5%	0.47
All four deflectors	0.393	44.5%	1.4
Spinning towards deflectors	0.426	56.6%	1.17
Spinning away from deflectors	0.442	62.5%	1.23
Upstream deflectors	0.407	49.6%	2.67

A preliminary investigation into drag force on the turbine was also conducted, and an approximation for the drag coefficient (accounting only for forces parallel to the flow) was found to be [Cd = 0.41*tsr – 0.16].

A primary source of error was the fluctuating revolution speed of the device caused by the large torque fluctuations involved; however, understanding of this error (up to 25° with the largest torque fluctuations down to only a few degrees for minimal fluctuations) renders the data presented suitable for validation of numerical models. Such a comparison was provided for both a free-stream and ducted numerical simulation created using a commercial RANS solver, and optimal correlation was obtained for the ducted comparison when reduced torque and revolution speed fluctuations were observed in the experimental results. Lastly, a sample case study was presented for a ducted 3.375m diameter by 3.375m span rotor operating in Quatsino Narrows on Vancouver Island capable of powering approximately 17 homes.

5.2 Recommendations for Future Work

Recommendations for tests conducted with the same or a similar setup are as follows:

- Application of a flywheel between the torque sensor and drive-train as a means to better regulate revolution speed control. Applying a flywheel connected by a shaft out of the top of the gearbox would allow for a variable revolution speed control by when adjusting the added weight, while still registering true torque values observed in the shaft.

- Replacement of the flexible coupling with a universal joint without backlash, or an alternative coupling.
- Use of a flume tank of suitable size and speed instead of a towing tank, as it would serve as a more reasonable facility for such turbine tests:
    - Allow for a more rigid, fixed structure
    - Permit longer run durations
    - Decrease testing time by not having to return to starting position
    - Simplify installation and removal of turbine

In addition to recommendations for improving the experimental setup used above, general understanding of the model testing of vertical axis hydro turbines may be greatly improved through the following:

- A study investigating how free-surface effects affect turbine performance. To do this, however, a deeper tank may be required so as to ensure interactions with the bottom of the tank are not a factor.
- An examination into performance differences (if any) between operation in a flume tank vs. a towing tank, potentially due to differing pressure field development upstream of the turbine
- A detailed investigation quantifying blockage effects on vertical axis turbine performance. This may be most effectively performed in a flume tank by reducing cross-sectional area through the addition of a series of false bottoms and walls. Alternatively, tests may also be conducted in tanks of varying dimensions.

Key factors suitable for experimental investigation and providing additional understanding of turbine operation and quantification of loading design requirements include:

- The complex interactions between blade lift and drag, parasitic drag forces, and drag on the shaft should be investigated to resolve net force fluctuations and directions on the bearings. Given the difficulty in simulating blade arms due to the computational cost of a 3D model, this research is likely best suited to an experimental study instrumented for measuring bearing forces in multiple directions.

- Detailed force data on an individual blade of a multi-blade device would be valuable for numerical model validation. This may include the use of strain gauges at the connection point between the arm and blade to resolve radial and tangential forces acting on the blade. The key challenge of such a study would be to get the low-signal strength data recorded using the underwater strain gauges synchronized with the revolution angle and transmitted to the stationary computer for analysis.

Numerical models are an invaluable tool for optimization studies pertaining to the duct shape, foil shape, and solidity ratio, as well as for understanding cavitation inception. Such numerical optimization should be ongoing, with the current limiting factor being high computational costs coupled with the high monetary costs to meet them.

Lastly, considering the device and its path towards commercial application, a number of factors require close examination and an exhaustive list is beyond the scope of this thesis; however, of primary significance from a hydrodynamics and mechanical engineering perspective are the requirement for:

- A detailed cost-benefit analysis assessing the use of ducting
- A mooring investigation to best understand how to overcome the fluctuating loads and how to best assure device stability
- Antifouling considerations to minimize performance reduction due to marine growth
- A detailed examination of cavitation avoidance/management caused by the pressure fluctuations on the blades

REFERENCES

[1] Intergovernmental Panel on Climate Change Fourth Assessment Report, "Climate Change 2007: Synthesis Report Summary for Policy Makers." Nov 2007. <http://www.ipcc.ch/>.

[2] Rifkin, Jeremy. *The Hydrogen Economy*. Penguin Group Inc., New York, 2002.

[3] Cornett, A. "Inventory of Canada's Marine Renewable Energy Resources." National Research Council of Canada CHC-TR-041, April 2006.

[4] "Evaluation of Nova Energy Ltd's Hydro Turbine." H.N. Halvorson Consultants, Victoria, Dec 1994.

[5] Siamack, Shojai and Bernard S. Katz. *The Oil Market in the 1980s: A Decade of Decline.* Praeger/Greenwood, 1992.

[6] "Green Energy Study for British Columbia Phase 2: Mainland – Tidal Current Energy." Triton Consultants Ltd., Vancouver, October 2002.

[7] Courtesy of Blue Energy Canada Inc., Dec 2007. <www.bluenergy.com>

[8] Templin, R.J. "Aerodynamic Performance Theory for the NRC Vertical-Axis Wind Turbine." National Research Council of Canada Laboratory Report LTR-LA-160, June 1974.

[9] White, Frank M. *Fluid Mechanics.* Fifth Edition, McGraw-Hill, New York, 2003.

[10] Davis, Barry V. "Water Turbine Model Trials." Nova Energy Limited for NRC Hydraulics Laboratory NEL-002, March 1980.

[11] Davis, B.V., D.H. Swan, and K.A. Jeffers "Ultra Low Head Hydroelectric Power Generation Using Ducted Vertical Axis Water Turbines." Nova Energy Limited for NRC Hydraulics Laboratory NEL-021, March 1981.

[12] Davis, B.V., D.H. Swan, and K.A. Jeffers. "Ultra Low Head Hydroelectric Power Generation Using Ducted Vertical Axis Water Turbines." Nova Energy Limited for NRC Hydraulics Laboratory NEL-022, October 1983.

[13] Davis, B.V., J.R. Farrell, D.H. Swan, and K.A. Jeffers. "Research and Development of a 50kW to 100kW Vertical Axis Hydro Turbine for a Restricted Flow Installation." Nova Energy Limited for NRC Hydraulics Laboratory NEL-038, March 1984.

[14] Davis, B.V., D.H. Swan, and K.A. Jeffers. "The Ducted Vertical Axis Hydro Turbine for Large Scale Tidal Energy Applications." Nova Energy Limited for H. A. Simmons NEL-070, March 1984.

[15] Davis, B.V. and D.H. Swan. "Commissioning and Testing of a 100kW Vertical Axis Hydraulic Turbine." Nova Energy Limited for NRC Hydraulics Laboratory NEL-081, December 1985.

[16] Gorlov, A. M., "Tidal Energy." Encyclopedia of Ocean Sciences, Academic Press, London, pp. 2955-2960, 2001.

[17] Coiro, D.P., A. De Marco, F. Nicolosi, S. Melone, F. Montella. "Dynamic Behaviour of the Patented Kobold Tidal Current Turbine: Numerical and Experimental Aspects." Acta Polytechnica Vol. 45 No. 3, pp. 77-84, 2005.

[18] Guido, C., S. Francesco, L. Greco, A. Moroso, H. Eriksson. "An Experimental Investigation and a Theoretical and Computational Methodology to Study an Innovative Technology for Marine Current Exploitation: the Kobold Turbine." Bolletino della Communita Scientifica in Australasia, December 2006.

[19] "Cycloidal Tidal Power Generation – Phase 2." QinetiQ Ltd. for the Department of Trade and Industry Contract T/06/00229/00/REP/2, 2004.

[20] Ponta, F. and P. Jacovkis. "Marine-Current Power Generation by Diffuser-Augmented Floating Hydro-Turbines." Renewable Energy, Elsevier, 2007, *in press.*

[21] "Variable Pitch Foil Vertical Axis Tidal Turbine." Edinburgh Designs Ltd. for the Department of Trade and Industry Contract T/06/00234/00/REP/2, March 2006.

[22] Shiono, M, K. Suzuki, S. Kiho. "Output Characteristics of Darrieus Water Turbine with Helical Blades for Tidal Current Generation." Proc. of the Twelfth International Offshore and Polar Engineering Conference, Kitakyushu, May 2002.

[23] Taylor, Julian. "Crossflow Turbine Developments & Testing for Ultra-Low Head Hydro Applications." Highquest Engineering Inc. DSS Contract File No.: 51SZ.23216-6-6156, Vancouver, Aug 1987.

[24] Alidaadi, M. (private communication), 2007.

[25] McCroskey, W.J. "The Phenomenon of Dynamic Stall." NASA Technical Memorandum B1264, Moffett Field, Ca, March 1981.

[26] Riley, Donald R. "Wind-Tunnel Investigation and Analysis of the Effects of End Plates of the Aerodynamic Characteristics of an Unswept Wing." National Advisory Committee for Aeronautics Technical Note 2440, Aug 1951.

[27] Klaptocz, V. (private communication), 2007.

[28] Nabavi, Y. "Numerical Study of the Duct Shape Effect on the Performance of a Ducted Vertical Axis Tidal Turbine." MASc thesis, University of British Columbia, Vancouver, B.C., Canada, 2007.

[29] Bahaj, A.S., A.F. Molland, J.R. Chaplin, and W.M.J. Batten. "Power and thrust measurements of marine current turbines under various hydrodynamic flow conditions in a cavitation tunnel and a towing tank." Renewable Energy, Volume 32 Issue 3 pp. 407-426, March 2007.

[30] B.C. Hydro (private communication), January 2008.

APPENDIX A: Design Calculations

SCALING AND CONSTANT DEFINITION

The term prototype refers to the full-scale unit, while model refers to the model being tested in the tank.

Variable	Notation	Value	Unit	Comments
Scale Factor	SF	22.214		<-- Scale factor to make Dm = 4 with Dp = 66.66 is 16.664
Prototype Diameter	Dp	20.32	m	(To make Dm = 3.5, SF = 19.045)
		66.66	ft	(To make Dm = 3, SF =22.214)
Prototype Radius	Rp	10.16	m	(to chord line if symmetrical, else pivot point)
		33.33	ft	
Proto Airfoil Chord Length	Lcp	1.52	m	
		5	ft	
Number of Blades	Nb	3		
Blade Height:Diameter	HD	0.75		(Based on value from NEL-002 p. 20)
Prototype Span Length	Lsp	15.24	m	
		50.0	ft	
Prototype Current Speed		6	knots	
	Scp	3.09	m/sec	
Prototype Water Density	Rhop	1025	kg/m^3	
Prototype Water Viscosity	Viscp	1.00E-03	kg/(m*s)	
Model Diameter	Dm	0.91	m	Use Tools -> Goal Seek.... to set a model diameter by changing SF or Dp
		3.001	ft	
Model Radius	Rm	0.46	m	
		1.50	ft	
Model Chord Length	Lcm	0.069	m	
		2.701	in	
Model Span Length	Lsm	0.686	m	
		2.25	ft	
Model Water Density	Rhom	998	kg/m^3	
Model Water Viscosity	Viscm	1.00E-03	kg/(m*s)	
Model Turbine Area	Am	0.63	m^2	

Model Current Speed

Model Current Speed	Scm =	Scp/sqrt(SF)		m/sec
	Scm =	**2.00**	**m/sec**	=Scp/SQRT(SF)
		6.56	ft/sec	

Solidity Ratio

Solidity Ratio	SR =	Nb*Lc/R
	SR =	**0.45**

Tip Speed Ratio

Tip Speed Ratio	TSR =	R*ω/Sc		where ω = angular frequency
Tip Speed Ratio	**TSR =**	**2.25**		Works for up to 3 blades max. If want more blades, then must change.
			3	Based on Eqn. p. 21 of NEL-002.
				Sets optimal TSR according to solidity from NEL-002

RPM and Tip Speed

Prototype RPM	RPMp =	TSR*Scp/(Rp*2*pi())*60		rev/min
	RPMp =	6.53	rev/min	
	Omega_p =	0.68	rad/s	
Prototype Tip Speed	TSp =	RPMp*2*PI()*Rp/60	m/s	
	TSp =	**6.94**	**m/s**	
Model RPM	RPMm =	TSR*Scm/(Rm*2*pi())*60		rev/min
	RPMm =	**93.97**	**rev/min**	
	Omega_m =	9.84	rad/s	
Model Tip Speed	TSm =	RPMm*2*PI()*Rm/60		
	TSm =	**4.50**	**m/s**	

Reynold's Number Estimation

Point in rotation	Pr =	0	deg	Where 0 deg is directly into the current (rotating ccw).
Prototype Re:	Rep =	Rhop*Vencp*Lcp/Viscp		
	Rep =	1.567E+07		
	Where:	Vencp =	Prototype encounter velocity	
		Vencp =	TSp + Scp*cos(Pr)	m/s
		Vencp =	10.03	m/s
Model Re:	Rem =	Rhom*Vencm*Lcm/Viscm		
	Rem =	4.450E+05		
	Where:	Vencm =	Model encounter velocity	
		Vencm =	TSm + Scm*cos(Pr)	m/s
		Vencm =	6.50	m/s

Stagnation Pressures **(to aid with calculating required P range for transducers)**

Prototype Stagnation P:	Pstagp =	1/2*Rhop*Vencp^2	Pa
	Pstagp =	5.16E+04	Pa
		7.5	psi
Model Stagnation P:	Pstagm =	1/2*Rhom*Vencm^2	
	Pstagm =	2.11E+04	Pa
		3.1	psi

FOIL VELOCITY AND ANGLE OF ATTACK

The parameters on this sheet adjust the force inputs into "Foil Strength Variable"

Diameter:	0.914608457 m	=Cm	
Foil Chord:	0.0686 m	=Lcm	
Foil Span:	0.6860 m	=Lsm	
Free-stream velocity:	2 m/s		
Preset AoA:	0 deg	(positive designates leading edge moving outwards radially)	
Tip Speed Ratio:	2.75		
Radius:	0.457 m		
Model revs per minute:	114.8 rpm		
Induced velocity:	5.50 m/s		
Fluid Density:	1000 kg/m^3		

Point in Rotation (deg) 0 deg directly into flow rotation is ccw	Direction Foil Moves: Vinduced X comp. (m/s)	Direction Foil Moves: Vinduced Y comp. (m/s)	Direction flow travels when hitting foil: Observed induced X (m/s)	Direction flow travels when hitting foil: Observed induced Y	Net Y component: Net Y incl. free stream	Total Observed flow (m/s)	(also = point in rotation less 90 degrees) Absolute heading of induced observed flow only (deg)
0	0.00	5.50	0.00	-5.50	-7.50	7.50	270.00
22.5	-2.10	5.08	2.10	-5.08	-7.08	7.39	292.50
45	-3.89	3.89	3.89	-3.89	-5.89	7.06	315.00
67.5	-5.08	2.10	5.08	-2.10	-4.10	6.53	337.50
90	-5.50	0.00	5.50	0.00	-2.00	5.85	0.00
112.5	-5.08	-2.10	5.08	2.10	0.10	5.08	22.50
135	-3.89	-3.89	3.89	3.89	1.89	4.32	45.00
157.5	-2.10	-5.08	2.10	5.08	3.08	3.73	67.50
180	0.00	-5.50	0.00	5.50	3.50	3.50	90.00
202.5	2.10	-5.08	-2.10	5.08	3.08	3.73	112.50
225	3.89	-3.89	-3.89	3.89	1.89	4.32	135.00
247.5	5.08	-2.10	-5.08	2.10	0.10	5.08	157.50
270	5.50	0.00	-5.50	0.00	-2.00	5.85	180.00
292.5	5.08	2.10	-5.08	-2.10	-4.10	6.53	202.50
315	3.89	3.89	-3.89	-3.89	-5.89	7.06	225.00
337.5	2.10	5.08	-2.10	-5.08	-7.08	7.39	247.50
360	0.00	5.50	0.00	-5.50	-7.50	7.50	270.00

Maximum Lift Force:	1318	N	**Max Drag (assume L/D = 20):**	65.92	N
	295	lbf		15	lbf

Point in Rotation (deg) 0 deg directly into flow rotation is ccw	Absolute heading of Net flow (deg)	Observed AoA (deg)	Corresponding Cl	=0.5*density*velocity^2*chord*span*Lift Coeff. Lift Force (N)	(assume L/D ~ 20) Drag Force (N)	Net FS Force (FS direction) (N)
0.00	270.00	0	0	0	0	
22.50	286.55	-6	0.80	1027	51	-341.9183366
45.00	303.44	-12	1.125	1318	66	[illegible]
67.50	321.07	-16	1.16	1165	58	[illegible]
90.00	-19.98	-20	1.1	886	44	-848.2373447
112.50	1.18	-21	Separation	0	0	0
135.00	25.91	-19	1.1125	489	24	-429.4805173
157.50	55.66	-12	1.125	369	18	[illegible]
180.00	90.00	0	0	0	0	
202.50	124.34	12	1.125	369	18	-192.881387
225.00	154.09	19	1.1125	489	24	-429.4805173
247.50	178.82	21	Separation	0	0	0
270.00	199.98	20	1.1	886	44	[illegible]
292.50	218.93	16	1.16	1165	58	[illegible]
315.00	236.56	12	1.125	1318	66	-781.5294788
337.50	253.45	6	0.8	1027	51	-341.9183366
360.00	270.00	0	0	0	0	

Totals at ~120 deg: -771.3788539; [illegible]; [illegible]; -1822.448211

AoA	Cl
0	0
1	0.11
2	0.22
3	0.3475
4	0.475
5	0.6375
6	0.8
7	0.8625
8	0.925
9	0.9875
10	1.05
11	1.0875
12	1.125
13	1.1375
14	1.15
15	1.155
16	1.16
17	1.1425
18	1.125
19	1.1125
20	1.1

Based on Re = 3E06, p.540 Theory of Wing Sections (Abbott)

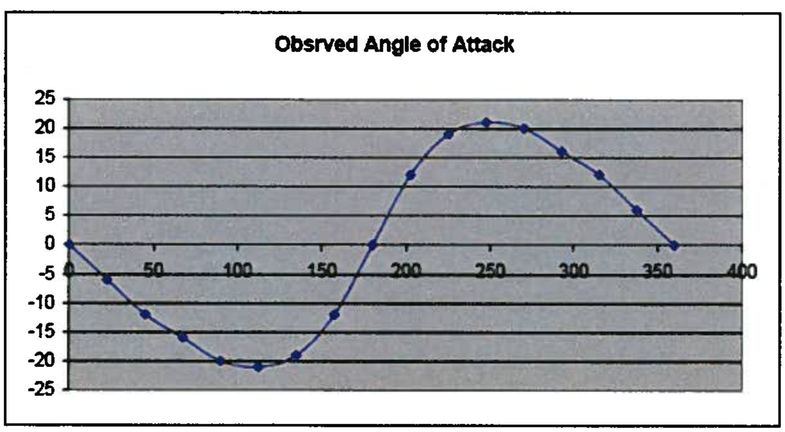

MODEL DRAG FORCE ESTIMATION

Model Chord Length	Lcm	0.0686	m
Maximum Model Airfoil Width	Wam	21.0%	percent of chord (p. 72 NEL-002 for NACA 63(4)-021
Actual Max Model Airfoil Width	Awam	0.0144	m
Model Span Length	Lsm	0.6860	m
Carriage Speed:	Scm or other	2.000	m/s

Drag Coefficient (central shaft):	Cdshaft	From Table White p. 485 for Re > 10 000	
	Cdshaft =	1.2	(Assume L/D very large)
Drag on central shaft:	=0.5*Rhom*Scm^2*Dshaft*Lshaft*Cdshaft		
	Lshaft =	1.32	m
	Dshaft =	0.04826	m
		1.9	in
Drag on central shaft:	152.7 N		

Drag on Mounting Arms:	Cdshaft =	1.2	
Drag on arm:	=0.5*Rhom*Scm^2*Darm*Larm*Cdshaft		
	Larm =	0.60957	m
	Darm =	0.0254	m
		1	in
Drag on arms:	37.1	N	

Total Drag:	# of items	Drag		
Central Shaft:	1	152.7	N	
Mounting arms:	6	74.2	N	six arms * 1/3 contributing to drag in free stream condition
Net FS direction force (from foil velocity and AoA')		-1885.1		

Total Drag Force:	**2112 N**
	475.2 lbf

Alternate pressure-based scenario for determining drag:

Head = Scm^2 / 2g		Current Speed: 2 m/s
0.203873598 m		
Turbine Area = Dm*Lsm		
0.63		
Pressure = rhom*g*Head		(pressure is also 1/2*rho*V^2)
1996 Pa		
Force = Pressure*Area		
Force =	1252 N	
=	281.8 lbf	

128 kg

Angular Natural Frequency of Loaded Beams

Reference: Sachs, Peter. Wind Forces in Engineering. Pergamon Press, Oxford, 1972.

Angular Natural Frequency, ω_n = λ_n^{2}*sqrt(YM*I/M*ln)

where:

λ_n = coefficient from reference table (Fig. 5.23 p. 167)

YM = Young's Modulus (Pa)

YM = 6.89E+10 E = 6.89E+10 Pa for Aluminum (matweb.com)

E = 1.93E+11 Pa for 304 Stainless Steel

Shaft outer diameter: od_shaft 1.9 in 0.04826 m

Shaft thickness: t_shaft 0.2 in 0.00508 m

I = Area moment of inertia of beam x-section (m^4)

I = pi()/64*(od_shaft^4 - (od_shaft - 2*t_shaft)^4)

I = 1.63E-07 m^4

ln = Length of beam (m)

ln = 1.52 m (assumed 5 feet)

m = Mass per unit length (kg / m)

Area: =pi()*(od_shaft^2 - (od_shaft - 2*t_shaft)^2) / 4

0.000689122 m^2

Density: 2700 kg/m^3

m = Area*density

m = **1.86 kg / m**

For a fixed-free cantilever

# nodes	λ_n^2	ω_n (rad/s)	freq (Hz)
1	3.52	221.4	35.2
2	22.4	1409.0	224.3
3	61.7	3881.1	617.7
4	121	7611.2	1211.4
5	200	12580.5	2002.3

For a fixed-hinged cantilever

# nodes	λ_n^2	ω_n	freq (Hz)
1	15.4	968.7	154.2
2	50	3145.1	500.6
3	104	6541.9	1041.2
4	178	11196.7	1782.0
5	272	17109.5	2723.1

For a hinged-hinged cantilever

# nodes	λ_n^2	ω_n	freq (Hz)
1	9.87	620.8	98.8
2	39.5	2484.7	395.4
3	88.9	5592.0	890.0
4	158	9938.6	1581.8
5	247	15536.9	2472.8

Shaft Excitation

Due to blade pulsing:

It is safe to assume that the shaft will experience a pulse at a rate of the number of blades * the rpm, assuming a pulse occurs as a blade passes a specific point in the rotation.

Pulse frequency = model rpm * number of blades
= RPMm * Nb
= 281.9 pulses / min
= 4.70 Hz

Due to vortex shedding on central shaft:

Ratio of surface to free stream velocity, alpha

alpha = od_shaft/2*Omega_m / Scm
alpha = 0.119

This ratio is so low that the relationship for a stationary cylinder will be deemed ok.

Shaft Reynold's number:

Res_m = Rhom*Scm*od_shaft / Viscm
Res_m = 96327 log(Res_m) = 4.98 For use in table referenced below

Shaft Strouhal number Sts_m = 1.8 (approx) Table p. 140 "Wind Forces in Engineering" by Sachs, Peter. Vol. 3 1972

Excitation Frequency = Scm*Sts_m / od_shaft
= 74.6 Hz

Vibrations Summary Table

Excitation Frequencies:

due to blade pulsing:	4.70	Hz
due to vortex shedding:	74.6	Hz

Natural Frequencies for fixed-free cantilever:

# nodes	freq (Hz)
1	35.2
2	224.3

Natural Frequencies for a fixed-hinged cantilever:

# nodes	freq (Hz)
1	154.2
2	500.6

Natural Frequencies for a hinged-hinged cantilever:

# nodes	freq (Hz)
1	98.8
2	395.4

Shaft Strength and Deflection

od_shaft = 0.04826 m 1.9 in
t_shaft = 0.00508 m 0.2 in

ln = Length of beam (m)
ln = 1.52 m

I = Area moment of inertia of beam x-section (m^4)
I = 1.63E-07 m^4

Drag Force: 2111.9 N (from Drag Estimation worksheet worst-case scenario)

With Bottom Locational Bearing: (Schigley p. 971)

Distance between bearings (AB): 75 in
1.905 m

Distance from upper bearing to force (AC): 50 in
1.270 m

Distance from force to lower bearing (CB): 25 in
0.635 m

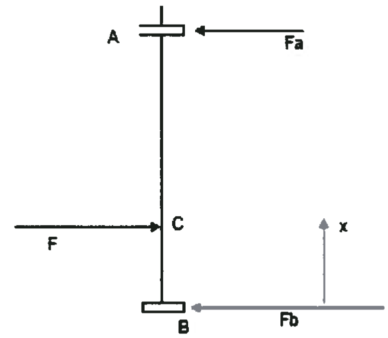

Sum Fx = 0; Fa + Fb = F
Sum Ma = 0; F*AC = Fb*AB

Fb = F*AC/AB
Fb = **1408** **N**

Fa = F - Fb
Fa = **704.0** **N**

Shear Force: From A -> C: 704.0
From C -> B: -1407.9

Moment: At A: 0
At C: 894.05 Nm
At B: 0

Stress: =M*y/I
y = 0.02413 m
M = 894.0 Nm
I = 1.63E-07 m^4

Stress = 1.32E+08 Pa
Stress = 132 MPa
FoS = 1.62

Tensile Yield Stress is: 215 MPa
Yield Stress for Aluminum: 276 Mpa
Yield Stress for Stainless Steel: 215 MPa

Deflections:
E = 1.93E+11 Pa
I = 1.63E-07 m^4
F = 2.11E+03 N

E = 6.89E+10 Pa for Aluminum
E = 1.93E+11 Pa for 304 Stainless Steel

Deflection from B -> C:
(x increasing from B -> C and must between 0 and 0.635 m)
x index: 0.554 m

Ybc = F*AC*x/(6*E*I*AB)*(x^2 + AC^2 - AB^2)
Ybc = **-0.0071** **m**

Deflection from C -> A:
(x must be between 0.635 and 1.905 m)
x index: 0.79 m

Yca = F*BC*(l-x) / (6*E*I*AB) * (x^2 + BC^2 - 2*AB*x)
Yca = **-0.0083** **m**

Cantilevered Design: (Schigley p. 969)

Distance between bearings (AB):		18 in	
		0.4572 m	
Distance from lower bearing to force (BC):		37 in	
		0.9398 m	

Sum Fx = 0; Fa + F = Fb
Sum Mb = 0; Fa*AB = F*BC

Fa =	F*BC/AB		
Fa =	4341	N	977 lbf
Fb =	Fa + F		
Fb =	6453	N	1452 lbf

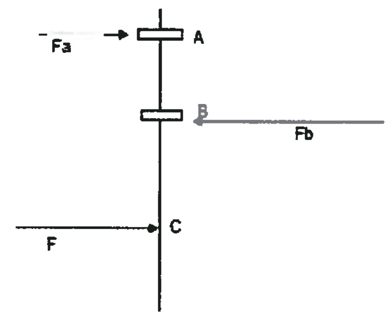

Shear Force:	From A -> B:	4341 N
	From B -> C:	-2112 N
	From C -> End:	0.0
Moment:	At B:	1984.8
	At C:	0.0

Stress: =M*y/I

y =	0.02413 m
M =	1984.8 Nm
I =	1.63E-07 m^4
Stress =	2.94E+08 Pa
Stress =	294 MPa
FoS =	0.73

Tensile Yield Stress is:	215 MPa	
Yield Stress for Aluminum:	276 Mpa	(matweb.com)
Yield Stress for Stainless Steel:	215 MPa	

Max Defl.: = F*(BC)^2 /(6*E*I) * (BC - 3*ln) Schigley p. 969

E =	1.93E+11 Pa	E =	6.89E+10 Pa for Aluminum
I =	1.63E-07 m^4	E =	1.93E+11 Pa for 304 Stainless Steel
BC =	0.9398 m		
F =	2111.9 N		
ln =	1.52 m (length of beam below bottom bearing) (ie from B to end)		

Max Defl.: **-0.036 m**

Shaft Critical Speed

Distance between bearings (AB):	68.8 in
	1.748 m
Distance from upper bearing to w1 (AC):	40.25 in
	1.022 m
Distance from w1 to w2 (CD):	13.5 in
	0.343 m
Distance from w2 to lower bearing (DB):	15.05 in
	0.382 m

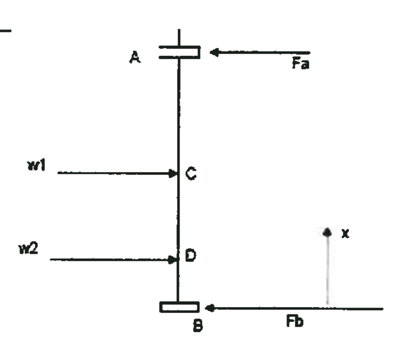

Critical Speed (no additional weight)

omega1 = (pi()/length)^2 * sqrt(E*I/m)

length:	1.748 m
E =	1.93E+11 Pa
I =	1.63E-07 m^4
m =	1.860629863
omega1 =	420.02 rad/s
omega1 =	4011 rpm

POWER OUTPUT PREDICTION

Constants:

Diameter:	0.914	m	(0.914)		0.2785872		
Span:	0.686	m	(.686)	Height:	0.382221638	Area:	0.6270 m²
Density of Water:	998	kg/m^3					
C_K (Global Efficiency):	0.35			C_P:	0.590		
Torque Ripple Factor:	6		Cp = power extracted / (0.593* power available in the water)				

Current	Tip Speed Ratio	Rotational Speed	Water Power per Area	Water Power	Power	Power Extracted (Based on C_K)	Torque (Extraction)	Torque w/ Ripple		Local Ck	Torque with local Ck	Torque w/ Ripple w/ local Ck	Power w/ Local Ck	Power w/ Local Ck
[m/s]	[]	[rev/min]	W/m^2	[Watts]	[hp]	[Watts]	[Nm]	[Nm]			[Nm]	[Nm]	[hp]	[kW]
0.5	0	0.00	62.38	39.11	0.05	13.69	-	-						
	1	10.45	62.38	39.11	0.05	13.69	12.511	75.067		0.07	2.50	15.01	0.004	0.002736
	2	20.90	62.38	39.11	0.05	13.69	6.256	37.533		0.175	3.13	18.77	0.009	0.006844
	3	31.34	62.38	39.11	0.05	13.69	4.170	25.022		0.245	2.92	17.52	0.013	0.009582
	4	41.79	62.38	39.11	0.05	13.69	3.128	18.767		0.35	3.13	18.77	0.018	0.013688
	5	52.24	62.38	39.11	0.05	13.69	2.502	15.013		0.35	2.50	15.01	0.018	0.013688
	6	62.69	62.38	39.11	0.05	13.69	2.085	12.511		0.35	2.09	12.51	0.018	0.013688
	7	73.13	62.38	39.11	0.05	13.69	1.787	10.724		0.28	1.43	8.58	0.015	0.010951
1	0	0.00	499.00	312.87	0.42	109.51	-	-						
	1	20.90	499.00	312.87	0.42	109.51	50.044	300.266		0.07	10.01	60.05	0.029	0.021901
	2	41.79	499.00	312.87	0.42	109.51	25.022	150.133		0.175	12.51	75.07	0.073	0.054753
	3	62.69	499.00	312.87	0.42	109.51	16.681	100.089		0.245	11.68	70.06	0.103	0.076654
	4	83.58	499.00	312.87	0.42	109.51	12.511	75.067		0.35	12.51	75.07	0.147	0.109506
	5	104.48	499.00	312.87	0.42	109.51	10.009	60.053		0.35	10.01	60.05	0.147	0.109506
	6	125.37	499.00	312.87	0.42	109.51	8.341	50.044		0.35	8.34	50.04	0.147	0.109506
	7	146.27	499.00	312.87	0.42	109.51	7.149	42.895		0.28	5.72	34.32	0.117	0.087605
1.5	0	0.00	1684.13	1055.95	1.42	369.58	-	-						
	1	31.34	1684.13	1055.95	1.42	369.58	112.600	675.599		0.07	22.52	135.12	0.099	0.073917
	2	62.69	1684.13	1055.95	1.42	369.58	56.300	337.799		0.175	28.15	168.90	0.248	0.184792
	3	94.03	1684.13	1055.95	1.42	369.58	37.533	225.200		0.245	26.27	157.64	0.347	0.258709
	4	125.37	1684.13	1055.95	1.42	369.58	28.150	168.900		0.35	28.15	168.90	0.496	0.369584
	5	156.72	1684.13	1055.95	1.42	369.58	22.520	135.120		0.35	22.52	135.12	0.496	0.369584
	6	188.06	1684.13	1055.95	1.42	369.58	18.767	112.600		0.35	18.77	112.60	0.496	0.369584
	7	219.40	1684.13	1055.95	1.42	369.58	16.086	96.514		0.28	12.87	77.21	0.396	0.295667
2	0	0.00	3992.00	2503.00	3.36	876.05	-	-						
	1	41.79	3992.00	2503.00	3.36	876.05	200.177	1201.065		0.07	40.04	240.21	0.235	0.17521
	2	83.58	3992.00	2503.00	3.36	876.05	100.089	600.532		0.175	50.04	300.27	0.587	0.438025
	3	125.37	3992.00	2503.00	3.36	876.05	66.726	400.355		0.245	46.71	280.25	0.822	0.613235
	4	167.16	3992.00	2503.00	3.36	876.05	50.044	300.266		0.35	50.04	300.27	1.175	0.87605
	5	208.96	3992.00	2503.00	3.36	876.05	40.035	240.213		0.35	40.04	240.21	1.175	0.87605
	6	250.75	3992.00	2503.00	3.36	876.05	33.363	200.177		0.35	33.36	200.18	1.175	0.87605
	7	292.54	3992.00	2503.00	3.36	876.05	28.597	171.581		0.28	22.88	137.26	0.940	0.70084
2.5	0	0.00	7796.88	4888.67	6.56	1711.04	-	-						
	1	52.24	7796.88	4888.67	6.56	1711.04	312.777	1876.663		0.07	62.56	375.33	0.459	0.342207
	2	104.48	7796.88	4888.67	6.56	1711.04	156.389	938.332		0.175	78.19	469.17	1.147	0.855518
	3	156.72	7796.88	4888.67	6.56	1711.04	104.259	625.554		0.245	72.98	437.89	1.606	1.197725
	4	208.96	7796.88	4888.67	6.56	1711.04	78.194	469.166		0.35	78.19	469.17	2.296	1.711036
	5	261.20	7796.88	4888.67	6.56	1711.04	62.555	375.333		0.35	62.56	375.33	2.296	1.711036
	6	313.43	7796.88	4888.67	6.56	1711.04	52.130	312.777		0.35	52.13	312.78	2.296	1.711036
	7	365.67	7796.88	4888.67	6.56	1711.04	44.682	268.095		0.28	36.76	214.48	1.836	1.368828

AIRFOIL STRENGTH CALCULATIONS

Model Span Length:	0.586 m	
Total Lift:	1318 N	Lift parameters on this sheet taken from "Foil velocity and AoA"
	302 lbf	
Number of struts:	2	
Force per strut (perp to airfoil):	659.19 N	
Distributed Lift: (Ldist)	1922 N/m	
Moment of Inertia:	8.88E-09 m^4	
Max Y Distance:	7.21E-03 m	
Tensile Yield Stress is:	276 MPa	

1/4 Span Supported Foils:

Distance from airfoil ends to support:	25% percent of airfoil span	
Max Moment for supports at 1/4 of the span from the ends:		28.3 Nm
(See hidden cells immediately below)		
Max stress in key:		3.06E+07 Pa
Safety Factor:		9.02

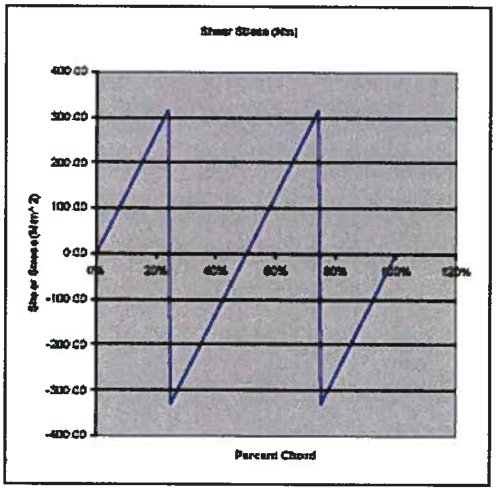

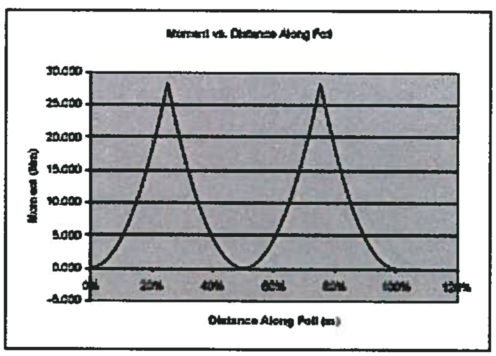

D along airfoil (%)	Distance Along Foil (m)	Shear Stress (N/m^2)	Moment (Nm)
0%	0.000	0.00	0.000
2%	0.014	26.37	0.181
4%	0.027	52.74	0.723
6%	0.041	79.10	1.628
8%	0.055	105.47	2.894
10%	0.069	131.84	4.522
12%	0.082	158.21	6.511
14%	0.096	184.57	8.863
16%	0.110	210.94	11.576
18%	0.123	237.31	14.651
20%	0.137	263.68	18.087
22%	0.151	290.05	21.885
24%	0.165	316.41	26.045
25%	0.171	-329.60	28.261
26%	0.178	-316.41	26.045
28%	0.192	-290.05	21.885
30%	0.206	-263.68	18.087
32%	0.220	-237.31	14.651
34%	0.233	-210.94	11.576
36%	0.247	-184.57	8.863
38%	0.261	-158.21	6.511
40%	0.274	-131.84	4.522
42%	0.288	-105.47	2.894
44%	0.302	-79.10	1.628
46%	0.316	-52.74	0.723
48%	0.329	-26.37	0.181
50%	0.343	0.00	0.000
52%	0.357	26.37	0.181
54%	0.370	52.74	0.723
56%	0.384	79.10	1.628
58%	0.398	105.47	2.894
60%	0.412	131.84	4.522
62%	0.425	158.21	6.511
64%	0.439	184.57	8.863
66%	0.453	210.94	11.576
68%	0.466	237.31	14.651
70%	0.480	263.68	18.087
72%	0.494	290.05	21.885
74%	0.508	316.41	26.045
75%	0.514	-329.60	28.261
76%	0.521	-316.41	26.045
78%	0.535	-290.05	21.885
80%	0.549	-263.68	18.087
82%	0.562	-237.31	14.651
84%	0.576	-210.94	11.576
86%	0.590	-184.57	8.863
88%	0.604	-158.21	6.511
90%	0.617	-131.84	4.522
92%	0.631	-105.47	2.894
94%	0.645	-79.10	1.628
96%	0.659	-52.74	0.723
98%	0.672	-26.37	0.181
100%	0.686	0.00	0.000

End-Supported Foils:

Max Moment for end supported beam = Ldist*Lsm/2*(Lsm - Lsm/2)

Max Moment for end supported beam = 113 Nm

(See hidden cells immediately below)

Max stress in key: 1.22E+08 Pa

Safety Factor: 2.29

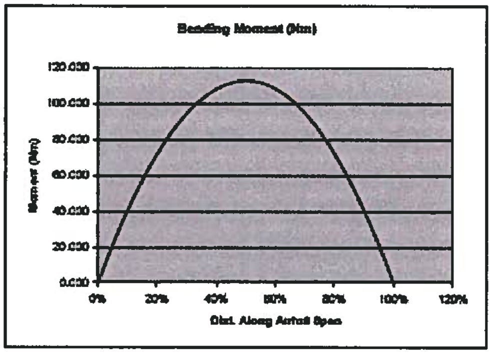

D along airfoil (%)	Distance Along Foil (m)	Moment (Nm)
0%	0.000	0.000
2%	0.014	8.863
4%	0.027	17.364
6%	0.041	25.503
8%	0.055	33.280
10%	0.069	40.696
12%	0.082	47.750
14%	0.096	54.442
16%	0.110	60.773
18%	0.123	66.742
20%	0.137	72.349
22%	0.151	77.594
24%	0.165	82.477
25%	0.171	84.784
26%	0.178	86.999
28%	0.192	91.159
30%	0.206	94.958
32%	0.220	98.394
34%	0.233	101.469
36%	0.247	104.182
38%	0.261	106.533
40%	0.274	108.523
42%	0.288	110.151
44%	0.302	111.417
46%	0.316	112.321
48%	0.329	112.864
50%	0.343	113.045
52%	0.357	112.864
54%	0.370	112.321
56%	0.384	111.417
58%	0.398	110.151
60%	0.412	108.523
62%	0.425	106.533
64%	0.439	104.182
66%	0.453	101.469
68%	0.466	98.394
70%	0.480	94.958
72%	0.494	91.159
74%	0.508	86.999
75%	0.514	84.784
76%	0.521	82.477
78%	0.535	77.594
80%	0.549	72.349
82%	0.562	66.742
84%	0.576	60.773
86%	0.590	54.442
88%	0.604	47.750
90%	0.617	40.696
92%	0.631	33.280
94%	0.645	25.503
96%	0.659	17.364
98%	0.672	8.863
100%	0.686	0.000

VERTICAL LOWER BEARING SUPPORT CALCULATIONS

Drag force on model:	2112 N			
	262 lbf			

(Ensure to change speed on drag for spreadsheet for checking different speeds!)

Number of struts: 2
Force per strut due to model drag: 1056.0 N

Strut length: 77 in 1.956 m
(from bottom of supporting beam on sub-carriage to plate with bearing)
Distance from bottom of sub-carriage to water: 19 in
Submerged length of bearing support arm: 58 in 1.473 m
(ie. underwater span)

Support arm dimensions: (rectangular tube)	Length =	4 in	(parallel to flow)
		0.1016 m	
	Width =	2 in	(perpendicular to flow)
		0.0508 m	
	Thickness =	0.1875 in	
		0.0048 m	
	Inertia =	1.75488E-06 m^4	

Speed: 2 m/s
Reynold Number: 2.03E+05

Drag coefficient of support arm: 0.2 (for a 2:1 ellipse in turbulent flow)
reference White p. 453

Reference Area: =underwater span * length parallel to flow
0.150 m^2

Drag due to a single bearing support arm: 60 N

Total drag force on a bearing support arm: 1116 N

Distance to centre of force: 50.5 in (rough approximation)
1.28 m

Maximum Moment: =Force * Distance to centre of force
1431 Nm

Maximum :=M*y/I
4.14E+07 Aluminum Yield Stress: 2.76E+08 Pa

FoS = 6.66

Ymax = =F*distance to force^2 / (6*E*I) * (distance to force - 3*length) (reference Schigley p. 969)
Ymax = -0.011601 m E = 6.89E+10 Pa for Aluminum

APPENDIX B: Component Drawings

Figure B-1: ¼ span rotor assembly.

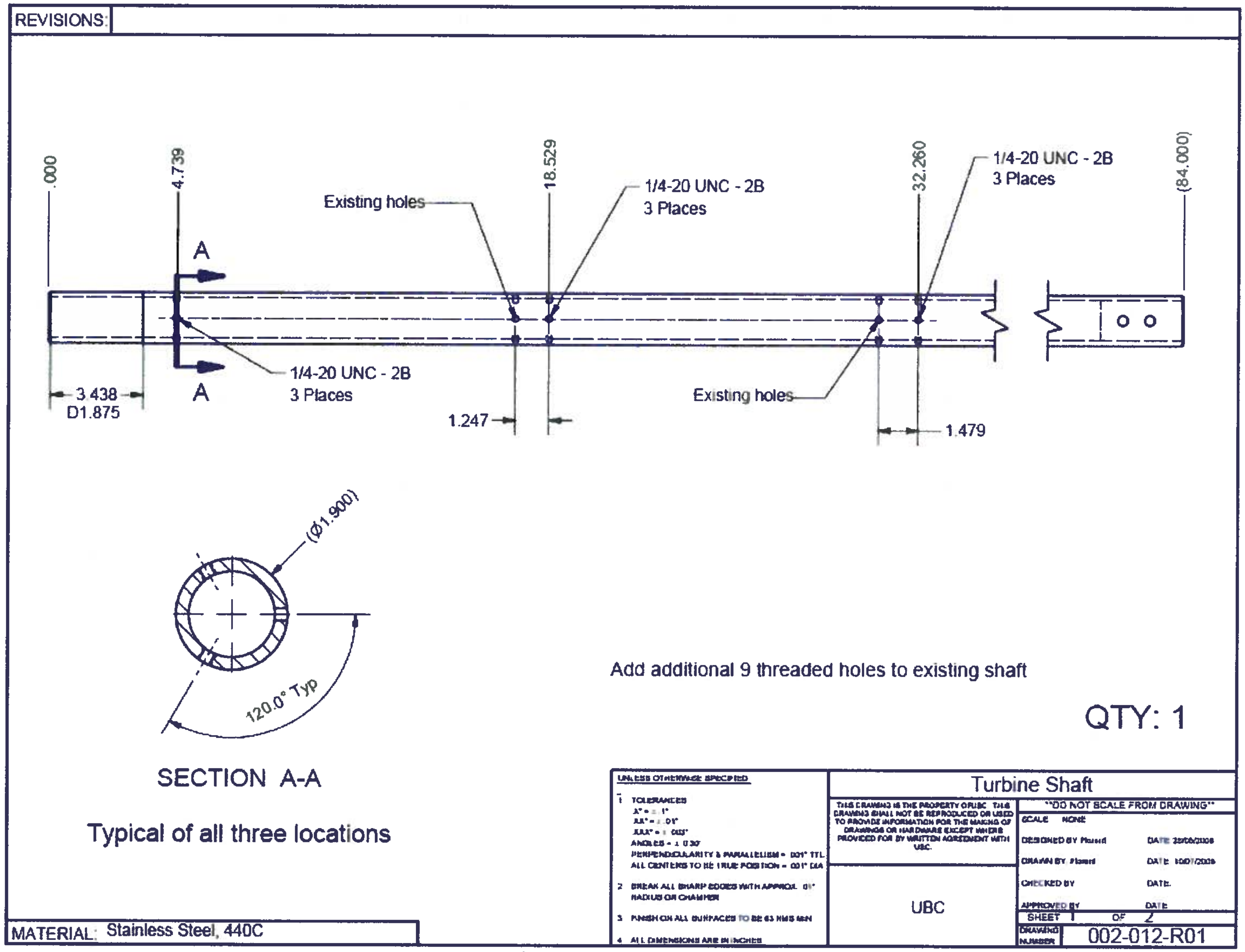

Figure B-2: Main shaft.

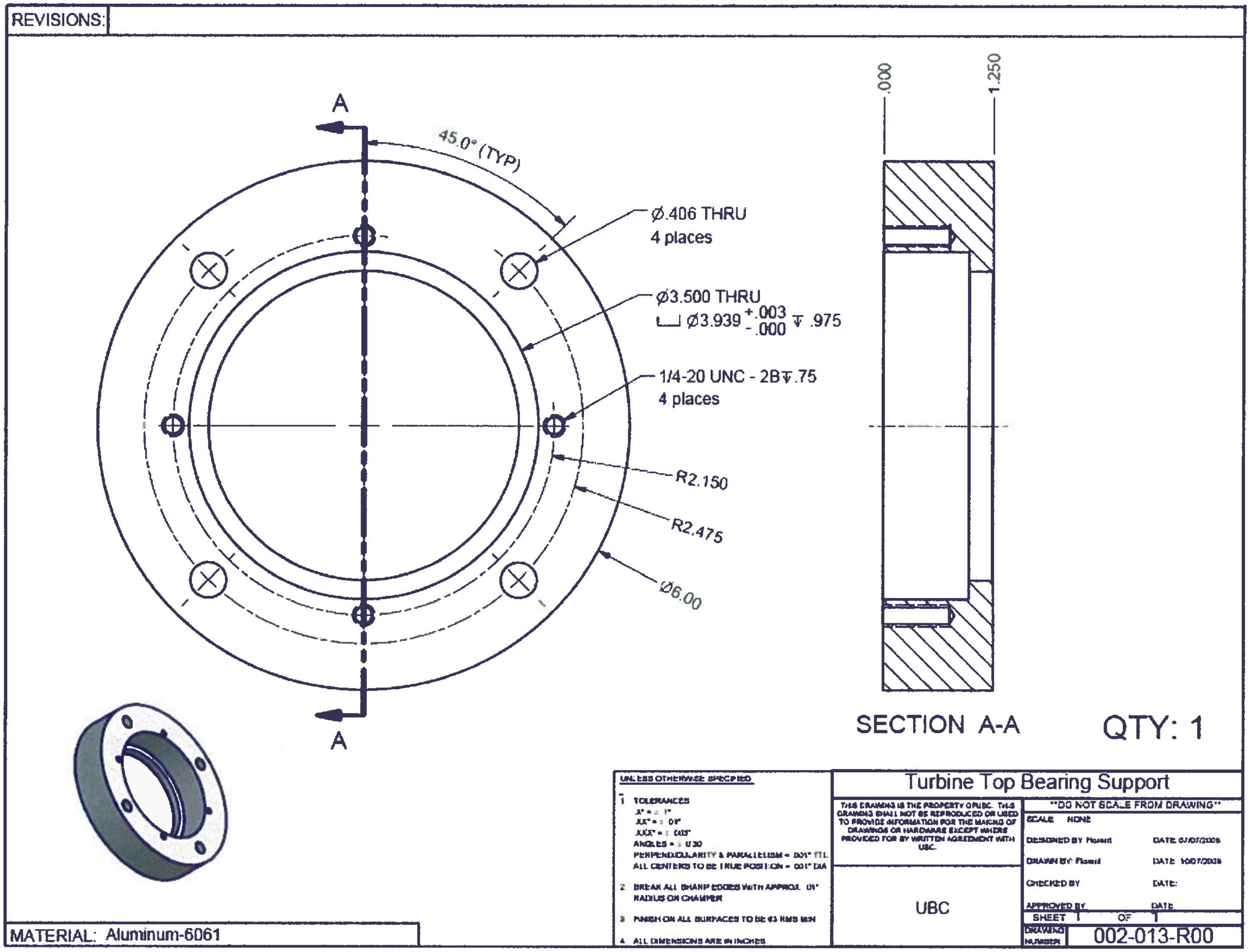

Figure B-3: Upper bearing mount.

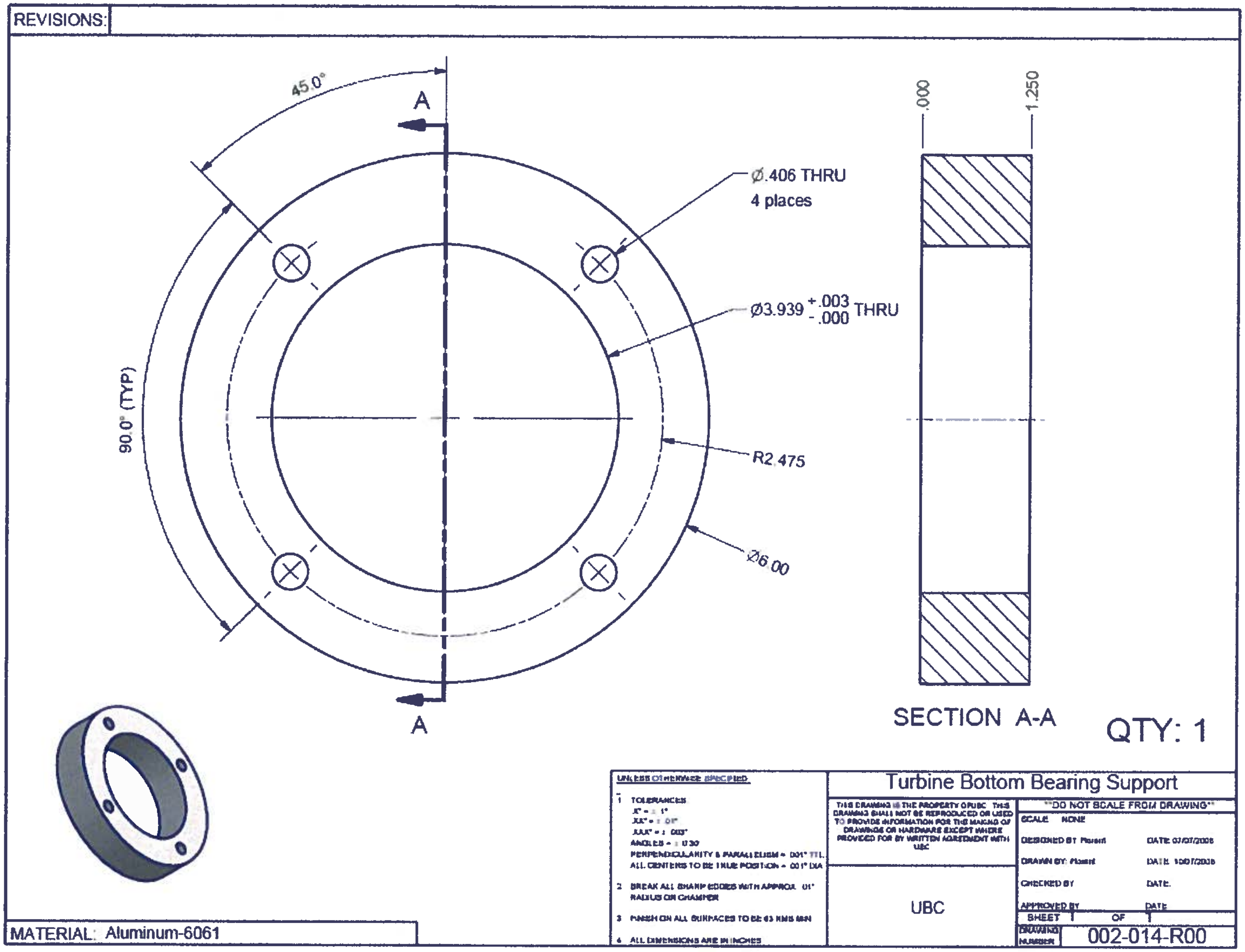

Figure B-4: Lower bearing mount.

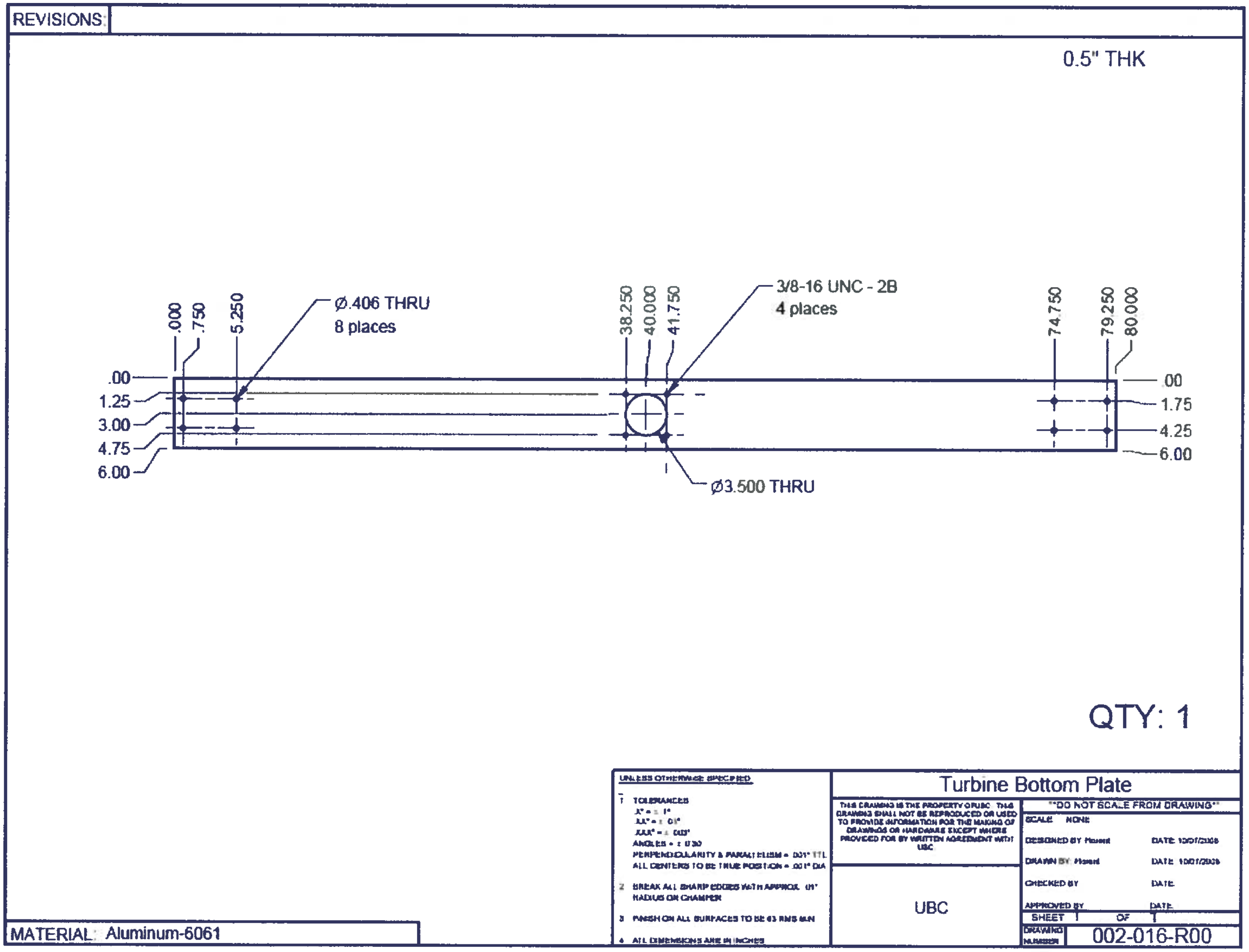

Figure B-5: Lower bearing support plate.

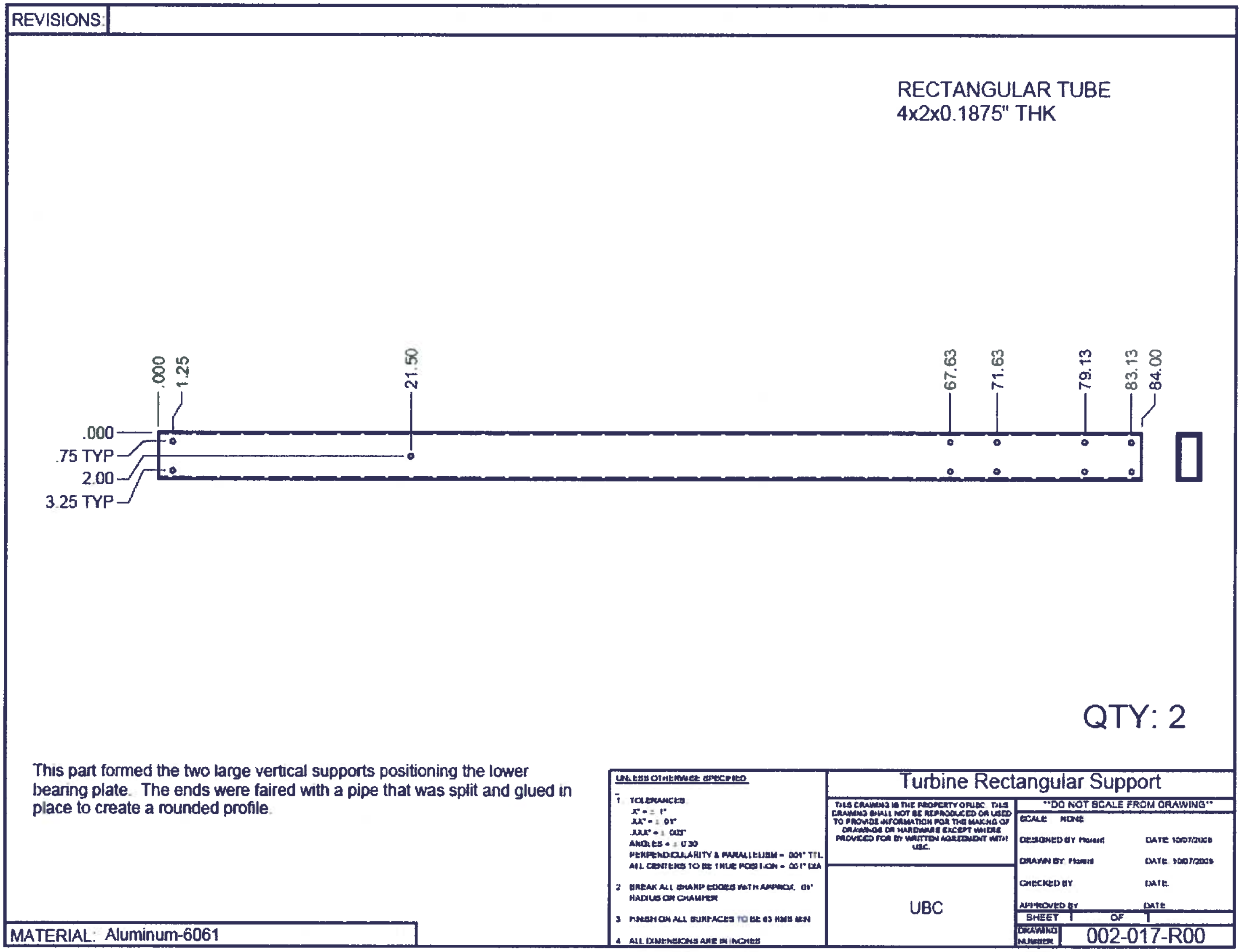

Figure B-6: Vertical supports for lower bearing support plate.

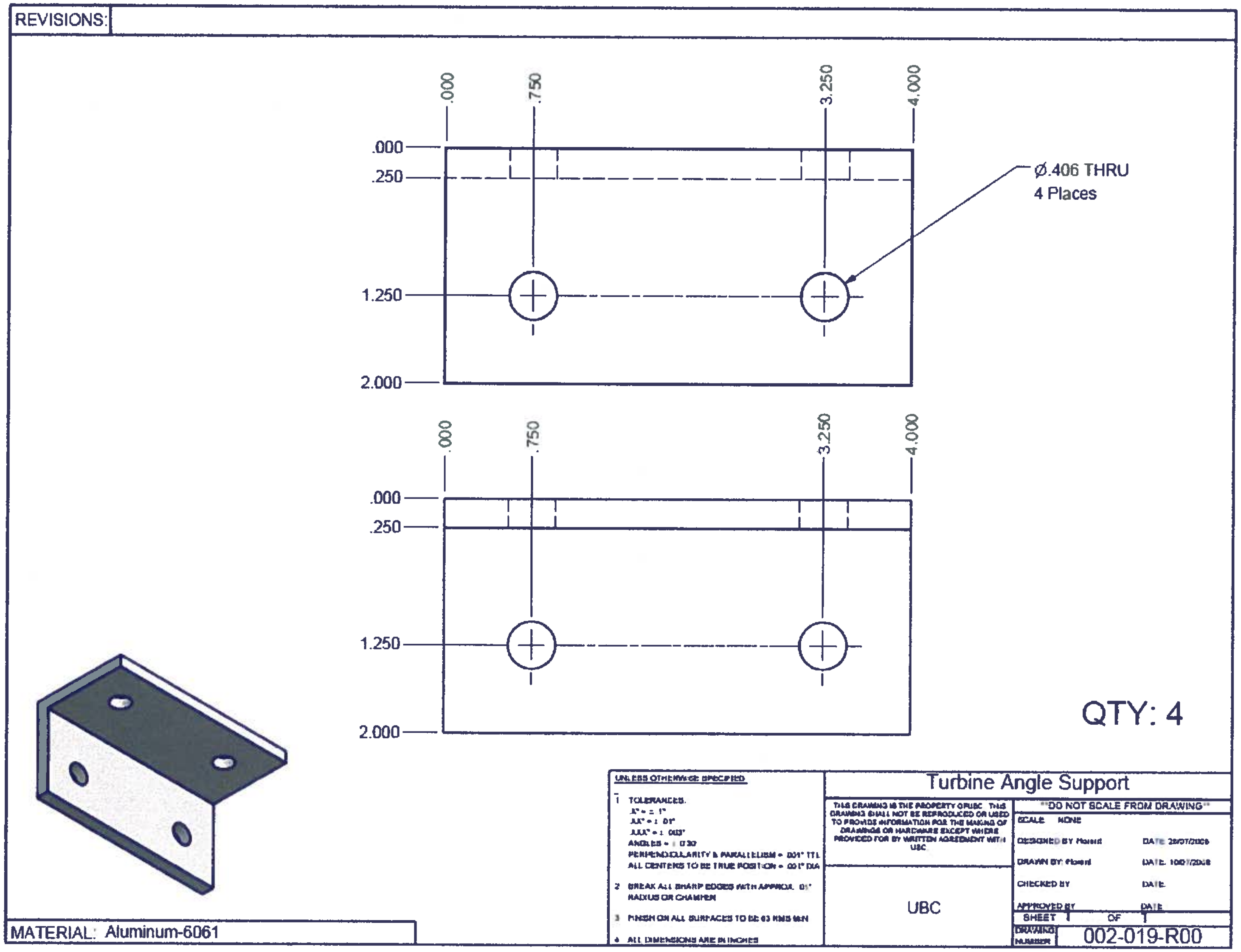

Figure B-7: Angle bracket connecting vertical supports to bottom plate.

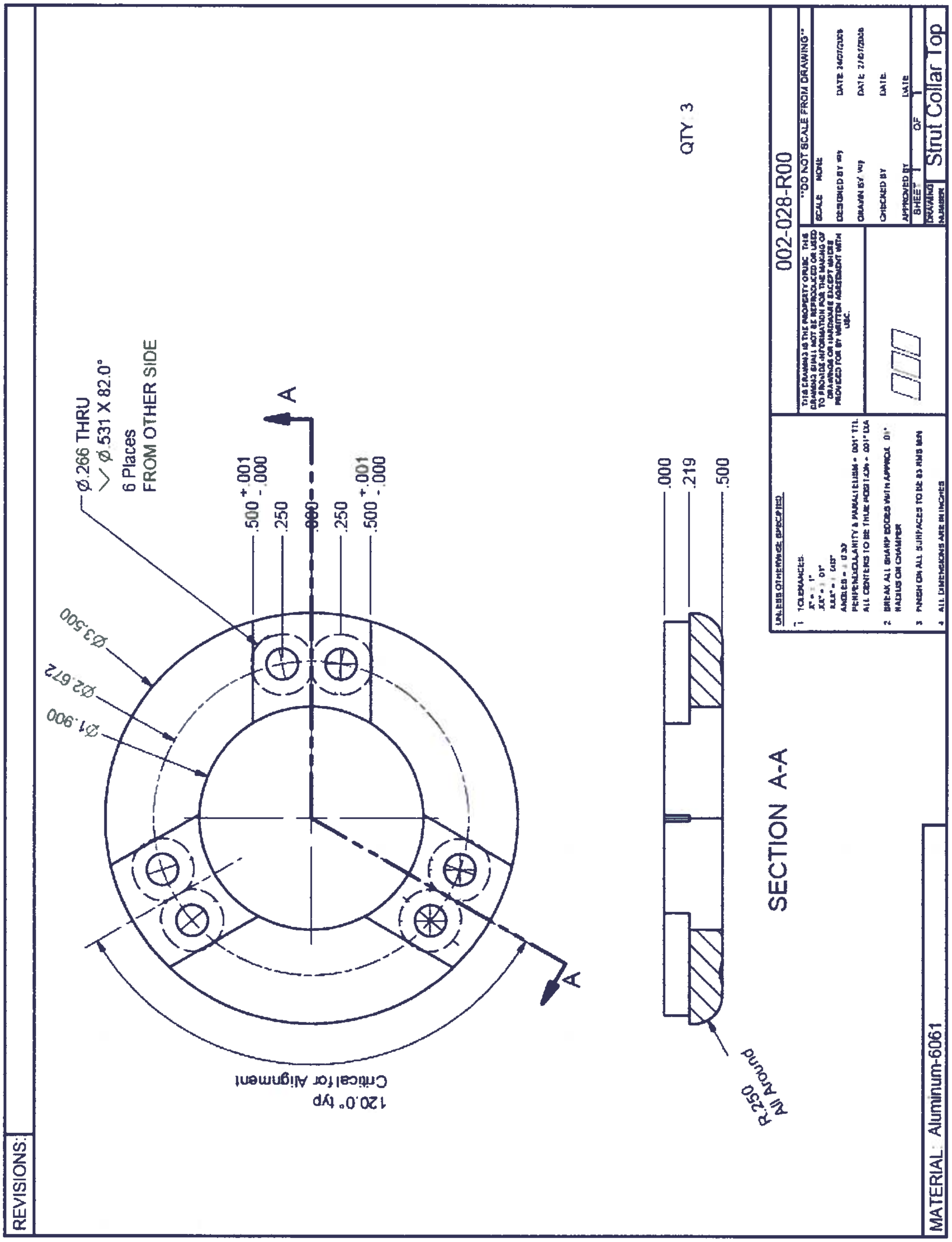

Figure B-8: Top of shaft collar for mounting arms to main shaft.

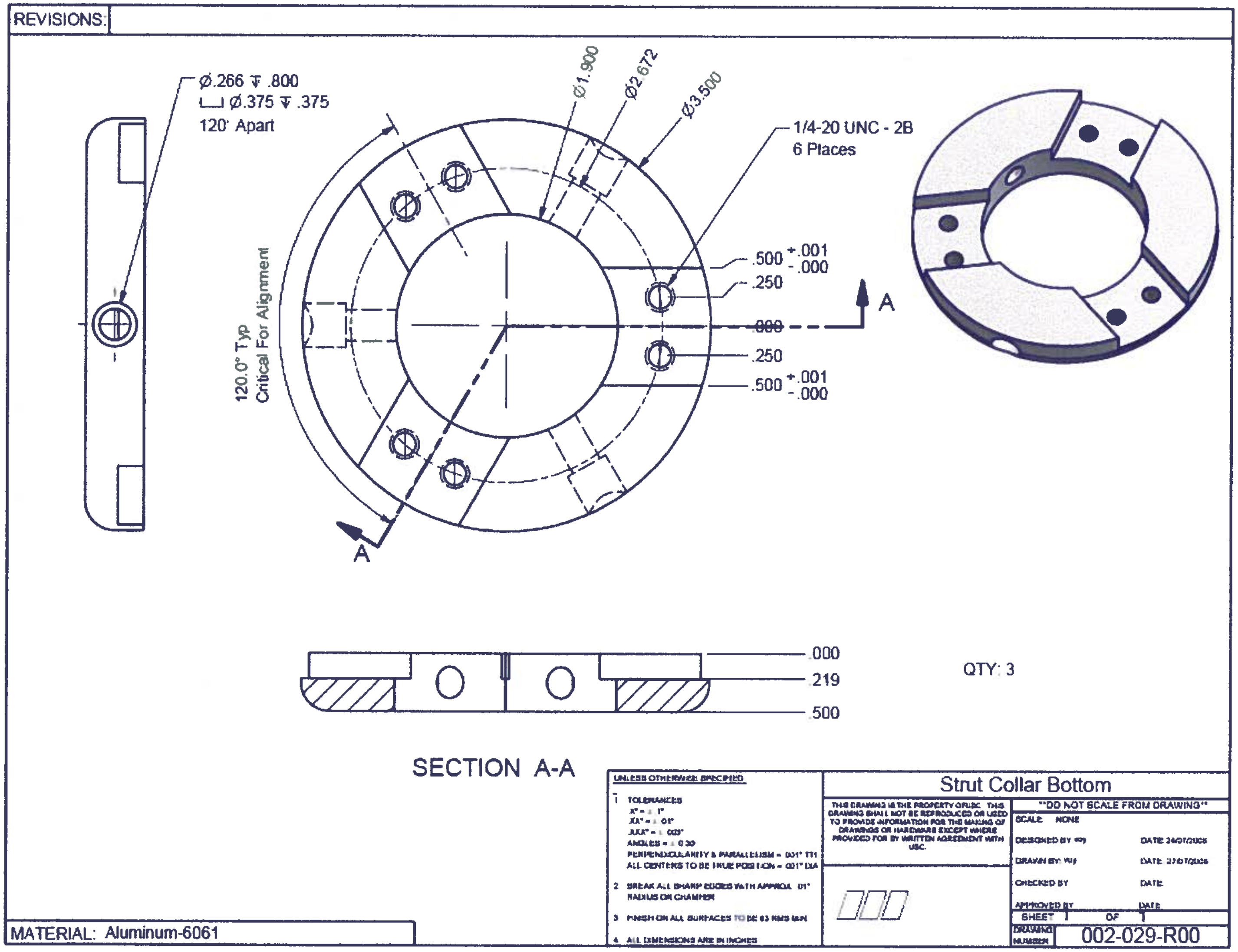

Figure B-9: Bottom of shaft collar for mounting arms to main shaft.

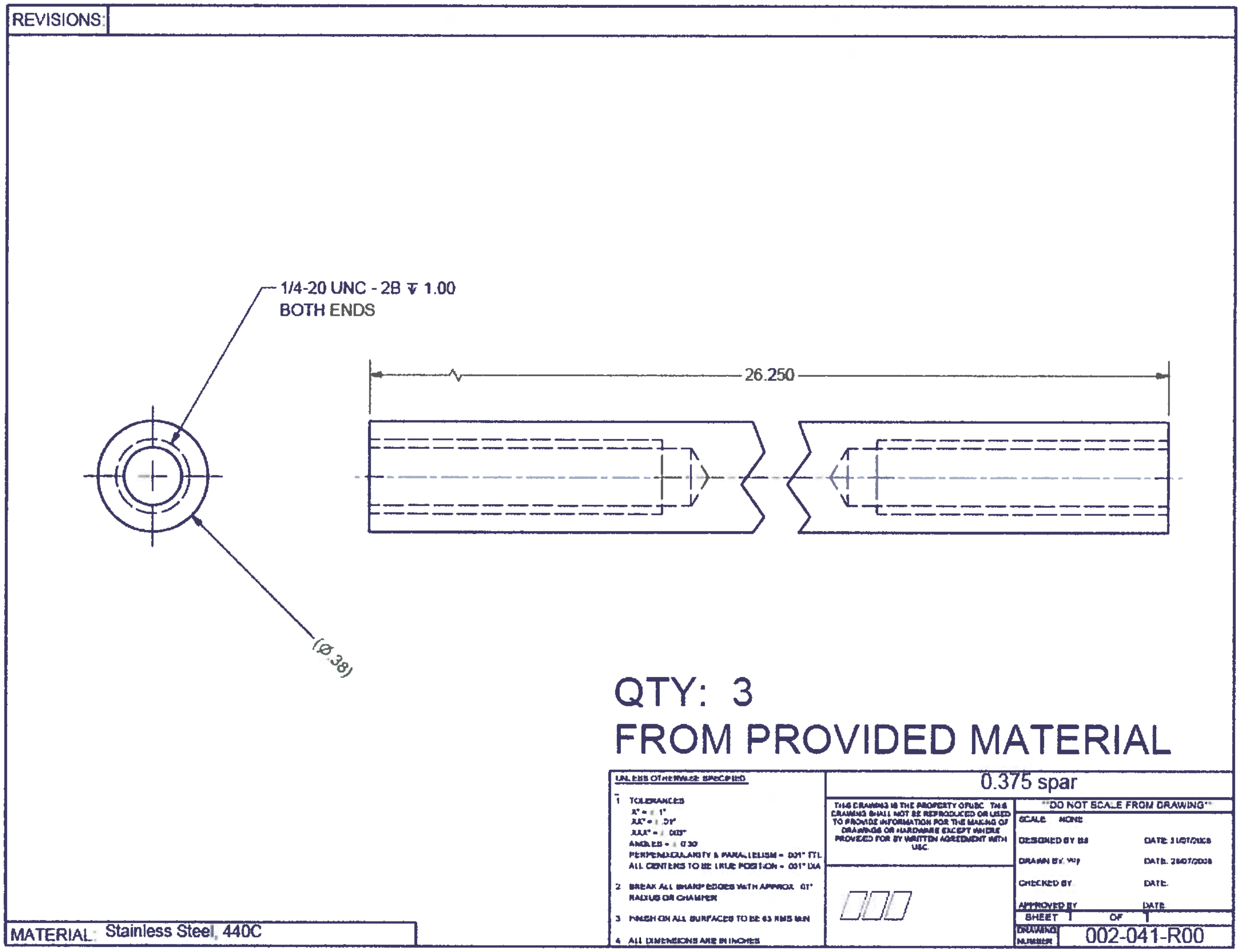

Figure B-10: 3/8" spar for foil assembly.

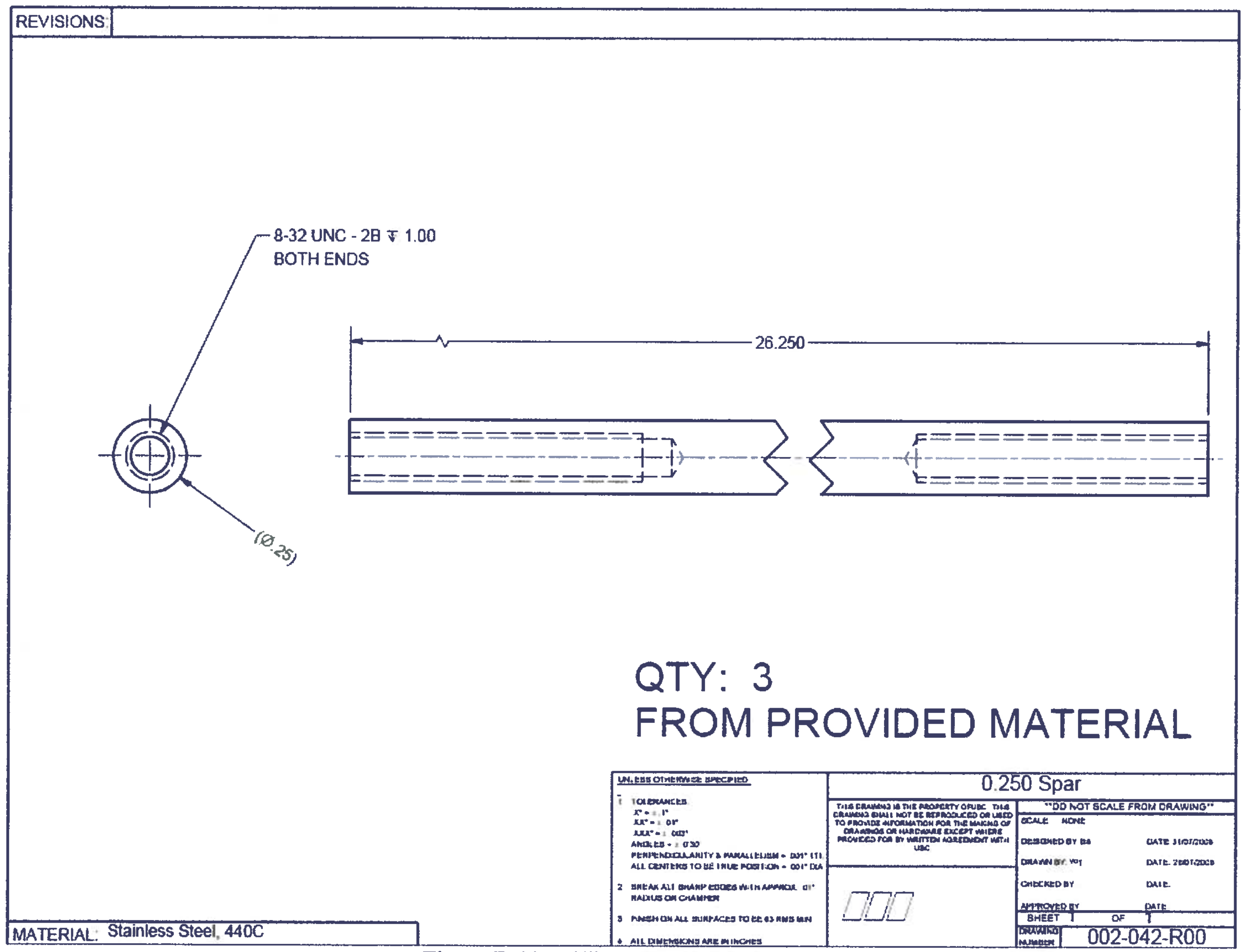

Figure B-11: 1/4" spar for foil assembly.

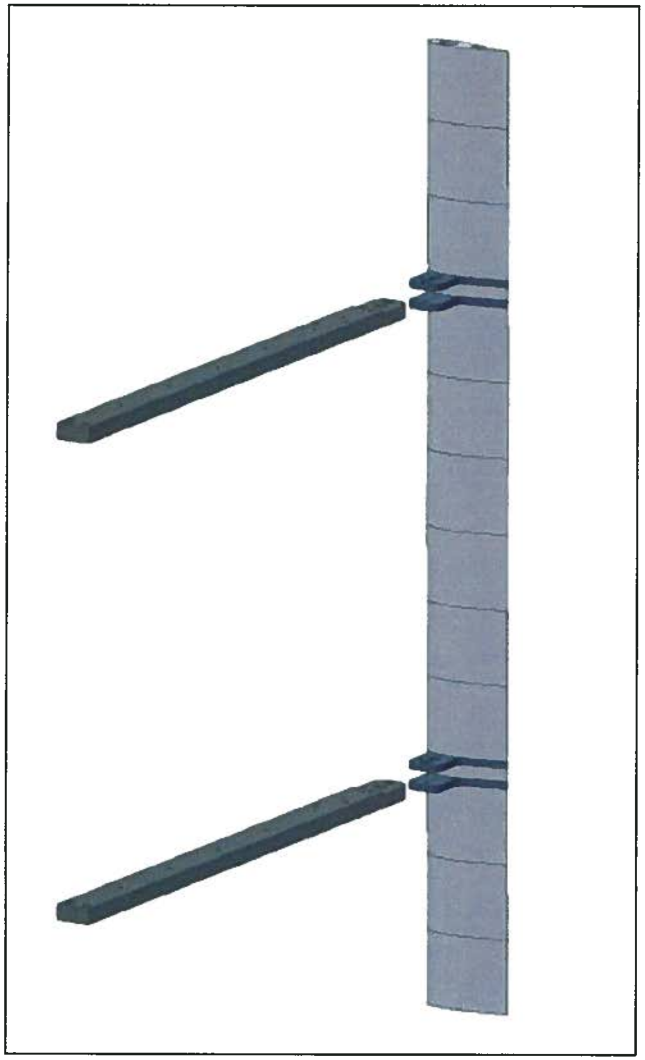

Figure B-12: ¼ span blade assembly as for arm profiles A and B.

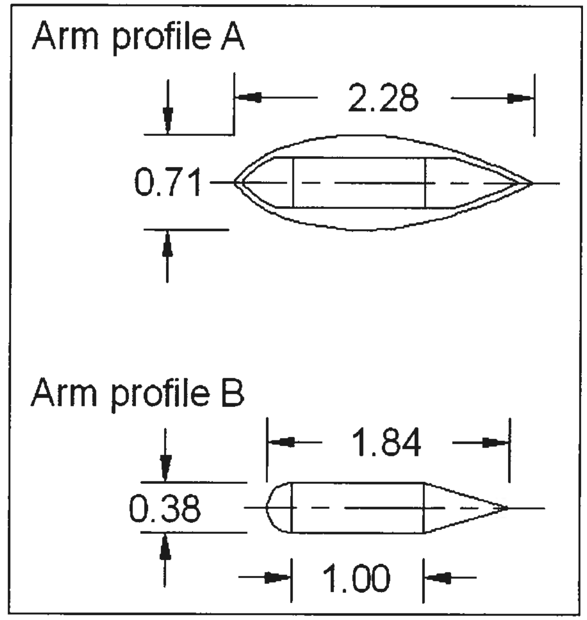

Figure B-13: Arm profiles A and B with fairings.

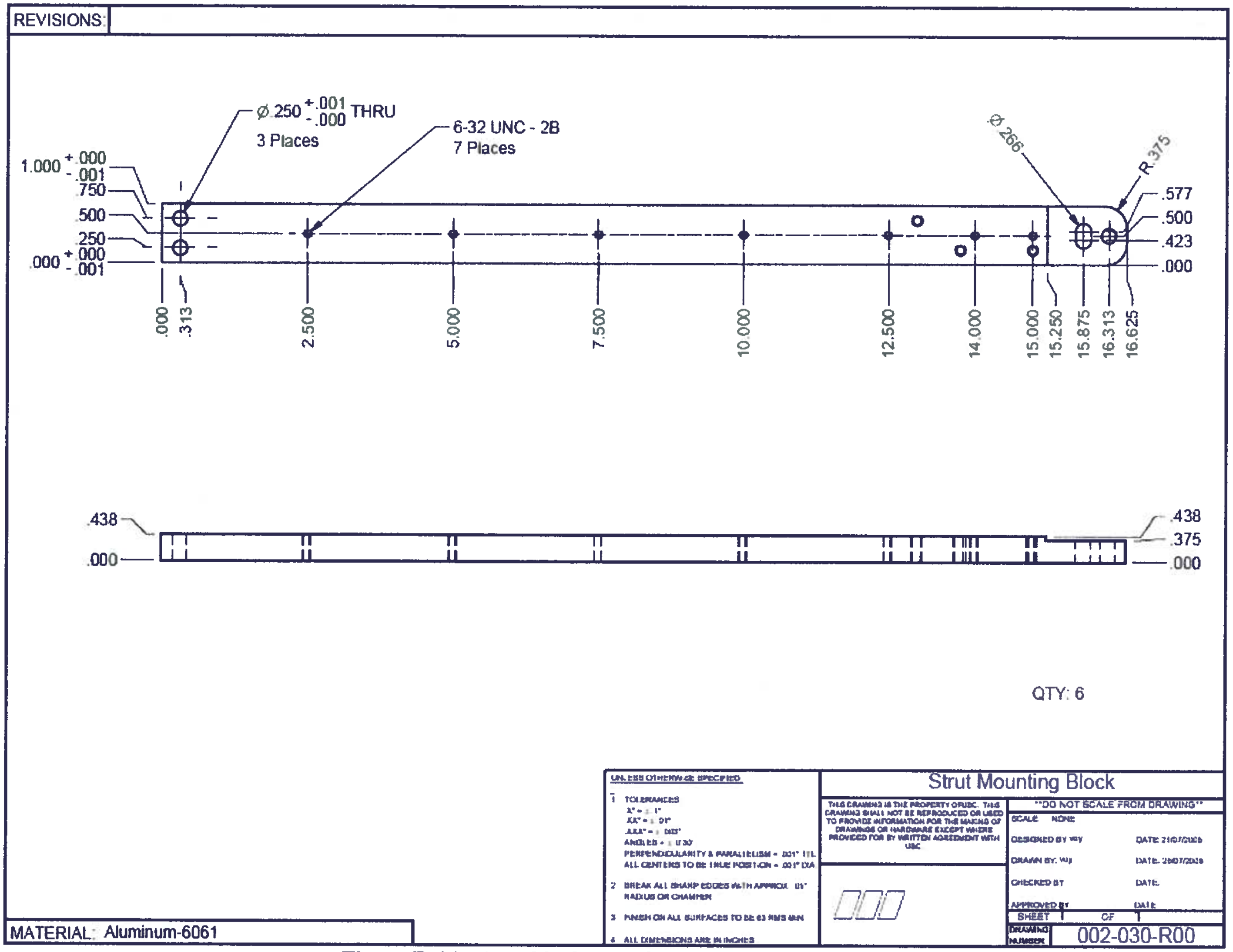

Figure B-14: Arm block used for arm profiles A and B.

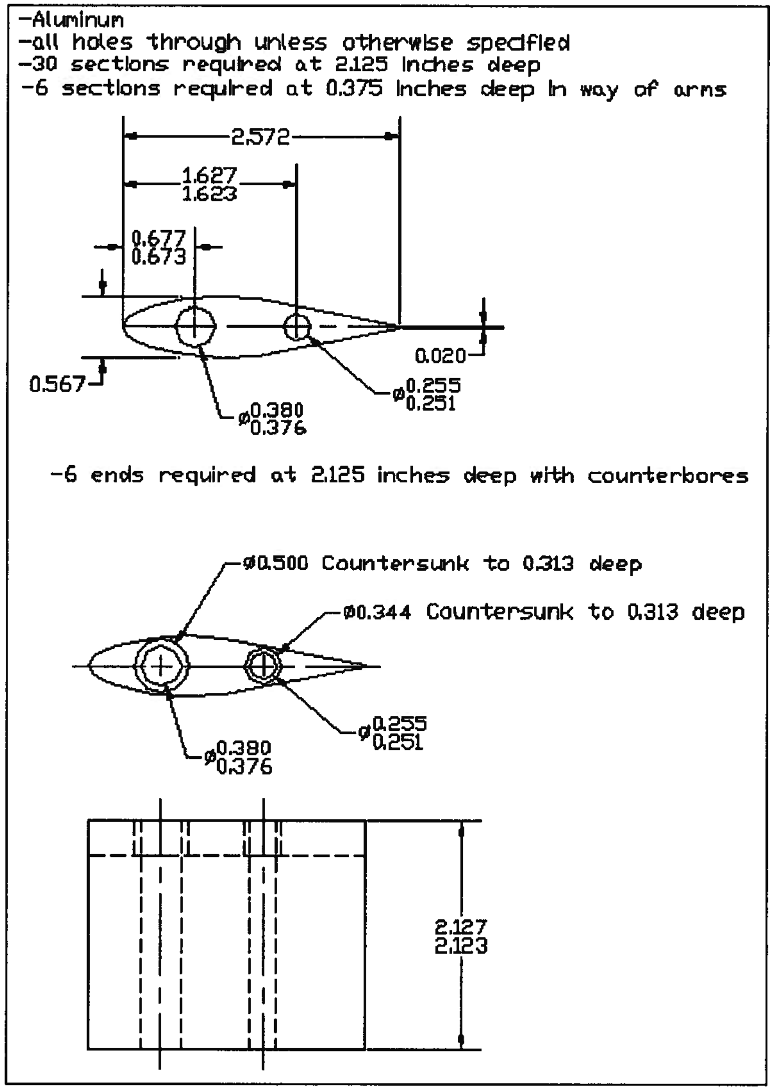

Figure B-15: 63_4-021 foil fabrication components.

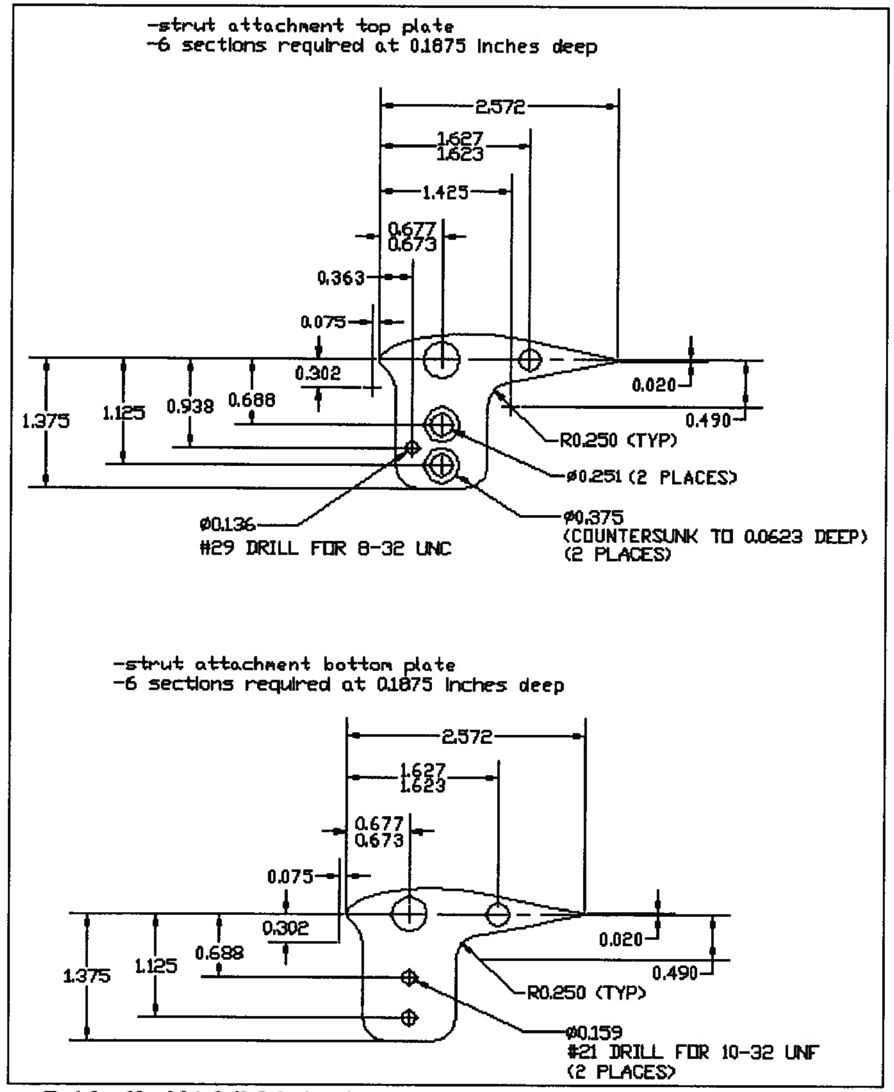

Figure B-16: 63_4-021 foil fabrication clamping components for ¼ span configuration.

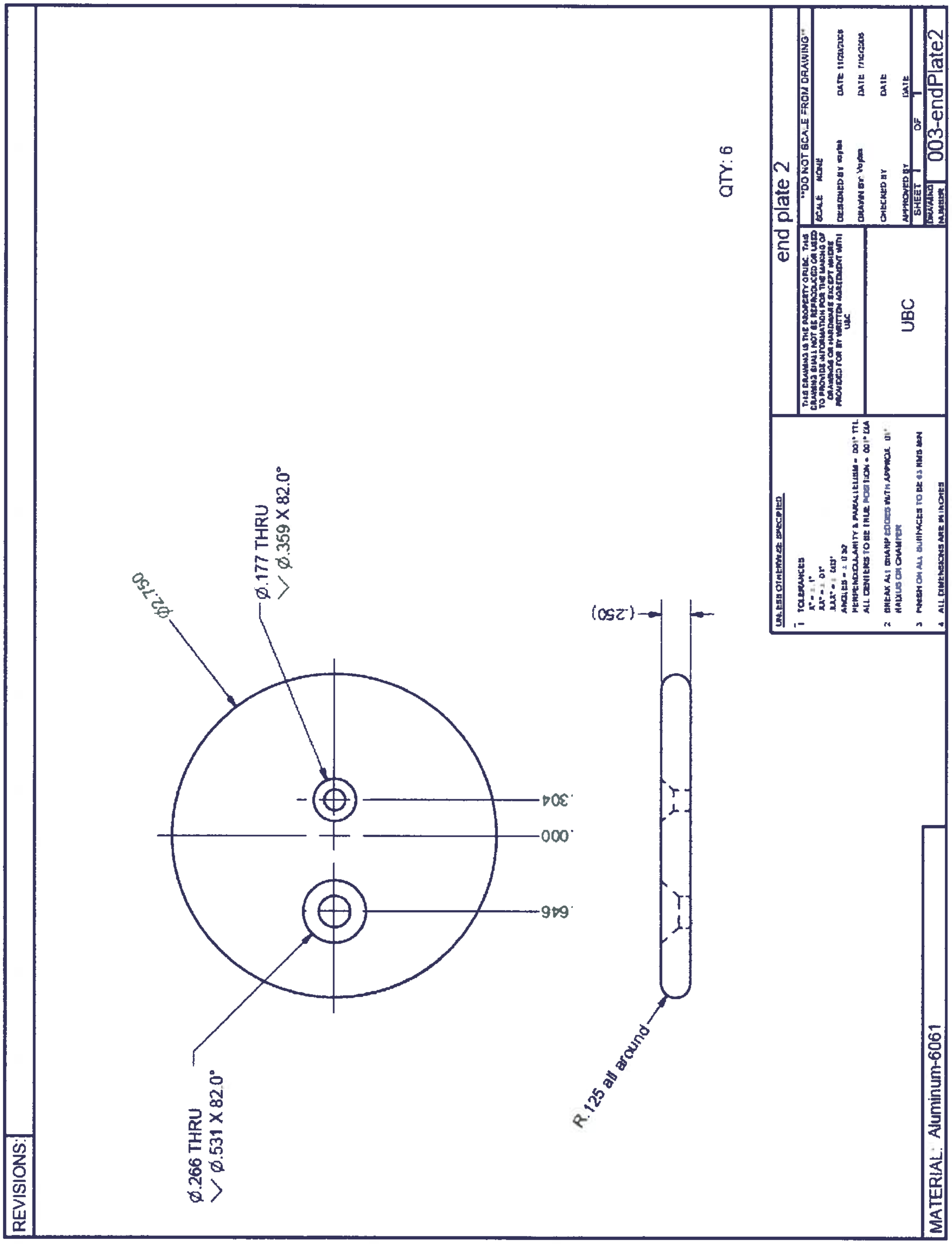

Figure B-17: Circular end plates.

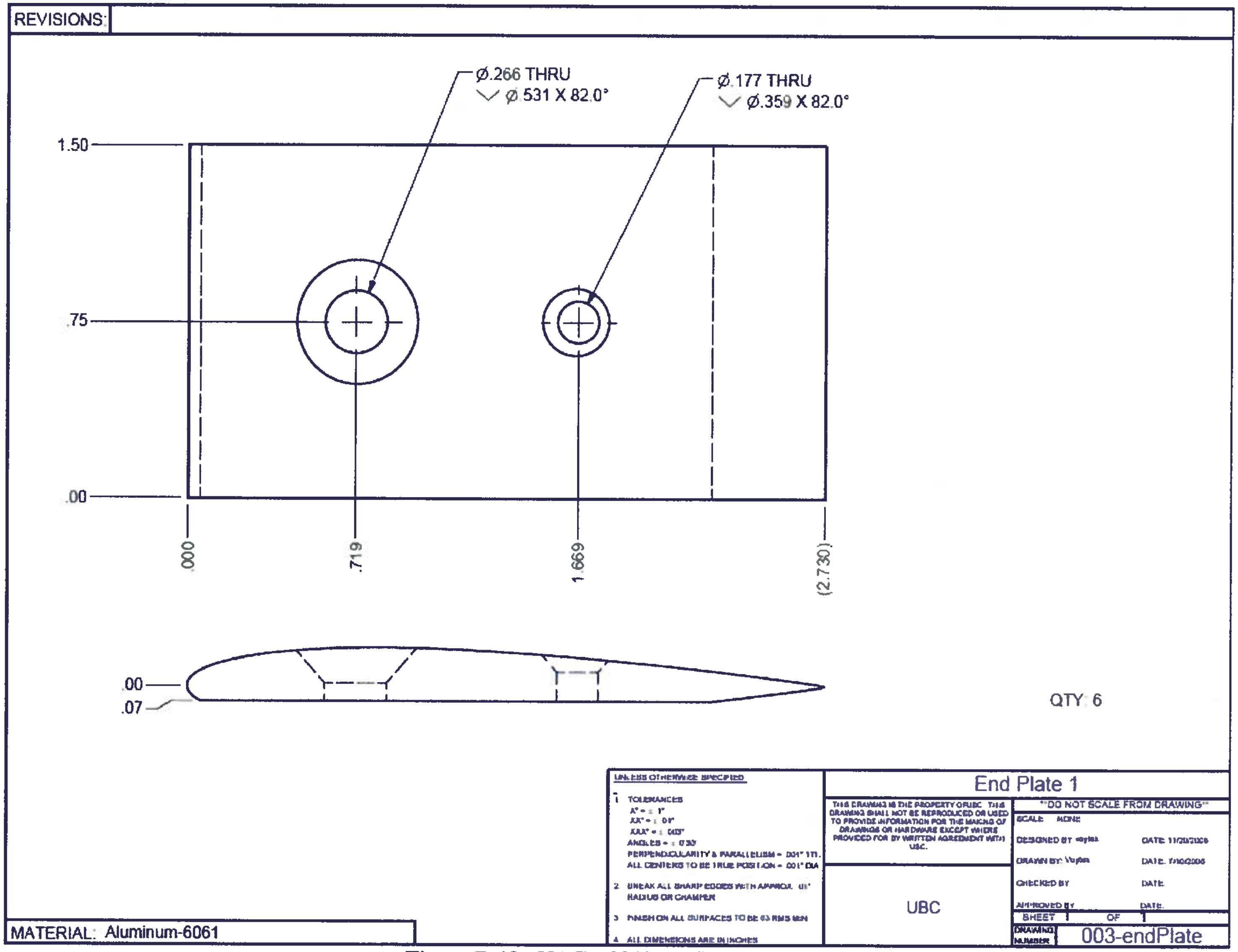

Figure B-18: NACA 0012 profile end plates.

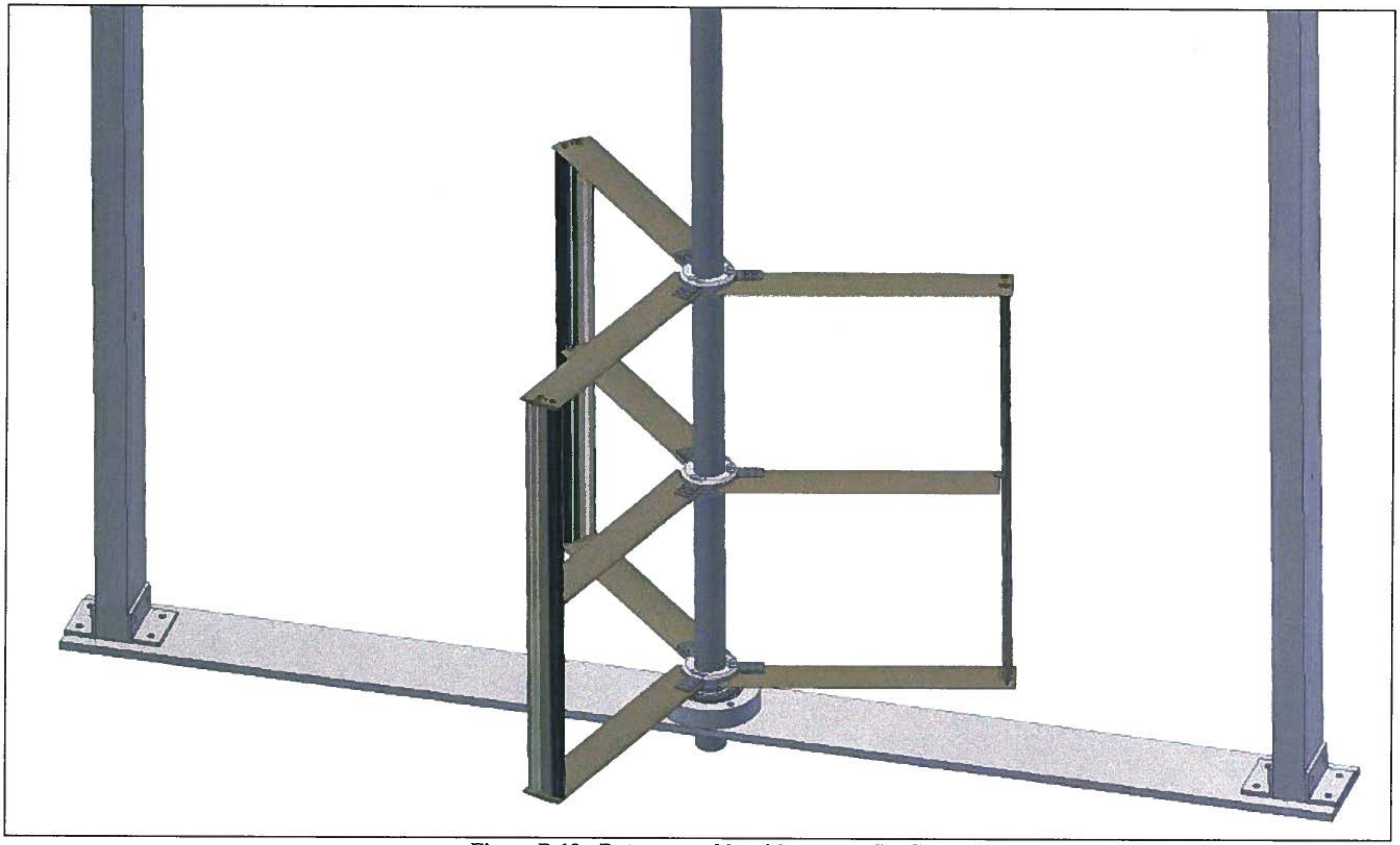

Figure B-19: Rotor assembly with arm profile C.

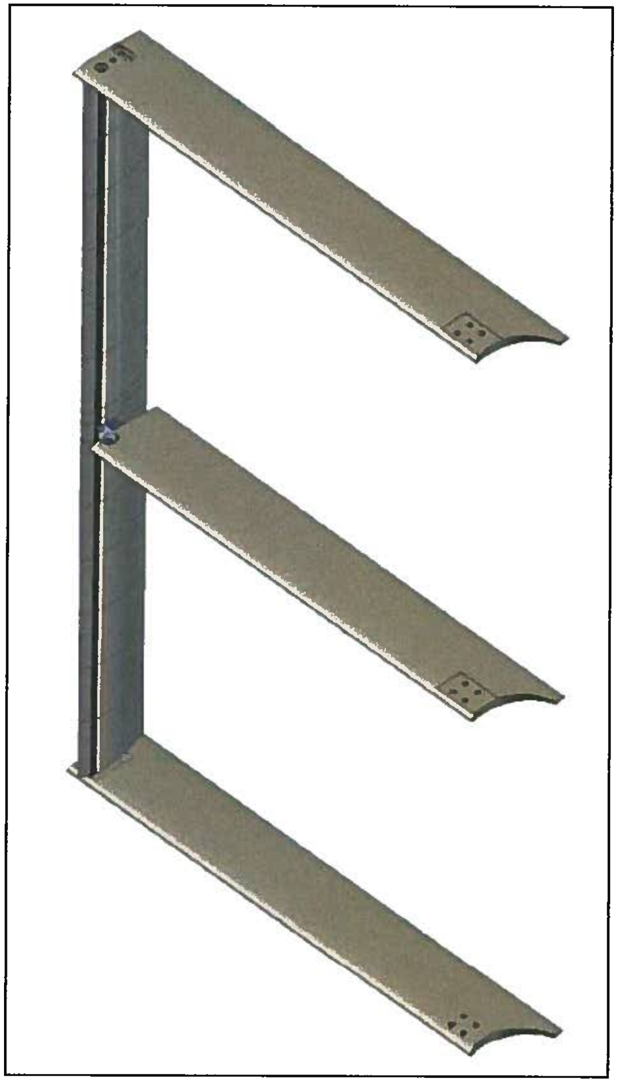

Figure B-20: Blade assembly with arm profile C.

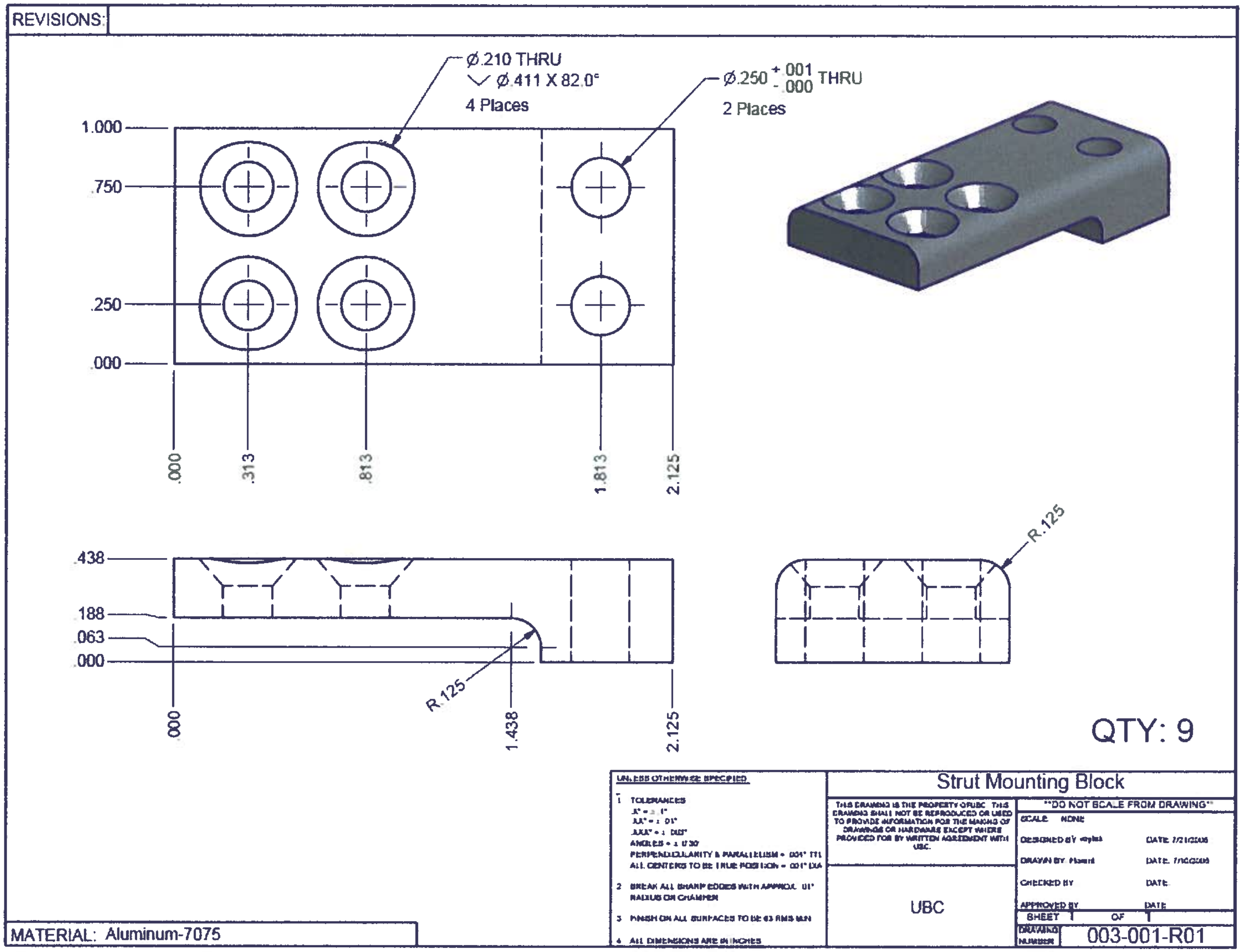

Figure B-21: Block for attaching profile C arms to shaft collars.

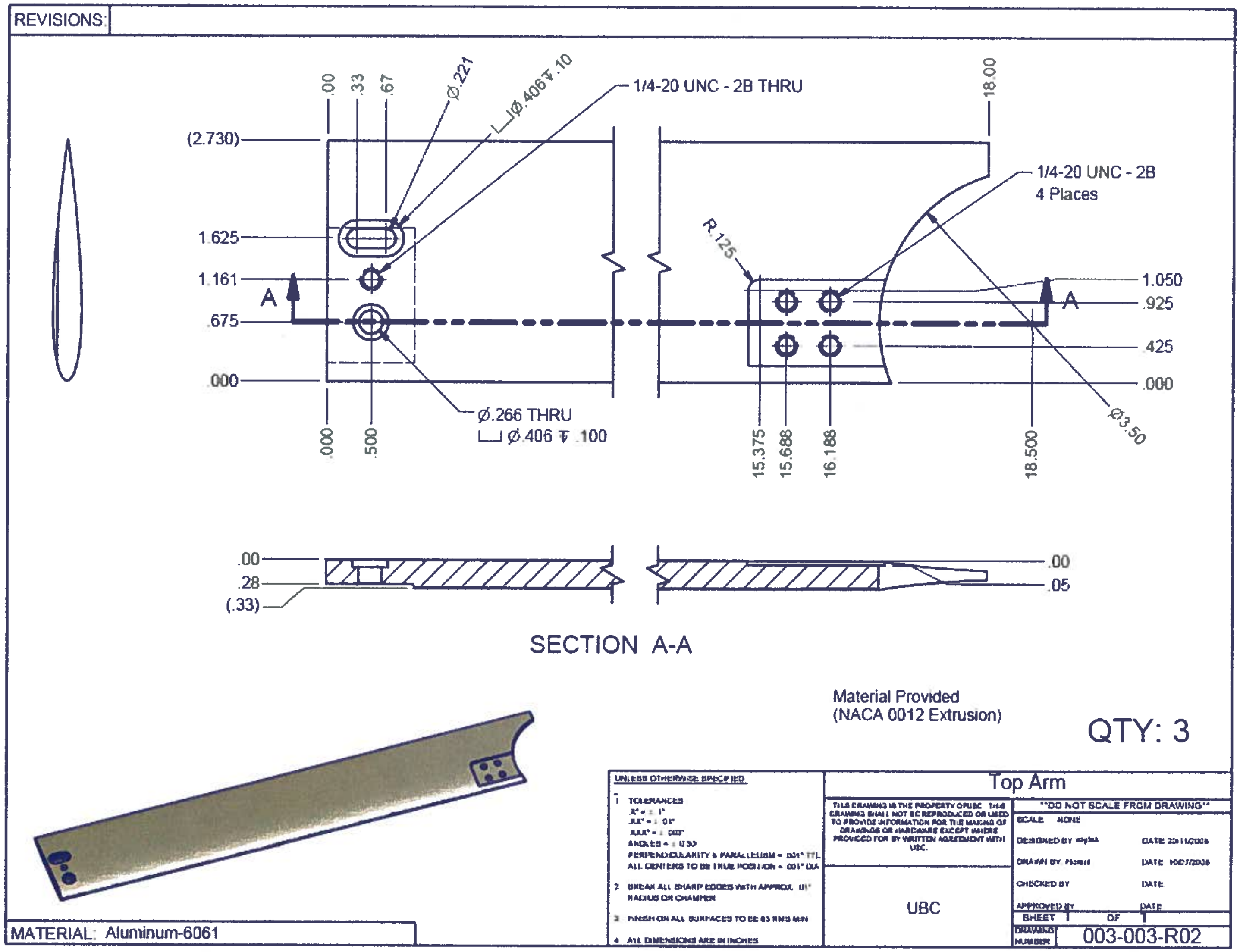

Figure B-22: Profile C upper arm.

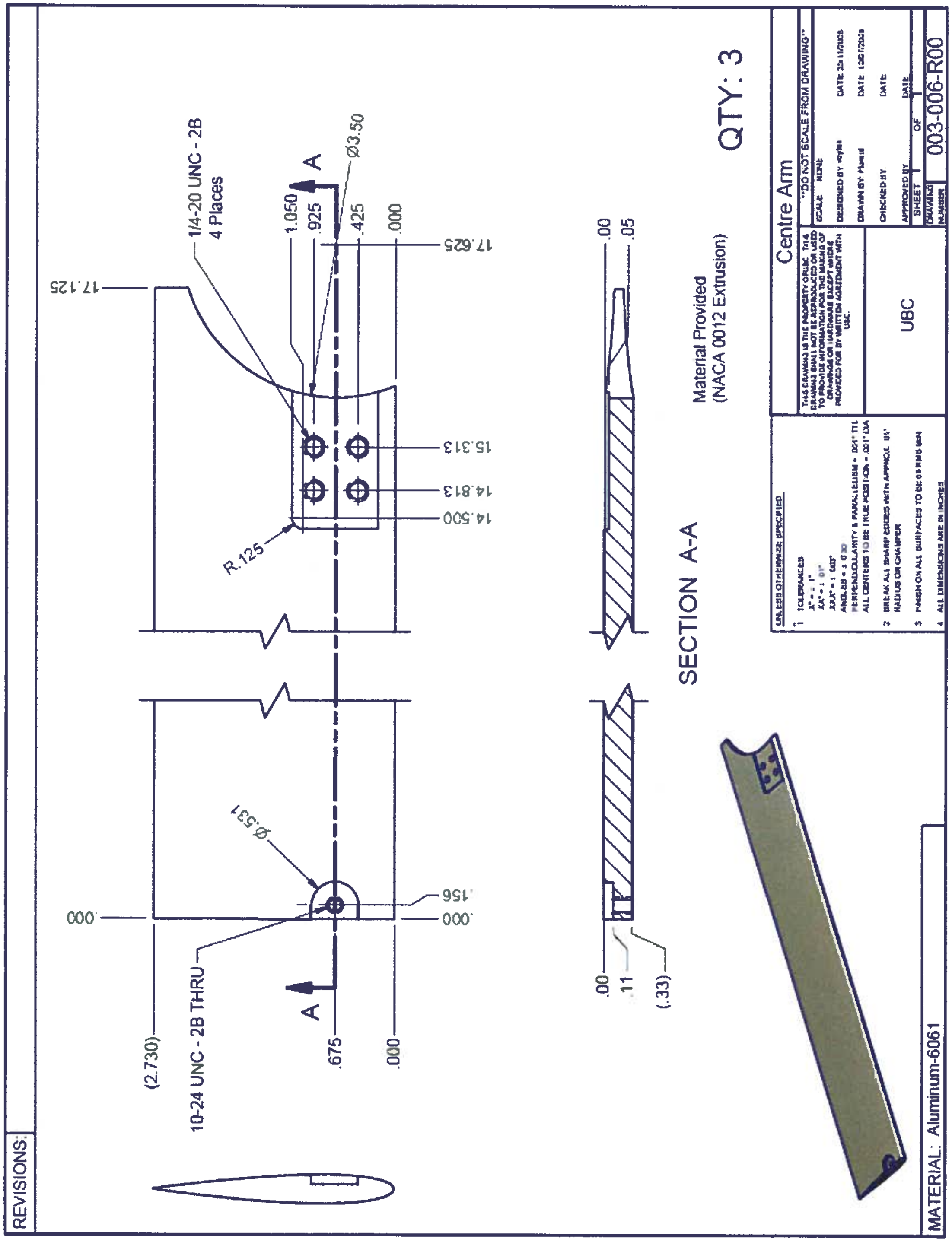

Figure B-23: Profile C central arm.

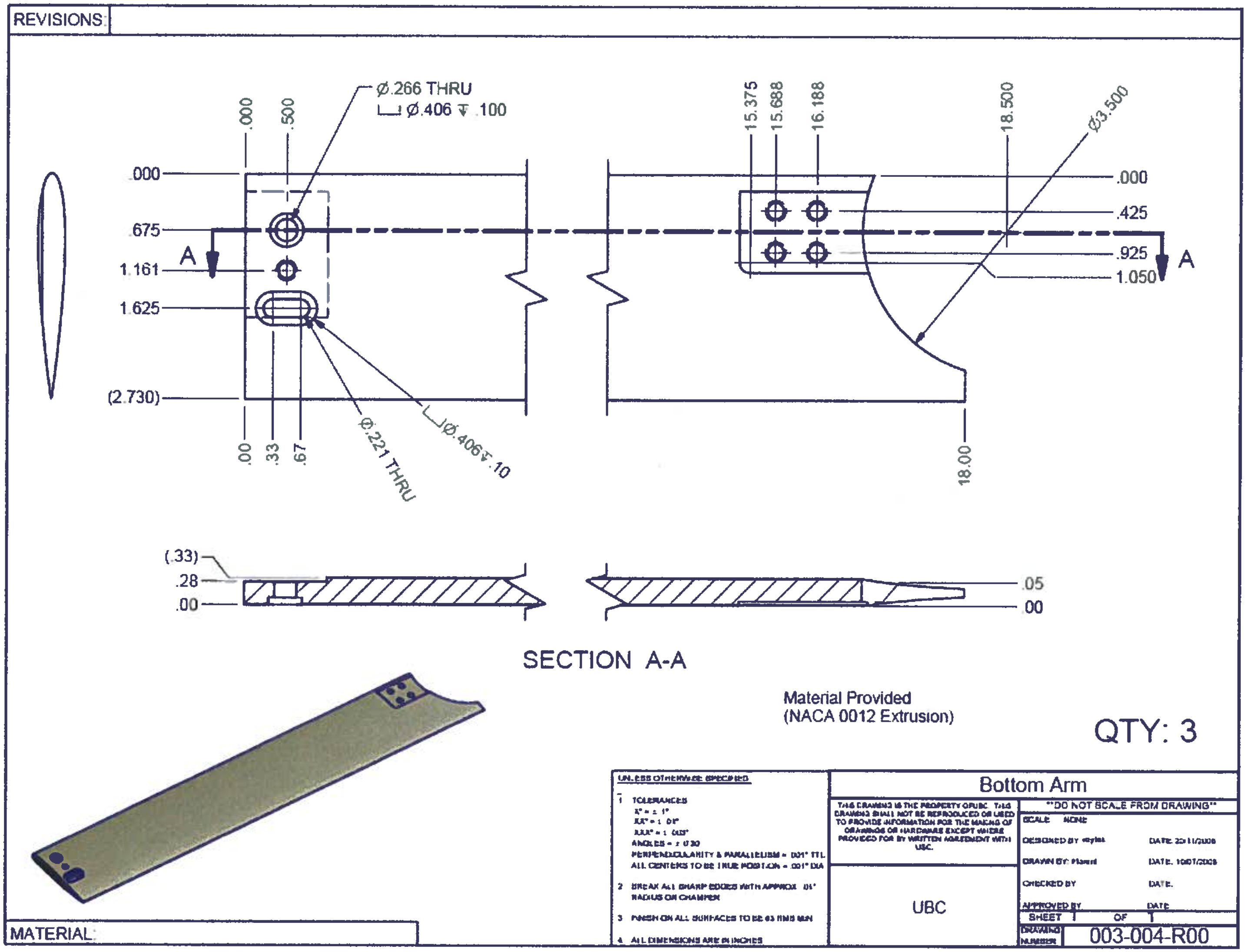

Figure B-24: Profile C lower arm.

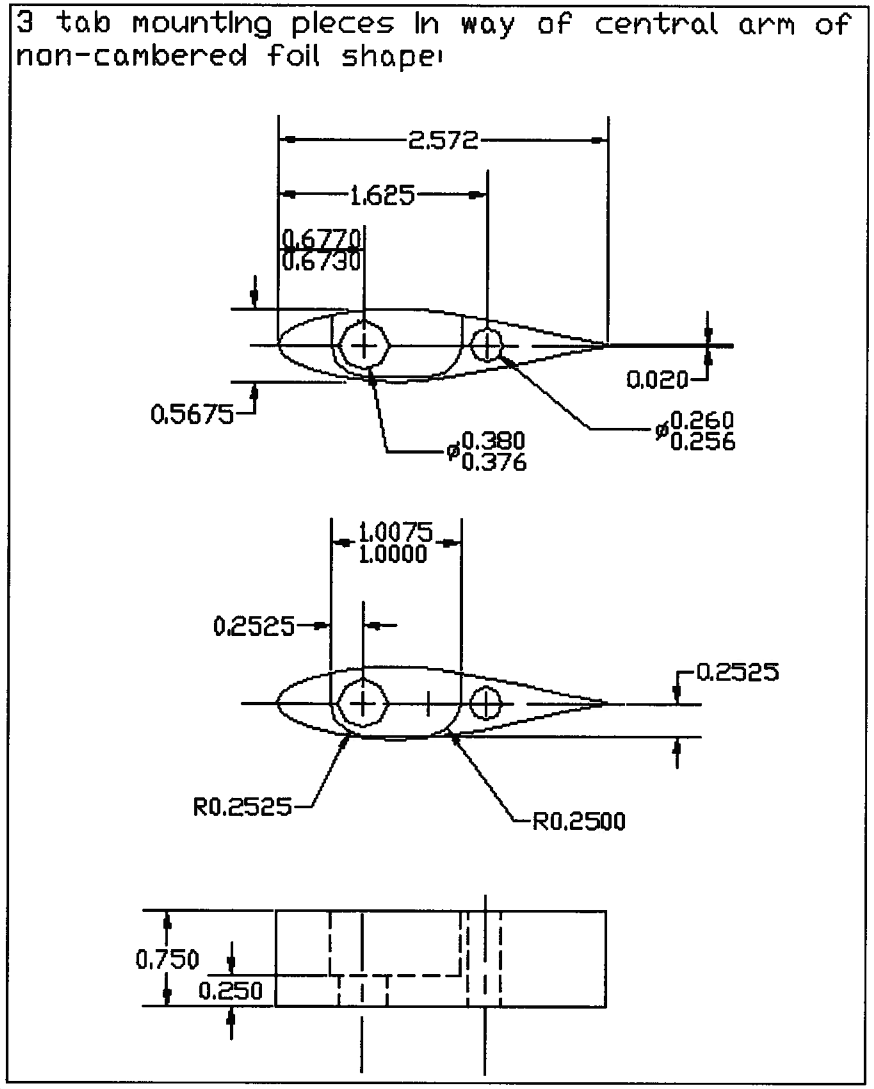

Figure B-25: Replacement 63_4-021 central foil pieces for use with arm profile C.

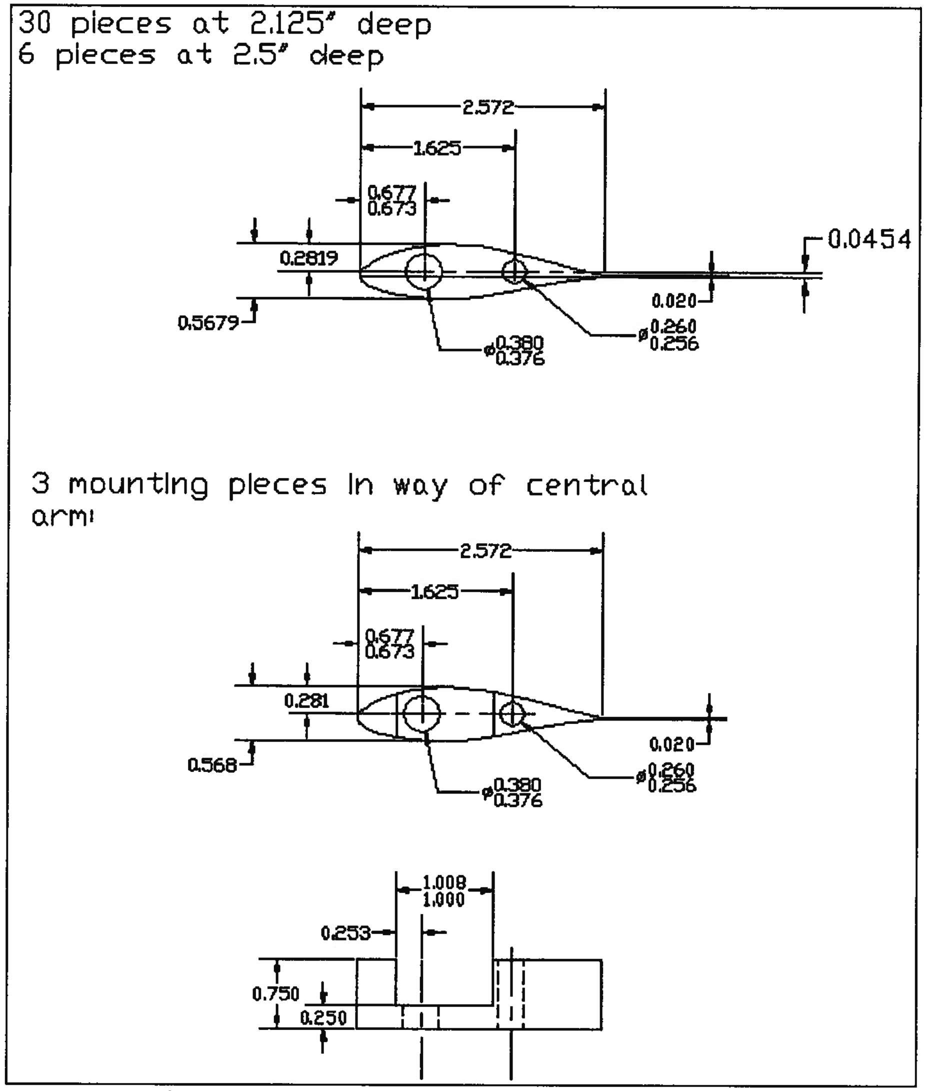

Figure B-26: 63_4-421 cambered blade foil components.

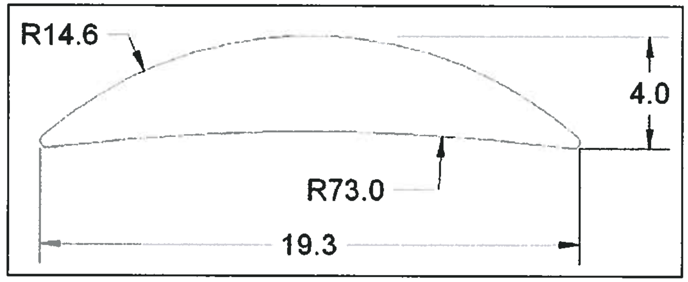

Figure B-27: Deflector details.

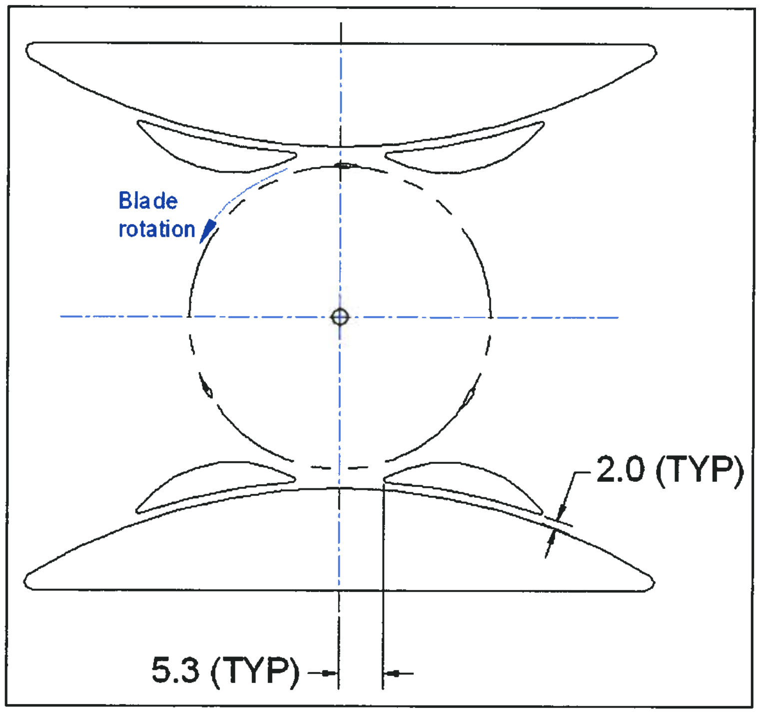

Figure B-28: Deflector positioning.

APPENDIX C: INSTRUMENTATION AND DAQ COMPONENTS

Instrumentation:

- 2 of PT-Global SG-PT4000-500 lb s-type load cells
  www.sensor-technik.co.uk/datasheets/pt4000.pdf
- Futek Torque Sensor, 0 - 369 ft lb, 0.2% accuracy, aluminum, 2mV/Voutput , 7" length (TRS300)
  http://www.futek.com/product.aspx?stock=FSH01992&acc2=acc
- Accu-Coder 776-B-S-2048-R-PP-E-P-A-N 1-7/8" through-bore encoder (2048 increments per revolution)
  http://www.encoder.com/model776.html
- Extech 0 - 18 Volts DC, 3 Amps, 2 digital/four digit display power supply
- BK Precision triple output 12V, 5V, and 0-30Volts DC, 5 Amp, 2 digital/three digit display power supply
- BK Precision 0-18 Volts DC, 5 Amp programmable power supply with Labview RS232
- U.S. Digital encoder digital-analog converter (used with encoder)
  www.usdigital.com/products/edac/

Drive-train:

- 3HP microMAX motor 182TCZ TEFC from Marathon Electric with Parker SSD AC 690+ vector drive controller and braking resistor kit (may be used for both driving and braking turbine) (7/8" shaft; 230V, 4.6A, 5400 max. safe rpm)
  www.marathonelectric.com/motors/docs/manuals/SB548.pdf
  www.ssddrives.com/usa/Resources/PDFs/Catalog/690%20Series%20AC%20Drives.pdf
- CONEX gearbox B091020.LAARJ, TEXTRON fluid and power. Ratio 20:1, SHC 634 lubrication, helicoidal gear geometry (used with gearbox configuration)
  www.akrongear.com/documents/catalogs/textron/Series%20B%2023293-0503.pdf

Data Acquisition Hardware:

- 1 cDAQ-9172 8-slot USB Chassis with rail mounting kit
  http://sine.ni.com/nips/cds/view/p/lang/fr/nid/202545
- 1 NI 9205 32-Channel +/- 10V 250 ks/s 16-bit analog input module used with encoder and carriage speed
  http://sine.ni.com/nips/cds/view/p/lang/fr/nid/202571
- 1 NI 9237 4-Ch 50 ks/s per channel 24-bit analog input module used with torque sensor
  http://sine.ni.com/nips/cds/view/p/lang/fr/nid/202632

APPENDIX D: RUN LOG

AUGUST 2006 RUNS

Arm Profile "A", chains and sprockets drive-train.

Run	Direction	AoA	Velocity	TSR	RPM	ω	Avg. Power	Ck
			m/s			(rad/s)	(W)	
'100'	'w'	0	1.00	1.25	25.97	2.72	-7.27	-0.0229
'101'	'd'	0	1.00	1.25	26.03	2.73	-6.64	-0.0207
'102'	'w'	0	1.00	1.49	30.94	3.24	-3.49	-0.0109
'103'	'd'	0	1.00	1.48	30.94	3.24	-4.28	-0.0133
'104'	'w'	0	1.00	1.74	36.34	3.81	0.22	0.0007
'105'	'd'	0	1.00	1.74	36.36	3.81	-0.55	-0.0017
'106'	'w'	0	1.00	2.00	41.77	4.37	8.20	0.0257
'107'	'd'	0	1.00	2.00	41.73	4.37	6.83	0.0213
'108'	'w'	0	1.00	2.24	46.61	4.88	17.25	0.0541
'109'	'd'	0	1.00	2.23	46.62	4.88	17.74	0.0554
'110'	'w'	0	1.00	2.50	52.05	5.45	19.45	0.0610
'111'	'd'	0	1.00	2.49	52.02	5.45	18.90	0.0590
'112'	'w'	0	1.00	2.75	57.27	6.00	7.84	0.0246
'113'	'd'	0	1.00	2.74	57.25	6.00	8.59	0.0268
'114'	'w'	0	1.00	2.99	62.21	6.51	-14.55	-0.0456
'115'	'd'	0	1.00	2.98	62.24	6.52	-13.64	-0.0426
'116'	'w'	0	1.00	3.25	67.71	7.09	-45.55	-0.1431
'117'	'd'	0	1.00	3.24	67.71	7.09	-45.88	-0.1431
'118'	'w'	0	1.00	3.50	72.93	7.64	-85.64	-0.2688
'119'	'd'	0	1.00	3.50	72.95	7.64	-82.75	-0.2583
'120'	'w'	0	1.25	1.25	32.66	3.42	-8.35	-0.0134
'121'	'd'	0	1.25	1.25	32.70	3.42	-9.44	-0.0151
'122'	'w'	0	1.25	1.50	39.01	4.09	0.01	0.0000
'123'	'd'	0	1.25	1.50	39.05	4.09	-1.02	-0.0016
'124'	'w'	0	1.25	1.76	45.71	4.79	10.11	0.0163
'125'	'd'	0	1.25	1.75	45.69	4.78	7.07	0.0113
'126'	'w'	0	1.25	2.00	52.02	5.45	23.35	0.0376
'127'	'd'	0	1.25	2.00	52.03	5.45	23.85	0.0382
'128'	'w'	0	1.25	2.24	58.42	6.12	46.15	0.0742
'129'	'd'	0	1.25	2.24	58.40	6.12	46.31	0.0743
'130'	'w'	0	1.25	2.49	64.84	6.79	44.29	0.0713
'131'	'd'	0	1.25	2.49	64.81	6.79	45.37	0.0727
'132'	'w'	0	1.25	2.75	71.53	7.49	20.62	0.0332
'133'	'd'	0	1.25	2.74	71.50	7.49	21.59	0.0346
'134'	'w'	0	1.25	3.00	78.06	8.17	-26.25	-0.0422
'135'	'd'	0	1.25	2.99	78.01	8.17	-22.33	-0.0358
'136'	'w'	0	1.25	3.25	84.53	8.85	-84.07	-0.1354
'137'	'd'	0	1.25	3.24	84.52	8.85	-84.49	-0.1355
'138'	'w'	0	1.25	3.50	91.04	9.53	-157.82	-0.2542
'139'	'd'	0	1.25	3.49	91.02	9.53	-159.46	-0.2557
'140'	'w'	0	1.50	1.25	39.08	4.09	-8.10	-0.0075
'141'	'd'	0	1.50	1.25	39.11	4.10	-10.79	-0.0100
'142'	'w'	0	1.49	1.50	46.87	4.91	12.35	0.0115
'143'	'd'	0	1.50	1.50	46.91	4.91	7.22	0.0067
'144'	'w'	0	1.49	1.75	54.53	5.71	29.46	0.0275

AUGUST 2006

Run	Direction	AoA	Vel	TSR	RPM	ω	Power	Ck
'145'	'd'	0	1.50	1.74	54.50	5.71	21.94	0.0204
'146'	'w'	0	1.49	2.00	62.36	6.53	65.33	0.0609
146b'	'w'	0	1.49	2.00	62.36	6.53	64.35	0.0600
'147'	'd'	0	1.50	2.00	62.36	6.53	56.05	0.0521
'147'	'd'	0	1.50	1.99	62.32	6.53	58.80	0.0546
'148'	'w'	0	1.49	2.24	69.92	7.32	91.60	0.0854
'149'	'd'	0	1.50	2.24	69.92	7.32	87.87	0.0817
'150'	'w'	0	1.49	2.49	77.84	8.15	78.96	0.0736
'151'	'd'	0	1.50	2.49	77.83	8.15	79.39	0.0738
'152'	'w'	0	1.49	2.74	85.55	8.96	38.04	0.0355
'153'	'd'	0	1.50	2.73	85.41	8.94	37.95	0.0353
'154'	'w'	0	1.49	3.00	93.60	9.80	-39.53	-0.0369
'155'	'd'	0	1.50	3.00	93.59	9.80	-43.27	-0.0403
'156'	'w'	0	1.49	3.24	101.16	10.59	-134.97	-0.1260
'157'	'd'	0	1.50	3.24	101.32	10.61	-138.92	-0.1292
'158'	'w'	0	1.49	3.51	109.40	11.46	-262.51	-0.2451
'159'	'd'	0	1.50	3.50	109.45	11.46	-268.28	-0.2497
'160'	'w'	0	1.74	1.23	44.62	4.67	-7.44	-0.0044
'161'	'd'	0	1.75	1.25	45.48	4.76	-13.50	-0.0079
'162'	'w'	0	1.74	1.50	54.47	5.70	37.44	0.0220
'163'	'd'	0	1.74	1.50	54.55	5.71	22.05	0.0129
'164'	'w'	0	1.74	1.74	63.49	6.65	59.47	0.0350
'165'	'd'	0	1.74	1.75	63.59	6.66	42.74	0.0251
'166'	'w'	0	1.74	2.00	72.62	7.60	128.40	0.0755
'167'	'd'	0	1.74	1.99	72.66	7.61	113.66	0.0667
'168'	'w'	0	1.74	2.24	81.65	8.55	150.42	0.0885
'169'	'd'	0	1.74	2.24	81.67	8.55	150.94	0.0886
'170'	'w'	0	1.74	2.49	90.55	9.48	130.20	0.0766
'171'	'd'	0	1.74	2.49	90.59	9.49	130.27	0.0765
'172'	'w'	0	1.74	2.74	99.71	10.44	68.38	0.0403
'173'	'd'	0	1.74	2.74	99.84	10.45	61.43	0.0361
'174'	'w'	0	1.74	2.99	108.81	11.39	-58.89	-0.0347
'175'	'd'	0	1.74	3.00	109.13	11.43	-59.87	-0.0352
'176'	'w'	0	1.74	3.19	115.88	12.13	-225.40	-0.1328
'177'	'd'	0	1.74	3.24	117.80	12.34	-201.19	-0.1182
'180'	'w'	0	1.99	1.25	52.12	5.46	0.19	0.0001
'181'	'd'	0	1.99	1.25	52.13	5.46	-12.14	-0.0048
'182'	'w'	0	1.99	1.52	63.13	6.61	71.55	0.0282
'183'	'd'	0	1.99	1.50	62.28	6.52	46.57	0.0183
'184'	'w'	0	1.99	1.75	72.69	7.61	103.48	0.0408
'185'	'd'	0	1.99	1.75	72.63	7.61	77.02	0.0303
'186'	'w'	0	1.99	2.00	83.14	8.71	209.48	0.0827
'187'	'd'	0	1.99	2.00	83.14	8.71	184.22	0.0726
'188'	'w'	0	1.99	2.24	93.20	9.76	229.84	0.0908
'189'	'd'	0	1.99	2.24	93.21	9.76	215.80	0.0851
'190'	'w'	0	1.99	2.49	103.60	10.85	184.51	0.0729
'191'	'd'	0	1.99	2.49	103.64	10.85	196.52	0.0775
'192'	'w'	0	1.99	2.74	113.84	11.92	91.02	0.0360
'193'	'd'	0	1.99	2.74	113.70	11.91	102.43	0.0404
'194'	'w'	0	1.99	2.91	121.06	12.68	-63.94	-0.0253
'195'	'd'	0	1.99	2.92	121.56	12.73	-73.84	-0.0292

AUGUST 2006

Run	Direction	AoA	Vel	TSR	RPM	ω	Power	Ck
'196'	'w'	0	1.99	2.00	83.08	8.70	205.50	0.0811
'197'	'd'	0	1.99	2.00	83.25	8.72	195.95	0.0772
'198'	'w'	0	1.99	1.50	62.57	6.55	69.89	0.0276
'199'	'd'	0	1.99	1.50	62.46		0.00	0.0000
'200'	'w'	0	0.75	1.25	19.61	2.05	-3.88	-0.0288
'201'	'd'	0	0.75	1.25	19.62	2.05	-3.89	-0.0286
'202'	'w'	0	0.75	1.51	23.55	2.47	-3.06	-0.0227
'203'	'd'	0	0.75	1.50	23.54	2.47	-3.08	-0.0227
'204'	'w'	0	0.75	1.74	27.25	2.85	-1.74	-0.0129
'205'	'd'	0	0.75	1.74	27.23	2.85	-2.19	-0.0161
'206'	'w'	0	0.75	2.01	31.42	3.29	0.44	0.0032
'207'	'd'	0	0.75	2.00	31.40	3.29	1.31	0.0096
'208'	'w'	0	0.75	2.25	35.10	3.68	3.91	0.0290
'209'	'd'	0	0.75	2.24	35.09	3.67	4.17	0.0307
'210'	'w'	0	0.75	2.50	39.02	4.09	4.76	0.0353
'211'	'd'	0	0.75	2.49	39.03	4.09	5.29	0.0390
'212'	'w'	0	0.75	2.75	42.98	4.50	1.66	0.0123
'213'	'd'	0	0.75	2.74	42.98	4.50	1.38	0.0102
'214'	'w'	0	0.75	2.99	46.70	4.89	-7.07	-0.0525
'215'	'd'	0	0.75	2.98	46.69	4.89	-8.04	-0.0592
'216'	'w'	0	0.75	3.26	50.93	5.33	-22.65	-0.1682
'217'	'd'	0	0.75	3.25	50.93	5.33	-21.33	-0.1570
'218'	'w'	0	0.75	2.01	31.38	3.29	0.01	0.0001
'219'	'd'	0	0.75	2.00	31.41	3.29	0.39	0.0028
'300'	'w'	5	1.00	1.25	26.00	2.72	-8.77	-0.0276
'301'	'd'	5	1.00	1.25	26.00	2.72	-8.08	-0.0251
'302'	'w'	5	1.00	1.48	30.92	3.24	-8.69	-0.0273
'303'	'd'	5	1.00	1.48	30.92	3.24	-9.20	-0.0286
'304'	'w'	5	1.00	1.75	36.37	3.81	-9.70	-0.0305
'305'	'd'	5	1.00	1.74	36.36	3.81	-10.13	-0.0315
'306'	'w'	5	1.00	2.00	41.75	4.37	-4.05	-0.0127
'306'	'w'	5	1.00	2.00	41.73	4.37	-3.27	-0.0103
'307'	'd'	5	1.00	2.00	41.76	4.37	-5.75	-0.0179
'307'	'd'	5	1.00	2.00	41.78	4.38	-5.72	-0.0178
'308'	'w'	5	1.00	2.24	46.67	4.89	4.16	0.0131
'309'	'd'	5	1.00	2.24	46.67	4.89	1.89	0.0059
'310'	'w'	5	1.00	2.50	52.06	5.45	9.70	0.0304
'311'	'd'	5	1.00	2.49	52.08	5.45	10.80	0.0337
'312'	'w'	5	1.00	2.77	57.65	6.04	9.88	0.0310
'313'	'd'	5	1.00	2.74	57.24	5.99	7.44	0.0232
'314'	'w'	5	1.00	2.99	62.20	6.51	-2.80	-0.0088
'315'	'd'	5	1.00	2.98	62.22	6.52	1.16	0.0036
'316'	'd'	5	1.00	3.24	67.69	7.09	-25.96	-0.0809
'317'	'w'	5	1.02	3.16	67.14	7.03	0.36	0.0011
'318'	'd'	5	1.00	3.49	72.90	7.63	-55.05	-0.1716
'319'	'w'	5	1.00	3.50	72.91	7.64	-57.99	-0.1821
'320'	'd'	5	1.50	1.25	39.10	4.09	-14.82	-0.0138
'321'	'w'	5	1.49	1.25	39.08	4.09	-10.65	-0.0099
'322'	'd'	5	1.50	1.50	46.92	4.91	-13.82	-0.0128
'323'	'w'	5	1.49	1.50	46.94	4.92	-6.61	-0.0062
'324'	'd'	5	1.50	1.75	54.58	5.72	-12.72	-0.0118

AUGUST 2006

Run	Direction	AoA	Vel	TSR	RPM	ω	Power	Ck
'325'	'w'	5	1.49	1.75	54.56	5.71	-4.20	-0.0039
'326'	'd'	5	1.50	2.00	62.39	6.53	16.47	0.0153
'327'	'w'	5	1.49	2.00	62.34	6.53	21.61	0.0201
'328'	'd'	5	1.50	2.24	70.04	7.33	60.06	0.0558
'329'	'w'	5	1.49	2.24	69.98	7.33	65.32	0.0609
'330'	'd'	5	1.50	2.49	77.83	8.15	78.47	0.0729
'331'	'w'	5	1.49	2.49	77.79	8.15	77.72	0.0725
'332'	'd'	5	1.50	2.76	86.12	9.02	73.31	0.0681
'333'	'w'	5	1.49	2.74	85.48	8.95	74.10	0.0691
'334'	'd'	5	1.50	2.99	93.53	9.79	17.66	0.0164
'335'	'w'	5	1.49	2.99	93.19	9.76	17.86	0.0167
'336'	'd'	5	1.50	3.24	101.24	10.60	-51.40	-0.0478
'337'	'w'	5	1.49	3.24	101.14	10.59	-56.56	-0.0528
'338'	'd'	5	1.50	3.50	109.27	11.44	-163.71	-0.1522
'339'	'w'	5	1.49	3.50	109.13	11.43	-156.67	-0.1463
'340'	'd'	5	1.99	1.25	52.19	5.47	-14.66	-0.0058
'341'	'w'	5	1.99	1.25	52.19	5.47	-2.27	-0.0009
'342'	'd'	5	1.99	1.50	62.49	6.54	-5.03	-0.0020
'343'	'w'	5	1.99	1.50	62.44	6.54	10.61	0.0042
'344'	'd'	5	1.99	1.75	72.84	7.63	19.54	0.0077
'345'	'w'	5	1.99	1.75	72.65	7.61	51.37	0.0203
'346'	'd'	5	1.99	2.00	83.23	8.72	113.45	0.0447
'347'	'w'	5	1.99	2.00	83.18	8.71	139.32	0.0550
'348'	'd'	5	1.99	2.24	93.26	9.77	195.67	0.0771
'349'	'w'	5	1.99	2.24	93.30	9.77	197.81	0.0781
'350'	'd'	5	1.99	2.49	103.63	10.85	237.29	0.0935
'351'	'w'	5	1.99	2.49	103.53	10.84	247.10	0.0976
'352'	'd'	5	1.99	2.73	113.54	11.89	185.10	0.0730
'353'	'w'	5	1.99	2.74	113.83	11.92	172.66	0.0683
'354'	d'	5	1.99	2.91	120.82	12.65	52.52	0.0207
'355'	'w'	5	1.99	2.93	121.67	12.74	75.15	0.0297
'364'	d'	5	1.99	2.95	122.71	12.85	30.22	0.0119
'365'	w'	5	1.99	0.56	23.22	2.43	2.29	0.0009
'366'	d'	5	1.99	2.99	124.23	13.01	30.67	0.0121
'400'	'w'	10	1.00	1.25	26.06	2.73	-11.65	-0.0366
'401'	'd'	10	1.00	1.25	26.06	2.73	-12.01	-0.0374
'402'	'w'	10	1.00	1.49	31.03	3.25	-17.96	-0.0566
'403'	'd'	10	1.00	1.48	31.01	3.25	-18.86	-0.0587
'404'	'w'	10	1.00	1.75	36.47	3.82	-30.71	-0.0969
'405'	'd'	10	1.00	1.75	36.45	3.82	-30.01	-0.0935
'406'	'w'	10	1.00	2.51	52.33	5.48	-79.95	-0.2510
'407'	'd'	10	1.00	2.51	52.34	5.48	-83.79	-0.2610
'408'	'w'	10	1.00	1.00	20.87	2.19	-7.24	-0.0227
'409'	'd'	10	1.00	1.00	20.85	2.18	-7.39	-0.0230
'410'	'w'	10	1.00	3.03	62.94	6.59	-105.30	-0.3317
'411'	'd'	10	1.00	2.99	62.43	6.54	-101.16	-0.3152
'420'	'w'	10	1.49	1.25	39.17	4.10	-29.21	-0.0272
'421'	'd'	10	1.50	1.25	39.17	4.10	-31.18	-0.0289
'422'	'w'	10	1.49	2.01	62.78	6.57	-138.89	-0.1295
'423'	'd'	10	1.50	2.01	62.81	6.58	-143.35	-0.1331
'500'	'w'	-5	1.00	1.25	26.02	2.72	-9.31	-0.0292

AUGUST 2006

Run	Direction	AoA	Vel	TSR	RPM	ω	Power	Ck
'501'	'd'	-5	1.00	1.25	26.01	2.72	-9.47	-0.0295
'502'	'w'	-5	1.00	1.49	30.95	3.24	-10.71	-0.0336
'503'	'd'	-5	1.00	1.48	30.96	3.24	-10.79	-0.0336
'504'	'w'	-5	1.00	1.75	36.40	3.81	-14.97	-0.0470
'505'	'd'	-5	1.00	1.74	36.40	3.81	-15.31	-0.0477
'506'	'w'	-5	1.00	2.01	41.80	4.38	-14.76	-0.0464
'507'	'd'	-5	1.00	2.00	41.81	4.38	-14.84	-0.0462
'508'	'w'	-5	1.00	2.24	46.72	4.89	-19.67	-0.0618
'509'	'd'	-5	1.00	2.24	46.74	4.89	-21.01	-0.0655
'510'	'w'	-5	1.00	2.51	52.20	5.47	-35.49	-0.1115
'511'	'd'	-5	1.00	2.50	52.20	5.47	-37.72	-0.1175
'512'	'w'	-5	1.00	2.76	57.41	6.01	-56.54	-0.1776
'513'	'd'	-5	1.00	2.75	57.41	6.01	-57.83	-0.1802
'520'	'w'	-5	1.49	1.25	39.08	4.09	-14.60	-0.0136
'521'	'd'	-5	1.50	1.25	39.05	4.09	-17.04	-0.0158
'522'	'w'	-5	1.49	1.51	47.00	4.92	-21.83	-0.0203
'523'	'd'	-5	1.50	1.50	47.01	4.92	-24.78	-0.0230
'524'	'w'	-5	1.49	1.75	54.63	5.72	-29.46	-0.0275
'525'	'd'	-5	1.50	1.75	54.62	5.72	-31.74	-0.0295
'526'	'w'	-5	1.49	2.51	78.17	8.19	-92.40	-0.0862
'527'	'd'	-5	1.50	2.50	78.17	8.19	-96.21	-0.0894
'540'	'w'	-5	1.99	1.25	52.14	5.46	-19.65	-0.0077
'541'	'd'	-5	1.99	1.25	52.11	5.46	-24.75	-0.0097
'542'	'w'	-5	1.99	1.50	62.53	6.55	-21.02	-0.0083
'543'	'd'	-5	1.99	1.50	62.46	6.54	-45.35	-0.0178
'544'	'w'	-5	1.99	1.75	72.87	7.63	-31.28	-0.0123
'545'	'd'	-5	1.99	1.75	72.78	7.62	-55.17	-0.0217
'546'	'w'	-5	1.99	2.51	104.15	10.91	-193.09	-0.0763
'547'	'd'	-5	1.99	2.51	104.21	10.91	-196.83	-0.0776
'600'	'w'	3	1.00	1.25	25.99	2.72	-7.68	-0.0241
'601'	'd'	3	1.00	1.26	26.37	2.76	-8.29	-0.0258
'602'	'w'	3	1.00	1.49	30.95	3.24	-7.96	-0.0249
'603'	'd'	3	1.00	1.48	30.97	3.24	-8.11	-0.0253
'604'	'w'	3	1.00	1.88	39.09	4.09	-8.08	-0.0253
'605'	'd'	3	1.00	1.80	37.56	3.93	-8.58	-0.0267
'606'	'w'	3	1.00	2.00	41.73	4.37	0.62	0.0020
'607'	'd'	3	1.00	2.00	41.76	4.37	-0.16	-0.0005
'608'	'w'	3	1.00	2.24	46.63	4.88	8.89	0.0279
'609'	'd'	3	1.00	2.23	46.61	4.88	7.85	0.0244
'610'	'w'	3	1.00	2.50	52.03	5.45	16.21	0.0509
'611'	'd'	3	1.00	2.49	52.04	5.45	16.60	0.0517
'612'	'w'	3	1.00	2.75	57.24	5.99	13.69	0.0430
'613'	'd'	3	1.00	2.74	57.23	5.99	17.33	0.0540
'614'	'w'	3	1.00	2.99	62.20	6.51	-3.57	-0.0112
'615'	'd'	3	1.00	2.98	62.19	6.51	1.64	0.0051
'616'	'w'	3	1.00	3.25	67.67	7.09	-28.49	-0.0894
'617'	'd'	3	1.00	3.24	67.69	7.09	-24.31	-0.0758
'618'	'w'	3	1.00	3.50	72.92	7.64	-64.34	-0.2019
'619'	'd'	3	1.00	3.49	72.88	7.63	-58.50	-0.1825
'620'	'w'	3	1.49	1.25	39.08	4.09	-10.93	-0.0102
'621'	'd'	3	1.50	1.25	39.14	4.10	-13.54	-0.0126

AUGUST 2006

Run	Direction	AoA	Vel	TSR	RPM	ω	Power	Ck
'622'	'w'	3	1.50	1.50	46.93	4.91	-6.69	-0.0062
'623'	'd'	3	1.50	1.50	46.96	4.92	-10.84	-0.0101
'624'	'w'	3	1.49	1.75	54.57	5.71	3.39	0.0032
'625'	'd'	3	1.50	1.75	54.58	5.72	-3.19	-0.0030
'626'	'w'	3	1.49	2.00	62.35	6.53	41.50	0.0387
'627'	'd'	3	1.50	2.00	62.38	6.53	31.38	0.0292
'628'	'w'	3	1.49	2.24	69.90	7.32	84.00	0.0783
'629'	'd'	3	1.50	2.24	69.96	7.33	75.28	0.0700
'630'	'w'	3	1.49	2.49	77.76	8.14	99.96	0.0932
'631'	'd'	3	1.50	2.49	77.79	8.15	96.25	0.0894
'632'	'w'	3	1.49	2.74	85.48	8.95	80.43	0.0750
'633'	'd'	3	1.50	2.74	85.46	8.95	73.69	0.0685
'634'	'w'	3	1.49	3.00	93.51	9.79	19.82	0.0185
'635'	'd'	3	1.50	2.99	93.47	9.79	16.05	0.0149
'636'	'w'	3	1.49	3.24	101.25	10.60	-60.49	-0.0564
'637'	'd'	3	1.50	3.24	101.23	10.60	-60.88	-0.0566
'638'	'w'	3	1.49	3.50	109.12	11.43	-162.29	-0.1515
'639'	'd'	3	1.50	3.50	109.26	11.44	-172.97	-0.1609
'640'	'w'	3	1.99	1.25	52.09	5.45	0.10	0.0000
'641'	'd'	3	1.99	1.25	52.13	5.46	-13.75	-0.0054
'642'	'w'	3	1.99	1.50	62.31	6.53	34.63	0.0136
'643'	'd'	3	1.99	1.50	62.47	6.54	3.76	0.0015
'644'	'w'	3	1.99	1.75	72.79	7.62	89.04	0.0351
'645'	'd'	3	1.99	1.75	72.73	7.62	36.97	0.0145
'646'	'w'	3	1.99	2.00	83.13	8.71	184.63	0.0729
'647'	'd'	3	1.99	2.00	83.16	8.71	144.69	0.0570
'648'	'w'	3	1.99	2.24	93.07	9.75	240.66	0.0950
'649'	'd'	3	1.99	2.24	93.27	9.77	227.74	0.0897
'650'	'w'	3	1.99	2.49	103.55	10.84	260.91	0.1030
'651'	'd'	3	1.99	2.48	103.29	10.82	259.27	0.1023
'652'	'w'	3	1.99	2.73	113.65	11.90	202.84	0.0801
'653'	'd'	3	1.99	2.72	113.10	11.84	200.61	0.0791
'654'	'w'	3	1.99	2.91	120.84	12.65	49.96	0.0197
'655'	'd'	3	1.99	2.94	122.15	12.79	77.25	0.0305
'660'	'd'	3	2.24	1.67	77.97	8.16	58.10	0.0161
'661'	'w'	3	2.24	1.67	78.32	8.20	94.02	0.0261
'662'	'd'	3	2.24	1.25	58.59	6.14	-9.09	-0.0025
'663'	'w'	3	2.24	1.25	58.58	6.13	8.97	0.0025
'664'	'd'	3	2.24	1.50	69.98	7.33	31.76	0.0088
'665'	'w'	3	2.24	1.51	70.56	7.39	53.29	0.0148
'666'	'd'	3	2.24	1.75	81.74	8.56	93.19	0.0258
'667'	'w'	3	2.24	1.79	83.88	8.78	152.63	0.0423
'668'	'd'	3	2.24	1.99	93.23	9.76	268.28	0.0743
'669'	'd'	3	2.24	2.25	104.97	10.99	360.96	0.1001
'670'	'd'	3	2.24	2.49	116.57	12.21	366.78	0.1018
'671'	'w'	3	2.24	0.79	37.13	3.89	0.30	0.0001
'672'	'd'	3	2.24	0.70	33.00	3.46	2.99	0.0008
'673'	'd'	3	2.24	3.00	140.05	14.67	40.15	0.0112
'674'	'd'	3	2.24	2.70	126.09	13.20	258.11	0.0717
'801'	'w'	parasit drag	1.00	1.25	25.99	2.72	-5.86	-0.0184
'802'	'd'	parasit drag	1.00	1.25	26.06	2.73	-6.04	-0.0188

AUGUST 2006

Run	Direction	AoA	Vel	TSR	RPM	ω	Power	Ck
'803'	'd'	parasit drag	1.00	1.74	36.34	3.81	-12.17	-0.0378
'804'	'w'	parasit drag	1.00	1.75	36.36	3.81	-12.02	-0.0377
'805'	'd'	parasit drag	1.00	2.24	46.71	4.89	-21.65	-0.0674
'806'	'w'	parasit drag	1.00	2.49	51.74	5.42	-23.54	-0.0742
'807'	'd'	parasit drag	1.00	2.75	57.38	6.01	-36.02	-0.1121
'808'	'w'	parasit drag	1.00	2.76	57.35	6.01	-35.48	-0.1118
'809'	'd'	parasit drag	1.00	3.24	67.76	7.10	-55.40	-0.1724
'810'	'w'	parasit drag	1.00	3.25	67.65	7.08	-54.62	-0.1721
'811'	'd'	parasit drag	1.50	1.25	39.12	4.10	-16.34	-0.0151
'812'	'w'	parasit drag	1.50	1.25	39.08	4.09	-15.86	-0.0148
'813'	'd'	parasit drag	1.50	1.75	54.64	5.72	-35.58	-0.0330
'814'	'w'	parasit drag	1.50	1.75	54.65	5.72	-34.97	-0.0325
'815'	'd'	parasit drag	1.50	2.25	70.30	7.36	-66.17	-0.0613
'816'	'w'	parasit drag	1.50	2.25	70.21	7.35	-65.04	-0.0605
'817'	'd'	parasit drag	1.50	2.70	84.48	8.85	-108.72	-0.1008
'818'	'w'	parasit drag	1.50	2.75	85.77	8.98	-109.50	-0.1019
'819'	'd'	parasit drag	1.50	3.00	93.91	9.83	-139.94	-0.1297
'820'	'w'	parasit drag	1.50	3.00	93.73	9.81	-138.70	-0.1290
'821'	'd'	parasit drag	1.50	3.50	109.52	11.47	-212.63	-0.1971
'822'	'w'	parasit drag	1.50	3.50	109.35	11.45	-210.43	-0.1958
'823'	'd'	parasit drag	1.99	1.25	52.26	5.47	-35.86	-0.0141
'824'	'w'	parasit drag	1.99	1.25	52.19	5.46	-34.96	-0.0137
'825'	'd'	parasit drag	1.99	1.75	72.95	7.64	-79.43	-0.0311
'826'	'w'	parasit drag	1.99	1.75	72.93	7.64	-77.94	-0.0306
'827'	'd'	parasit drag	1.99	2.23	92.75	9.71	-147.04	-0.0576
'828'	'w'	parasit drag	1.99	2.25	93.78	9.82	-146.63	-0.0576
'829'	'd'	parasit drag	1.99	2.75	114.37	11.98	-249.60	-0.0979
'830'	'w'	parasit drag	1.99	2.74	114.17	11.96	-247.44	-0.0972
'831'	'd'	parasit drag	1.99	2.91	121.43	12.72	-303.50	-0.1190
'832'	'w'	parasit drag	1.99	2.91	121.22	12.69	-300.76	-0.1182
'833'	'd'	parasit drag	2.24	1.30	60.95	6.38	-51.06	-0.0141
'834'	'w'	parasit drag	2.24	1.25	58.64	6.14	-48.49	-0.0134
'835'	'd'	parasit drag	2.24	1.75	82.05	8.59	-110.80	-0.0305
'836'	'w'	parasit drag	2.24	1.75	82.09	8.60	-109.63	-0.0303
'837'	'd'	parasit drag	2.24	2.25	105.43	11.04	-208.28	-0.0574
'838'	'w'	parasit drag	2.24	2.26	105.65	11.06	-206.88	-0.0571
'839'	'd'	parasit drag	2.24	2.54	118.94	12.46	-303.73	-0.0838
'840'	'w'	parasit drag	2.24	2.43	113.86	11.92	-289.00	-0.0797
'841'	'd'	parasit drag	0.75	1.26	19.69	2.06	-2.94	-0.0216
'842'	'w'	parasit drag	0.76	1.27	20.13	2.11	-2.62	-0.0188
'843'	'd'	parasit drag	0.75	1.74	27.25	2.85	-5.76	-0.0423
'844'	'w'	parasit drag	0.75	1.55	24.11	2.53	-5.20	-0.0388
'845'	'd'	parasit drag	0.75	2.24	35.16	3.68	-10.21	-0.0750
'846'	'w'	parasit drag	0.75	2.24	35.03	3.67	-10.38	-0.0767
'847'	'd'	parasit drag	0.75	2.75	43.05	4.51	-16.58	-0.1218
'848'	'w'	parasit drag	0.75	2.76	43.04	4.51	-16.24	-0.1210
'849'	'd'	parasit drag	0.75	3.25	50.91	5.33	-25.20	-0.1853
'850'	'w'	parasit drag	0.75	3.07	48.01	5.03	-23.45	-0.1745
'851'	'd'	parasit drag	1.75	1.25	45.52	4.77	-24.18	-0.0141
'852'	'w'	parasit drag	1.74	1.24	45.36	4.75	-23.81	-0.0140
'853'	'd'	parasit drag	1.75	1.75	63.78	6.68	-54.20	-0.0317

AUGUST 2006

Run	Direction	AoA	Vel	TSR	RPM	ω	Power	Ck
'854'	'w'	*parasit drag*	1.74	1.75	63.78	6.68	-53.66	-0.0314
'855'	'd'	*parasit drag*	1.75	2.30	83.80	8.78	-103.81	-0.0607
'856'	'w'	*parasit drag*	1.74	2.25	82.05	8.59	-101.00	-0.0592
'857'	'd'	*parasit drag*	1.75	2.75	100.16	10.49	-170.40	-0.0996
'858'	'w'	*parasit drag*	1.74	2.79	101.69	10.65	-172.16	-0.1009
'859'	'd'	*parasit drag*	1.75	2.96	108.10	11.32	-243.96	-0.1426
'860'	'w'	*parasit drag*	1.74	3.24	117.94	12.35	-264.60	-0.1551
'861'	'd'	*parasit drag*	1.75	3.43	124.92	13.08	-319.57	-0.1868
'862'	'w'	*parasit drag*	1.74	3.43	125.04	13.09	-319.67	-0.1874
'863'	'd'	*parasit drag*	1.25	1.25	32.63	3.42	-10.06	-0.0161
'864'	'w'	*parasit drag*	1.25	1.25	32.67	3.42	-9.93	-0.0160
'865'	'd'	*parasit drag*	1.25	1.75	45.73	4.79	-21.53	-0.0344
'866'	'w'	*parasit drag*	1.25	1.76	45.75	4.79	-21.46	-0.0345
'867'	'd'	*parasit drag*	1.25	2.25	58.61	6.14	-39.65	-0.0634
'868'	'w'	*parasit drag*	1.25	2.25	58.56	6.13	-39.23	-0.0630
'869'	'd'	*parasit drag*	1.25	2.75	71.72	7.51	-66.07	-0.1056
'870'	'w'	*parasit drag*	1.25	2.75	71.68	7.51	-65.80	-0.1057
'871'	'd'	*parasit drag*	1.25	3.24	84.57	8.86	-102.42	-0.1637
'872'	'w'	*parasit drag*	1.25	3.24	84.38	8.84	-101.94	-0.1637
'873'	'd'	*parasit drag*	1.25	3.49	91.13	9.54	-124.74	-0.1994
'874'	'w'	*parasit drag*	1.25	3.49	90.99	9.53	-124.37	-0.1998

November 2006 runs

Arm Profile "B", chains and sprockets drive-train.

	Target Conditions			Achieved Conditions							Drag Data		
run no	v (m/s)	ω	TSR	v (m/s)	ω	TSR	Avg Torque	ω torqueM	Power	Ck	Initial load	Avg drag	Cd
0 AoA		(rad/s)			(rad/s)		(Nm)	(rad/sec)	(W)		(lbf)	(N)	
1001	1.00	3.28	1.50	1.00	3.23	1.47	0.29	5.82	1.66	-0.0053	-6.95	257.43	0.821
1002	1.00	3.83	1.75	1.00	3.81	1.74	-0.86	6.86	-5.89	0.0187	-6.25	257.07	0.820
1003	1.00	4.37	2.00	1.00	4.36	1.99	-1.63	7.86	-12.77	0.0405	-5.56	262.95	0.839
1004	1.00	4.92	2.25	1.00	4.88	2.23	-2.91	8.78	-25.58	0.0813	-5.06	289.75	0.924
1005	1.00	5.47	2.50	1.00	5.44	2.49	-3.22	9.80	-31.57	0.1003	-6.96	351.44	1.121
1006	1.00	6.01	2.75	1.00	5.99	2.74	-2.16	10.78	-23.25	0.0739	-5.81	364.92	1.164
1007	1.00	6.56	3.00	1.00	6.51	2.97	-0.31	11.72	-3.68	0.0117	-6.60	402.48	1.284
1040	1.50	4.10	1.25	1.50	4.11	1.25	0.28	7.40	2.11	-0.0020			
1041	1.50	4.92	1.50	1.50	4.87	1.48	-2.56	8.76	-22.38	0.0212	3.81	247.19	0.350
1042	1.50	5.74	1.75	1.50	5.66	1.73	-4.57	10.19	-46.63	0.0441	-3.46	351.02	0.498
1043	1.50	6.56	2.00	1.50	6.54	1.99	-7.48	11.77	-87.98	0.0833	-4.71	459.28	0.651
1044	1.50	7.38	2.25	1.50	7.21	2.20	-9.63	12.97	-124.94	0.1183	-0.74	462.05	0.655
1045	1.50	8.20	2.50	1.50	8.11	2.54	-9.29	14.60	-135.59	0.1284	-6.83	607.63	0.861
1046	1.50	9.02	2.75	1.50	8.94	2.73	-6.30	16.09	-101.37	0.0960	-5.08	699.22	0.991
1047	1.50	9.84	3.00	1.50	9.14	2.89	-2.38	16.44	-39.11	0.0371	-4.66	789.27	1.119
1048	1.50	10.66	3.25	1.50	10.24	3.13	1.56	18.44	28.68	-0.0272			
1049	1.50	11.48	3.50	1.50	11.52	3.51	6.75	20.73	139.95	-0.1327			
1061	1.75	5.74	1.50	1.75	5.70	1.49	-5.33	10.27	-54.76	0.0327	-7.80	467.72	0.487
1062	1.75	6.70	1.75	1.75	6.65	1.74	-7.62	11.97	-91.18	0.0545	-6.91	489.98	0.510
1063	1.75	7.66	2.00	1.75	7.59	1.99	-12.55	13.67	-171.53	0.1025	-6.91	596.96	0.622
1064	1.75	8.61	2.25	1.75	8.53	2.23	-14.35	15.36	-220.41	0.1318	-7.77	690.20	0.719
1065	1.75	9.57	2.50	1.75	9.47	2.48	-13.14	17.05	-224.07	0.1341	-6.27	765.56	0.797
1066	1.75	10.53	2.75	1.75	10.43	2.73	-9.35	18.77	-175.56	0.1051	-6.49	896.88	0.934
1067	1.75	11.48	3.00	1.75	11.38	2.98	-4.27	20.48	-87.47	0.0524	-6.82	1035.48	1.078
1080	2.00	5.47	1.25	2.00	5.45	1.25	-1.97	9.81	-19.31	0.0077	-4.99	68.59	0.055
1081b	2.00	6.56	1.50	2.00	6.52	1.49	-7.61	11.73	-89.21	0.0358	-19.84	690.26	0.550
1082b	2.00	7.66	1.75	1.99	7.66	1.76	-11.10	13.79	-153.09	0.0616	-17.46	758.00	0.604
1083	2.00	8.75	2.00	1.99	8.76	2.01	-17.96	15.77	-283.24	0.1142	-12.34	808.61	0.645
1084	2.00	9.84	2.25	1.99	9.75	2.23	-19.73	17.54	-346.03	0.1391	-15.19	928.89	0.741
1085	2.00	10.94	2.50	1.99	10.74	2.46	-17.58	19.32	-339.81	0.1367	-4.94	931.88	0.743
1086	2.00	12.03	2.75	1.99	11.91	2.73	-13.16	21.44	-282.19	0.1136	-22.54	1324.84	1.056
1087	2.00	13.12	3.00	1.99	12.82	2.94	-1.57	23.08	-36.13	0.0146	-22.06	1558.44	1.243
3 AoA													
1200	1.00	2.73	1.25	1.00	2.73	1.24	1.04	4.91	5.10	-0.0162			
1201	1.00	3.28	1.50	1.00	3.26	1.49	0.54	5.88	3.18	-0.0101	-7.02	193.71	0.618
1202	1.00	3.83	1.75	1.00	3.71	1.69	-0.47	6.68	-3.13	0.0099	-6.80	218.83	0.698
1203	1.00	4.37	2.00	1.00	4.36	1.99	-1.99	7.85	-15.60	0.0495	-9.26	267.76	0.854
1204	1.00	4.92	2.25	1.00	5.03	2.29	-3.52	9.05	-31.83	0.1010	-7.74	260.17	0.830
1205	1.00	5.47	2.50	1.00	5.25	2.40	-4.22	9.46	-39.91	0.1266	-8.06	302.28	0.964
1206	1.00	6.01	2.75	1.00	6.12	2.79	-2.87	11.01	-31.56	0.1001	-7.94	326.52	1.041
1207	1.00	6.56	3.00	1.00	6.51	2.97	-1.38	11.72	-16.23	0.0515	-7.67	349.61	1.115
1240	1.50	4.10	1.25	1.50	4.09	1.25	0.48	7.36	3.53	-0.0033			
1241	1.50	4.92	1.50	1.50	4.91	1.50	-1.34	8.84	-11.86	0.0112	-6.63	403.01	0.571
1242	1.50	5.74	1.75	1.50	5.63	1.72	-5.25	10.14	-53.17	0.0503	-7.00	385.53	0.546
1243	1.50	6.56	2.00	1.50	6.52	1.99	-7.96	11.73	-93.44	0.0884	-7.05	423.77	0.601
1244	1.50	7.38	2.25	1.50	7.07	2.16	-11.73	12.73	-149.42	0.1414	-7.52	486.53	0.690
1245	1.50	8.20	2.50	1.50	8.11	2.47	-11.23	14.60	-164.05	0.1553	-7.03	560.49	0.794
1246	1.50	9.02	2.75	1.50	8.94	2.73	-8.67	16.10	-139.52	0.1321	-6.48	636.23	0.902
1247	1.50	9.84	3.00	1.50	9.63	2.94	-5.01	17.34	-86.84	0.0823	-7.34	740.08	1.049
1248	1.50	10.66	3.25	1.50	10.45	3.19	-0.93	18.80	-17.43	0.0165			
1249	1.50	11.48	3.50	1.50	11.26	3.44	3.77	20.27	76.38	-0.0724			

November 2006 runs

Arm Profile "B", chains and sprockets drive-train.

	Target Conditions			Achieved Conditions							Drag Data		
run no	v (m/s)	ω	TSR	v (m/s)	ω	TSR	Avg Torque	ω torqueM	Power	Ck	Initial load	Avg drag	Cd
1260	1.75	*4.78*	1.25	1.75	4.80	*1.25*	-0.10	8.64	-0.84	0.0005			
1261	1.75	*5.74*	1.50	1.75	5.69	*1.49*	-2.88	10.23	-29.47	0.0176	-14.86	578.16	0.602
1262	1.75	*6.70*	1.75	1.75	6.65	*1.74*	-8.13	11.97	-97.36	0.0582	-16.41	597.77	0.623
1263	1.75		2.00			*1.99*	22.50				-14.93	639.71	0.666
1264	1.75	*8.61*	2.25	1.75	8.54	*2.23*	-16.93	15.37	-260.19	0.1556	-18.93	757.22	0.789
1265	1.75		2.50			*2.48*	28.80				-15.40	807.67	0.841
1266	1.75	*10.53*	2.75	1.75	11.38	*2.59*	-7.32	20.48	-150.00	0.0898	-15.12	930.94	0.969
1267	1.75		3.00			*2.98*	13.16				-17.30	1073.23	1.118
1280	2.00	*5.47*	1.25	2.00	5.45	*1.25*	-2.14	9.80	-21.00	0.0084			
1281	2.00	*6.56*	1.50	2.00	6.52	*1.49*	-7.61	11.74	-89.37	0.0358	-7.24	591.67	0.472
1282	2.00	*7.66*	1.75	2.00	7.66	*1.75*	-12.24	13.78	-168.62	0.0676	-12.84	685.35	0.546
1283	2.00	*8.75*	2.00	2.00	8.19	*1.88*	-19.51	14.73	-287.42	0.1154	-13.03	765.73	0.611
1284	2.00	*9.84*	2.25	1.99	9.83	*2.25*	-22.94	17.69	-405.90	0.1631	-13.08	897.77	0.716
1285	2.00	*10.94*	2.50	1.99	10.64	*2.44*	-18.96	19.15	-363.02	0.1459	-13.57	1064.41	0.849
1286	2.00	*12.03*	2.75	1.99	11.23	*2.58*	-17.21	20.21	-347.82	0.1399	-13.66	1127.64	0.899
1287	2.00	*13.12*	3.00	1.99	13.57	*3.15*	-6.14	24.43	-149.93	0.0604	-13.59	1405.58	1.121
1288	2.00	*6.56*	1.50	2.00	6.49	*1.49*	-6.88	11.69	-80.37	0.0322			
5 AoA													
1340	1.50	*4.10*	1.25	1.50	4.10	*1.25*	1.19	7.38	8.79	-0.0083			
1341	1.50	*4.92*	1.50	1.50	4.97	*1.52*	-0.66	8.95	-5.93	0.0056			
1342	1.50	*5.74*	1.75	1.50	5.71	*1.74*	-1.52	10.29	-15.59	0.0147			
1343	1.50	*6.56*	2.00	1.50	6.31	*1.92*	-5.15	11.35	-58.52	0.0554			
1344	1.50	*7.38*	2.25	1.50	7.15	*2.18*	-9.60	12.87	-123.52	0.1169			
1345	1.50	*8.20*	2.50	1.50	8.10	*2.47*	-10.66	14.58	-155.51	0.1472			
1346	1.50	*9.02*	2.75	1.50	9.17	*2.80*	-9.10	16.51	-150.19	0.1423			
1347	1.50	*9.84*	3.00	1.50	9.78	*2.99*	-5.63	17.61	-99.08	0.0939			
1348	1.50	*10.66*	3.25	1.50	10.60	*3.23*	-1.89	19.07	-36.05	0.0342			
1349	1.50	*11.48*	3.50	1.50	11.44	*3.49*	2.61	20.59	53.67	-0.0509			
1380	2.00	*5.47*	1.25	2.00	5.45	*1.25*	-0.54	9.81	-5.30	0.0021			
1381	2.00	*6.56*	1.50	2.00	6.53	*1.50*	-2.97	11.76	-34.93	0.0140			
1382	2.00	*7.66*	1.75	2.00	7.80	*1.79*	-7.80	14.03	-109.46	0.0439			
1383	2.00	*8.75*	2.00	2.00	8.74	*2.00*	-15.02	15.73	-236.23	0.0949			
1384	2.00	*9.84*	2.25	2.00	9.74	*2.23*	-21.72	17.54	-380.97	0.1530			
1385	2.00	*10.94*	2.50	1.99	10.79	*2.47*	-21.65	19.42	-420.36	0.1689			
1386	2.00	*12.03*	2.75	1.99	11.89	*2.73*	-17.23	21.40	-368.75	0.1483			
1387	2.00	*13.12*	3.00	1.99	13.30	*3.05*	-9.43	23.94	-225.80	0.0908			
-3 AoA													
1400	1.00	*2.73*	1.25	1.00	2.67	*1.22*	1.37	4.81	6.59	-0.0209			
1401	1.00	*3.28*	1.50	1.00	3.09	*1.41*	0.46	5.56	2.58	-0.0082			
1402	1.00	*3.83*	1.75	1.00	3.77	*1.72*	0.40	6.79	2.69	-0.0085			
1403	1.00	*4.37*	2.00	1.00	4.39	*2.00*	-0.63	7.89	-4.98	0.0158			
1404	1.00	*4.92*	2.25	1.00	4.90	*2.24*	-1.10	8.82	-9.68	0.0307			
1405	1.00	*5.47*	2.50	1.00	5.44	*2.48*	-0.34	9.79	-3.32	0.0105			
1406	1.00	*6.01*	2.75	1.00	6.01	*2.74*	0.32	10.82	3.52	-0.0112			
1407	1.00	*6.56*	3.00	1.00	6.53	*2.98*	1.75	11.76	20.55	-0.0652			
1408	1.00	*7.11*	3.25	1.00	7.11	*3.25*	3.98	12.80	50.87	-0.1615			
1409	1.00	*7.66*	3.50	1.00	7.66	*3.50*	6.28	13.78	86.50	-0.2746			
1460	1.75	*4.78*	1.25	1.75	4.66	*1.22*	0.15	8.40	1.29	-0.0008			
1461	1.75	*5.74*	1.50	1.75	5.68	*1.49*	-3.07	10.23	-31.40	0.0188			
1462	1.75	*6.70*	1.75	1.75	6.62	*1.73*	-3.60	11.91	-42.93	0.0257			
1463	1.75	*7.66*	2.00	1.75	7.56	*1.98*	-7.50	13.61	-102.07	0.0610			
1464	1.75	*8.61*	2.25	1.75	7.70	*2.01*	-7.85	13.85	-108.68	0.0650			
1464b	1.75	*8.61*	2.25	1.75	8.44	*2.21*	-7.75	15.19	-117.71	0.0704			
1465	1.75	*9.57*	2.50	1.75	9.90	*2.59*	-6.29	17.82	-112.09	0.0671			
1466	1.75	*10.53*	2.75	1.75	10.31	*2.70*	-3.56	18.56	-66.00	0.0395			

August / September 2007 Tests – Free Stream, Gearbox Drive-train

		Target Conditions				Achieved conditions				Measured Data		
		run no	v	w	TSR	v	RPM	w	TSR	Avg Torque	Power	Ck
			(m/s)	(rad/s)		(m/s)		(rad/s)		(Nm)	(W)	
Exp 1	New Drivetrain	11	1.50	5.74	1.75	1.50	54.70	5.73	1.75	5.56	31.85	0.030
		12	1.50	7.38	2.25	1.50	70.40	7.37	2.25	15.37	113.31	0.107
		13	1.50	8.20	2.50	1.50	77.90	8.16	2.40	16.17	131.91	0.125
	Nov2006 arms (Profile B)	14	1.50	9.02	2.75	1.50	85.60	8.96	2.73	12.17	109.09	0.103
	AoA = 0	15	1.50	7.38	2.25	1.50	70.30	7.36	2.24	15.60	114.84	0.109
	634-021 blades	16	1.50	8.20	2.50	1.50	79.30	8.30	2.53	15.31	127.14	0.120
		17	1.50	9.02	2.75	1.50	85.60	8.96	2.73	11.86	106.31	0.100
		30	2.00	9.84	2.25	2.00	92.50	9.68	2.21	33.95	328.69	0.131
		31	2.00	9.84	2.25	2.00	92.80	9.71	2.22	35.10	340.93	0.136
		32	2.00	9.84	2.25	2.00	92.80	9.71	2.22	34.08	331.02	0.132
		33	2.00	9.84	2.25	2.00	92.70	9.70	2.22	33.97	329.60	0.131
		34	2.00	10.94	2.50	2.00	102.90	10.77	2.46	32.45	349.49	0.139
		35	2.00	12.03	2.75	2.00	113.20	11.85	2.71	24.32	288.15	0.115
												#DIV/0!
Exp 2	End Plates: NACA 0012	40	1.50	4.10	1.25	1.50	39.10	4.09	1.25	-1.28	-5.24	-0.005
		41	1.50	4.92	1.50	1.50	47.00	4.92	1.50	5.11	25.14	0.024
	Nov2006 arms (Profile B)	42	1.50	5.74	1.75	1.50	54.70	5.73	1.75	6.33	36.24	0.034
	AoA = 0	43	1.50	6.56	2.00	1.50	62.50	6.54	1.99	9.72	63.59	0.060
	634-021 blades	44	1.50	7.38	2.25	1.50	70.40	7.37	2.25	16.94	124.82	0.118
		45	1.50	8.20	2.50	1.50	77.80	8.14	2.48	18.15	147.80	0.140
		46	1.50	9.02	2.75	1.50	85.70	8.97	2.73	14.05	126.03	0.119
		47	1.50	9.84	3.00	1.50	93.30	9.77	2.98	7.57	73.92	0.070
		48	1.50	10.66	3.25	1.50	101.20	10.59	3.23	0.29	3.07	0.003
												#DIV/0!
		60	2.00	5.47	1.25	2.00	52.10	5.45	1.25	2.42	13.20	0.005
		61	2.00	6.56	1.50	2.00	62.70	6.56	1.50	15.51	101.79	0.041
		62	2.00	7.66	1.75	2.00	72.80	7.62	1.74	19.12	145.69	0.058
		63	2.00	8.75	2.00	2.00	82.50	8.64	1.97	25.57	220.80	0.088
		64	2.00	9.84	2.25	2.00	92.50	9.68	2.21	38.85	376.13	0.150
		65	2.00	10.94	2.50	2.00	102.80	10.76	2.46	36.33	390.90	0.156
		66	2.00	12.03	2.75	2.00	113.20	11.85	2.71	27.23	322.63	0.129
Exp 3	End Plates: Circular	80	1.50	4.10	1.25	1.50	39.00	4.08	1.24	-1.18	-4.82	-0.005
		81	1.50	4.92	1.50	1.50	47.00	4.92	1.50	5.11	25.14	0.024
	Nov2006 arms (Profile B)	82	1.50	5.74	1.75	1.50	54.60	5.71	1.74	6.28	35.89	0.034
	AoA = 0	83	1.50	6.56	2.00	1.50	62.60	6.55	2.00	9.09	59.56	0.056
	634-021 blades	84	1.50	7.38	2.25	1.50	70.30	7.36	2.24	16.14	118.76	0.112
		85	1.50	8.20	2.50	1.50	77.90	8.15	2.49	17.79	145.05	0.137
		86	1.50	9.02	2.75	1.50	85.60	8.96	2.73	13.29	119.07	0.113
		87	1.50	9.84	3.00	1.50	93.30	9.77	2.98	5.47	53.42	0.050
		88	1.50	10.66	3.25	1.50	101.10	10.58	3.23	-3.09	-32.70	-0.031
												#DIV/0!
		100	2.00	5.47	1.25	2.00	52.10	5.45	1.25	4.42	24.10	0.010
		101	2.00	6.56	1.50	2.00	62.50	6.54	1.50	11.98	78.37	0.031
		102	2.00	7.66	1.75	2.00	72.80	7.62	1.74	15.22	115.97	0.046
		103	2.00	8.75	2.00	2.00	82.70	8.66	1.98	22.76	197.01	0.079
		104	2.00	9.84	2.25	2.00	92.50	9.68	2.21	33.63	325.59	0.130
		105	2.00	10.94	2.50	2.00	102.70	10.75	2.46	33.74	362.68	0.145
		106	2.00	12.03	2.75	2.00	112.90	11.82	2.70	25.24	298.26	0.119
		110	2.00	5.47	1.25	2.00	52.10	5.45	1.25	1.12	6.11	0.002
								0.00				#DIV/0!
	Repeat w/o end plates	111	1.50	6.56	2.00	1.50	62.60	6.55	2.00	8.37	54.84	0.052
		112	1.50	7.38	2.25	1.50	70.50	7.38	2.25	15.36	113.34	0.107
		113	1.50	8.20	2.50	1.50	78.00	8.16	2.40	16.58	135.36	0.128
		114	1.50	9.02	2.75	1.50	85.80	8.98	2.74	12.33	110.73	0.105
								0.00				#DIV/0!
	Repeat w/o end plates	115	2.00	8.75	2.00	2.00	82.70	8.66	1.98	23.15	200.38	0.080
		116	2.00	9.84	2.25	2.00	92.90	9.72	2.22	33.94	330.02	0.132
		117	2.00	10.94	2.50	2.00	102.70	10.75	2.46	32.13	345.37	0.138
		118	2.00	12.03	2.75	2.00	113.10	11.84	2.71	24.33	288.01	0.115

August / September 2007 Tests – Free Stream

Exp		run no	v	w	TSR	v	RPM	w	TSR	Avg Torque	Power	Ck
Exp 4	November Arms Only	120	1.50	4.10	1.25	1.50	39.10	4.09	1.25	-2.80	-11.46	-0.011
		121	1.50	4.92	1.50	1.50	47.10	4.93	1.50	-3.40	-16.76	-0.016
	(BLADES REMOVED)	122	1.50	5.74	1.75	1.50	54.70	5.73	1.75	-4.16	-23.82	-0.023
	Nov2006 arms (Profile B)	123	1.50	6.56	2.00	1.50	62.60	6.55	2.00	-4.64	-30.40	-0.029
	AoA = 0	124	1.50	7.38	2.25	1.50	70.50	7.38	2.25	-5.62	-41.47	-0.039
	634-021 blades	125	1.50	8.20	2.50	1.50	78.40	8.21	2.50	-6.40	-52.52	-0.050
		126	1.50	9.02	2.75	1.50	86.10	9.01	2.75	-7.39	-66.60	-0.063
		127	1.50	9.84	3.00	1.50	93.90	9.83	3.00	-8.63	-84.82	-0.080
		128	1.50	10.66	3.25	1.50	101.70	10.64	3.24	-9.78	-104.10	-0.098
		129	1.50	11.48	3.50	1.50	109.40	11.45	3.49	-10.96	-125.73	-0.119
								0.00				#DIV/0!
		140	2.00	5.47	1.25	2.00	52.20	5.46	1.25	-4.25	-23.22	-0.009
		141	2.00	6.56	1.50	2.00	62.50	6.54	1.50	-5.18	-33.89	-0.014
		142	2.00	7.66	1.75	2.00	73.00	7.64	1.75	-6.41	-48.98	-0.020
		143	2.00	8.75	2.00	2.00	83.30	8.72	1.99	-7.65	-66.70	-0.027
		144	2.00	9.84	2.25	2.00	93.80	9.82	2.24	-9.18	-90.13	-0.036
		145	2.00	10.94	2.50	2.00	104.00	10.89	2.49	-10.83	-117.89	-0.047
		146	2.00	12.03	2.75	2.00	114.50	11.98	2.74	-12.59	-150.88	-0.060
Exp 5	Single Blade, B Arms	160	1.50	4.10	1.25	1.50	39 00	4.06	1.24	-2.57	-10.49	-0.010
		161	1.50	4.92	1.50	1.50	47 00	4.92	1 50	-0.69	-3.39	-0 003
	Nov2006 arms (Profile B)	162	1.50	5.74	1.75	1.50	54 60	5.71	1 74	2.58	14 74	0.014
	AoA = 0	163	1.50	6.56	2.00	1.50	62.60	6 55	2.00	4.08	26 73	0.025
	634-021 blades	164	1.50	7.38	2.25	1.50	70.40	7.37	2.25	5.26	38.76	0.037
		165	1.50	8.20	2.50	1.50	78.20	8 16	2.49	8.55	69.98	0.066
		166	1.50	9.02	2.75	1.50	85 80	8.98	2.74	9 30	83 52	0.079
		167	1.50	9.84	3 00	1.50	93.50	9.79	2.98	8.88	86 90	0.082
		168	1.50	10 66	3.25	1.50	101.50	10 62	3 24	7 64	8 .16	0.077
		170	1.50	8.20	2.50	1.50	78.20	8.16	2.49	8.47	69.33	0.066
								0 00				#DIV/0!
		180	2.00	5.47	1.25	2.00	52.20	5 46	1 25	-2.16	- 1 80	-0 005
		181	2.00	6 56	1.50	2.00	62.60	6.55	1 50	0.33	2.16	0.001
		182	2.00	7.66	1.75	2.00	72.90	7.63	1 74	5 55	42.35	0.017
		183	2.00	8.75	2 00	2.00	83.10	8 70	1 99	7 00	60.88	0.024
		184	2.00	9.84	2.25	2.00	93.40	9.78	2.23	13 12	128.26	0.051
		185	2.00	10.94	2.50	2.00	103.70	10 85	2.48	16.32	177.14	0.071
		186	2.00	12.03	2.75	2.00	113.40	11.87	2.71	16.26	192.99	0.077

Exp		run no	v	w	TSR	v	RPM	w	TSR	Avg Torque	Power	Ck
Exp 6	New Arms: 3,0 AoA = 0	201	1.50	4.92	1.50	1.50	46.90	4.91	1 50	15 68	76.97	0.073
		202	1.50	6 56	2.00	1.50	62.40	6.53	1 99	21.56	140.81	0.133
	2007 Arms (profile C)	203	1.50	7.38	2.25	1.50	70.30	7.36	2.24	30.60	225.16	0.213
	AoA = 0	204	1.50	8.20	2.50	1.50	78.00	8.16	2.49	33.78	275.78	0.261
	634-021 blades	206	1.50	9.84	3.00	1.50	93.40	9.78	2.98	28.52	278.81	0.263
	free-stream	207	1.50	11.48	3.50	1.50	108.70	11.38	3.47	17.20	195.69	0 185
		203.1	1.50	7.38	2.25	1.50	72.20	7.56	2.30	29.19	220.59	0.208
		204.1	1.50	8.20	2.50	1.50	78.40	8.21	2.50	32.72	268.50	0.254
		203.2	1.50	7.36	2.25	1.50	70.20	7.35	2.24	30.17	221.68	0.209
		204.2	1.50	8.20	2.50	1.50	77.90	8.15	2.49	33.01	269 15	0.254
		202.1	1.50	6.56	2.00	1.50	62.40	6.53	1 99	21.29	139 05	0 131
		204.3	1.50	8.20	2.50	1.50	78.60	8.23	2.51	34.36	282.67	0.267
		205.1	1.50	9.02	2.75	1.50	85.50	8.95	2.73	32.14	287.62	0.272
		203.3	1.50	7.38	2.25	1.50	70.60	7.39	2.25	29.47	217.77	0.206
		204.4	1.50	8.20	2.50	1.50	77.90	8.15	2.49	32.78	267.27	0.253
								0.00				#DIV/0!

August / September 2007 Tests – Free Stream

		211	2.00	6.56	1.50	2.00	62.50	6.54	1.50	28.16	184.21	0.073
		212	2.00	8.75	2.00	2.00	82.70	8.66	1.98	44.81	387.87	0.155
		212.1	2.00	8.75	2.00	2.00	82.80	8.67	1.98	46.15	399.95	0.159
		213	2.00	9.84	2.25	2.00	92.70	9.70	2.22	56.51	548.29	0.219
		214	2.00	10.94	2.50	2.00	102.90	10.77	2.46	64.51	694.79	0.277
		215	2.00	12.03	2.75	2.00	112.00	11.72	2.68	59.74	700.31	0.279
		216	2.00	13.12	3.00	2.00		0.00	0.00		0.00	0.000
		217	2.00	15.31	3.50	2.00		0.00	0.00		0.00	0.000
		213.1	2.00	9.84	2.25	2.00	92.60	9.69	2.22	55.26	535.59	0.214
		214.1	2.00	10.94	2.50	2.00	103.20	10.80	2.47	63.99	691.19	0.276
		213.2	2.00	9.84	2.25	2.00	92.90	9.72	2.22	56.08	545.30	0.217
		214.2	2.00	10.94	2.50	2.00	103.20	10.80	2.47	64.24	693.89	0.277
		214.3	2.00	10.94	2.50	2.00	103.20	10.80	2.47	63.25	683.20	0.272
		212.1	2.00	8.75	2.00	2.00	82.80	8.67	1.98	46.15	399.95	0.159
		214.4	2.00	10.94	2.50	2.00	103.10	10.79	2.47	64.17	692.47	0.276
		215.1	2.00	12.03	2.75	2.00	112.90	11.82	2.70	61.49	726.62	0.290
		213.3	2.00	9.84	2.25	2.00	92.80	9.71	2.22	56.09	544.81	0.217
		214.5	2.00	10.94	2.50	2.00	103.00	10.78	2.46	64.64	696.86	0.278
		215.5	2.00	12.03	2.75	2.00	112.00	11.72	2.68	59.74	700.31	0.279
		run no	v	w	TSR	v	RPM	w	TSR	Avg Torque	Power	Ck
Exp	Shaft Fairing	221	1.50	4.92	1.50	1.50	47.10	4.93	1.50	11.44	56.40	0.053
7		222	1.50	6.56	2.00	1.50	62.50	6.54	1.99	19.11	125.01	0.118
	2007 Arms (profile C)	223	1.50	7.38	2.25	1.50	70.30	7.36	2.24	28.55	210.07	0.199
	AoA = 0	224	1.50	8.20	2.50	1.50	77.90	8.15	2.49	31.08	253.41	0.239
	634-021 blades	225	1.50	9.02	2.75	1.50	85.80	8.98	2.74	30.00	269.41	0.255
	free-stream	226	1.50	9.84	3.00	1.50	93.30	9.77	2.98	24.85	242.67	0.229
		227	1.50	11.48	3.50	1.50	108.70	11.38	3.47	14.92	169.75	0.160
		224.1	1.50	8.20	2.50	1.50	77.90	8.15	2.49	30.41	247.95	0.234
								0.00				#DIV/0!
		231	2.00	6.56	1.50	2.00	62.50	6.54	1.50	26.19	171.33	0.068
		232	2.00	8.75	2.00	2.00	83.20	8.71	1.99	41.79	363.92	0.145
		233	2.00	9.84	2.25	2.00	92.70	9.70	2.22	51.94	503.95	0.201
		234	2.00	10.94	2.50	2.00	103.20	10.80	2.47	63.81	689.25	0.275
		235	2.00	12.03	2.75	2.00	112.80	11.81	2.70	57.88	683.35	0.272
		run no	v	w	TSR	v	RPM	w	TSR	Avg Torque	Power	Ck
Exp	New Arms: 2 ONLY	241	1.50	4.92	1.50	1.50	46.10	4.83	1.47	15.76	76.04	0.072
8		242	1.50	6.56	2.00	1.50	62.00	6.49	1.98	21.95	142.44	0.135
	2 arms only	243	1.50	7.38	2.25	1.50	70.30	7.36	2.24	29.93	220.23	0.208
	2007 Arms (profile C)	244	1.50	8.20	2.50	1.50	77.80	8.14	2.48	33.27	270.92	0.256
	AoA = 0	245	1.50	9.02	2.75	1.50	85.40	8.94	2.72	35.85	320.45	0.303
	634-021 blades	246	1.50	9.84	3.00	1.50	93.20	9.75	2.97	32.91	321.03	0.303
	free-stream	247	1.50	11.48	3.50	1.50	108.50	11.36	3.46	26.53	301.28	0.285
		243.1	1.50	7.38	2.25	1.50	70.20	7.35	2.24	31.63	232.40	0.220
		244.1	1.50	8.20	2.50	1.50	77.80	8.14	2.48	34.04	277.19	0.262
								0.00				#DIV/0!
		251	2.00	6.56	1.50	2.00	62.30	6.52	1.49	31.39	204.69	0.082
		252	2.00	8.75	2.00	2.00	82.60	8.65	1.98	47.96	414.64	0.165
		253	2.00	9.84	2.25	2.00	92.90	9.72	2.22	59.27	576.31	0.230
		254	2.00	10.94	2.50	2.00	104.00	10.89	2.49	67.82	738.24	0.294
		255	2.00	12.03	2.75	2.00	113.30	11.86	2.71	66.11	783.98	0.313
		253.1	2.00	9.84	2.25	2.00	92.90	9.72	2.22	63.27	615.21	0.245
		254.1	2.00	10.94	2.50	2.00	103.90	10.87	2.49	69.30	753.63	0.300

August / September 2007 Tests – Free Stream

Exp 10

Cambered Blade: AoA = 0

2007 Arms (profile C)
AoA = 0
634-421 blades
free-stream

run no	v	w	TSR	v	RPM	w	TSR	Avg Torque	Power	Ck
281	1.50	4.92	1.50	1.50	47.20	4.94	1.51	15.03	74.25	0.070
282	1.50	6.56	2.00	1.50	62.50	6.54	1.99	23.98	156.87	0.148
283	1.50	7.38	2.25	1.50	70.60	7.39	2.25	33.00	243.85	0.230
284	1.50	8.20	2.50	1.50	78.00	8.16	2.49	34.62	282.64	0.267
285	1.50	9.02	2.75	1.50	85.90	8.99	2.74	33.59	302.00	0.285
286	1.50	9.84	3.00	1.50	93.40	9.78	2.98	29.85	291.81	0.276
287	1.50	11.48	3.50	1.50	108.60	11.37	3.46	19.86	225.74	0.213
283.1	1.50	7.38	2.25	1.50	71.00	7.43	2.27	33.01	245.31	0.232
284.1	1.50	8.20	2.50	1.50	77.90	8.15	2.49	34.72	283.09	0.268
						0.00				#DIV/0!
291	2.00	6.56	1.50	2.00	62.50	6.54	1.50	31.50	206.06	0.082
292	2.00	8.75	2.00	2.00	82.80	8.67	1.98	52.33	453.51	0.181
293	2.00	9.84	2.25	2.00	92.10	9.64	2.20	61.19	589.86	0.235
294	2.00	10.94	2.50	2.00	103.00	10.78	2.46	66.59	717.88	0.286
295	2.00	12.03	2.75	2.00	113.10	11.84	2.71	63.16	747.68	0.298
293.1	2.00	9.84	2.25	2.00	92.70	9.70	2.22	60.68	588.75	0.235
294.1	2.00	10.94	2.50	2.00	102.60	10.76	2.46	65.26	702.18	0.280

Exp 11

Cambered Blade: AoA = 5

2007 Arms (profile C)
AoA = 5
634-421 blades
free-stream

run no	v	w	TSR	v	RPM	w	TSR	Avg Torque	Power	Ck
301	1.50	4.92	1.50	1.50	47.10	4.93	1.50	10.12	49.89	0.047
302	1.50	6.56	2.00	1.50	62.40	6.53	1.99	24.53	160.21	0.151
303	1.50	7.38	2.25	1.50	70.20	7.35	2.24	31.57	231.96	0.219
304	1.50	8.20	2.50	1.50	77.90	8.15	2.49	38.87	316.93	0.299
305	1.50	9.02	2.75	1.50	85.60	8.96	2.73	37.64	337.23	0.319
306	1.50	9.84	3.00	1.50	93.30	9.77	2.98	34.00	332.02	0.314
307	1.50	11.48	3.50	1.50	108.50	11.36	3.46	22.73	258.13	0.244
304.1	1.50	8.20	2.50	1.50	77.80	8.14	2.48	37.99	309.36	0.292
						0.00				#DIV/0!
311	2.00	6.56	1.50	2.00	60.10	6.29	1.44	28.50	179.28	0.071
312	2.00	8.75	2.00	2.00	84.40	8.83	2.02	51.00	450.53	0.180
313	2.00	9.84	2.25	2.00	92.90	9.72	2.22	61.54	598.39	0.239
314	2.00	10.94	2.50	2.00	103.10	10.79	2.47	69.68	751.93	0.300
315	2.00	12.03	2.75	2.00	112.60	11.79	2.69	68.87	811.67	0.324
314.1	2.00	10.94	2.50	2.00	103.20	10.80	2.47	70.22	758.49	0.302

Exp 13

3 New Arms Only

No blades
free-stream

run no	v	w	TSR	v	RPM	w	TSR	Avg Torque	Power	Ck
341	1.50	4.92	1.50	1.50	47.00	4.92	1.50	-3.40	-16.73	-0.016
342	1.50	6.56	2.00	1.50	62.50	6.54	1.99	-4.22	-27.61	-0.026
343	1.50	7.38	2.25	1.50	70.40	7.37	2.25	-4.39	-32.35	-0.031
344	1.50	8.20	2.50	1.50	78.20	8.18	2.49	-5.01	-41.01	-0.039
345	1.50	9.02	2.75	1.50	85.90	8.99	2.74	-5.55	-49.90	-0.047
346	1.50	9.84	3.00	1.50	93.90	9.83	3.00	-6.19	-60.84	-0.057
347	1.50	11.48	3.50	1.50	109.20	11.43	3.48	-7.38	-84.35	-0.080
						0.00				#DIV/0!
351	2.00	6.56	1.50	2.00	62.60	6.55	1.50	-4.22	-27.65	-0.011
352	2.00	8.75	2.00	2.00	83.20	8.71	1.99	-5.47	-47.63	-0.019
353	2.00	9.84	2.25	2.00	93.80	9.82	2.24	-6.49	-63.72	-0.025
354	2.00	10.94	2.50	2.00	104.20	10.91	2.49	-7.51	-81.91	-0.033
355	2.00	12.03	2.75	2.00	114.20	11.95	2.73	-8.31	-99.33	-0.040

August / September 2007 Tests – Free Stream

Exp		run no	v	w	TSR	v	RPM	w	*TSR*	Avg Torque	Power	Ck
Exp 14	Single Blade	361	1.50	4.92	1.50	1.50	47.00	4.92	*1.50*	2.86	14.07	0.013
	3 arms profile C	362	1.50	6.56	2.00	1.50	58.30	6.10	*1.86*	8.56	52.23	0.049
	634-021 blade	363	1.50	7.38	2.25	1.50	73.50	7.69	2.34	11.87	91.32	0.086
	free-stream	364	1.50	8.20	2.50	1.50	78.10	8.17	2.49	15.38	125.72	0.119
		365	1.50	9.02	2.75	1.50	85.90	8.99	2.74	17.82	160.22	0.151
		366	1.50	9.84	3.00	1.50	93.50	9.79	2.98	19.17	187.60	0.177
		367	1.50	11.48	3.50	1.50	108.80	11.39	3.47	18.09	206.00	0.195
		368	1.50	7.38	2.25	1.50	70.40	7.37	2.25	11.82	87.10	0.082
		369	1.50	8.20	2.50	1.50	78.20	8.18	2.49	15.01	122.86	0.116
								0.00				#DIV/0!
		371	2.00	6.56	1.50	2.00	62.50	6.54	*1.50*	7.45	48.74	0.019
		372	2.00	8.75	2.00	2.00	83.00	8.69	*1.99*	16.63	135.78	0.054
		373	2.00	9.84	2.25	2.00	93.40	9.78	2.23	24.12	235.79	0.094
		374	2.00	10.94	2.50	2.00	103.60	10.84	2.48	27.50	298.20	0.119
		375	2.00	12.03	2.75	2.00	113.30	11.86	2.71	29.63	351.37	0.140
		376	2.00	10.94	2.50	2.00	103.50	10.83	2.48	27.96	302.89	0.121

Exp		run no	v	w	TSR	v	RPM	w	*TSR*	Avg Torque	Power	Ck
Exp 15	Fairing:One Blade	381	1.50	4.92	1.50	1.50	47.00	4.92	*1.50*	1.37	6.74	0.006
	New Arms:3	382	1.50	6.56	2.00	1.50	62.50	6.54	*1.99*	8.01	62.40	0.060
	AoA = 0	383	1.50	7.38	2.25	1.50	70.40	7.37	2.25	11.27	83.04	0.078
	634-021 blades	384	1.50	8.20	2.50	1.50	78.20	8.18	2.49	14.60	119.50	0.113
	free-stream	385	1.50	9.02	2.75	1.50	85.90	8.99	2.74	17.05	153.29	0.145
		386	1.50	9.84	3.00	1.50	93.60	9.80	2.99	18.90	185.16	0.175
		387	1.50	11.48	3.50	1.50	108.70	11.38	3.47	18.43	209.68	0.198
		384.1	1.50	8.20	2.50	1.50	78.10	8.17	2.49	14.29	116.81	0.110
								0.00				#DIV/0!
		391	2.00	6.56	1.50	2.00	62.60	6.55	*1.50*	3.30	21.62	0.009
		392	2.00	8.75	2.00	2.00	82.90	8.68	*1.98*	14.41	125.03	0.050
		393	2.00	9.84	2.25	2.00	93.40	9.78	2.23	23.83	232.96	0.093
		394	2.00	10.94	2.50	2.00	103.60	10.84	2.48	27.27	295.70	0.118
		395	2.00	12.03	2.75	2.00	113.30	11.86	2.71	29.72	352.44	0.141

August / September 2007 Tests – Ducted, Gearbox drive-train

Exp 15

Ducts + 4 Bumps

Profile C arms
AoA = 0
634-021 blades

run no	Target v (m/s)	Target TSR	Achieved v (m/s)	RPM	w (rad/s)	TSR	Torque (Nm)	Power (W)	Ck
400	1.60	1.25	1.50		4.08	1.24	4.19	17.10	0.016
401	1.60	1.50	1.50		4.92	1.60	8.69	42.77	0.040
402	1.60	1.75	1.50		5.72	1.74	13.93	79.62	0.075
403	1.60	2.00	1.50		6.54	1.99	23.95	156.75	0.148
404	1.60	2.25	1.50		7.35	2.24	24.96	183.48	0.173
405	1.60	2.50	1.50		8.13	2.48	33.06	268.62	0.254
406	1.60	2.75	1.50		8.93	2.72	47.72	426.25	0.403
407	1.60	3.00	1.50		9.73	2.97	42.79	416.25	0.393
408	1.60	3.25	1.50		10.55	3.21	34.18	360.45	0.341
409	1.60	3.50	1.50		11.33	3.45	26.08	295.55	0.279
410	1.60	3.7	1.50		12.01	3.66	18.94	227.50	0.215
401.1	1.60	1.50	1.50		4.93	1.60	8.72	42.98	0.041
403.1	1.60	2.00	1.50		6.54	1.99	22.26	145.68	0.138
405.1	1.60	2.50	1.50		8.14	2.48	31.80	258.74	0.245
407.1	1.60	3.00	1.50		9.70	2.96	43.36	420.47	0.397
409.1	1.60	3.50	1.50		11.35	3.46	26.14	296.78	0.280
420	2.00	1.25	2.00			0.00		0.00	0.000
421	2.00	1.50	2.00			0.00		0.00	0.000
422	2.00	1.75	2.00	72.6	7.60	1.74	44.73	340.07	0.136
423	2.00	2.00	2.00	83.3	8.72	1.99	50.26	438.38	0.175
424	2.00	2.25	2.00	90.4	9.47	2.16	50.30	476.14	0.190
425	2.00	2.50	2.00	106.7	11.17	2.55	81.68	912.65	0.364
426	2.00	2.75	2.00	112.7	11.80	2.70	84.22	993.90	0.396
426.1	2.00	2.75	2.00	112.70	11.80	2.70	84.26	994.39	0.396

Exp 16

Duct: 2 bumps

Profile C arms
AoA = 0
634-021 blades

Bump diag. opposite turbine spinning towards

run no	Target v (m/s)	Target TSR	Achieved v (m/s)	RPM	w (rad/s)	TSR	Torque (Nm)	Power (W)	Ck
440	1.60	1.50	1.50	47.00	4.92	1.60	7.08	34.85	0.033
441	1.60	2.00	1.50	62.50	6.54	1.99	29.42	186.01	0.176
442	1.60	2.25	1.50	70.40	7.37	2.25	31.26	230.45	0.218
443	1.60	2.50	1.50	77.60	8.13	2.48	44.86	364.50	0.344
444	1.60	2.75	1.50	85.30	8.93	2.72	51.37	455.87	0.434
445	1.60	3.00	1.50	93.20	9.76	2.97	46.22	451.10	0.426
446	1.60	3.25	1.50	100.60	10.53	3.21	38.83	409.01	0.387
447	1.60	3.50	1.50	109.40	11.46	3.49	29.74	340.67	0.322
443.1	1.60	2.50	1.50	77.60	8.13	2.48	46.36	376.73	0.356
430	2.00	1.75	2.00	72.80	7.62	1.74	49.36	376.32	0.150
431	2.00	2.00	2.00	83.00	8.69	1.99	57.33	498.30	0.199
432	2.00	2.25	2.00	89.10	9.33	2.13	60.31	562.71	0.224
433	2.00	2.50	2.00	102.60	10.74	2.46	89.50	961.60	0.383
434	2.00	2.75	2.00	112.60	11.79	2.70	93.35	1100.74	0.439

Exp 17

Duct No Bumps

Profile C arms
AoA = 0
634-021 blades

run no	Target v (m/s)	Target TSR	Achieved v (m/s)	RPM	w (rad/s)	TSR	Torque (Nm)	Power (W)	Ck
460	1.60	1.50	1.5	47.1	4.93	1.60	9.75	48.09	0.045
461	1.60	2.00	1.50	62.50	6.54	1.99	30.16	197.37	0.187
462	1.60	2.25	1.50	70.10	7.34	2.24	34.51	253.33	0.239
463	1.60	2.50	1.50	75.90	7.95	2.42	47.13	374.60	0.354
464	1.60	2.75	1.50	81.40	8.52	2.60	54.71	466.36	0.441
465	1.60	3.00	1.50	92.80	9.72	2.96	51.53	500.81	0.473
466	1.60	3.25	1.50	100.50	10.52	3.21	43.87	461.70	0.436
467	1.60	3.50	1.50	108.20	11.33	3.45	34.97	396.23	0.374
460.1	1.60	1.50	1.50	47.00	4.92	1.60	10.38	51.10	0.048
490	2.00	1.75	2.00	72.50	7.59	1.74	56.33	427.68	0.171
491	2.00	2.00	2.00	83.30	8.72	1.99	64.57	563.25	0.225
492	2.00	2.25	2.00	90.40	9.47	2.16	70.76	669.81	0.267
493	2.00	2.50	2.00	102.50	10.73	2.45	97.00	1041.13	0.415
494	2.00	2.75	2.00	112.40	11.77	2.69	96.97	1141.33	0.455
494.1	2.00	2.75	2.00	112.50	11.78	2.69	99.96	1177.53	0.469

August / September 2007 Tests – Ducted

		run no	v	TSR	v	RPM	w	TSR	Torque	Power	Ck
Exp	Duct no bumps_Direction	601	1.60	2.75	1.5	85.30	8.93	2.72	54.60	487.72	0.461
	wavemaker	602	1.60	2.75	1.50	85.30	8.93	2.72	53.98	482.19	0.456
18	dock	603	1.60	3.00	1.50	92.80	9.72	2.96	49.82	484.15	0.458
	wavemaker	604	1.60	3.00	1.50	92.80	9.72	2.96	47.93	465.78	0.440
	dock	610	2.00	2.75	2.00	112.60	11.79	2.70	100.29	1182.56	0.471
	wavemaker	611	2.00	2.75	2.00	112.40	11.77	2.69	98.89	1163.98	0.464
Exp	Duct: 2 Bumps Downstream	620	1.60	1.50				#DIV/0!		0.00	#DIV/0!
19		621	1.60	2.00	1.50	62.50	6.54	1.99	21.55	141.04	0.133
	Profile C arms	622	1.60	2.25	1.50	70.40	7.37	2.26	29.157	215.25	0.203
	AoA = 0	623	1.60	2.50	1.50	78.00	8.17	2.49	40.755	332.89	0.315
	634-021 blades	624	1.60	2.75	1.50	85.30	8.93	2.72	51.875	463.38	0.438
		626	1.60	3.00	1.50	92.90	9.73	2.97	48.12	468.13	0.442
		628	1.60	3.50	1.50	108.40	11.35	3.46	29.983	340.36	0.322
	runs towards dock	627	1.60	2.75	1.50	85.30	8.93	2.72	52.32	467.35	0.442
		633	2.00	2.50	2.00	102.50	10.73	2.46	83.46	895.84	0.357
		634	2.00	2.75	2.00	112.50	11.78	2.69	93.53	1101.87	0.439
Exp	Duct: 2 Bumps Upstream	640	1.60	1.50				#DIV/0!		0.00	#DIV/0!
22		641	1.60	2.00	1.50	62.60	6.56	2.00	31.12	204.01	0.193
	Profile C arms	642	1.60	2.25	1.50	70.20	7.35	2.24	34.446	253.22	0.239
	AoA = 0	643	1.60	2.50	1.50	77.60	8.13	2.48	46.442	377.40	0.357
	634-021 blades	644	1.60	2.75	1.50	85.10	8.91	2.72	46.5	414.39	0.392
		646	1.60	3.00	1.50	92.70	9.71	2.96	44.386	430.88	0.407
	runs towards wavemaker	648	1.60	3.50	1.50	108.30	11.34	3.46	27.734	314.54	0.297
		647	1.60	2.75	1.50	85.10	8.91	2.72	48.61	433.20	0.409
		663	2.00	2.50	2.00	102.80	10.77	2.46	92.13	991.80	0.398
		664	2.00	2.75	2.00	112.70	11.80	2.70	90.87	1072.44	0.428
Exp	Duct: 2 bumps	680	1.60	1.50	1.50	47.2	4.94	1.51	12.1	59.81	0.057
23		681	1.60	2.00	1.50	62.60	6.56	2.00	27.92	183.03	0.173
	Profile C arms	682	1.60	2.25	1.50	70.40	7.37	2.26	31.14	229.57	0.217
	AoA = 0	683	1.60	2.50	1.50	77.50	8.12	2.47	44.69	362.69	0.343
	634-021 blades	684	1.60	2.75	1.50	85.50	8.95	2.73	51.95	465.14	0.440
		686	1.60	3.00	1.50	92.50	9.69	2.96	48.317	468.03	0.442
	Bumps are diagonally opp.	688	1.60	3.50	1.50	108.70	11.38	3.47	31.154	354.63	0.335
	turbine rotating away	684.1	1.60	2.75	1.50	85.40	8.94	2.73	51.39	459.58	0.434
		670	2.00	1.75	2.00	72.90	7.63	1.75	55.062	420.27	0.168
		672	2.00	2.25	2.00	87.40	9.15	2.09	63.59	582.01	0.232
		673	2.00	2.50	2.00	102.60	10.74	2.46	90.29	970.10	0.387
		674	2.00	2.75	2.00	112.60	11.79	2.70	94.185	1110.59	0.443

August / September 2007 Tests – Ducted

Exp	Description	run no	v	TSR	v	RPM	w	*TSR*	Torque	Power	Ck
Exp	Duct: Barge	600	1.50	1.50			0.00	*#DIV/0!*		0.00	#DIV/0!
25		601	1.50	2.00	1.50	62.60	6.56	*2.00*	28.3	185.52	0.175
	Profile C arms	602	1.50	2.25	1.50	70.20	7.35	*2.24*	34.845	256.16	0.242
	AoA = 0	603	1.50	2.50	1.50	77.60	8.13	*2.48*	44.77	363.81	0.344
	634-021 blades	604	1.50	2.75	1.50	85.40	8.94	*2.73*	54.33	485.88	0.459
		605	1.50	3.00	1.50	92.90	9.73	*2.97*	50.65	492.75	0.466
		606	1.50	3.50			0.00	*#DIV/0!*		0.00	#DIV/0!
		604.1	1.50	2.75	1.50	85.30	8.93	*2.72*	54.32	485.22	0.459
Exp	Duct no bumps repeat	620	1.50	1.50				*#DIV/0!*		0.00	#DIV/0!
26	Profile C arms	621	1.50	2.00	1.50	62.50	6.54	*1.99*	29.695	194.35	0.184
	AoA = 0	622	1.50	2.25	1.50	70.40	7.37	*2.25*	33.9	249.92	0.236
	634-021 blades	623	1.50	2.50	1.50	77.60	8.13	*2.48*	47.862	388.94	0.368
		624	1.50	2.75	1.50	85.30	8.93	*2.72*	53.92	481.65	0.455
		625	1.50	3.00	1.50	92.90	9.73	*2.97*	50.776	493.97	0.467
		632	2.00	2.25	2.00	91.90	9.62	*2.20*	80.86	778.18	0.310
		633	2.00	2.50	2.00	102.60	10.74	*2.46*	94.58	1016.19	0.405
		634	2.00	2.75	2.00	112.60	11.79	*2.70*	97.82	1153.44	0.460
Exp		640	1.50	1.50				*#DIV/0!*		0.00	#DIV/0!
27	Duct w/ shaft fairing	641	1.50	2.00	1.50	62.50	6.54	*1.99*	26.98	176.58	0.167
		642	1.50	2.25	1.50	70.10	7.34	*2.24*	32.725	240.23	0.227
		643	1.50	2.50	1.50	77.70	8.14	*2.48*	43.967	357.75	0.338
	Profile C arms	644	1.50	2.75	1.50	85.50	8.95	*2.73*	53.186	476.20	0.450
	AoA = 0	645	1.50	3.00	1.50	93.00	9.74	*2.97*	48.05	467.96	0.442
	634-021 blades	646	1.50	3.50						0.00	
		644.1	1.50	2.75	1.50	85.40	8.94	*2.73*	52.752	471.76	0.446
		652	2.00	2.25	2.00	90	9.42	*2.15*	66.472	626.48	0.250
		653	2.00	2.50	2.00	102.2	10.70	*2.45*	91.06	974.56	0.389
		654	2.00	2.75	2.00	112.6	11.79	*2.70*	104.24	1229.14	0.490